

1.3 GA BIMODAL VOLCANISM IN SOUTHEASTERN LABRADOR: FOX HARBOUR

by

James T. Haley, B.Sc. (Hons.)

A thesis submitted to the School of Graduate Studies in partial fulfillment of the
requirements for the degree of

Master of Science

Department of Earth Sciences/Faculty of Science

Memorial University of Newfoundland

May 2014

St. John's, Newfoundland

ABSTRACT

The Fox Harbour bimodal volcanic package, newly discovered in 2010 during exploration by Search Minerals Inc. for rare earth elements (REE) is located in southeastern Labrador (northern Grenville Province). This package of rocks consists of three separate belts, known as the Road Belt, MT Belt, and South Belt. They are highly deformed, with an age of formation of 1.3 Ga, determined via U-Pb analysis of zircon from rhyolitic units. A metamorphic age of 1.05 Ga has also been determined for this package of rocks, which is taken to represent time that the Grenville Orogeny affected this area, exposing it to amphibolite facies metamorphism. The Grenville Orogeny is responsible for much of the observed deformation. The MT Belt has undergone the most exploration, due to the fact that the Foxtrot Deposit is located in this belt. This means that a detailed stratigraphy is available, and a much better correlation between rock types and lithogeochemistry is possible for this belt. Geochemically, many of the rhyolite units are peralkaline, determined geochemically, and by the presence of sodic amphiboles and sodic pyroxenes. The REE-bearing mineral in the volcanic units was determined to be a Y-Nb oxide called fergusonite, determined via electron probe micro-analysis (EPMA). Although not analyzed, allanite is also an important REE-bearing mineral found in all mineralized units. Zircon was also analyzed via EPMA, revealing that a zircon population consisting of large microporous grains was different than the general population observed in Fox Harbour. These microporous grains are believed to be 1.05 Ga based on the limited success in obtaining U-Pb dates from them. *In-situ* determinations of Hf isotopes on the 1.3 Ga zircon crystals reveal that partial melting of 1.5 to 1.9 Ga felsic crustal

sources derived the Fox Harbour volcanic units. *In-situ* Hf determinations of the 1.05 Ga zircon crystal population suggest that these zircon have the same Hf-crustal evolution array for 1.5 to 1.9 Ga sources. This suggests that the 1.05 Ga metamorphism event was a closed system for Lu-Hf, and that there was no flux of REE into or out of the rocks during metamorphism.

ACKNOWLEDGEMENTS

First of all, I would like to thank my supervisor Paul J. Sylvester for overseeing this project, along with providing guidance throughout. The Research and Development Corporation of Newfoundland Labrador, and Search Minerals Inc. supported this research. This project would not have been possible without the generous contributions by these organizations.

I would like to thank Search Minerals Inc., for allowing me propagate my career via providing me with invaluable industry experience, all while allowing me to continue my academic pursuits. Vice President of Exploration, Randy R. Miller, is especially thanked for providing geological guidance and mentoring during my time with Search Minerals Inc. The many hours spent discussing Labrador geology, and regional tectonics will not soon be forgotten.

Many mentors at Memorial University of Newfoundland have provided me with invaluable knowledge that I will take with me for the rest of my career. First and foremost, I'd like to thank Greg Dunning, for taking the time to truly understand my projects issues, and helping me solve those problems in the best way possible. Toby Rivers, and Aphrodite Indares are also thanked for their thoughtful discussion and guidance with regards to the Grenville Province.

My mother and father are also thanked for the love and support through the years, and always having confidence in me.

Lastly, but certainly not least I would like to thank the love of my life, Amanda Langille for the loving support provided throughout the duration of this project. Taking care of two dogs (Beans, and Wilbur) while I was working in Labrador was never an easy task, but you always did it with a smile on your face.

TABLE OF CONTENTS

ABSTRACT.....	ii
ACKNOWLEDGEMENTS	iv
LIST OF TABLES.....	ix
LIST OF FIGURES	x
LIST OF ABBREVIATIONS	xiii
LIST OF APPENDICIES.....	xv
CO-AUTHORSHIP STATEMENT	xvi
CHAPTER 1 Introduction and overview	1
1-1 History and previous work	2
1-2 Thesis Objectives	4
1-3 Methods	5
1-4 Chapter overview	6
1-5 Summary	11
CHAPTER 2 Discovery of 1.3 Ga REE-enriched bimodal volcanism in the Grenville Province of southeastern Labrador, Canada	19
2-1 Introduction	20
2-2 Regional Geology	24
2-2-1 Lake Melville Terrane.....	28
2-2-2 Mealy Mountains Terrane	29

2-2-3	Pinware Terrane	30
2-3	Mapping, Sampling, and Exploration Methods	31
2-4	Local Geology	34
2-4-1	Metamorphic Grade	35
2-4-2	Description of the Volcanic Belts	36
2-5	U-Pb Zircon Geochronology of the Volcanic Rocks	49
2-5-1	Sample Description And Petrography	50
2-5-2	Analytical Methods	53
2-6	Zircon Morphology and U-Pb Zircon Ages	60
2-6-1	FHWT-6-02 – Rhyolite unit from South Belt.....	63
2-6-2	FH-10-02 (8.4m) – Granitic vein/pegmatite within folded basalt	71
2-6-3	FHC-44-01 – Rhyolite unit in MT Belt	72
2-6-4	FHC-45-01 – Rhyolite unit in MT Belt	74
2-6-5	Sample FHC-33-01A – Road Belt	76
2-6-6	Sample FHC-34-03 – Road Belt	78
2-7	Discussion	80
2-7-1	Recognition of large supracrustal package	80
2-7-2	U-Pb age of volcanic package.....	80
2-7-3	Tectonic implications	85
2-8	Conclusions	89
2-9	References	91

CHAPTER 3	The 1.3 Ga bimodal REE-enriched Fox Harbour volcanic belts: a study of the lithgeochemical, mineralogical, and isotopic characteristics	106
3-1	Introduction	107
3-2	Geological Setting	108
3-3	Local Geology	114
3-3-1	South Belt.....	114
3-3-2	MT Belt.....	114
3-3-3	Road Belt	117
3-4	Analytical Techniques.....	118
3-4-1	Lithogeochemical Sampling From Channel Samples and Diamond Drill Core	118
3-4-2	Lithogeochemical Analysis.....	119
3-4-3	Electron Probe Micro-Analysis of Zircon and Fergusonite.....	120
3-4-4	In-situ Lutetium-Hafnium Isotope Analysis of Zircon	121
3-5	Results	123
3-5-1	Lithogeochemistry	123
3-5-2	Electron Probe-Micro Analysis.....	149
3-5-3	In-situ Lutetium-Hafnium Analysis of Zircon	164
3-6	Discussion	169
3-7	Conclusions	174
3-8	References	174

SUMMARY.....185

APPENDIX A.....187

LIST OF TABLES

Table 2-1: Zircon reference material, sample: Harvard 91500.....	55
Table 2-2: Zircon reference material, sample: Plesovice.....	56
Table 2-3: LA-ICPMS U-Pb data table for the Fox Harbour rocks.....	66
Table 2-4: TIMS U-Pb data for sample FHWT-6-02.	70
Table 3-1: Electron microprobe analyses (wt.%) for fergusonite.....	152
Table 3-2: Electron microprobe analyses (wt.%) for zircon.....	159
Table 3-3: Lu-Hf isotope measurements of zircon from Fox Harbour volcanic rocks by LA-MC-ICPMS	168

LIST OF FIGURES

Figure 2-1: Geological provinces of southern Laurentia in Mesoproterozoic	21
Figure 2-2: Location of the Fox Harbour project in Labrador	23
Figure 2-3: Legend for geological map of Labrador.....	26
Figure 2-4: Geological map of the Grenville Province in eastern Labrador.....	27
Figure 2-5: Airborne magnetometer survey for the Fox Harbour project.....	33
Figure 2-6: Geology map for Fox Harbour project area.....	35
Figure 2-7: Typical rock type appearances in the South Belt	38
Figure 2-8: General outcrop appearances of units in the MT Belt.....	42
Figure 2-9: Geology map for the general vicinity of Foxtrot Deposit	45
Figure 2-10: Stratigraphy observed in the Foxtrot deposit	46
Figure 2-11: Channel and diamond drill sections chosen for U-Pb dating.....	51
Figure 2-12: Harvard 91500, and Plešovice zircon reference materials: Concordia diagrams.....	57
Figure 2-13: Cathodoluminescence photos of zircon from samples analyzed for U-Pb. ..	61
Figure 2-14: Cathodoluminescence photos of zircon from samples analyzed for U-Pb. ..	62
Figure 2-15: Cathodoluminescence photos of zircon from samples analyzed for U-Pb. ..	63
Figure 2-16a: LA-ICPMS U-Pb zircon data for sample FHWT-6-02 plotted on a Concordia diagram.....	65
Figure 2-17: LA-ICPMS U-Pb zircon data for sample FH-10-02 (8.4m) plotted on a Concordia diagram.....	72

Figure 2-18: LA-ICPMS U-Pb zircon data for sample FHC-44-01 plotted on a Concordia diagram	74
Figure 2-19: LA-ICPMS U-Pb zircon data for sample FHC-45-01 plotted on a Concordia diagram	75
Figure 2-20: LA-ICPMS U-Pb zircon data for sample FHC-33-01A plotted on a Concordia diagram	79
Figure 2-22: Photos of representative amazonite-bearing pegmatites from the Foxtrot Project	84
Figure 2-23: Airborne magnetometer survey for the southeastern coast of Labrador	89
Figure 3-1: Generalized geological map of Labrador	110
Figure 3-2: Geological map of the Grenville Province in eastern Labrador	111
Figure 3-3: Fox Harbour geology, depicting three volcanic belts mapped and sampled.	113
Figure 3-4: Geology map of the Foxtrot Deposit (MT Belt)	115
Figure 3-5: Stratigraphy observed in the Foxtrot Deposit	117
Figure 3-6: Photomicrographs from the most mineralized units in the Foxtrot Deposit.	124
Figure 3-7: Geology map of the Foxtrot Deposit.....	128
Figure 3-8: Geochemical diagrams for the South Belt	130
Figure 3-9: Harker Diagrams for the South Belt.	131
Figure 3-10: Geochemical diagrams for the South Belt	133
Figure 3-11: Geology map of the Foxtrot Deposit, within the MT Belt.....	134
Figure 3-12: Geochemical diagrams for the MT Belt.....	136
Figure 3-13: Harker Diagrams for MT Belt.....	137
Figure 3-14: Geochemical diagrams for the MT Belt.....	139

Figure 3-15: Spider diagrams for each unit in the MT Belt.....	140
Figure 3-16: Geochemical diagrams for the Road Belt.	143
Figure 3-17: Harker Diagrams for the Road Belt	145
Figure 3-18: Geochemical diagrams for the rhyolitic units of the Road Belt.....	147
Figure 3-19: Spider diagrams for the rhyolitic, basaltic, and aplitic units of the Road Belt.	148
Figure 3-20: Plot designed by Ercit (2005) utilized in distinguishing yttrium-niobate mineral groups	150
Figure 3-21: Chondrite-normalized REE patterns for fergusonite grains from sample FHWT-17-13.....	153
Figure 3-22: Chondrite-normalized REE patterns for fergusonite grains from sample FT- 11-10 (187.5m).	154
Figure 3-23: EPMA data for zircon in the Fox Harbour area	158
Figure 3-24: Cathodoluminescence images of zircon from the Fox Harbour area.....	165
Figure 3-25: $\varepsilon\text{Hf}(t)$ results for zircon from the Fox Harbour area.	167

LIST OF ABBREVIATIONS

AMCG	anorthosite-mangerite-charnockite-granite
Amph	amphibole
APFU	atoms per formula unit
BSE	back scattered electron
ca	circa
CA-TIMS	chemical abrasion thermal ionization mass spectrometer
CPS	counts per second
CHUR	Chondritic uniform reservoir
CL	cathodoluminescence
CPX	clinopyroxene
CV1, CV2	canonical variables 1, and 2
DDH	diamond drill hole
EDX	energy dispersive X-ray
ϵ Hf(t)	epsilon hafnium at time (t)
EPMA	electron probe microanalyzer
FH	Fox Harbour
FHC	Fox Harbour channel
FHWT	Fox Harbour west transect
FHRBC	Fox Harbour Road Belt channel
FTC	Foxtrot channel
FP	Fox Pond project

FT	Foxtrot deposit
HF	hydrofluoric acid
HFSE	high field strength element(s)
HREE	heavy rare earth element(s)
Ga	gigannum
LA-ICPMS	laser ablation inductively coupled mass spectrometer
LREE	light rare earth element(s)
Ma	megaannum
MC-ICPMS	multi-collector inductively coupled mass spectrometer
MLA	mineral liberation analyzer
MREE	middle rare earth element(s)
MSWD	mean square of the weighted deviates
MTB	MT Belt
MUN	Memorial University of Newfoundland
PHS	Port Hope Simpson
ppb	parts per billion
ppm	parts per million
REE	rare earth element(s)
RB	Road Belt
SB	South Belt
SEM	scanning electron microscope
wt%	weight percent

LIST OF APPENDICES

Appendix 1	Lithogeochemical data.....	187
-------------------	----------------------------	-----

CO-AUTHORSHIP STATEMENT

The manuscript presented as Chapter 2, entitled “Discovery of 1.3 Ga REE-enriched bimodal volcanism in the Grenville Province of southeastern Labrador, Canada,” and the manuscript presented as Chapter 3, entitled “Lithogeochemical, and isotopic study of the 1.3 Ga Fox Harbour bimodal volcanic package, Grenville Province, southeastern Labrador” contains contributions from three authors. These include, James T. Haley (Memorial University of Newfoundland), Paul J. Sylvester (Memorial University of Newfoundland), and Randy R. Miller (Search Minerals Inc.). As the first author, I was responsible for all aspects of the project, from project planning, formulating scientific hypotheses, literature research, data collection, and analysis. Coauthors provided guidance on geological hypotheses, data collection, data reduction, interpretation, and corrected the manuscript before submission.

CHAPTER 1 INTRODUCTION AND OVERVIEW

The Fox Harbour bimodal volcanic belts, located in southeastern Labrador have been the focus for rare earth element (REE) exploration by Search Minerals Inc. since late 2009 (Delaney and Haley, 2011; *unpublished* assessment report). The regional geology of the area is complicated, as it straddles three lithotectonic terranes, from north to south, the Lake Melville terrane, the Mealy Mountain terrane, and the Pinware terrane. The geology in the area generally consists of granitoids, highly deformed supracrustal packages, mafic intrusives, and pegmatites.

This project focuses on three volcanic belts named the Road Belt, MT Belt, and the South Belt (north to south). Rock types within these volcanic belts include: high field strength element (HFSE) enriched peralkaline rhyolite (comendite and pantellerite), subalkaline tholeiitic basalt, quartzite, garnetiferous volcaniclastic/metasedimentary units, along with discordant mafic dykes, and granitoid dykes. Observed textures and mineral assemblages indicate metamorphism at amphibolite facies. The belts have been mapped and sampled for 35 km, and are assumed to extend another 25 km based on limited grab samples (exhibiting similar mineralogy, textures, and geochemistry), and aeromagnetic patterns.

1-1 HISTORY AND PREVIOUS WORK

Early knowledge of the area is based mainly on descriptions of coastal localities (Lieber, 1860; Packard, 1891; Daly, 1902; Kranck, 1939; Christie, 1951; Douglas, 1953) and 1:500,000 scale reconnaissance mapping (Eade, 1962).

Complete aeromagnetic coverage and lake-sediment geochemical surveys were conducted for the region (Geological Survey of Canada, 1974a, 1974b, 1984). The Newfoundland and Labrador Geological Survey released a detailed lake sediment survey in 2010 for southeastern Labrador.

Geological mapping at 1:100,000 scale, as a 5-year Canada - Newfoundland joint project aimed at mapping an 80 km coastal fringe of the Grenville Province in southern Labrador, was carried out from 1984 to 1987 by Charles F. Gower of the Newfoundland and Labrador Geological Survey (Gower and Owen, 1984; Gower, 1985; Gower et al., 1987; Gower and Erdmer, 1988; Gower et al., 1992; Gower, 1994; Gower and van Nostrand, 1994; Gower, 1996a; Gower, 1996b; Gower et al., 1997; Gower and Krogh, 2002; Gower, 2003; Gower 2005, Gower, 2007; Gower et al., 2008a; Gower et al., 2008b; Gower, 2009, Gower, 2010).

Meyer and Dean visited the area in 1988 to investigate a Pb-Cd-W-Cu lake sediment anomaly (Meyer and Dean, 1988).

Scott et al. (1994) used U-Pb geochronology to directly determine the age of deformation within shear zones developed throughout the region.

Devonian Resources Inc. conducted work from June 1st – June 27th, 1996 in the eastern boundary of the current project area (assessment file 003D/05/0021). Work

conducted was ground follow up of a Geological Survey of Canada lake sediment survey that indicated anomalous copper, nickel and cobalt values. They concluded saying that no further exploration is recommended. They also attempted to relocate the sample location found by the Newfoundland Geological Survey in 1988 with anomalous zirconium (Zr) values. They did not find the rock described by the Newfoundland Geological Survey, and did not take any samples.

Greenshield Resources Inc. conducted work from May 29th – August 3rd 1996 on the eastern edge of the current project area (assessment file LAB/1205). This file describes a program of geological mapping, prospecting, lithogeochemical sampling, and diamond drilling. Most of the focus was towards the west (*i.e.*: outside of) the current project area. Exploration focused on assessing the potential for economic magmatic copper-nickel mineralized areas within the Alexis River Anorthosite. The program was completed with no significant economic mineralization discovered.

Rockhopper Corporation and Cartaway Resources conducted work between 1994 and 1996 in the center of the current project area, and focused on locating gem quality sapphires (assessment file LAB/1203). Work described consists of stripping, and prospecting, along with subsequent laboratory evaluations of the gems from the deposit.

Alterra Resources Inc. (Search Minerals Inc.) have worked on the Fox Harbour project since late 2009. Work thus far consists of an airborne radiometric survey, prospecting, lithogeochemical sampling, mapping, trenching, channel sampling, diamond drilling, and detailed magnetometer surveys.

1-2 THESIS OBJECTIVES

The main objectives of this thesis are:

- 1. To fully characterize the Fox Harbour bimodal volcanic belts.*

The newly discovered Fox Harbour bimodal volcanic belts have never been described in literature. Recording and interpreting the physical characteristics of the belts, such as their location, main rock types, subdivisions, stratigraphy (if discernable), mineralogy, and petrography is an important first step for these packages of rocks.

- 2. Determine the absolute age of formation for the supracrustal units, along with the age of metamorphism for the general area (via dating the rhyolitic units).*

The location of this volcanic package in southeastern Labrador is very interesting, as it straddles three separate lithotectonic terranes (Lake Melville, Mealy Mountain, and Pinware terranes). Dating of this volcanic package is essential for the full geological interpretation of the area.

- 3. Utilize the 10,000-lithogeochemical samples taken in the area for a full lithogeochemical study of the area.*

Often times, when a mineral exploration company conducts work, the lithogeochemical assay package chosen is one that gives only elements of interest, and is not suitable for academic studies. Search Minerals Inc. decided to conduct a full assay package (i.e.: major, minor, and trace elements) on every single sample analyzed. This allows for a unique situation, where there is an abundance of lithogeochemical data

suitable for academic research. Utilizing this geochemistry data to further understand the geochemical processes that affected the area is of utmost importance in this project.

4. Incorporate the Fox Harbour bimodal volcanic packages into the regional tectonic model for southeastern Labrador, and the Grenville Province.

Once fully characterized via mapping, petrography, lithogeochemistry, U-Pb geochronology, and isotopic studies, the volcanic package must be introduced into the tectonic model for southeastern Labrador.

1-3 METHODS

Southeastern Labrador has had a large amount of regional geological interpretation, including geological mapping, terrane identification, lithotectonic models, and U-Pb dating (refer to section 1-1). The Geological Survey of Newfoundland and Labrador, and the Geological Survey of Canada have completed much the work in this area. The Fox Harbour volcanic belts are a complex package of rocks, which have undergone very interesting igneous and metamorphic processes. Understanding, and characterizing this package of rocks requires a multidisciplinary approach, utilizing fieldwork, petrography (including polarizing microscopes, SEM-MLA, and CL), lithogeochemistry, U-Pb geochronology (using the laser ablation inductively coupled mass spectrometer, and the thermal ionization mass spectrometer, or LA-ICPMS, and TIMS, respectively), and understanding of accessory mineral geochemistry, by utilizing electron probe microanalysis (EPMA).

1-4 CHAPTER OVERVIEW

Chapter 2: Discovery of 1.3 Ga REE-enriched bimodal volcanism in the Grenville Province of southeastern Labrador.

The Fox Harbour volcanic package underwent a vast array of exploration within the first three years of its discovery (Delaney and Haley, 2011; *unpublished* assessment report). Exploration techniques include airborne radiometric survey, prospecting, mapping, lithogeochemical sampling, channeling, and diamond drilling. These exploration methods allowed for a detailed interpretation of the area on the surface, and extending to the subsurface in the case of the Foxtrot Deposit. The Fox Harbour volcanic belts, discovered in 2010, have not been described in literature; therefore a thorough write-up of the belts was required, and is presented in this chapter.

A regional geology map for the area between the town of St. Lewis and the intersection of highway 510 and 513 was created, identifying three separate volcanic belts (the South Belt, MT belt, and Road Belt) extending beyond the extent of this initial project area. A detailed understanding of each belt was conducted, attempting to identify the physical extent of the belts, and individual units within each belt.

This project set out to fully characterize each belt, along with the currently identified units within each respective belt. This characterization includes its lateral extent, size, rock types, stratigraphy, mineralogy, and U-Pb age, as recorded in zircon.

Representative thin sections from each belt were chosen for U-Pb dating via *in-situ* laser ablation inductively coupled mass spectrometry (LA-ICPMS), and thermal

ionization mass spectrometry (TIMS). Zircon crystals were identified using the scanning electron microscope, coupled with the mineral liberation analyzer, otherwise known as the SEM-MLA. Complex zircon textures were identified, and subsequently analyzed. These data provide an absolute age of formation for the rhyolite units (1.3 Ga), along with the age of metamorphism for the area (1.05 Ga).

The South Belt was dated via LA-ICPMS and TIMS, confirming an age of 1297 ± 21 Ma (2σ) via LA-ICPMS, and 1300 ± 2.5 Ma via TIMS. A number of samples were analyzed for U-Pb on the MT Belt (dated via LA-ICPMS), which identified both the age of formation, and age of metamorphism. Absolute age of formation range from 1346 ± 51 Ma (2σ), and 1250 ± 20 Ma (2σ), while the recorded metamorphic age is 1018 ± 30 Ma (2σ). The Road Belt was analyzed via LA-ICPMS, and like the MT Belt recorded both the age of formation and age of metamorphism. The recorded age of formation is 1256 ± 24 Ma (2σ), while the metamorphic ages range from 1050 ± 21 Ma (2σ), and 1047 ± 17 Ma (2σ).

Chapter 3 The 1.3 Ga bimodal REE-enriched Fox Harbour volcanic belts: a study of the lithogeochemical, mineralogical, and isotopic characteristics.

Upwards of 10,000 lithogeochemical samples have been taken from the Fox Harbour area, with sampling methods ranging from hand samples, channel samples, and diamond drill hole samples. The combination of field observations, and stratigraphic reconstruction for the area allows for a detailed interpretation of this lithogeochemical

data. Representative lithogeochemical samples were taken from each belt to fully characterize the volcanic belts geochemically.

Rhyolitic units in the Fox Harbour area tend to be peralkaline (i.e.: ~1.0 on the alkalinity index), and are further classified as comendite and pantellerite (Winchester and Floyd, 1977; Macdonald, 1974). Many of the more mineralized units contain peralkaline-indicator minerals, such as sodic pyroxenes and amphiboles. Lithogeochemical classification is done by utilizing geochemical diagrams designed for altered volcanic rocks (Harker, 1909; Shand, 1927; Macdonald, 1974; Winchester and Floyd, 1977; and Sun and McDonough, 1989).

The rhyolite units of the South Belt are generally peralkaline (as defined by Shand (1927), which may not be applicable to altered volcanics). Indicator minerals within the units suggest that the entirety of the South Belt is peralkaline, and roughly transitions from pantellerite in the north to comendite in the south, roughly in the center of the belt (Shand, 1927; Macdonald, 1974; Winchester and Floyd, 1977). These subdivisions are determined solely geochemically, as the South Belt is extremely homogenous on the surface. This makes individual unit identification near impossible. Mafic volcanic rocks in the South Belt are subalkaline tholeiitic basalts (Irvine and Barager, 1971). Rhyolitic units (comendite and pantellerite) display very slight differences in light rare earth element (LREE) and heavy rare earth element (HREE) slopes when plotted on a Chondrite normalized spider diagram.

Rhyolitic units of the MT Belt, are peralkaline, and are further classified to comendite (FT2) and pantellerite (FT2x, FT3, FT3b, and FT4) (Macdonald, 1974; Winchester and Floyd, 1977). Basalt in the MT Belt is generally subalkaline tholeiites

(Irvine and Baragar, 1971). Major elements in the rhyolitic units of the MT Belt are generally immobile, except for Al_2O_3 , Na_2O , and K_2O , which when plotted on simple Harker diagrams display erratic behavior (Harker, 1909). Simple immobile vs immobile element plots (i.e.: Zr vs Y, Zr vs Dy) suggest that these elements remained largely immobile (plot at a consistent ratio with respect to each other, throughout the full geochemical spectrum observed). Rhyolite units of the MT Belt display very similar patterns, with only slight LREE and HREE variations when plotted on the chondrite normalized spider diagrams.

Rhyolite units of the Road Belt are very similar to those found in the MT Belt, displaying similar lithological units, mineralogy, and geochemistry. Rhyolitic units are classified as comendite and pantellerite, and are peralkaline in nature (Macdonald, 1974; Maniar and Piccoli, 1989). As with the South Belt, the further subdivision (i.e.: comendite or pantellerite) of the rhyolite units is made solely on the geochemical characteristics. The Road Belt is heavily deformed, and identifying individual units prior to acquiring lithogeochemistry is near impossible (Haley et al., 2013). The only exception to this is the pantelleritic units, which commonly contain a high amount of magnetite, amazonite, sodic pyroxene, \pm sodic amphibole, similar to units FT2x, FT3, FT3b, and FT4 in the MT Belt. As with the other belts, mafic volcanic rocks plot as subalkaline tholeiites, with a small amount of samples plotting as andesite/basalt (Irvine and Baragar, 1971; Winchester and Floyd, 1977). Due to the nature of volcanic systems, some of the major elements (Na, Ca, and K) appear to have been affected, likely by post deposition metasomatism often associated with subaerial volcanics. It is also possible that the metamorphism this unit experienced also affected the major elements. This creates a scattered affect on the Harker

(1909) diagrams. Elements that were greatest affected include Al₂O₃, Na₂O, and K₂O, while FeO, CaO, TiO₂, and P₂O₅ decrease with increasing SiO₂. Although the major elements were affected, XY immobile vs immobile plots reveal that the trace elements have remained relatively immobile, as they plot consistently throughout the full range of geochemical values (i.e.: simple XY immobile vs immobile diagrams plot in a straight line). Patterns observed on the chondrite normalized spider diagrams are all very similar, with very little variation within each respective geochemical unit.

Electron microprobe analysis of the yttrium-niobate mineral identified via SEM-MLA confirms that the mineral is fergusonite, a Y-Nb oxide. Fergusonite grains were shown to contain ~20-29 wt.% REE, and are believed to be the main carrier of REE in the Fox Harbour area. Chondrite normalized REE patterns are fairly consistent in the two samples analyzed. Differences consist of slightly different Eu depletion anomalies, along with slight variations in the LREE and HREE slopes. Although not analyzed, allanite is also an important REE-bearing minerals observed throughout all units of the Fox Harbour area.

Electron microprobe analysis of zircon was conducted on a representative sample from all three belts, and the adjacent granitic augen gneiss. Many of the analyzed zircon crystals are consistent, with Zr (APFU: atoms per formula unit) ranging from 0.97-0.99, while U+Th (APFU) ranges from 0.0000-0.001, Nb+Ta (APFU) ranges from 0.000-0.001, and Y+Gd+Dy+Yb (APFU) ranges from 0.000-0.020. Zircon morphology in the Fox Harbour area is quite interesting, with many different textures, described by Haley et al. (2013). A population of microporous zircon crystals was analyzed by the EPMA, unveiling interesting results. These microporous zircon contained much less Zr (APFU)

from approximately 0.92-0.95, much lower than the majority of the crystals analyzed in the Fox Harbour area. This means other elements are in the place of Zr. Looking at the U+Th, Nb+Ta, and Y+Gd+Dy+Yb (APFU) values for this specific zircon population quantifies this observation. This reveals that they are elevated with respect to the general population zircon in the Fox Harbour area. U+Th (APFU) ranges from 0.002-0.005, while Nb+Ta (APFU) ranges from 0.001-0.008, and Y+Gd+Dy+Yb (APFU) ranges from 0.010-0.080.

In-situ lutetium-hafnium (Lu-Hf) analysis of zircon crystals in the Fox Harbour area reveals interesting results as well. All three belts were analyzed, along with the two main age populations (1.3 Ga, and 1.05 Ga) as determined by Haley et al. (2013). *In-situ* Hf analysis reveals that the 1.3 Ga has an $\epsilon\text{Hf}(t)$ that ranges from -0.65 to $+7.59$, and the 1.05 Ga zircon population has an $\epsilon\text{Hf}(t)$ that ranges from $+0.62$ to -4.21 . This suggests, first of all, that the 1.3 Ga rhyolite units in Fox Harbour were derived by partial melting of 1.5 to 1.9 Ga felsic crustal sources. Second of all, the 1.05 Ga zircon crystals have the same Hf-isotope crustal evolution array for 1.5 to 1.9 Ga sources, suggesting that the 1.05 Ga metamorphic event was a closed system for Lu-Hf. This suggests that there was no flux of REE into or out of the rocks, and that REE were remobilized within the volcanic package, and not added during Grenvillian metamorphism.

1-5 SUMMARY

The data presented in this thesis suggest that the age of formation for the Fox Harbour rhyolite units (and adjacent supracrustal units) is 1.3 Ga, determined via U-Pb

age analysis of zircon. Many of the rhyolitic units in the belt are peralkaline, while almost as they display peralkaline indicator minerals (such as sodic pyroxenes and sodic amphiboles). The continent-continent collision, known as the Grenville Orogeny affected this package of rocks at 1.05 Ga, exposing it to amphibolite facies metamorphism, based on characteristic metamorphic mineral assemblages. Although heavily disturbed by deformation, it is suggested that there was no flux of HFSE (high field strength elements) into or out of the volcanic packages during deformation. This requires that all REE mineralization occurring in the packages be of a primary origin. The main REE-bearing mineral in Fox Harbour is shown to be fergusonite, a Y-Nb oxide.

REFERENCES

- Andrews, R., and Beecham, A.W. 1997: First, second and third year assessment report on geological exploration for licenses 646M, 709M, 4460M, 4484M, 4485M, 4555M, 4664M- 4666M, 4808M-4810M and 50009M-5010M on claims in the Doreen Pond area, near St. Lewis Inlet, southeastern Labrador, 2 reports. Rockhopper Corporation, Cartaway Resources Corporation, Peruvian Gold Limited, Clouston, I.B., McCarthy, A.W. NTS: 13D/05, 13A/08. Newfoundland and Labrador Geological Survey, Assessment File LAB/1203, 1997, 42 pages.
- Christie, A.M. (1951). Geology of the southern coast of Labrador from Forteau Bay to Cape Porcupine. *Geological Survey of Canada*, Paper 51-13, 19 pages.

- Christie, A.M., Roscoe, S.M. and Fahrig, W.F. (1953). Preliminary map. Central Labrador coast Newfoundland (descriptive notes). *Geological Survey of Canada*, Paper 53-14, 3 pages.
- Daly, R.A. (1902). The geology of the northeast coast of Labrador. *Bulletin of the Museum of Comparative Zoology*, (38-5), 205-270. .
- Delaney, P., and Haley, J.T. (2011; *unpublished*). Report on mapping, prospecting, geochemical sampling, trenching, diamond drilling, and airborne radiometric/magnetometer survey on the Fox Harbour property, Port Hope Simpson, Labrador. 1st year assessment report, Alterra Resources Inc, pp. 429.
- Douglas, G.V. (1953). Notes on localities visited on the Labrador coast in 1946 and 1947. *Geological Survey of Canada*, Paper 53-1, 67 pages.
- Eade, K.E. (1962). Geology, Battle Harbour - Cartwright, coast of Labrador, Newfoundland. *Geological Survey of Canada*, Map 22-1962.
- Gower, C.F. (1985). Correlations between the Grenville Province and Sveconorwegian Orogenic Belt — Implications for Proterozoic Evolution of the Southern Margins of the Canadian and Baltic Shields. *The deep Proterozoic Crust in the North Atlantic Provinces*, 247–257. doi:10.1007/978-94-009-5450-2_15.
- Gower, C.F. (1994). Distribution of pre-1400 Ma crust in the Grenville province: Implications for rifting in Laurentia-Baltica during geon 14. *Geology*, 22, 827-830.
- Gower, C.F. (1996a). The evolution of the Grenville Province in eastern Labrador, Canada. *Geological Society London Special Publications*, 112(1), 197-218. doi: 10.1144/GSL.SP.1996.112.01.11

- Gower, C.F. (1996b). Geology of the southeast Mealy Mountains Region, Grenville Province, Southeast Labrador. *Current Research, Newfoundland and Labrador Department of Natural Resources*. 96-1, 55-71.
- Gower, C.F. (2003). Geological map of the Grenville Province in eastern Labrador. *Newfoundland and Labrador Department of Mines and Energy, Geological Survey, Map 2003-11*. Open file: LAB/1379.
- Gower, C.F. (2005). Kinematic evidence for terrane displacements in the Grenville province. *Current Research, Newfoundland and Labrador Department of Natural Resources*. Report 05-01, pp. 73-92.
- Gower, C. F. (2007). Protolith recognition of metamorphosed felsic volcanic/volcaniclastic rocks, with special reference to the Grenville Province in southeast Labrador. *Current Research. Newfoundland and Labrador Department of Natural Resources*. Report 07-01, pp. 11-23.
- Gower, C.F. (2009). Battle Island – A geological treasure in coastal eastern Labrador. Government of Newfoundland and Labrador, Department of Natural Resources, Geological Survey, Open File 003D/05/0031, 38 pages.
- Gower, C.F. (2010a). Geology of the St. Lewis River area (NTS sheets 03D/04 and 05; 13A/01, 02, 07 and 08), southeastern Labrador. Geological Survey, Mines Branch, Department of Natural Resources, Government of Newfoundland and Labrador, Map 2010-24, Open File LAB/1566.
- Gower, C.F. (2010b). Geology of the Port Hope Simpson area (NTS sheets 03D/12 and 13; 13A/09, 10, 15 and 16), southeastern Labrador. Geological Survey, Mines

Branch, Department of Natural Resources, Government of Newfoundland and Labrador, Map 2010-20, Open File LAB/1565.

Gower, C., & Owen, V. (1984). Pre-Grenvillian and Grenvillian lithotectonic regions in eastern Labrador-correlations with the Sveconorwegian Orogenic Belt in Sweden.

Canadian Journal of Earth Sciences, 21(6), 678–693.

Gower, C.F., Neuland, S., Newman, M., Smyth, J., 1987: Geology of the Port Hope Simpson map region, Grenville province, eastern Labrador, *Current Research (1987) Newfoundland Department of Mines and Energy, Mineral Development Division*, Report 87-1, 183-199.

Gower, C. F., & Erdmer, P. (1988). Proterozoic metamorphism in the Grenville Province: a study in the Double Mer-Lake Melville area, eastern Labrador. *Canadian Journal of Earth Sciences*, 25(11), 1895–1905.

Gower, C., Schärer, U., & Heaman, L. (1992). The Labradorian orogeny in the Grenville Province, eastern Labrador, Canada. *Canadian Journal of Earth Sciences*, 29(9), 1944–1957.

Gower, C.F., van Nostrand, T. (1994). Geology of the Pinware River Region, southeast Labrador. *Current Research, Newfoundland and Labrador Department of Natural Resources*. 94-1, 347-369.

Gower, C., Hall, J., Kilfoil, G., Quinlan, G., & Wardle, R. (1997). Roots of the Labradorian orogen in the Grenville Province in southeast Labrador: Evidence from marine, deep-seismic reflection data. *Tectonics*, 16(5), 795–809.

- Gower, C., & Krogh, T. (2002). A U–Pb geochronological review of the Proterozoic history of the eastern Grenville Province. *Canadian Journal of Earth Sciences*, 39(5), 795–829. doi: 10.1139/E01-090
- Gower, C., Kamo, S., & Krogh, T. (2008). Indentor tectonism in the eastern Grenville Province. *Precambrian Research*, 167(1-2), 201–212.
- Gower, C., Kamo, S., Kwok, K., & Krogh, T. (2008). Proterozoic southward accretion and Grenvillian orogenesis in the interior Grenville Province in eastern Labrador: Evidence from U-Pb geochronological investigations. *Precambrian Research*, 165(1-2), 61–95.
- Haley, J.T., Sylvester, P.J., Miller, R.R. (2013). Discovery of 1.3 Ga REE-enriched bimodal volcanism in the Grenville Province of southeastern Labrador, Canada.
- Harker, A., (1909). The Natural History of Igneous Rocks. London, Methuen, 384 pp.
- Hodge, R. (1996). First year assessment report on prospecting for licence 4087m on claims in the Fox Harbour area, southeastern Labrador, *Newfoundland and Labrador Geological Survey*, 3D/05/0021, 13 pages.
- Irvine, T. N., & Baragar, W. (1971). A Guide to the Chemical Classification of the Common Volcanic Rocks. *Canadian Journal of Earth Sciences*, (8), 523-548.
- Jolliffe, T.S. (1997). Second year assessment report on geological, geochemical and diamond drilling exploration for licences 2559m-2560m, 4160m-4166m, 4367m-4375m, 4412m-4413m, 4602m, 4689m and 4766m-4772m on claims in the Alexis River and Fox Harbour areas, southeastern Newfoundland, *Newfoundland and Labrador Geological Survey*, LAB/1205, 115 pages.

- Kranck, E.H. (1939). Bedrock geology of the seaboard region of Newfoundland Labrador. *Newfoundland Geological Survey*, Bulletin 19, 50 pages. [LAB/0071].
- Lieber, O.M. (1860). Geology of the coast of Labrador. *United States Coast Survey Report* (Eclipse Expedition).
- Macdonald, R. (1974). Nomenclature and petrochemistry of the peralkaline oversaturated extrusive rocks. *Bulletin volcanologique*, 38(2), 498–516.
- Maniar, P.D., Piccoli, P.M. (1989). Tectonic discrimination of granitoids, *Geological Society of America Bulletin*, 101(5), 635–643.
doi:10.1130/00167606(1989)101<0635:TDOG>2.3.CO;2
- Meyer, J.R., Dean, P.L. (1988). Industrial minerals and follow-up of lake- and stream-sediment geochemical anomalies in Labrador, in *Current research, Newfoundland and Labrador Mineral Development Division*, Report No. 88-1, 1988, p. 247-259.
- Packard, A.S. (1891). The Labrador coast: a journal of two summer cruises to that region, with notes on its early discovery, on the Eskimo, on its physical geography, geology and natural history. *N.D.C. Hodges*, New York (publisher), 513 pages.
- Scott, D., Machado, N., Hanmer, S., & Gariépy, C. (1993). Dating ductile deformation using U-Pb geochronology: examples from the Gilbert River Belt, Grenville Province, Labrador, Canada. *Canadian Journal of Earth Sciences*, 30(7), 1458–1469.
- Shand, S.J. (1927). On the relations between silica, alumina, and the bases in eruptive rocks, considered as a means of classification. *Geological Magazine*, (64), 446–446.

- Shand, S. J. (1951). *Eruptive Rocks*. New York: J. Wiley.
- Sun, S. S., & McDonough, W. F. (1989). Chemical and isotopic systematics of oceanic basalts: implications for mantle composition and processes. *Geological Society, London, Special Publications*, (42), 313-345.
- Winchester, J. A., & Floyd, P. A. (1977). Geochemical discrimination of different magma series and their differentiation products using immobile elements. *Chemical Geology*, (20), 325–343. doi:10.1016/0009-2541(77)90057-2

CHAPTER 2 DISCOVERY AND U-PB DATING OF 1.3 GA REE-ENRICHED BIMODAL VOLCANISM IN THE GRENVILLE PROVINCE OF SOUTHEASTERN LABRADOR, CANADA

James T. Haley¹, Paul J. Sylvester¹, Randy R. Miller²

¹*Department of Earth Sciences, Memorial University, St. John's, NL, Canada,*

A1B 3X5

²*Search Minerals Inc., Toronto, ON, Canada, M5H 3B7*

E-mail: j.haley@mun.ca

ABSTRACT

The Fox Harbour bimodal volcanic package, located in southeastern Labrador Canada is a highly deformed package of rocks. There are three volcanic belts in the area (South Belt, MT Belt, and Road Belt), with rock types within the volcanic packages consisting of rhyolite (containing sodic pyroxene and amphibole, suggesting that they are peralkaline), subalkaline tholeiitic basalt, quartzite, aplitic dykes, and andesitic dykes. The mineralogy, surficial extent, and description of individual units within each volcanic belt are presented. Rhyolitic units from each volcanic belt have been dated via U-Pb zircon geochronology (LA-ICPMS, and TIMS). Zircon grains from each belt revealed an age of formation 1.3 Ga, and an age of metamorphism ~1.05 Ga (i.e.: Grenvillian deformation). This demonstrates that there was volcanic activity along this area of the

Laurentian margin during this time, coinciding with other occurrences of 1.3 Ga supracrustal packages throughout the Grenville Province. The Fox Harbour volcanic packages underwent amphibolite facies metamorphism during the Grenvillian orogenic event, at 1.05 Ga.

2-1 INTRODUCTION

Rock packages are intensely deformed and metamorphosed during large-scale continental collisions, obscuring their original age and character, limiting their recognition in the geological record, and biasing the record of crustal growth. One of the largest continental collisions in Earth history is represented by the Grenville Province, which extends for over 2000 km from southern Ontario to eastern Labrador, with a width ranging from 300-400 km for most of its length (up to 600 km in the south) (Figure 2-1). It is known to extend several thousand kilometers further to the southwest but is largely concealed by Paleozoic cover in the southeastern United States (Hynes and Rivers, 2010).

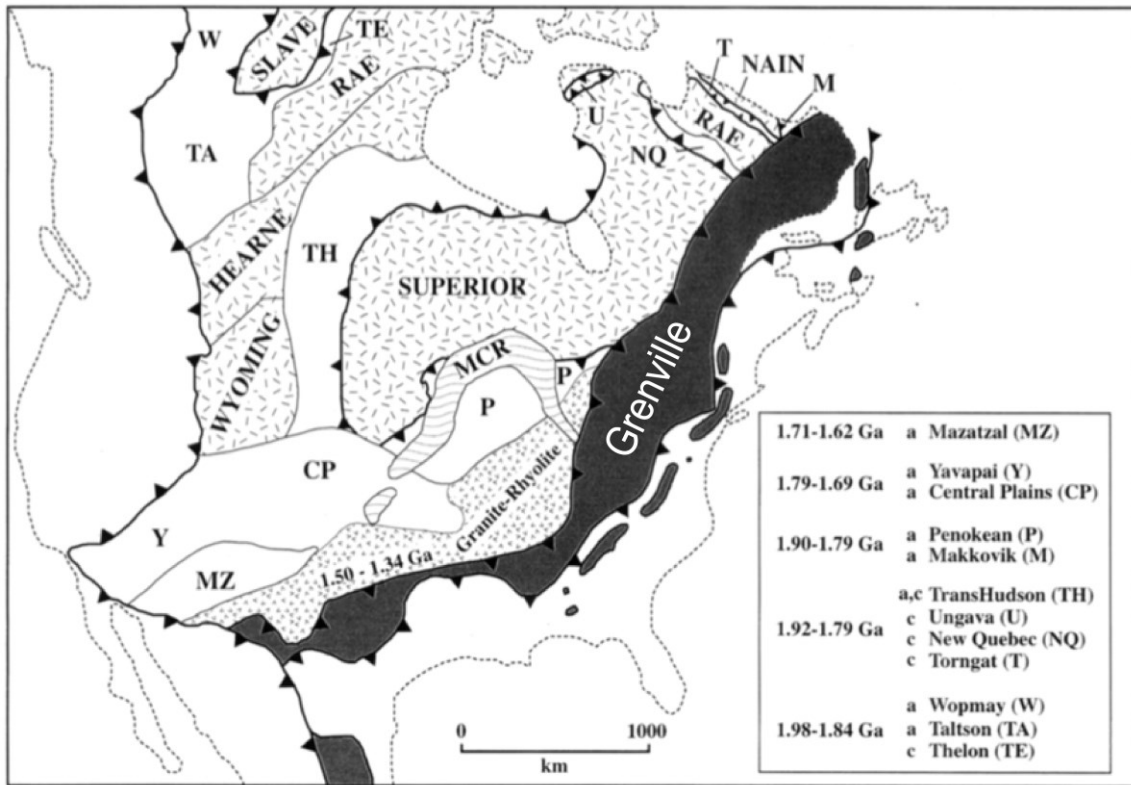


Figure 2-1: Geological provinces of southern Laurentia in Mesoproterozoic. Modified after Hoffman (1989) and Rivers (1997).

Determining the protolith of supracrustal rocks in medium to high-grade metamorphic terranes of the Grenville Province is generally a challenge. The supracrustal rocks are largely concealed by and structurally concordant to granitoid units in high-grade gneissic terranes (Corriveau and Bonnet, 2005; van Breemen and Corriveau, 2005; Gower, 2007; Kamo et al., 2011). Unless obvious primary textures are observed, or there is a field spatial relationship with obvious supracrustal rocks, they often go unrecorded (Gower, 2007).

The Fox Harbour project of the Port Hope Simpson area of southeastern Labrador (Figure 2-2) has been a focus for rare earth element (REE) exploration in felsic gneisses

by Search Minerals Inc. since late 2009 (Delaney and Haley, 2010 *unpublished*; Srivastava et al., 2012). The Foxtrot deposit (Defined as the occurrence of a thick sequence of volcanic rocks within the MT Belt, as seen in Figure 2-2, and 2-9), within the Fox Harbour project has undergone the majority of the exploration in the project area. The region is located in the northeastern portion of the Grenville Province, on the Laurentian margin of present day North America. Laurentia includes the Archean Superior and Nain cratons, and several accreted terranes of Paleoproterozoic orogens such as the Trans-Hudson, Torngat, Penokean, Makkovik, Yavapai and Mazatzal (Figure 2-1), each of which may now be deformed constituents of the Grenville Province (Gower et al., 1997; Hynes and Rivers, 2010).



Figure 2-2: Location of the Fox Harbour project in Labrador. Inset depicts detailed outline of project area. Star depicts location of the Foxtrot deposit within the Fox Harbour project area.

During the 2010 exploration season, a bimodal mafic and felsic volcanic package was discovered, near the communities of St. Lewis and Port Hope Simpson. This contribution is the first detailed description of the geology of the Fox Harbour bimodal volcanic packages. A geological map and tectonostratigraphy is presented, along with a petrographic description and geochemical characterization of the major lithologies present in each belt in the area. New U-Pb zircon geochronology for six rhyolitic units are also presented, documenting that the volcanic rocks formed during *ca.* 1.3 Ga magmatism and were strongly recrystallized during the subsequent *ca.* 1.1 Ga Grenville orogeny.

2-2 REGIONAL GEOLOGY

The Grenville Province in Labrador generally consists of medium- to high- grade rocks (Gower, 1996; Rivers, 1997, 2002, 2008, and 2009). The geology within the study area consists of granitoids, highly deformed supracrustal packages, mafic intrusive rocks, and later pegmatites, intruding all previously mentioned units. All have been affected by one or more phases of deformation (even the later pegmatites, which are often seen deformed), making primary features and protolith recognition often difficult to determine. Intrusives consist of K-feldspar megacrystic granite, granodiorite to diorite, quartz monzonite, and syenite, in many places with intruded amphibolite mafic dykes.

Most previous work in the eastern Grenville Province of southern and central Labrador has been dedicated to large-area regional mapping of consistent terranes. In this context, a terrane is defined as a fault-bounded crustal block or metamorphic domain with a common Grenvillian metamorphic history, following Gower (1996) and Rivers (2009).

Terranes have thus been distinguished on the basis of distinct lithologies, structures, metamorphic facies, along with numerous crystallization and metamorphic ages.

The regional geology of the Port Hope Simpson area straddles three separate lithotectonic terranes within the eastern Grenville Province (Gower, 1996, 2005; Gower and Krogh, 2002). These include the Lake Melville terrane, Mealy Mountain terrane, and the Pinware terrane, from north to south, respectively (Figure 2-4). Differing lithologies, structures, metamorphic facies, along with distinctive crystallization and metamorphic events characterize these terranes (Gower and Owen, 1984; Schärer and Krogh, 1986; Schärer and Gower, 1988; Gower and Schärer, 1992; Scott et al., 1993; Tucker and Gower, 1994; Gower, 1994, 1996, 1997, 2005, 2009; Kamo et al., 1996, 2011; Wasteneys et al. 1997; Rivers, 1997). Rivers (2009) described the Lake Melville terrane as an allochthonous medium- to low-pressure metamorphic belt of granulite to amphibolite facies rocks (800 MPa, 820 °C) formed during the early Ottawan phase (1088-1046 Ma) of the Grenville Orogeny. It is separated from the down-dropped Mealy Mountains terrane, which largely escaped Grenville metamorphic reworking, along the transtensional English River shear zone. The Pinware terrane is an allochthonous medium-pressure metamorphic belt of amphibolite facies rocks formed during the later stages of the Ottawan phase (1036-1020 Ma) of the Grenville Orogeny (Rivers 2009).

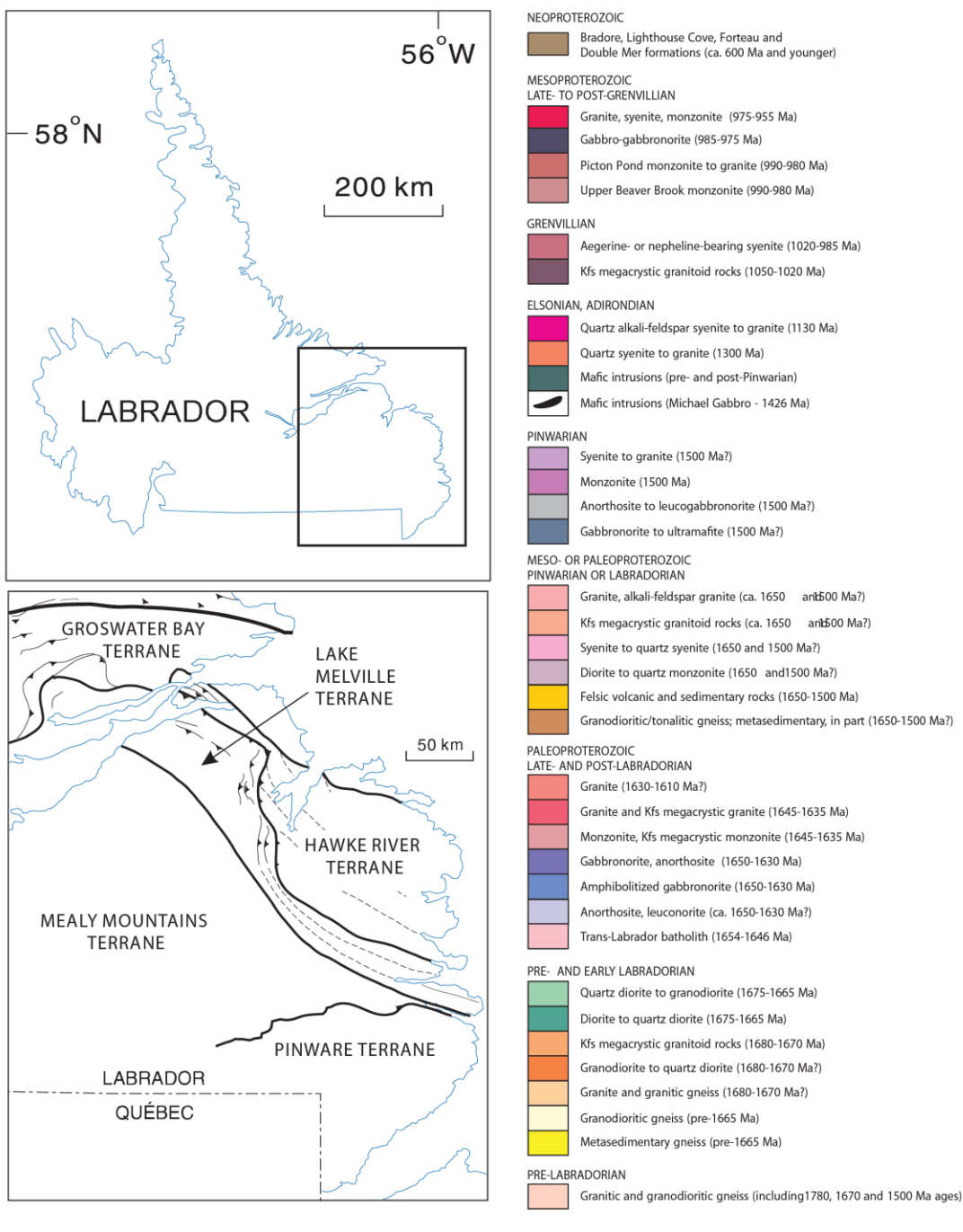


Figure 2-3: Legend for geological map of Labrador. Upper left inset depicts area drawn in the following figure, and lower left inset depicts lithotectonic terranes located in eastern Labrador (Gower, 2003).

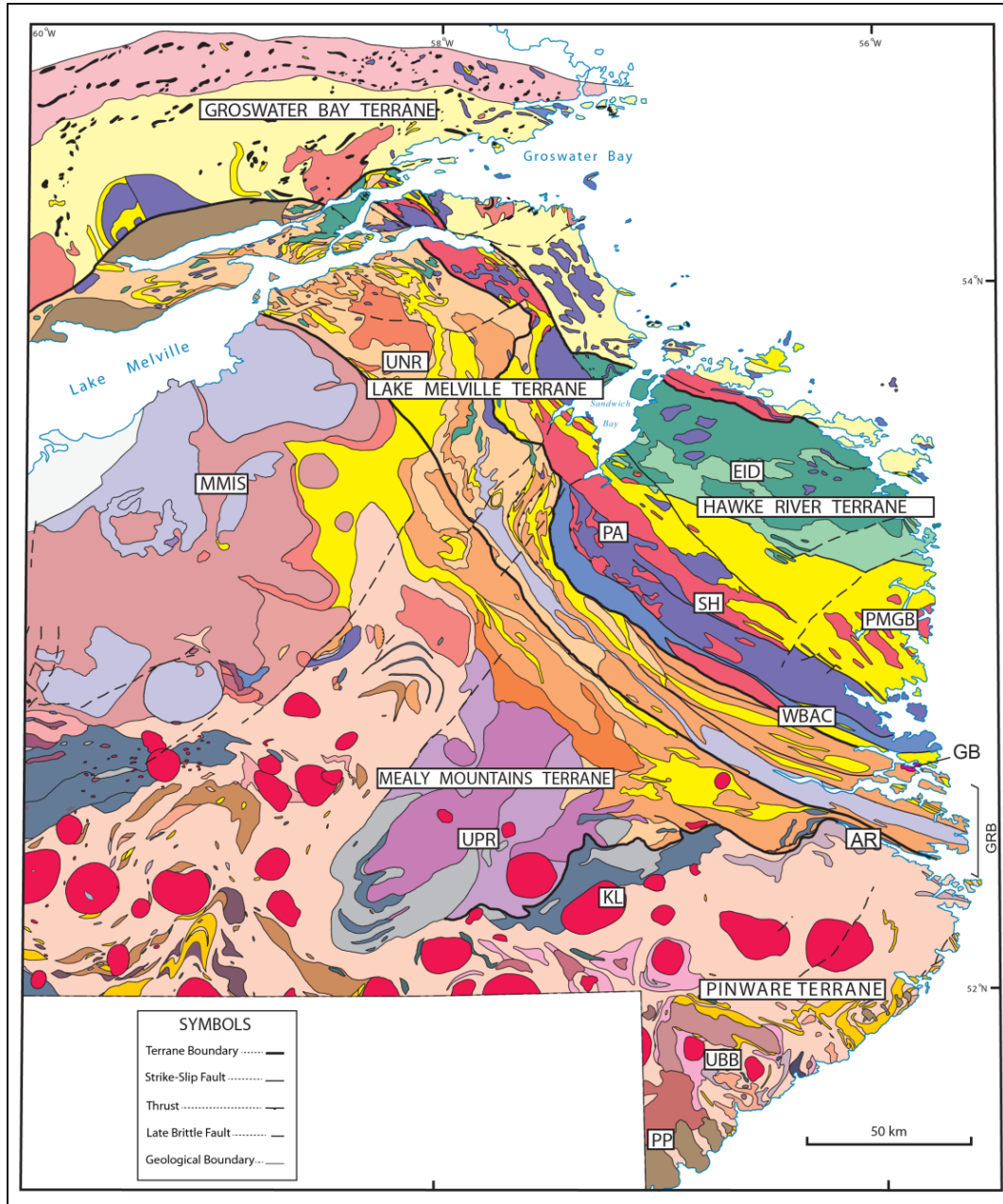


Figure 2-4: Geological map of the Grenville Province in eastern Labrador (Gower, 2003). AR - Alexis River anorthosite; EID - Earl Island domain; GB - Gilbert Bay pluton; GRB - Gilbert River belt; KL - Kyfanan Lake layered mafic intrusion; MMIS - Mealy Mountains Intrusive Suite; PA - Paradise Arm pluton; PMGB - Paradise metasedimentary gneiss belt; PP - Picton Pond pluton; SH - Sand Hill Big Pond gabbro-norite; UBB - Upper Beaver Brook pluton; UNR - Upper North River pluton; UPR - Upper Paradise River pluton; WBAC - White Bear Arm complex.

2-2-1 LAKE MELVILLE TERRANE

The Lake Melville terrane is up to 60 km wide in the northeastern section of the terrane, but thins to 20 km in the southeast portion of the terrane (Figure 2-3). This southeastern section has been referred to as the Gilbert River Shear belt (Figure 2-4), and subsequently as the Gilbert River belt, following the investigation of Hanmer and Scott (1990) (Gower and Owen, 1984; Gower et al., 1987, 1996; Hanmer and Scott, 1990). The Lake Melville terrane consists of K-feldspar megacrystic granitoids, biotite-bearing granite, granodiorite, quartz-to-diorite gneiss, metasedimentary gneisses, as well as layered mafic to anorthositic rocks (Gower and Owen, 1984; Gower et al., 1987, 1988, 1994; Gower, 1996). The most prominent rock types within the Gilbert River section are K-feldspar megacrystic granites, and the Alexis River anorthosite, which is approximately 5 km wide, but can be traced along strike length for over 150 km (Gower et al., 1985, 1987, van Nostrand 1992, van Nostrand et al., 1992). In the project area, the Fox Harbour fault zone (Gower, 2005) defines the tectonic boundary between the Lake Melville terrane and the Mealy Mountain terrane to the south. This fault zone contains high-grade mylonites, and is characterized by changes in lineations and differences in garnet abundances of rocks of similar composition north and south of the fault (Gower 1996, 2005). Published magmatic ages for the protoliths of the Lake Melville terrane are generally 1.6-1.7 Ga in age (known as Labradorian). A megacrystic granitoid was dated at 1678 ± 6 Ma, and a banded migmatitic orthogneiss was dated at $1677+16/-15$ Ma (Shärer et al., 1986; Gower, 1996). A granitic vein, which is deformed itself, and a megacrystic granitoid rock were dated at $1664+14/-9$ Ma, and $1644+8/-6$ Ma, respectively (Scott et al., 1993). The next event dated in this area is the intrusion of a pyroxene bearing syenite to

granite, which is strongly deformed and referred to as the Upper North River syenite, dated at 1296+13/-12 Ma (Shärer et al., 1986).

2-2-2 MEALY MOUNTAINS TERRANE

The Mealy Mountain terrane is the central terrane in the Port Hope Simpson area, and thins drastically from 100 km in the west to 10 km in the southeast (i.e.: adjacent the study area). This terrane contains two different lithologies that are concentrated in different areas. The northern section consists of a large anorthositic, leucogabbroic, and leucotroctolitic intrusive complex named the Mealy Mountains Intrusive Suite, along with younger pyroxene dominated quartz monzonite intrusions (Emslie, 1976). To the southeast, tracts of silliminite-bearing pelitic gneisses dominate the Mealy Mountain terrane, along with granitic and mafic intrusives throughout. Granitic rocks consist of quartz diorite, quartz monzonite, granodiorite, granite and K-feldspar megacrystic intrusions (Gower, 1996). An extensive mylonite zone separates the Lake Melville and Mealy Mountain terranes and is present within the study area. Published magmatic ages in the Mealy Mountain terrane range from 1646 ± 2 Ma to 962 ± 3 Ma (Emslie & Hunt, 1990; Gower, 1996). The previously mentioned anorthositic bodies in the northern portion of the Mealy Mountains terrane contain ages of 1646 ± 2 Ma, and $1635+22/-8$ Ma, found within a pyroxene monzonite, and a pyroxene granite, respectively (Emslie & Hunt, 1990; Gower, 1996). A deformed discordant aplite vein, just south of this studies project area, which cross-cuts a mylonite gave a lower intercept of $1509 +11/-12$, and was taken as the minimum age of emplacement (Scott et al., 1993). The Mealy Dykes, which

are northeast-trending olivine tholeiitic gabbros and diabases have been dated at 1250 ± 2 Ma (Emslie et al., 1997). Finally, a small granite pluton in the southeast part of the terrane has been dated. The age of this pluton is 962 ± 3 Ma, and is apart of a widespread suite found throughout the Grenville Province (Gower et al., 1996).

2-2-3 PINWARE TERRANE

The third and most southern terrane is the Pinware terrane (Figure 2-4), originally defined by Gower et al. (1988). Lithologies in this terrane consist of felsic and mafic supracrustal units, foliated to gneissic granitoids, layered mafic intrusions, mafic dykes, syn- to late- Grenvillian granitoid rocks and late- to post- Grenvillian granitoid rocks (Gower 1988, 1996, 2005). Supracrustal rocks are largely recrystallized, commonly quartzofeldspathic rocks with inhomogeneous texture (Gower 1996). It is often extremely difficult to confidently define the protolith of these fine-grained rocks; therefore protolith determination is often based on adjacent rock types that have an unambiguous supracrustal parentage (Gower, 1996, 2007, 2008, 2009; Kamo et al., 2011). U-Pb dating within the Pinware terrane has been focused largely on the granitoid rocks, which comprise much of the terrane. The oldest dated rocks in the Pinware terrane come from a quartz monzonite intrusion, yielding ages of $1650+18/-19$ Ma, and 1649 ± 7 Ma (Wasteneys et al., 1997; Heaman et al., 2004). Other likely volcaniclastic rocks dated by Tucker and Gower (1994), and Wasteneys et al. (1997), produced ages of 1640 ± 7 Ma, and 1637 ± 8 Ma (Tucker and Gower, 1994; Wasteneys et al., 1997). Granitoids located just south of the project area for this study have been dated at 1490 ± 5 Ma, 1479 ± 2 Ma,

and 1472 ± 3 Ma (Tucker and Gower, 1994). The discordant aplitic dyke mentioned earlier revealed an age of $1509 +11/-12$ Ma (Scott et al., 1993). The last plutonic addition to the Pinware terrane are a large suite of granitoid plutons, ranging in age from 1043 to 951 Ma, thought to be emplaced shortly after Grenvillian orogenesis (Tucker and Gower, 1994; Wasteneys et al., 1997; Heaman et al., 1996; Heaman et al., 2004; Gower et al., 2008).

2-3 MAPPING, SAMPLING, AND EXPLORATION METHODS

The Foxtrot deposit (located in the MT Belt) area was mapped to 1:10,000. The mapping was supported by a wide array of exploration studies carried out by Search Minerals Inc., including: airborne radiometric and magnetometer surveys, a detailed ground based magnetometer survey, channel sampling, and diamond drilling. Search collected over 1000 samples from surface bedrock outcrops (hand and channel samples) for chemical analysis. They also completed a total of 57 diamond drill holes at the Foxtrot deposit, totaling 18,000 m of core, and accounting for over 10,000 lithogeochemical analyses. Channel samples were from 10 cm deep by 8 cm wide cuts, made using a gas-powered diamond saw from cleared outcrops. Each channel was cut into two vertical sections, similar to drill core, with a 6 cm thick section (weathering removed) being sent out for assay. A 2 cm thick section is stored in channel boxes for reference and to provide due diligence/verification samples. The channels were cut perpendicular to strike, pieced together, logged, and photographed to produce geological and geochemical sections, similar to diamond drill holes.

Airborne radiometric maps were utilized during initial mapping of the volcanic belts (Delaney and Haley, 2011, *unpublished*). The airborne magnetometer survey proved invaluable, as many units in the belts contain abundant magnetite, appearing as positive anomalies on the magnetometer map (Figure 2-5). The mapping technique involved traverses that were conducted perpendicular to general strike of the area (traverses were generally north-south), mapping the north and south contact of the belts at a spacing of approximately 0.25-1.0 km. Hand-held gamma radiations detectors (RS-125 Super-SPEC) were also utilized in locating the exact location of the volcanic belts during traverses, as the rocks exhibit anomalous enrichments of HFSE (high-field strength elements including Th and U).

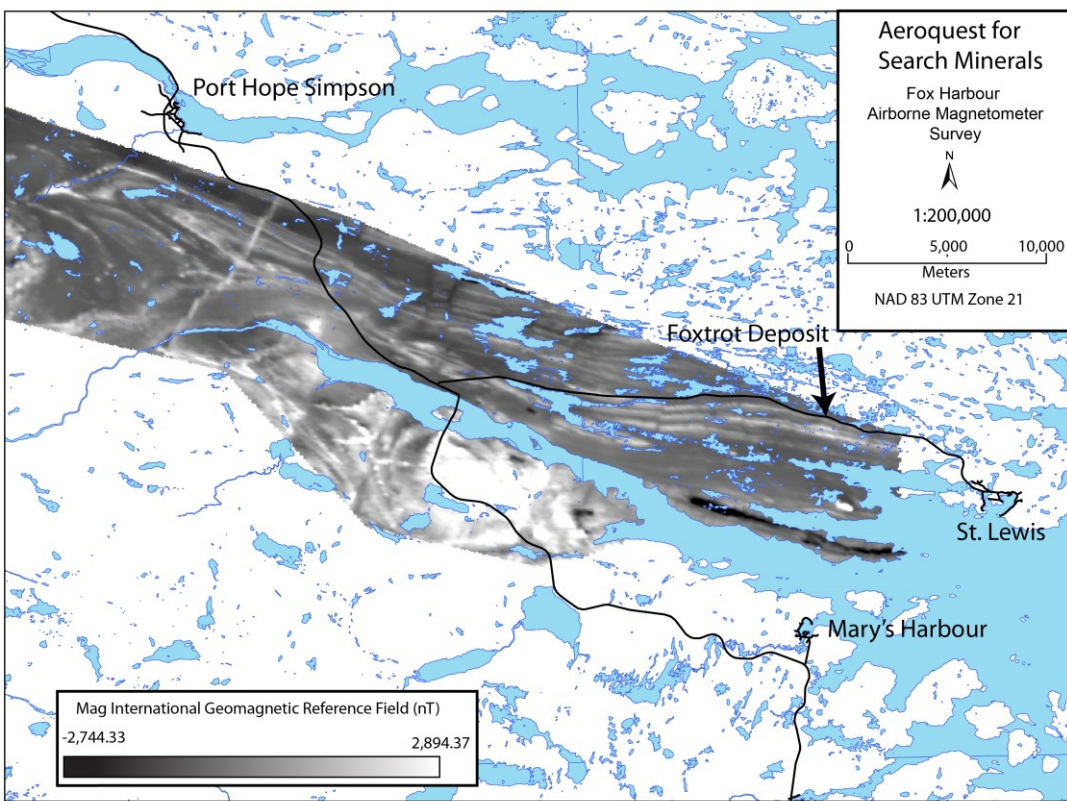


Figure 2-5: Airborne magnetometer survey for the Fox Harbour project (Delaney and Haley, 2011, *unpublished*).

Representative samples were taken from all units in the area, regardless of counts per second (CPS) recorded on the spectrometer, with preference given to units with higher CPS. Moderately detailed lithogeochemical sampling has been completed across 30 km of the packages, from the coast adjacent St. Lewis to the junction of Highway 510 and 513 (Figure 2-6). Less detailed sampling has been completed on the remaining 25km, due to limited exposure and outcrop, and fewer traverses.

2-4 LOCAL GEOLOGY

The Fox Harbour bimodal felsic and mafic volcanic package was discovered and recognized as having a volcanic origin while attempting to identify rock units prospective for REE mineralization (Delaney and Haley, 2011, *unpublished*). The felsic volcanic rocks, presumed to be highly deformed rhyolitic flows, within this volcanic package tend to be enriched in HFSE, and have been the subject of detailed mineral exploration. Within these volcanic belts, rock types include: rhyolite, basalt, quartzite, and garnetiferous volcaniclastic/metasedimentary units, along with discordant mafic and granitoid dykes. The garnetiferous volcaniclastic/metasedimentary unit is thought to be supracrustal as it is always found adjacent obvious basaltic units, with very characteristic geochemistry. Adjacent to the volcanic packages, rock types include mylonitic to megacrystic granitic augen gneiss with concordant amphibolite dykes, and metagabbroic gneiss.

The volcanic protolith determination for the felsic magmatic rocks is based on their association with basalt units adjacent, the volcaniclastic/metasedimentary rocks, and the quartzite units (Section 2-4-2). Some of the felsic units may be subvolcanic intrusions but deformation makes detailed interpretations of specific units difficult.

Three bimodal mafic and felsic volcanic belts have been mapped within the Fox Harbour area, from south to north: South Belt, MT Belt, and Road Belt (Figure 2-6). These volcanic belts possibly extend up to 55km from the coast adjacent to the town of St. Lewis to Port Hope Simpson. All three volcanic belts have been confirmed from St. Lewis to 30 km to the west.

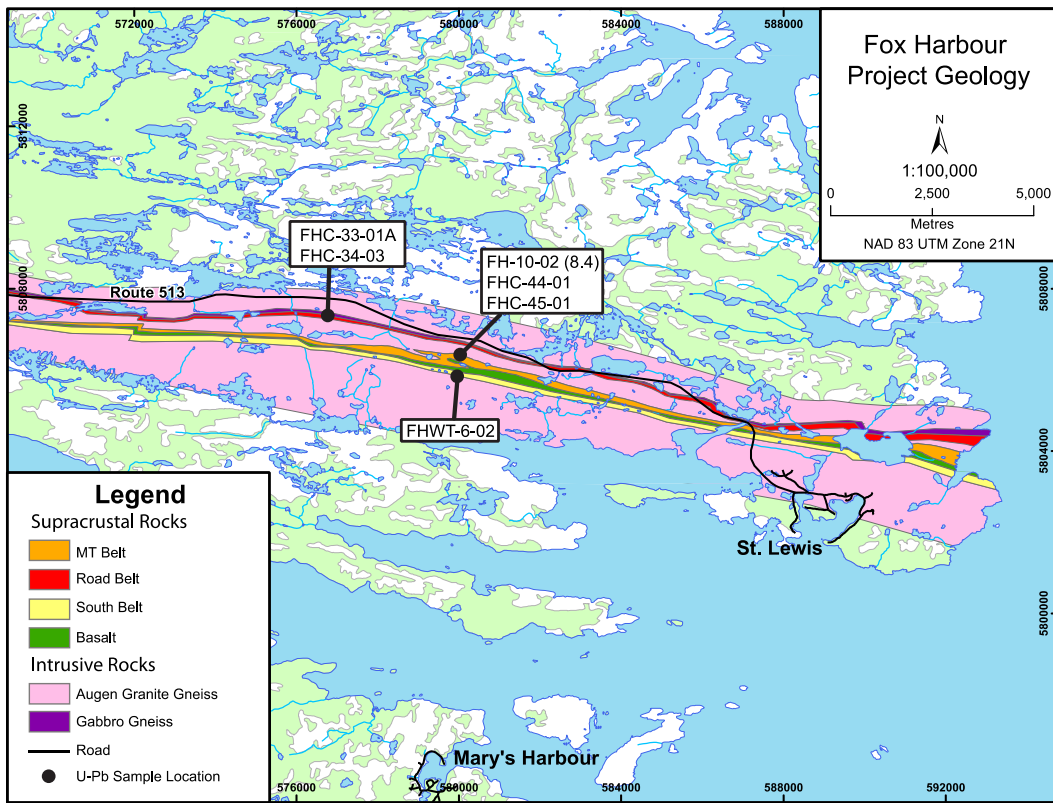


Figure 2-6: Geology map for Fox Harbour project area. Sample locations from U-Pb dating are shown. Note: Due to the scale of the figure, the granitic augen gneiss unit separating the MT Belt and South Belt is not visible, although present.

2-4-1 METAMORPHIC GRADE

The metamorphic grade of the volcanic package is amphibolite facies, as determined from the observed mineral assemblages. Basaltic units commonly exhibit coarse recrystallized hornblende, and occasionally garnet, which have since in part retrograded to chlorite. Large epidote pods observed within the basaltic units have small (1-2 cm) amphibole rich zones around them, but are largely intact (Figure 2-8g). These

metamorphic mineral assemblages suggest that the volcanic packages were exposed to amphibolite grade.

2-4-2 DESCRIPTION OF THE VOLCANIC BELTS

All three belts have very similar lithological units, and display very similar textures, and geochemistry. All three belts have been traced and mapped from the coastline adjacent to St. Lewis for approximately 30 km, and are postulated to extend at least another 25 km based on airborne magnetometer survey and limited grab samples (Figure 2-5). The physiography of the area consists of approximately 50% outcrop in the coastal areas, and 10-25% in the inland areas. Grab samples in the inland area are limited due to lack of outcrop, as the weathering profile of the felsic volcanic rocks causes it to form low-lying areas, which are commonly filled by bogs and marsh. The representative grab samples show very similar textures and geochemistry to those found in the main (eastern) Fox Harbour area.

2-4-2-1 *South Belt*

The South Belt is the most southern belt currently identified within the Fox Harbour volcanic area (Figure 2-6). As seen in Figure 2-5, there is another magnetic anomaly that runs parallel to the volcanic belts in Fox Harbour, south of the South Belt. This belt was shown to exhibit similar mineralization to the rest of the Fox Harbour area, but was not the focus of exploration; therefore little is known about it. The South Belt has the thickest package of rhyolitic and basaltic rocks, ranging in thickness from 100-250 m

(in the general vicinity of the Foxtrot Deposit) along strike. The basalt units within the South Belt are resistant to erosion with respect to other units in the area. This resistance has created an E-W trending ridge that extends for approximately 10 km, with an elevation up to 120 m, known locally as Deer Harbour Ridge. The main units within the South Belt are, highly deformed rhyolites, basalts, quartzite, a discordant mafic sill, and an unmineralized rhyolite (i.e.: no elevated Zr, Y, and REE) or aplite intrusion, all of which are discussed below.



Figure 2-7: Typical rock type appearances in the South Belt. Note: Pen tip direction points towards north in all photos. (A) Typical appearance of the rhyolite unit located in the South Belt. Darker continuous bands are rich in mafic material (magnetite, and biotite). (B) 2m wide quartzite located within the southern edge of the Deer Harbour Ridge basaltic unit, and north of the rhyolite package within the South Belt. (C) Typical outcrop appearance of the Deer Harbour Ridge basaltic unit.

The rhyolite unit in the South Belt ranges in thickness from approximately 50-100 m (in the general vicinity of the Foxtrot Deposit), and occurs on the south side of Deer Harbour Ridge. It is bound to the south by the mylonitic to megacrystic granitic augen gneiss, and to the north by a large basaltic package. It is an extremely homogenous package with very characteristic weathering appearance and outcrop color (Figure 2-7a). On surface it tends to weather to a sandy-like material, and is generally pink to grey in

color. Little to no lichen tends to grow on the rhyolite units, which makes field identification with respect to adjacent units (granite, basalts) easier. The rhyolitic unit is fine-grained (~1-3mm grain size), and is largely recrystallized. The mineralogy is dominated by orthoclase, albite, and quartz, accounting for approximately 75% of the mode, with minor minerals consisting of biotite (Fe-rich end-member annite), magnetite, allanite, fluorite, chlorite and zircon. Much of this unit has small concordant quartz veins (1-5 cm), which are often extremely folded, often displaying buckle folds. It should be noted that the South Belt is largely devoid of the boudinaged pegmatitic intrusions, often seen in the Foxtrot Deposit.

The basaltic unit in the South Belt also defines a large outcrop pattern, and ranges in thickness from approximately 50-100 m. The mafic volcanics make up the majority of Deer Harbour Ridge; therefore this mafic unit is named the Deer Harbour basalt. It is bound to the south by the rhyolite unit of the South Belt, and to the north by mylonitic megacrystic granitic augen gneiss. It displays characteristic differential weathering due to the variable grain sizes of individual layers. It is dark brown/green to black in color, and the mineralogy largely consists of hornblende, biotite, plagioclase feldspar, epidote and magnetite in places (Figure 2-7c). There are large epidote pods observed in other parts of the mafic volcanic unit, which are not as prevalent in this large pile, but are present, displayed as strung out blebs of epidote. This may reflect primary differences between the units, or possibly differences in metamorphic grade and/or deformation.

A 2 m thick quartzite unit that has been confirmed and traced for approximately 3 km is bound entirely by mafic volcanics within the southern margin of the volcanic pile (Figure 2-7b). Another thinner quartzite unit is present in the center of the Deer Harbour

mafic volcanic package. Exposure of this second quartzite is limited, but it is >1 m wide, where observed. The quartzite units are weathered to a dull white color, and are dominated by quartz with minor biotite and epidote.

Finally there is a fine-grained felsic unit, likely a separate rhyolitic flow or aplitic dyke/sill, in the South Belt. It is located within the northern margin of the belt, within the Deer Harbour mafic volcanics, and is approximately 30 m thick and extends for approximately 1 km. It is characterized by quartz, K-feldspar, plagioclase feldspar, biotite, and very minor magnetite. The outcrop appearance is very similar to that of the felsic volcanics in the southern section of South Belt, where it is fine-grained and recrystallized, but contains much less magnetite. It is extremely deformed with tight folds affecting the entire unit. It is possible that this unit is part of a felsic volcanic pile with a geochemical affinity that is different from the rest of the felsic volcanics, or it may be a later granitic sill/dyke that intruded the volcanic units.

2-4-2-2 *MT Belt*

The MT Belt is the central belt within the Fox Harbour volcanic units, located just north of Deer Harbour Ridge, and is in general 20-150 m thick. The MT Belt has been the main focus of detailed exploration for REE within the Fox Harbour area due to the fact that specific rhyolite units within the volcanic package are much more enriched in REE (Delaney and Haley, 2011, *unpublished*; Srivastava & Gauthier, 2012). The area has been explored with the most detailed channeling and diamond drilling, and with a ground-based magnetometer survey. The ongoing exploration has provided a much better

understanding of the apparent stratigraphy within the MT belt and many units have been identified and mapped at surface, along strike, and at depth. The main rock types within the MT Belt are highly deformed rhyolites, basalts, quartzite, discordant mafic and granitic intrusions, and intermediate garnetiferous volcaniclastic/metasedimentary units (Figure 2-8). Many individual rhyolitic units have been identified within the MT belt, but here, only a general overview of the units is described.

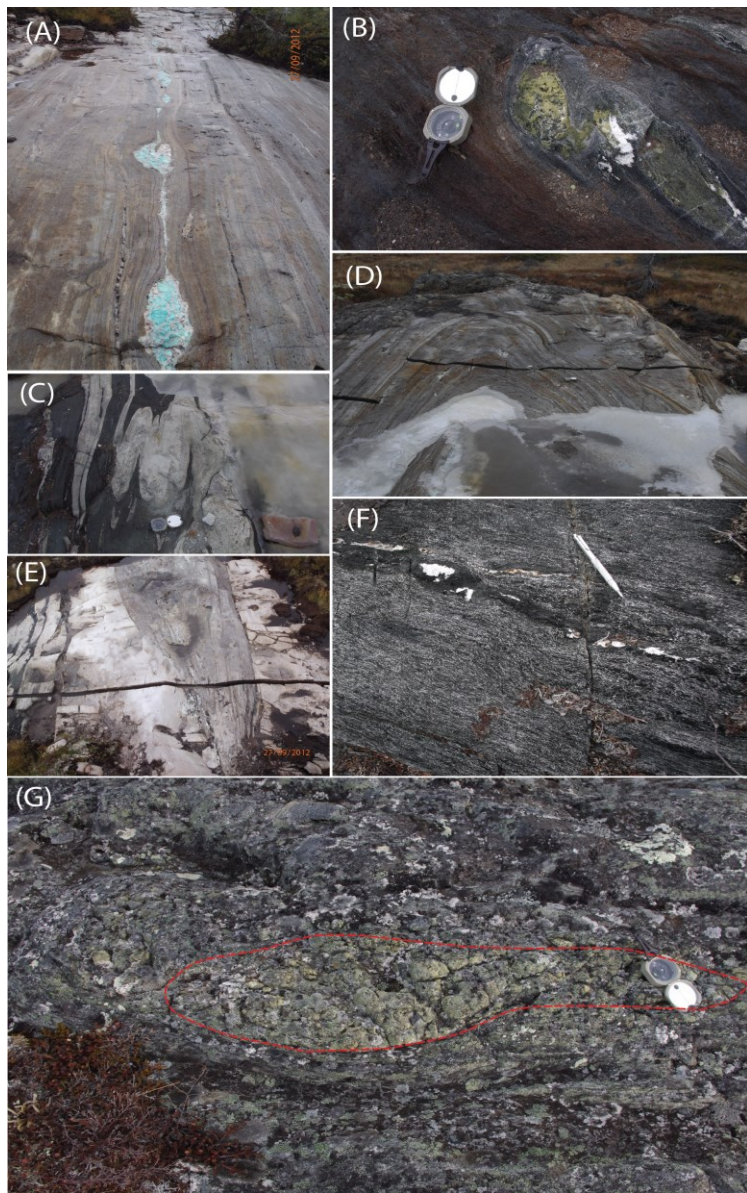


Figure 2-8: General outcrop appearances of units in the MT Belt; all photos taken from the Foxtrot Project, within the MT Belt. (A) Boudinaged amazonite pegmatite within fine-grained rhyolite unit (FT3). This pegmatite extends over 40 m. (B) Epidote pod within basaltic unit, located between FT2 and FT3. (C) Intense cuspatate and lobate folding within rhyolite unit (FT4) and adjacent basaltic unit. (D) Third-order folding, observed folding rhyolite unit FT4; folds are plunging to the east. (E) Third-order folding, units observed in FTBuff (white to cream color, observed on outer part of limbs), and FT4 (grey unit, in center of fold). (F) Mafic dyke. Notice coarser grained, and small seam of tonalitic melt rock beneath pen magnet. (G) Basaltic unit with large epidote pod preserved. Epidote pod is outlined in red.

The MT Belt contains several different units of fine-grained recrystallized variably mylonitic and migmatized rhyolite units. Variably thick basaltic units often separate the rhyolite units from one another. On surface they are weathered similarly to the South Belt, but do not break down to a sandy texture as readily, and often exhibit very smooth weathered surfaces. The color of the units on surface ranges from pink to green, which is largely controlled by mineralogy. With respect to the other units in this area, the felsic units are preferentially weathered, where it is typical to locate the felsic volcanic package in low-lying areas. Where outcrop is visible, very little lichen tends to grow on these outcrops, similar to the South Belt. Mineralogy varies between each separate sub-unit, but generally consists of K-feldspar, plagioclase feldspar, quartz, magnetite, aegirine-augite, biotite, K-hastingsite, calcite, allanite, zircon, and fergusonite. Some mineralized (i.e.: containing anomalous Zr, Nb, Y, and REE) units contain concordant boudinaged granitic pegmatites stretched over 10's of meters, observed best in outcrop. These pegmatites also tend to have a variety of K-feldspar called amazonite (Figure 2-8a), which is a deep turquoise/green color, thought to be a result of elevated contents of lead in the mineral, possibly also with high levels of divalent Fe (Arnaudov et al., 1967; Plyusnin, 1969; Szuzkiewicz and Körber, 2010). Some of the rhyolite units have many late stage quartz veins, some of which are concordant and some are discordant, often displaying buckle folds.

The mineralized rhyolite units often contain aegirine-augite and a Na-rich amphibole indicating that they are peralkaline rhyolites. Lesser-mineralized felsic volcanic units, especially in the MT zone often exhibit these same minerals but they are present in lower abundances and are seen reacting to other minerals, often biotite,

magnetite, and K-feldspar. Therefore it is believed that these units are often peralkaline, which aids in understanding the HFSE enrichment, and aids in determining the tectonics of that time, which will be discussed later.

The main zone of exploration within the MT Belt has been undertaken on the Foxtrot Deposit. This area has been studied intensely since exploration began on this property in 2009. The rhyolite units within the Foxtrot Deposit are subdivided as: FT2a, FT2b, FT2x, FT3, FT3b, FT4, and FT5. These subdivisions are based on mineralogical and textural differences, along with stratigraphy, and geochemistry. For all intents and purposes, these units can be treated as separate volcanic packages, separated by small basalt units. A generalized geology map for the Foxtrot Deposit, located within the MT belt is presented below (Figure 2-9). This map shows the surficial extent of the three belts on surface in the Foxtrot Deposit area. The stratigraphy observed in the Foxtrot Project is shown in Figure 2-10.

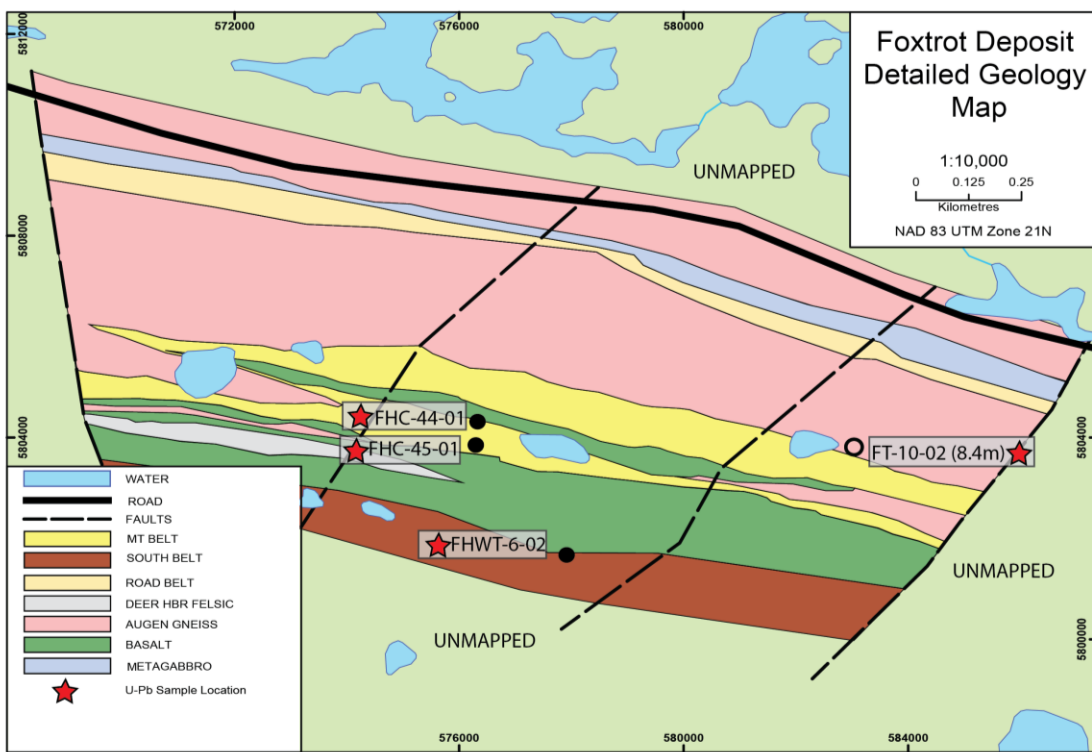


Figure 2-9: Geology map for the general vicinity of Foxtrot Deposit, (located within the MT Belt). Sample locations are indicated via filled circles (channel), or a hollow circle (diamond drill hole collar location).

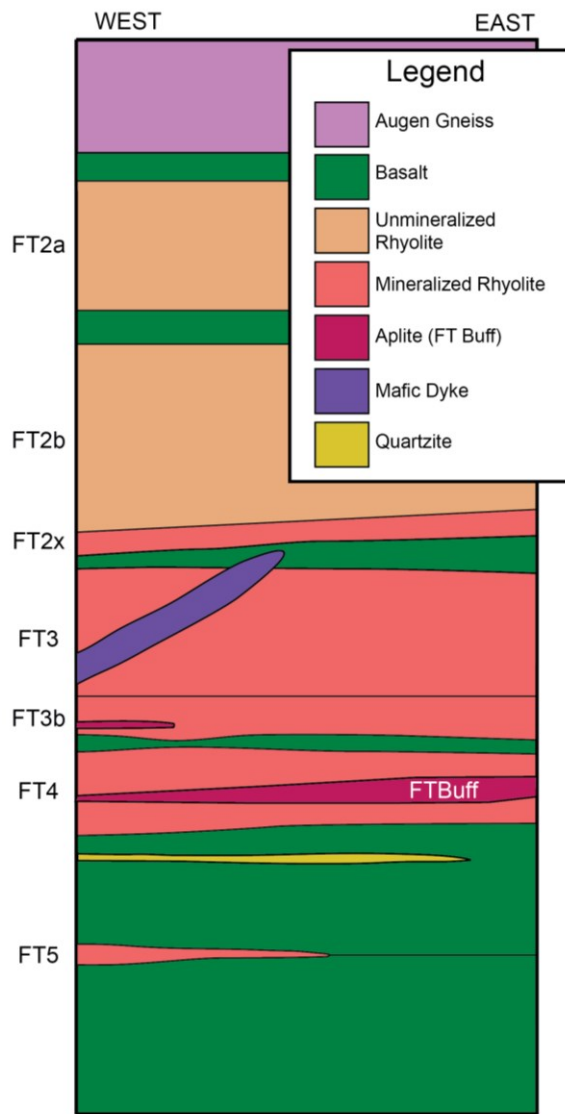


Figure 2-10: Stratigraphy observed in the Foxtrot deposit. The dyke/sill units (i.e.: the mafic dyke, and FT Buff) are likely pre-deformation discordant intrusions into the volcanic pile.

The basalt units in the MT Belt are similar to the South Belt volcanics, in that they display characteristic differential weathering, and are dark brown/green to black in color. The mineralogy consists of hornblende, biotite, plagioclase feldspar, epidote and magnetite in places. Certain mafic volcanic units have large epidote “pods,” up to 1.5 x

1.0 m in length and width (Figure 2-8b). These epidote pods often are assumed to be alteration “pipes/veins” within the volcanic package, often associated with basaltic rocks. Much like the Deer Harbour Ridge mafic volcanics, this pile contains a quartzite unit, but it is much smaller, ranging in thickness from 0.2-0.5 m and extends along strike for ~500 m.

Small intermediate garnetiferous volcaniclastic/metasedimentary units are also present within the MT belt. The thickness and stratigraphic position of the unit is extremely variable. It is almost always associated with the basalt packages, often at contacts between individual units. It weathers to a dark grey surface, with a mineralogy consisting of quartz, biotite ± garnet ± magnetite, with biotite and garnet varying from unit to unit. Garnet often appears to be porphyroblastic and occurs as very small grains (0.5-2 mm).

A large discordant mafic sill/dyke occurs within the bimodal volcanic package (Figure 2-8f). The unit weathers to a very dark brown/green to black color, with grain sizes varying from 0.5-1.0 cm. A visible grain size reduction is visible at contacts with its host, which is likely caused by a chilled margin contact, and/or subsequent shearing after formation. Its observed thickness at surface and depth ranges from approximately 2-13 m. The unit is discerned from the adjacent mafic volcanic units by its coarse grained nature, and it also lacks the intermediate garnetiferous metasedimentary unit that is commonly associated with the mafic volcanics. Where the unit is thin, either due to primary thinning, or reduction in size due to shearing, the only way to be certain it is the sill is the absence of the associated intermediate volcaniclastic unit. On surface this unit is much more

competent and lacks the characteristic differential weathering observed in the mafic volcanics.

Another discordant intrusion observed within the MT belt is a felsic granitic intrusion within the volcanic pile, which is geochemically and texturally distinct from the rhyolitic units (Figure 2-8e). Similarly to the mafic sill, it is found solely within the bimodal volcanic package in the Fox Harbour area. This unit has been identified in both the MT Belt and the Road Belt (discussed below). It tends to be extremely fine grained, with a mineralogy consisting of quartz, K-feldspar, and biotite, and is named FT Buff, or RB Buff depending on its host belt. This unit is distinguished from the felsic volcanics by its cream buff color, and negligible magnetite content. This intrusion also has a much different geochemical signature than the rhyolite units. This unit is similar to the felsic intrusive/volcanic unit at the northern side of the Deer Harbour Ridge basaltic unit, but the relationship between them is not clear.

Two discordant sills/dykes have been identified in the area with the thickest volcanic units, where exploration has been focused on this area. Both units intrude the volcanic pile similarly: they occur in the bottom of the pile in the west, and higher up in the stratigraphy in the east. These units appear to be nearly concordant presently, due to the shearing that has occurred since the time of formation.

2-4-2-3 *Road Belt*

Lithologically the Road Belt and MT Belt display similar units, mainly rhyolitic units, basalt, and the discordant felsic intrusion. The Road Belt has experienced much

more deformation; therefore identifying units based solely on stratigraphy is very difficult.

A unit that is not observed within the adjacent belts in the area is a metagabbroic gneiss that is found consistently to the north of the rhyolite units of the Road Belt. It occurs as an internally complexly deformed unit, but is extremely consistent along strike, and has been mapped for approximately 30 km, and is inferred for another 25 km. It does not weather readily, and is generally a positive topographic feature. The mineralogy consists of plagioclase feldspar, hornblende, biotite, garnet, quartz and titanite, where titanite is often associated with hornblende.

2-5 U-PB ZIRCON GEOCHRONOLOGY OF THE VOLCANIC ROCKS

Polished thin sections from different rhyolitic units within each volcanic belt were chosen for U-Pb analysis via thin section on the laser ablation inductively coupled mass spectrometer (LA-ICPMS). A total of 6 thin sections were chosen for the representative dating; one from the South Belt, three from the MT Belt, and two from the Road Belt. One sample was also analyzed via CA-TIMS (chemical-abrasion thermal ionization mass spectrometry). All samples have been taken from either surface outcrops (via channel saw) or diamond drill hole.

Laser ablation-ICPMS was first chosen for U-Pb dating because the rhyolite thin sections contained so many zircon grains, making the *in-situ* technique ideal for a preliminary pass. Age determinations were initially intended to simply determine which tectonic terrane (section 2) the Fox Harbour volcanic package belonged to. It quickly

became evident that these rocks weren't going to simply fit into a tectonic package. Laser ablation-ICPMS was successful in identifying the metamorphic age of these rocks, but gave inconclusive data for the igneous age of the rocks. Therefore, one sample was chosen for more precise dating via CA-TIMS, to determine the igneous primary age of these volcanic rocks.

2-5-1 SAMPLE DESCRIPTION AND PETROGRAPHY

The first sample, taken from the South Belt, (FHWT-6-02), consisting of highly deformed and folded section of fine grained rhyolite near the center of the South Belt stratigraphy (Figure 2-9). Outcrop appearance is pink to grey in color, weathering to a sandy material. Mineralogy consists of K-feldspar (orthoclase) with sericite alteration, quartz, magnetite, biotite, allanite, zircon, epidote, titanite, chlorite, apatite, and fluorite along grain boundaries. This thin section has a zone (approximately 2 mm wide, extending the width of the section) of alteration, rich in zircon, and allanite. Potassium feldspar grains around this zone of alteration appear to have abundant fluid inclusions, suggesting possible fluid interaction.

The next three samples are from the MT Belt, (FT-10-02 (8.4m), FHC-44-01, and FHC-45-01), all of which sample highly deformed fine-grained rhyolite units within the Foxtrot Project (Figure 2-9).

(A) FHWT-6-02 (South Belt)



(B) FH-10-02 (8.4 (MT Belt))



(C) FHC-44-01 (MT Belt)



(D) FHC-45-01 (MT Belt)



(E) FHC-33-01A (Road Belt)



(F) FHC-34-03 (Road Belt)



Figure 2-11: Channel and diamond drill sections chosen for U-Pb dating. Thin section slab cuts can be seen in the majority of the samples. Scale for channel sections is 1 m, and 1.5 m for diamond drill core. (A) FHWT-6-02; sample taken in synform. (B) FH-10-02 (8.4m); sample cut visible in second row of core, at approximately 10m. (C) FHC-44-01; sample taken from first piece of rock. (D) FHC-45-01; sample taken from first section of rock pictured. (E) FHC-33-01A; sample taken from first section of rock pictured. (F) FHC-34-03; sample taken from last section of rock pictured.

FT-10-02 (8.4m) is a small (10 cm) patch of granitic vein/pegmatite; this interpretation is due to the coarser nature of the rock, with respect to the adjacent rhyolite (FT2). It is located within fine-grained basaltic rocks at the top of the MT Belt supracrustal package (FT2), and is from a diamond drill hole (Figure 2-11b). Mineralogy consists of plagioclase feldspar, K-feldspar, quartz, magnetite, allanite, and zircon. Magnetite and allanite are closely related, and tend to form magnetite, allanite, and zircon bands through the thin section.

FHC-44-01 and FHC-45-01 sample outcrops on the southern limb of the regional scale fold that affects the Foxtrot Project (Figure 2-6). Outcrop appearance is bleached white to pink, with variable magnetite, and abundant folding (Figure 2-11c). The mineralogy in sample FHC-44-01 consists of K-feldspar, quartz, magnetite, biotite, titanite, and epidote. Minerals epidote, zircon, and allanite are all closely associated with magnetite. Epidote, zircon, and allanite form discrete 1-2mm layers/bands through the thin section.

Sample FHC-45-01 consists of K-feldspar, quartz, magnetite, garnet, allanite, biotite, epidote, titanite, and \pm pyroxene (Figure 2-11d). As previously observed, minerals epidote, garnet, and allanite are all closely associated with magnetite.

The final two samples are from the Road Belt (FHC-33-01A and FHC-34-03), both of which sample a 30-40 m thick rhyolitic package approximately 16 km from the coast adjacent St. Lewis (Figure 2-6). Outcrops appear white to grey, with small positive relief equigranular magnetite grains spotting the outcrop.

Sample FHC-33-01A mineralogy consists of K-feldspar, quartz, magnetite, allanite, garnet, zircon, pyroxene, epidote, titanite and fluorite (Figure 2-11e). Pyroxene is skeletal and is observed reacting to allanite, magnetite, and K-feldspar. Allanite and zircon are very closely associated with magnetite.

Sample FHC-34-03 is fine-grained and recrystallized, consisting of K-feldspar, quartz, biotite, magnetite, allanite, zircon, \pm fluorite, \pm amphibole, and \pm pyroxene (Figure 2-11f). Allanite is closely associated to magnetite, often times with zircon. Abundant zircon grains are present through the entire thin section, within most minerals, except coarser grained K-feldspar.

2-5-2 ANALYTICAL METHODS

2-5-2-1 *Zircon Imaging by Scanning Electron Microscopy*

High-resolution images of zircon grains in polished thin sections of the rocks were acquired using backscattered electron (BSE) and cathodoluminescence (Gatan ChromaCL) detectors on an FEI Quanta 650F field emission scanning electron microscope (SEM). The microscope was operated under high vacuum conditions with an accelerating voltage of 25 keV, a beam current of 10 nA and at a 10 mm working distance. The zircon imaging characterized the nature and distribution of compositional domains and zones within grains that were targeted for subsequent LA-ICPMS U-Pb analysis.

2-5-2-2 *In-Situ U-Pb – Laser Ablation Inductively Coupled Mass Spectrometry*

(LA-ICPMS)

U-Pb isotopic data were acquired using a Thermo-Scientific ELEMENT XR magnetic sector, single-collector ICPMS and Lambda Physik ComPex Pro 110 ArF GeoLas laser ablation system, using procedures described in detail by Košler and Sylvester (2003). For analysis, a 10 µm laser beam with an energy density of ~ 5 J/cm² at a repetition rate of 10 Hz was scanned across the sample surface by moving the sample stage at a velocity of 10 µm/sec, ablating a 40 x 40 µm box. The sample aerosol was transported from the sample cell to the ICP using a He-carrier gas to improve sample transport efficiency. During data acquisition, ²⁰²Hg, ²⁰⁴Hg, ²⁰⁶Pb, ²⁰⁷Pb, ²⁰⁸Pb, ²³²Th and ²³⁸U isotopes from the zircon and gas were measured along with a mixed ²⁰³Tl, ²⁰⁵Tl, ²⁰⁹Bi, ²³³U, ²³⁷Np internal standard tracer solution, simultaneously nebulized throughout each analysis. The tracer solution was used for matrix-independent, real-time instrumental mass bias correction of the U-Pb and Pb-Pb ratios using the known isotopic composition of the tracer solution. Data acquisition for each analysis was 3 minutes, with the first ~30 seconds used to measure the gas background and tracer solution followed by ~150 sec of laser ablation. Raw data were reduced off-line using the LAMDATE macro-based spreadsheet program (Košler et al. 2008). An instrumental mass bias correction was made using the measured ratios of the tracer solution. Laser-induced U-Pb fractionation was corrected using the intercept method of Sylvester and Ghaderi (1997). No common Pb correction was applied to any data; an analysis is rejected when ²⁰⁴Pb was detected above background. Standard reference zircons Harvard 91500 (1065 ± 3 Ma; Wiedenbeck et al.

1995) and Plesovice (337 ± 0.37 Ma; Slama et al. 2008) were each analyzed between every ~ 8 unknowns during the analytical session in order to monitor the accuracy and reproducibility of U-Pb analyses. Final ages and Concordia diagrams were produced using the Isoplot/Ex 3 macro (Ludwig 2008). The Concordia age for all analyses of the 91500 zircon are 1069 ± 13 Ma (2σ , MSWD of concordance = 0.24; Probability of concordance = 0.63, n = 21) and for Plesovice zircon is 334 ± 4 Ma (2σ , MSWD of concordance = 0.25; Probability of concordance = 0.62, n = 16) over the course of all the U-Pb analytical sessions (Table 2-1, 2-2; and Figure 2-12).

Table 2-1: Zircon reference material, sample: Harvard 91500.

Harvard 91500 LA-ICPMS U-Pb Data																			
SAMPLE spot #	file	ISOTOPIC RATIOS						AGES Ma						% concordancy			Th232 ppm	U238 ppm	Th/U Ratio
		207/235	7/5 err	206/238	6/8 err	Rho	207/206	7/6 err	7/5 age	1 sigma	6/8 age	1 sigma	7/6 age	1 sigma	concordancy				
3	au15a02	1.8395	0.1515	0.1777	0.0063	0.2168	0.0688	0.0053	1060	54	1054	35	1187	37	89	36	99	0.37	
8	au15a29	1.7824	0.1160	0.1802	0.0074	0.3170	0.0663	0.0043	1039	42	1068	41	1050	43	102	26	73	0.35	
15	au15a14	1.8232	0.1426	0.1888	0.0075	0.2531	0.0646	0.0057	1054	51	1115	41	1059	45	105	23	67	0.34	
28	au15a27	1.7800	0.0967	0.1834	0.0046	0.2589	0.0688	0.0036	1038	32	1086	25	987	45	110	30	85	0.36	
13	au15a41	1.7781	0.1133	0.1830	0.0061	0.2596	0.0654	0.0042	1037	41	1084	33	1076	43	101	30	85	0.35	
24	au15a52	1.9680	0.0879	0.1806	0.0045	0.2777	0.0739	0.0032	1105	30	1070	24	1129	37	95	31	83	0.37	
25	au15a53	1.9348	0.1476	0.1764	0.0089	0.3288	0.0745	0.0047	1083	51	1047	48	1080	43	97	31	85	0.36	
2	au15a55	1.8086	0.1307	0.1808	0.0073	0.2777	0.0752	0.0049	1049	47	1071	40	1223	48	88	29	83	0.34	
3	au15a56	1.8957	0.1021	0.1793	0.0067	0.3457	0.0773	0.0040	1080	36	1063	37	1093	44	97	30	84	0.35	
14	au15a67	1.8780	0.1236	0.1801	0.0066	0.2783	0.0754	0.0048	1073	44	1067	36	1258	45	85	30	78	0.39	
24	au15a77	1.9438	0.1014	0.1829	0.0066	0.3479	0.0745	0.0043	1096	35	1083	36	1167	41	93	27	81	0.34	
1	au15a92	1.8069	0.1044	0.1777	0.0070	0.3401	0.0710	0.0044	1048	38	1054	38	1090	40	97	37	101	0.37	
9	au15a86	1.6666	0.1360	0.1782	0.0088	0.3057	0.0686	0.0053	1003	51	1057	48	1049	49	101	20	62	0.32	
14	au15a91	1.8417	0.0900	0.1837	0.0054	0.2987	0.0681	0.0034	1060	32	1087	29	1019	36	107	36	97	0.37	
2	au10a70	1.8207	0.0995	0.1814	0.0052	0.2644	0.0727	0.0038	1053	36	1075	29	1139	43	94	19	59	0.33	
11	au10a79	1.8231	0.1516	0.1807	0.0103	0.3437	0.0732	0.0054	1054	55	1071	56	1055	38	102	34	92	0.37	
13	au10a50	1.9308	0.0938	0.1716	0.0050	0.2980	0.0776	0.0038	1092	33	1021	27	1109	42	92	38	103	0.37	
1	au10a01	1.8788	0.1227	0.1831	0.0057	0.2399	0.0747	0.0039	1074	43	1084	31	1193	32	91	37	100	0.37	
3	au10a03	1.8395	0.0873	0.1795	0.0048	0.2824	0.0727	0.0030	1060	31	1064	26	1088	36	98	25	75	0.34	
15	au10a14	1.9617	0.1149	0.1833	0.0085	0.3951	0.0714	0.0043	1102	39	1085	46	1025	37	106	24	68	0.35	
22	au10a21	1.8790	0.1021	0.1846	0.0055	0.2735	0.0739	0.0042	1074	36	1092	30	1075	40	102	26	74	0.35	

Table 2-2: Zircon reference material, sample: Pleisovice

Plesovice LA-ICPMS U-Pb Data																			
SAMPLE spot #	file	ISOTOPIC RATIOS						AGES Ma						% concordancy			Th232 ppm	U238 ppm	Th/U Ratio
		207/235	7/5 err	206/238	6/8 err	Rho	207/206	7/6 err	7/5 age	1 sigma	6/8 age	1sigma	7/6 age	1 sigma	concordancy				
5	au15a04	0.4034	0.0242	0.0525	0.0017	0.2679	0.0530	0.0027	344	18	330	10	377	36	88	79	729	0.11	
5	au15a05	0.3731	0.0314	0.0539	0.0020	0.2202	0.0469	0.0035	322	23	338	12	330	45	103	60	572	0.11	
7	au15a06	0.3874	0.0160	0.0523	0.0012	0.2704	0.0501	0.0019	332	12	329	7	402	33	82	106	780	0.14	
16	au15a15	0.3832	0.0241	0.0531	0.0014	0.2142	0.0506	0.0026	329	18	334	9	345	35	97	94	794	0.12	
29	au15a28	0.4040	0.0157	0.0541	0.0013	0.3081	0.0524	0.0020	345	11	339	8	381	32	89	125	895	0.14	
1	au15a54	0.3973	0.0222	0.0530	0.0017	0.2863	0.0487	0.0026	340	16	333	10	303	42	110	92	817	0.11	
14	au15a42	0.4075	0.0175	0.0542	0.0012	0.2498	0.0517	0.0018	347	13	340	7	320	34	106	88	822	0.11	
4	au15a57	0.3872	0.0177	0.0522	0.0013	0.2774	0.0522	0.0021	332	13	328	8	371	37	89	93	836	0.11	
15	au15a68	0.3917	0.0149	0.0530	0.0011	0.2758	0.0518	0.0018	336	11	333	7	399	31	83	103	877	0.12	
14	au10a51	0.3982	0.0382	0.0528	0.0036	0.3580	0.0538	0.0042	340	28	331	22	394	49	84	59	680	0.09	
23	au10a60	0.3803	0.0147	0.0527	0.0010	0.2470	0.0515	0.0020	327	11	331	6	310	39	107	52	646	0.08	
4	au10a04	0.3918	0.0222	0.0530	0.0018	0.2974	0.0522	0.0024	336	16	333	11	339	32	98	69	645	0.11	
5	au10a05	0.4000	0.0257	0.0537	0.0022	0.3180	0.0522	0.0026	342	19	337	13	360	36	94	59	564	0.10	
6	au10a06	0.3977	0.0222	0.0543	0.0016	0.2590	0.0525	0.0025	340	16	341	10	351	36	97	64	610	0.11	
7	au10a22	0.4008	0.0231	0.0537	0.0017	0.2830	0.0531	0.0025	342	17	337	11	373	35	90	58	577	0.10	
16	au10a15	0.3760	0.0169	0.0531	0.0012	0.2469	0.0496	0.0021	324	12	333	7	323	36	103	67	623	0.11	

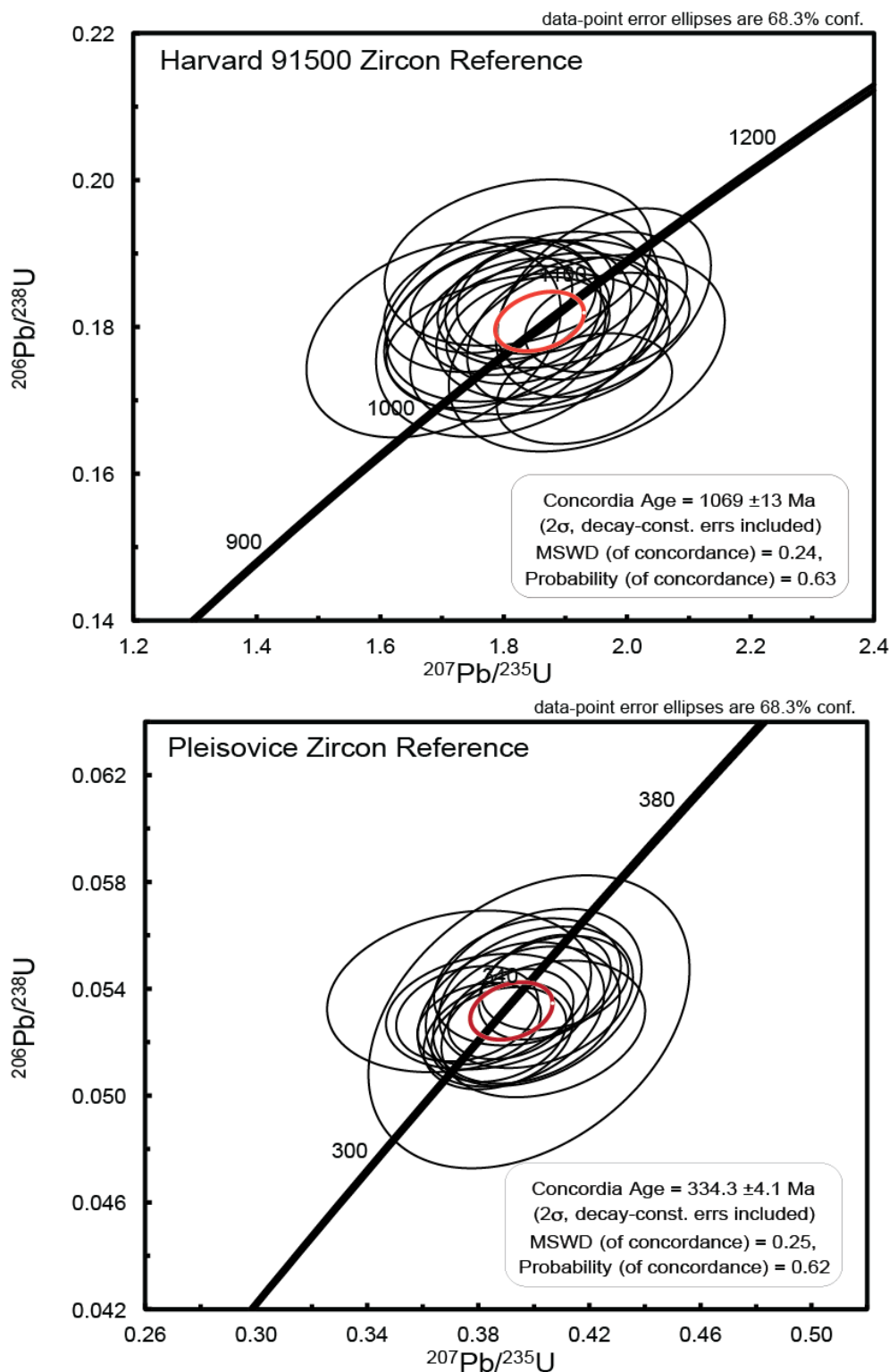


Figure 2-12: Harvard 91500, and Plešovice zircon reference materials: Concordia diagrams.

2-5-2-3 *U-Pb – Chemical Abrasion – Thermal Ionization Mass Spectrometry*

(CA-TIMS)

CA-TIMS requires a number of time intensive steps prior to analyzing. These include, crushing, heavy mineral separation via heavy liquids, and the Frantz magnetic separator, initial picking, annealing, physical abrasion, etching, final picking, and finally dissolution and loading of chosen zircon for analysis on the TIMS (Krogh, 1973; Krogh, 1982; Mattinson, 2005). These steps are discussed in detail in the following.

Due to the large amount of zircon within the rhyolite units, an extremely small sample (leftover thin section puck measuring approximately 2x4 cm) was required for crushing, and heavy mineral separation. This sample was initially broken down into smaller chips via hammering in a large sample bag, along with mortar and pestle. It was then crushed into a fine powder using the disk mill. Once crushed, heavy minerals were extracted using methylene iodide (3.32 g/cm), where minerals that are heavier than the methylene sink, and those that are lighter, float. Once collected this heavy mineral concentrate was allowed to dry, and underwent further separation by using a Frantz magnetic separator. The Frantz separates the heavy mineral concentrates into groups based on the magnetism of different minerals. Magnetic, and non-magnetic separates are collected through a number of steps, while changing the tilt, and magnetic field strength of the Frantz. Once separated, zircons were picked based on a number of parameters. Grains chosen tend to be the clearest, least magnetic, inclusion and crack free grains in the mineral separates.

Once picked, zircon grains were physically abraded using the technique developed and described by Krogh (1982). Zircon grains are abraded in the physical abrader for 10 hours, with pyrite grains being used to abrade the grains (Krogh, 1982). This technique allows for the removal of the outer skin of the zircon grains, which were shown to (via CL imaging) have U-rich outer rims, which would likely cause the zircon to be discordant.

Physically abraded zircon grains were then hand-picked and annealed in a high purity alumina crucible in a furnace at 900°C for 36 hours, following techniques described by Mattinson (2005). Once annealed, grains are etched, effectively removing zones in the zircon with radiation damage, where Pb loss has likely occurred (Mattinson, 2005). Etching involves putting the grains in a TEFILON bomb, with concentrated hydrofluoric acid (HF), at 200°C. Once abraded, annealed and etched, they are then examined using binocular microscope, and the best grains (i.e.: clearest, fracture/inclusion free) grains were chosen for isotope dilution.

Prior to dissolution of the sample, a $^{205}\text{Pb}/^{235}\text{U}$ spike was added to the Teflon dissolution capsules. The zircon were then dissolved using ~0.10 mL of concentrated HF, and 0.2 mL of 8N HNO₃ at 210°C for 5 days, then dried to a precipitate, and re-dissolved in~0.15 mL of 3N hydrochloric acid (HCL) (Krogh, 1973).

Uranium and Pb are then isolated from the zircon solutions using standard column ion exchange chromatography techniques (Krogh, 1973). Once isolated, the U and Pb are deposited on an outgassed rhenium filament with silica gel and are evaporated through heating in a clean box (Gerstenberger and Haase, 1997).

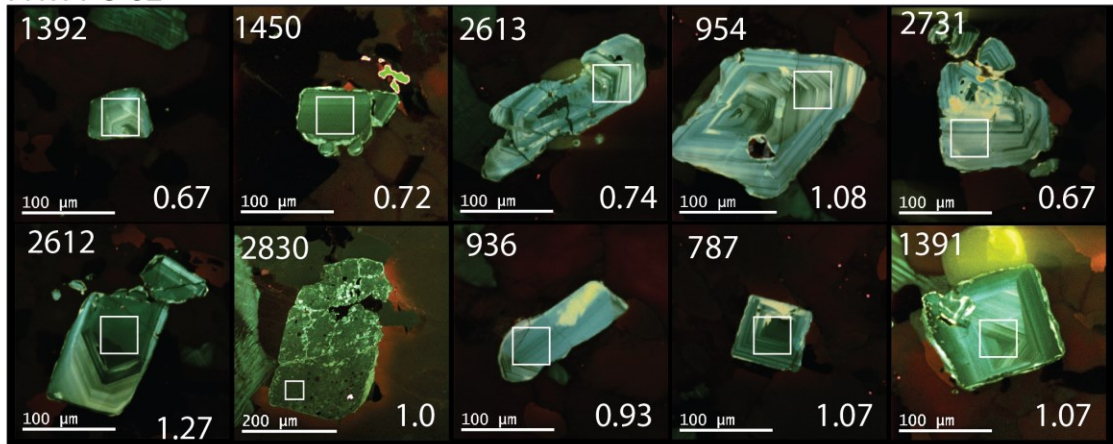
The U and Pb were analyzed a MAT 262 thermal ionization mass spectrometer, at Memorial University of Newfoundland. Techniques used generally followed those outlined in Sánchez-García et al. (2008), except for a few differences, discussed below. First of all, as mentioned previously (section 5.2.3.2.) zircon grains were physically abraded following Krogh (1982) to remove the thin-skin U-rich rim present on some zircon grains, to avoid Pb-loss. Both U and Pb were measured on the axial ion-counting secondary electron multiplier.

2-6 ZIRCON MORPHOLOGY AND U-PB ZIRCON AGES

Zircon grains from these samples display many interesting textures, and are often quite complicated. Common textures include well to poorly defined oscillatory zoning, sector zoning, bimodal (cauliflower) zoning, local recrystallization, along with variable amounts of cracking, and voids/pits.

It should be noted that all LA-ICPMS laser spots were placed on the most homogeneous domains of the zircon grains (Figures 2-13, to 2-15). Occasionally due to small zircon size, or large amounts of internal complexities (zoning, cracking, inclusions, voids), somewhat heterogeneous domains could not be avoided.

FHTW-6-02



FHC-45-01

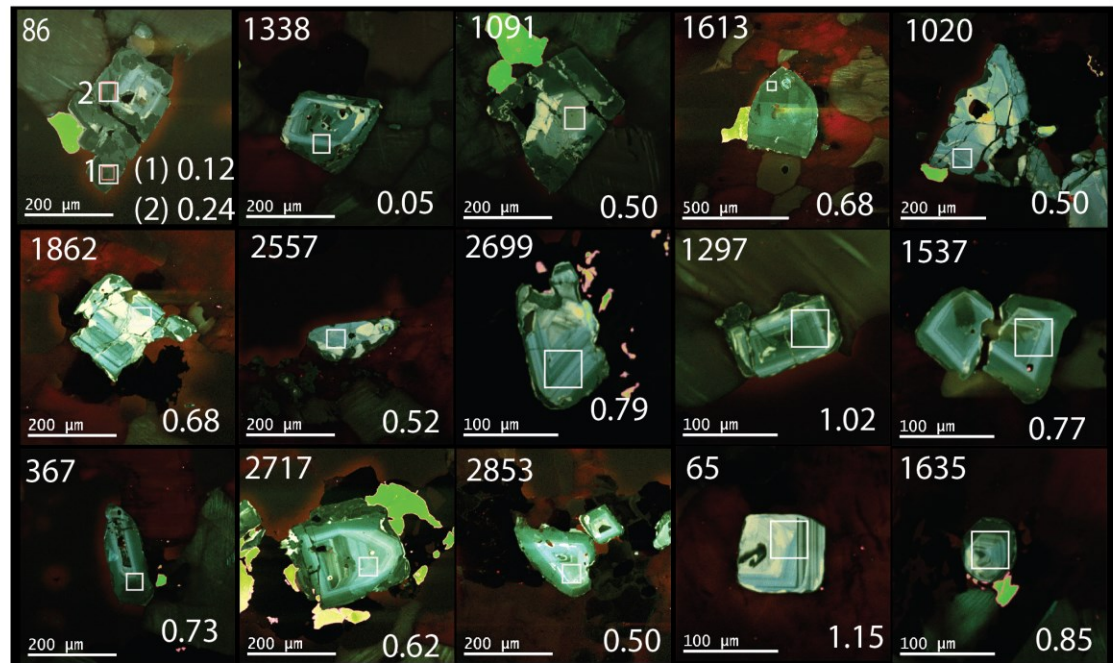


Figure 2-13: Cathodoluminescence photos of zircon from samples analyzed for U-Pb. Grain number located in top left corner. Scale bars are either 100 µm or 200 µm. Laser spots are represented with white box, measuring 40x40 µm. Th/U ratio is shown in the bottom right corner of each image.

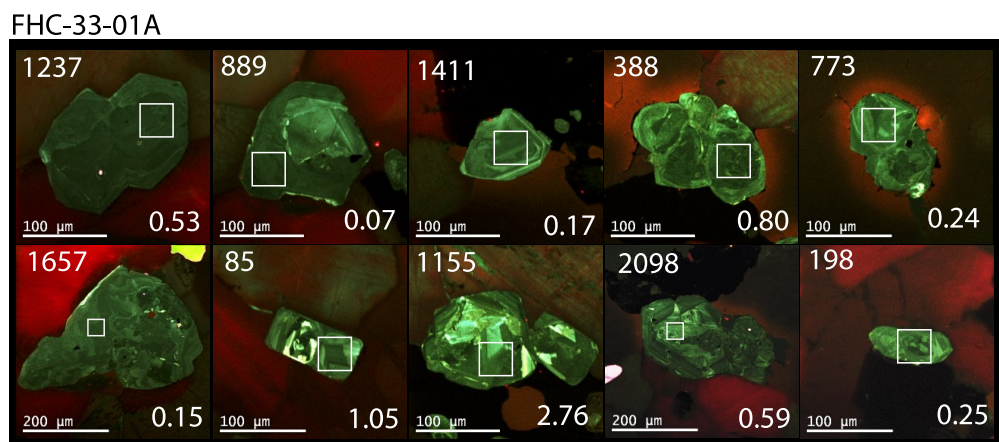
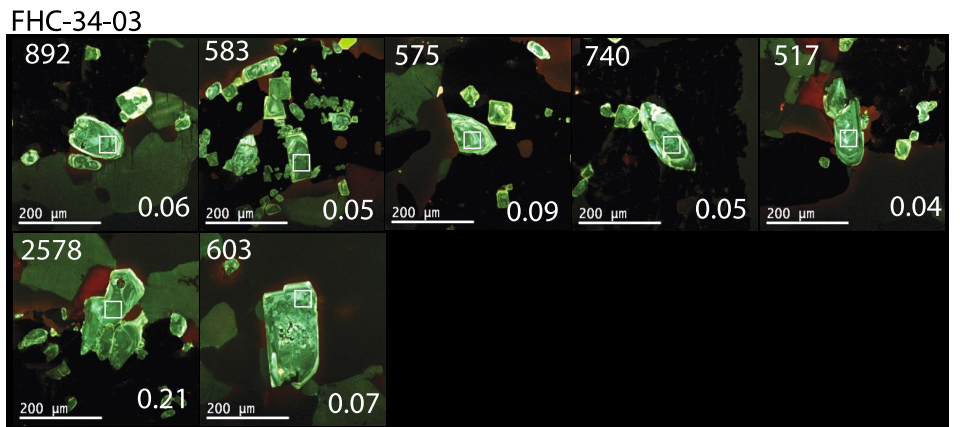


Figure 2-14: Cathodoluminescence photos of zircon from samples analyzed for U-Pb. Grain number located in top left corner. Scale bars are either 100 μm or 200 μm . Laser spots are represented with white box, measuring 40x40 μm . Th/U ratio is shown in the bottom right corner of each image.

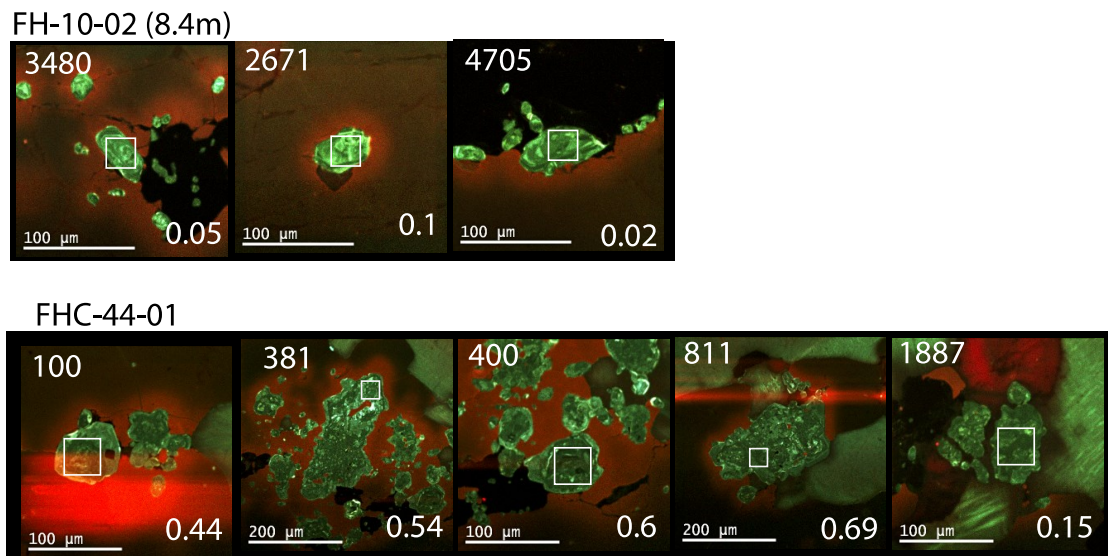


Figure 2-15: Cathodoluminescence photos of zircon from samples analyzed for U-Pb. Grain number located in top left corner. Scale bars are either 100 μm or 200 μm . Laser spots are represented with white box, measuring 40x40 μm . Th/U ratio is shown in the bottom right corner of each image.

2-6-1

FHWT-6-02 – RHYOLITE UNIT FROM SOUTH BELT

The morphologies of zircon grains from sample FHWT-6-02 are fairly consistently sub-equant to somewhat elongated with rounded edges, but there are some differences with respect to their internal zoning patterns. Grains are 100-300 μm in size. The majority of the grains analyzed display well-developed oscillatory zoning (e.g., grains 954, 2731 in Figure 2-13), and often contain a small-recrystallized rim around them that luminesce brightly in CL. Other grains exhibit more diffuse zoning (e.g., grains 1450, 936). Some grains have been locally recrystallized, with small embayments (e.g., grain 2613). One grain is quite different where it is large, luminesces poorly, and looks completely recrystallized (grain 2830).

2-6-I-1 *FHWT-6-02 via LA-ICPMS*

Twelve zircon grains were analyzed for U-Pb age by LA-ICPMS (Table 2-3) including those with oscillatory and more diffuse zoning. Thorium/U ratios from all analyzed zircon grains are consistently in the range of 0.5-1.1, typical of magmatic zircon (Hoskin and Schaltegger, 2003). Eleven of the U-Pb analyses give a Concordia age (Ludwig, 2008) of 1297 ± 21 Ma (2σ) but with a low probability of concordance (<0.003) (Figure 2-16a). U-Pb analysis of recrystallized grain 2830 is significantly more discordant than the others and was excluded from the age calculation.

FHWT-6-02

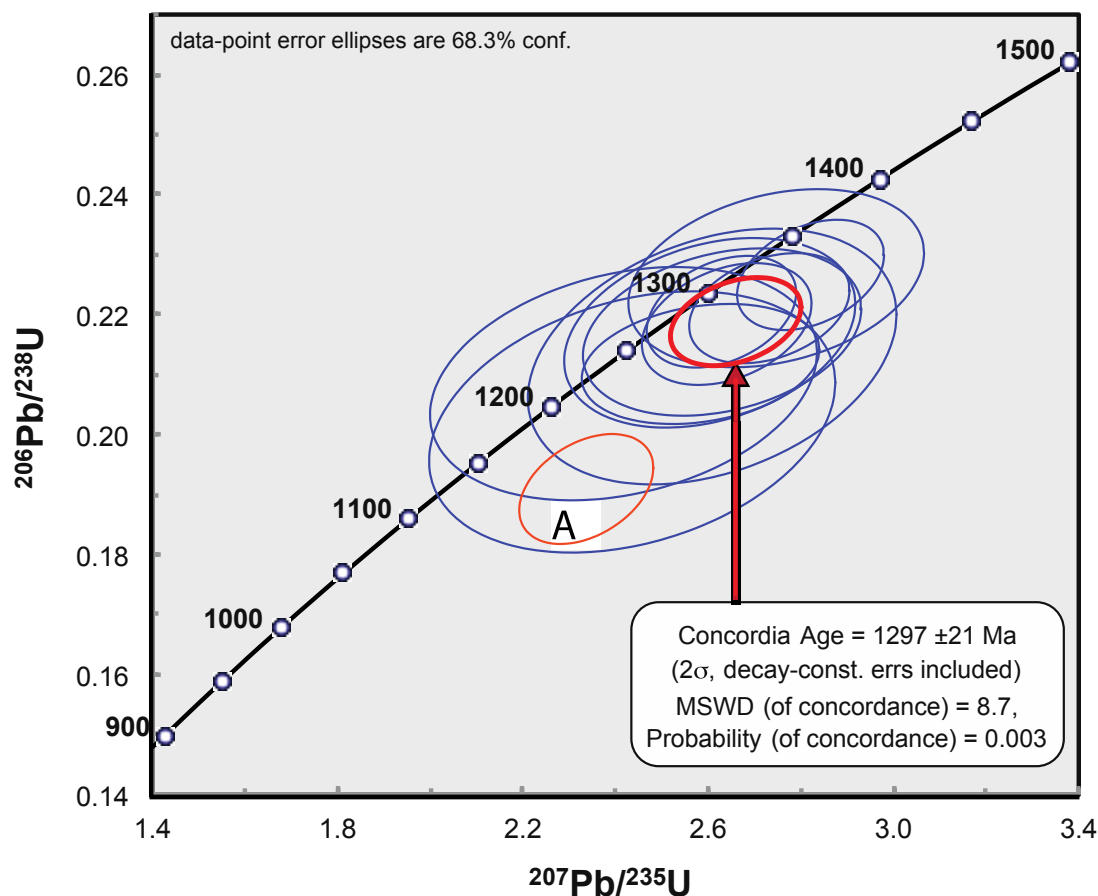


Figure 2-16a: LA-ICPMS U-Pb zircon data for sample FHWT-6-02 plotted on a Concordia diagram. Eleven analyses shown in blue ellipses give a Concordia age of 1297 ± 21 Ma (2σ). One analysis, grain 2830, labeled "A" and shown in orange ellipse is 12% discordant and excluded from the age calculation.

Table 2-3: LA-ICPMS U-Pb data table for the Fox Harbour rocks.

SAMPLE FHWT-6-02			ISOTOPIC RATIOS								AGES Ma								Th (232)			U (238)		Th/U	
Spot #	Grain #	File	207Pb/ 235U	1 sigma	206Pb/ 238U	1 sigma	Rho	207Pb/ 206Pb	1 sigma	207Pb/ 235U	1 sigma	206Pb/ 238U	1 sigma	207Pb/ 206Pb	1 sigma	% U-Pb concordancy	ppm	ppm	ratio						
7	511	au15a35	2.4170	0.2759	0.2085	0.0128	0.2695	0.0849	0.0014	1248	82	1221	68	1314	31	93	144	177	0.82						
8	611	au15a36	2.6284	0.1065	0.2205	0.0061	0.3437	0.0815	0.0014	1309	30	1284	32	1234	34	104	63	80	0.79						
9	787	au15a37	2.6083	0.2628	0.2130	0.0141	0.3277	0.0849	0.0013	1303	74	1245	75	1312	29	95	198	185	1.07						
10	936	au15a38	2.7466	0.2108	0.2261	0.0098	0.2824	0.0887	0.0017	1341	57	1314	52	1398	37	94	57	61	0.93						
11	954	au15a39	2.6299	0.1985	0.2171	0.0092	0.2808	0.0890	0.0019	1309	56	1267	49	1404	40	90	73	68	1.08						
12	1391	au15a40	2.6031	0.2076	0.2170	0.0104	0.3014	0.0853	0.0013	1302	58	1266	55	1323	30	96	196	183	1.07						
15	1392	au15a43	2.7319	0.1144	0.2211	0.0061	0.3274	0.0850	0.0014	1337	31	1288	32	1316	32	98	82	123	0.67						
16	1450	au15a44	2.5833	0.1693	0.2118	0.0066	0.2379	0.0850	0.0011	1296	48	1238	35	1316	25	94	313	433	0.72						
19	2612	au15a47	2.8209	0.1047	0.2266	0.0061	0.3607	0.0852	0.0012	1361	28	1317	32	1319	27	100	568	449	1.27						
20	2613	au15a48	2.6398	0.1209	0.2184	0.0067	0.3347	0.0894	0.0013	1312	34	1274	35	1412	28	90	92	125	0.74						
22	2731	au15a50	2.4356	0.2895	0.2021	0.0144	0.2991	0.0852	0.0019	1253	86	1187	77	1321	42	90	81	120	0.67						
23	2830	au15a51	2.3365	0.0956	0.1909	0.0060	0.3871	0.0835	0.0009	1223	29	1126	33	1280	22	88	1059	1060	1.00						
SAMPLE FH-10-02 (8.4m)																									
14	2671	au10a13	1.7195	0.0972	0.1686	0.0058	0.3058	0.0740	0.0009	1016	36	1004	32	1041	25	96	20	197	0.10						
18	3480	au10a17	1.9477	0.1183	0.1746	0.0062	0.2900	0.0813	0.0013	1098	41	1038	34	1229	31	84	8	173	0.05						
21	4705	au10a20	1.7171	0.0632	0.1654	0.0054	0.4435	0.0746	0.0009	1015	24	987	30	1058	23	93	5	313	0.02						
SAMPLE FHC-44-01																									
7	100	au10a75	2.3949	0.1200	0.1963	0.0077	0.3895	0.0885	0.0010	1241	36	1155	41	1393	22	83	186	426	0.44						
8	381	au10a76	2.5197	0.1334	0.2095	0.0083	0.3755	0.0886	0.0009	1278	38	1226	44	1395	20	88	184	340	0.54						
9	395	au10a77	1.6222	0.1359	0.1240	0.0105	0.5052	0.0945	0.0007	979	53	754	60	1519	14	50	1060	1174	0.90						
10	400	au10a78	2.0493	0.0480	0.1794	0.0034	0.4070	0.0811	0.0007	1132	16	1064	19	1224	18	87	353	593	0.60						
14	636	au10a82	2.4025	0.1585	0.1958	0.0074	0.2850	0.0949	0.0010	1243	47	1153	40	1527	19	76	351	334	1.05						
16	811	au10a84	2.4417	0.0869	0.2022	0.0043	0.3015	0.0839	0.0009	1255	26	1187	23	1290	20	92	290	418	0.69						
17	1887	au10a85	2.2207	0.0699	0.1786	0.0063	0.5639	0.0849	0.0009	1188	22	1060	35	1314	20	81	75	503	0.15						
18	2111	au10a86	2.5085	0.0939	0.2142	0.0056	0.3497	0.0863	0.0014	1274	27	1251	30	1346	30	93	29	90	0.33						
SAMPLE FHC-45-01																									
1	65	au15a07	2.9087	0.1340	0.2421	0.0091	0.4076	0.0915	0.0022	1384	35	1398	47	1458	45	96	57	50	1.15						
9	86	au15a08	1.7730	0.1528	0.1731	0.0074	0.2473	0.0781	0.0010	1036	56	1029	41	1150	26	89	59	510	0.12						
10	86	au15a09	2.1086	0.1244	0.1912	0.0075	0.3326	0.0804	0.0010	1152	41	1128	41	1208	24	93	81	331	0.24						
11	367	au15a10	2.5835	0.2012	0.2160	0.0121	0.3606	0.0852	0.0008	1296	57	1261	64	1321	18	95	289	394	0.73						
12	422	au15a11	2.4714	0.1678	0.2113	0.0115	0.4021	0.0814	0.0011	1264	49	1236	61	1232	25	100	311	383	0.81						
13	1020	au15a12	2.5477	0.1437	0.2163	0.0070	0.2862	0.0897	0.0019	1286	41	1262	37	1420	41	89	29	58	0.50						
14	1091	au15a13	2.3499	0.1132	0.2099	0.0067	0.3302	0.0842	0.0016	1227	34	1228	36	1296	36	95	35	71	0.50						
17	1297	au15a16	2.2166	0.1319	0.2025	0.0064	0.2635	0.0753	0.0031	1186	42	1189	34	1249	28	95	172	168	1.02						
18	1338	au15a17	2.3406	0.1667	0.2158	0.0068	0.2206	0.0844	0.0015	1225	51	1260	36	1302	34	97	78	134	0.58						
19	1537	au15a18	2.5155	0.1609	0.2125	0.0075	0.2755	0.0916	0.0020	1277	46	1242	40	1459	41	85	81	105	0.77						
20	1613	au15a19	2.6236	0.2059	0.2188	0.0124	0.3619	0.0835	0.0010	1307	58	1276	66	1280	24	100	207	303	0.68						
21	1635	au15a20	2.6288	0.2520	0.2186	0.0159	0.3797	0.0844	0.0015	1309	71	1275	84	1302	34	98	115	132	0.87						
22	1862	au15a21	2.5930	0.1943	0.2201	0.0120	0.3649	0.0825	0.0017	1299	55	1282	64	1258	41	102	44	65	0.68						
23	2557	au15a22	2.4296	0.2240	0.2065	0.0158	0.4145	0.0822	0.0015	1251	66	1210	84	1250	36	97	46	88	0.52						
24	2699	au15a23	2.3545	0.1454	0.2095	0.0084	0.3251	0.0850	0.0015	1229	44	1226	45	1316	34	93	74	94	0.79						
25	2717	au15a24	2.5767	0.2693	0.2176	0.0131	0.2877	0.0885	0.0017	1294	76	1269	69	1394	38	91	54	87	0.62						
26	2853	au15a25	2.5595	0.2062	0.2142	0.0098	0.2847	0.0921	0.0022	1289	59	1251	52	1470	46	85	43	85	0.50						
27	1635	au15a26	2.4968	0.1077	0.2151	0.0075	0.4030	0.0844	0.0013	1271	31	1256	40	1301	31	97	67	126	0.53						

Table 2-3 (continued): LA-ICPMS U-Pb data table for the Fox Harbour rocks.

Spot #	Grain #	File	ISOTOPIC RATIOS						AGES Ma						Th (232) ppm	U (238) ppm	Th/U ratio		
			207Pb/ 235U	1 sigma	206Pb/ 238U	1 sigma	Rho	207Pb/ 206Pb	1 sigma	207Pb/ 235U	1 sigma	206Pb/ 238U	1 sigma	207Pb/ 206Pb	1 sigma	% U-Pb concordancy			
SAMPLE FHC-33-01A																			
6	85	au15a59	2.4577	0.0978	0.2073	0.0056	0.3374	0.0859	0.0011	1260	29	1214	30	1335	25	91	269	256	1.05
7	198	au15a60	1.8415	0.0516	0.1775	0.0037	0.3684	0.0761	0.0009	1060	18	1053	20	1098	22	96	127	516	0.25
8	388	au15a61	2.5405	0.2047	0.2115	0.0128	0.3748	0.0874	0.0009	1284	59	1237	68	1369	19	90	687	863	0.80
11	773	au15a64	2.3813	0.2090	0.2026	0.0105	0.2966	0.0866	0.0010	1237	63	1189	57	1352	22	88	167	698	0.24
13	889	au15a66	1.7356	0.1275	0.1730	0.0082	0.3230	0.0737	0.0007	1022	47	1029	45	1033	20	100	55	747	0.07
17	986	au15a70	2.5123	0.0630	0.2186	0.0041	0.3780	0.0798	0.0007	1276	18	1275	22	1193	18	107	200	598	0.34
18	1008	au15a71	2.1331	0.1449	0.1852	0.0091	0.3611	0.0841	0.0009	1160	47	1095	49	1296	20	85	143	466	0.31
22	1155	au15a75	2.3742	0.1803	0.2034	0.0108	0.3508	0.0841	0.0009	1235	54	1193	58	1296	22	92	1408	511	2.76
2	1237	au15a79	1.8790	0.1167	0.1775	0.0064	0.2909	0.0764	0.0008	1074	41	1053	35	1105	22	95	307	578	0.53
3	1411	au15a80	1.7925	0.0942	0.1728	0.0063	0.3475	0.0760	0.0009	1043	34	1028	35	1096	24	94	84	502	0.17
4	1657	au15a81	1.8417	0.0713	0.1705	0.0061	0.4586	0.0748	0.0010	1060	25	1015	33	1064	26	95	47	324	0.15
8	2098	au15a85	3.0035	0.1056	0.2469	0.0084	0.4817	0.0858	0.0012	1409	27	1423	43	1333	26	107	134	227	0.59
SAMPLE FHC-34-03																			
6	517	au10a43	1.7487	0.0896	0.1748	0.0061	0.34	0.0747	0.0011	1027	33	1039	34	1061	31	98	10	249	0.04
7	575	au10a44	1.7099	0.1215	0.1712	0.0059	0.24	0.0815	0.0014	1012	46	1019	33	1233	34	83	8	167	0.05
8	583	au10a45	1.9587	0.1214	0.1885	0.0068	0.29	0.0776	0.0012	1101	42	1113	37	1137	31	98	13	235	0.05
10	603	au10a47	1.6605	0.0996	0.1671	0.0071	0.36	0.0727	0.0010	994	38	996	39	1004	29	99	19	289	0.07
12	674	au10a49	1.7917	0.0757	0.1759	0.0042	0.28	0.0784	0.0012	1042	28	1044	23	1158	30	90	11	210	0.05
15	740	au10a52	1.9009	0.1293	0.1802	0.0068	0.28	0.0803	0.0012	1081	45	1068	37	1205	30	89	23	267	0.09
17	892	au10a54	1.8625	0.0746	0.1802	0.0044	0.30	0.0757	0.0012	1068	26	1068	24	1087	31	98	12	218	0.06
24	1372	au10a61	1.8710	0.1260	0.1806	0.0059	0.24	0.0774	0.0014	1071	45	1070	32	1131	36	95	10	224	0.04
26	2578	au10a63	1.7643	0.0813	0.1739	0.0059	0.37	0.0745	0.0011	1032	30	1033	32	1056	29	98	73	344	0.21
29	3358	au10a66	1.7155	0.1309	0.1704	0.0102	0.39	0.0746	0.0010	1014	49	1014	56	1057	26	96	38	395	0.10

% U-Pb concordancy = $100 \times (206\text{Pb}/238\text{U} \text{ age})/(207\text{Pb}/206\text{Pb} \text{ age})$

2-6-1-2 *FHWT-6-02 via CA-TIMS*

This sample was chosen for CA-TIMS because it contains a large number of large (100-300 μm) grains with oscillatory zoning (imaged via SEM and CL) of likely igneous origin. A total of 6 zircon fractions were analyzed, where two fractions contained single grains (Z1, and Z4), three fractions contained two grains (Z2, Z5, and Z6), and one contained three grains (Z3) (Table 2-4). All six zircon fractions were concordant, with five of the analysis (Z1, 2, 3, 4, and 6) superimposed on one another in the U-Pb Concordia diagram, yielding a weighted average $^{206}\text{Pb}/^{238}\text{U}$ age of 1300 ± 2.5 Ma. One fraction (Z5) exhibited Pb-loss along a Discordia line to ~ 1050 Ma, and was not included in the weighted average (Figure 2-16b).

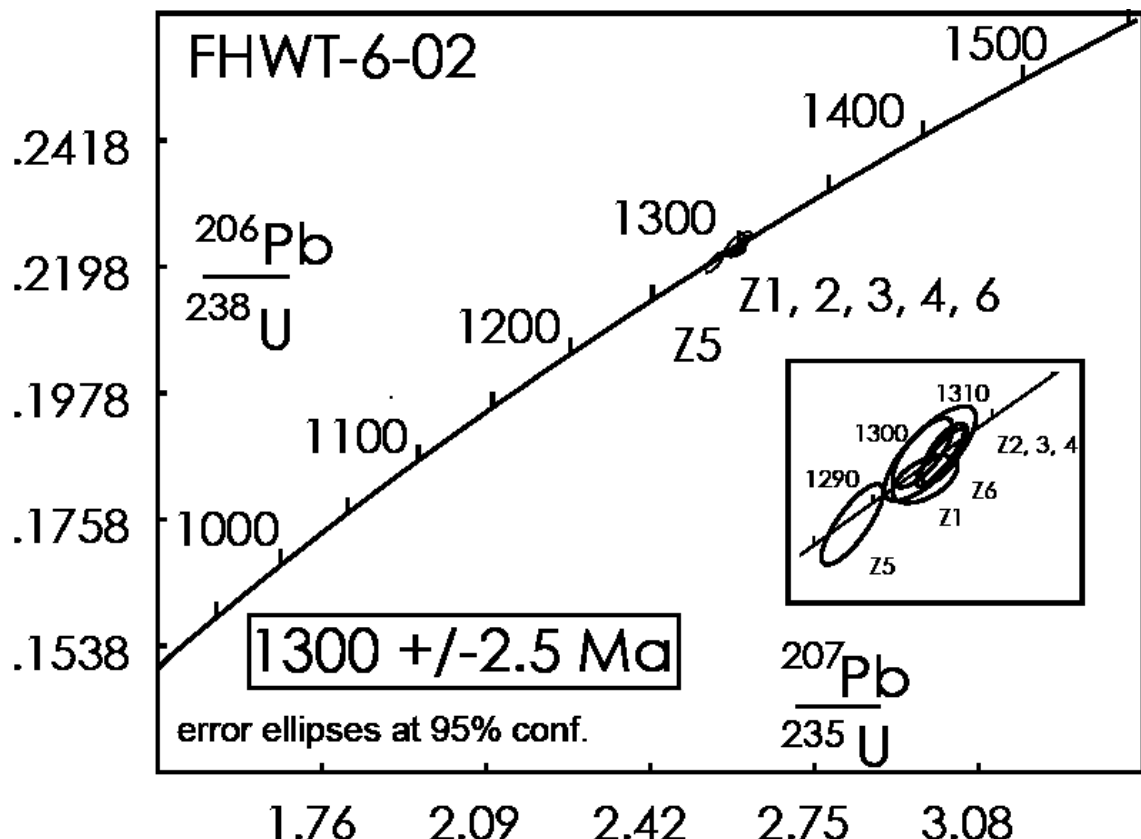


Figure 2-16b: CA-TIMS U-Pb zircon age for FHWT-6-02 plotted on a Concordia diagram

Table 2-4: TIMS U-Pb data for sample FHWT-6-02.

Fraction	Weight (mg)	Concentration		Measured		Corrected Atomic Ratios						Age (Ma)			
		U (ppm) (a)	Pb rad (ppm) (b)	Total commo n Pb (pg)	206Pb/ 204Pb	208Pb/ 206Pb 238U	206Pb/ 238U	±	207Pb/ 235U	207Pb/ 206Pb	±	207Pb/ 206Pb	206Pb/ 238U	207Pb/ 235U	207Pb/ 206Pb
Z1 1 lrg prm	0.002	117	29	9	387	0.2058	0.22259	86	2.5934	156	0.0845	44	1296	1299	1304
Z2 1 lrg + 1 sml prm	0.003	196	52.1	2	4903	0.297	0.22356	106	2.6024	116	0.08443	20	1301	1301	1302
Z3 3 sml prm	0.003	76	19.5	3	1218	0.2419	0.22377	126	2.5921	146	0.08401	34	1302	1298	1293
Z4 1 lrg prm	0.002	123	30.1	2	2164	0.1855	0.22374	110	2.6048	112	0.08444	30	1302	1302	1303
Z5 2 sml prm	0.002	208	54	2	2620	0.2843	0.22057	146	2.5503	150	0.08386	34	1285	1287	1289
Z6 2 sml prm	0.002	86	22.4	1	1943	0.2646	0.22374	172	2.5965	222	0.08417	48	1302	1300	1296

Notes: All zircon was physically abraded (Krogh, 1982), and chemically abraded (Mattinson 2005) prior to dissolution. Z,zircon; 1,2 number of grains in analysis; prm, prism; sml, small; frag, fragment.

a. weights of grains were estimated, with potential uncertainties of 25-50% for these small samples.

b. radiogenic lead

c. Atomic ratios corrected for fractionation, spike, laboratory blank of 0.6- 2 picograms (pg) common lead, and initial common lead at the age of the sample calculated from the model of Stacey and Kramers (1975), and 0.3 pg U blank. Two sigma uncertainties are reported after the ratios and refer to the final

*2-6-2 FH-10-02 (8.4M) – GRANITIC VEIN/PEGMATITE WITHIN FOLDED BASALT,
FROM THE FOXTROT DEPOSIT (MT BELT)*

The morphologies of zircon grains from sample FH-10-02 (8.4m) are all consistently elongated with aspect ratios of ca. 2:1. Grains are small (50-100 μm), luminesce poorly, and contain complex internal features, such as poorly developed oscillatory zoning, and sector zoning (Figures 2-13 to 2-15). BSE images reveal that the grains are largely featureless, except for some very small cracks.

LA-ICPMS analyses of three zircon grains (Table 2-3) yield a U-Pb Concordia age of 1018 ± 30 Ma (2σ) (Figure 2-23). Thorium/U ratios for the 3 analyzed zircon grains are quite low, 0.02, 0.05 and 0.10, typical of metamorphic zircon (Hoskin and Schaltegger, 2003).

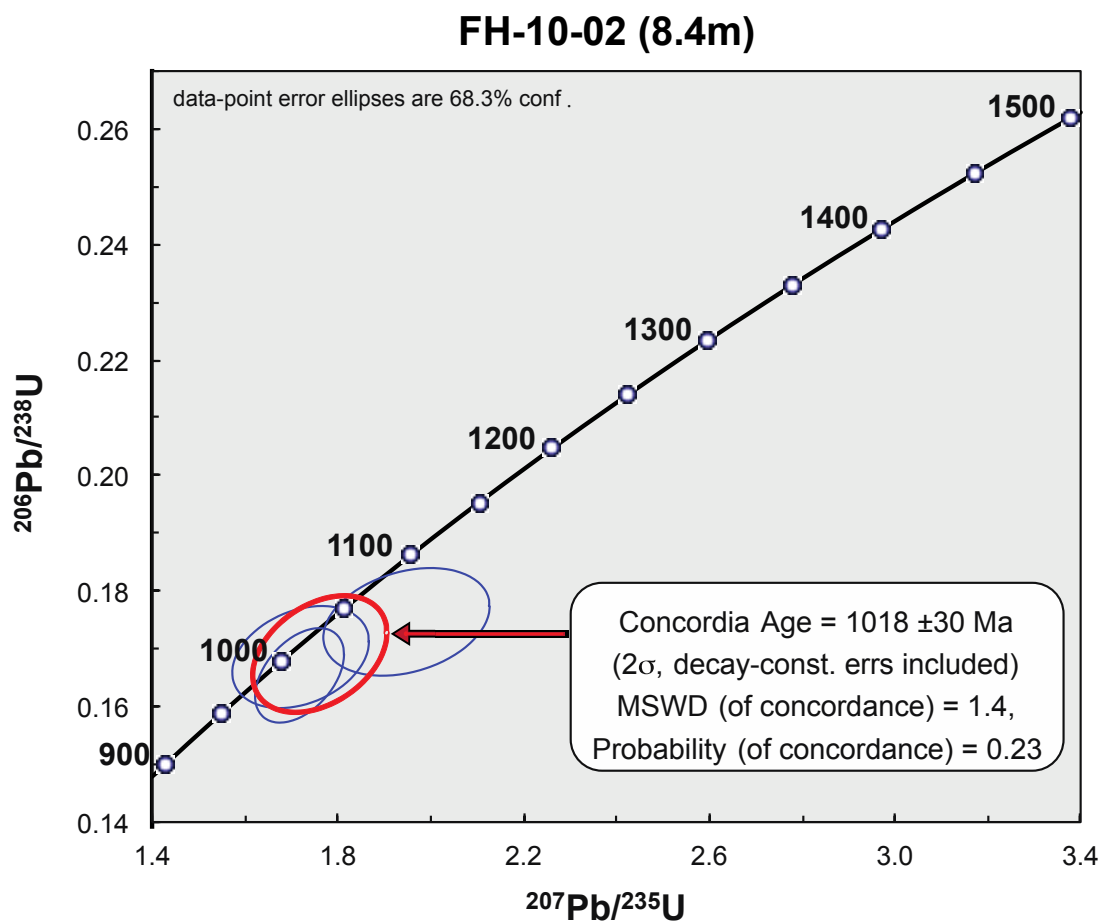


Figure 2-17: LA-ICPMS U-Pb zircon data for sample FH-10-02 (8.4m) plotted on a Concordia diagram.

2-6-3 FHC-44-01 – RHYOLITE UNIT IN MT BELT

The morphologies of zircon grains from sample FHC-44-01 are all quite irregular and complicated. Grains are 100-200 μm in size, and display complex internal features. Zircon grains do not display well-developed oscillatory zoning, but appear to be composite resorbed, with bimodal zoning. All grains contain numerous barren voids/pits, and are variably cracked.

LA-ICPMS U-Pb analyses for 8 grains (Table 2-3) indicate that the zircon is moderately (7-13%, for 4 grains) to highly discordant (50%, grain 395) with a trend on the Concordia diagram suggesting recent Pb loss. The U-Pb data can be fit by a model 1 solution, with an upper intercept age of 1346 ± 51 Ma, and a lower intercept at the origin (Figure 2-18). Thorium/U ratios range from 0.15 to 1.05 in zircon grains analyzed from this sample. Grain 395, which is most discordant, contains the most Th (1060 ppm) and U (1174 ppm).

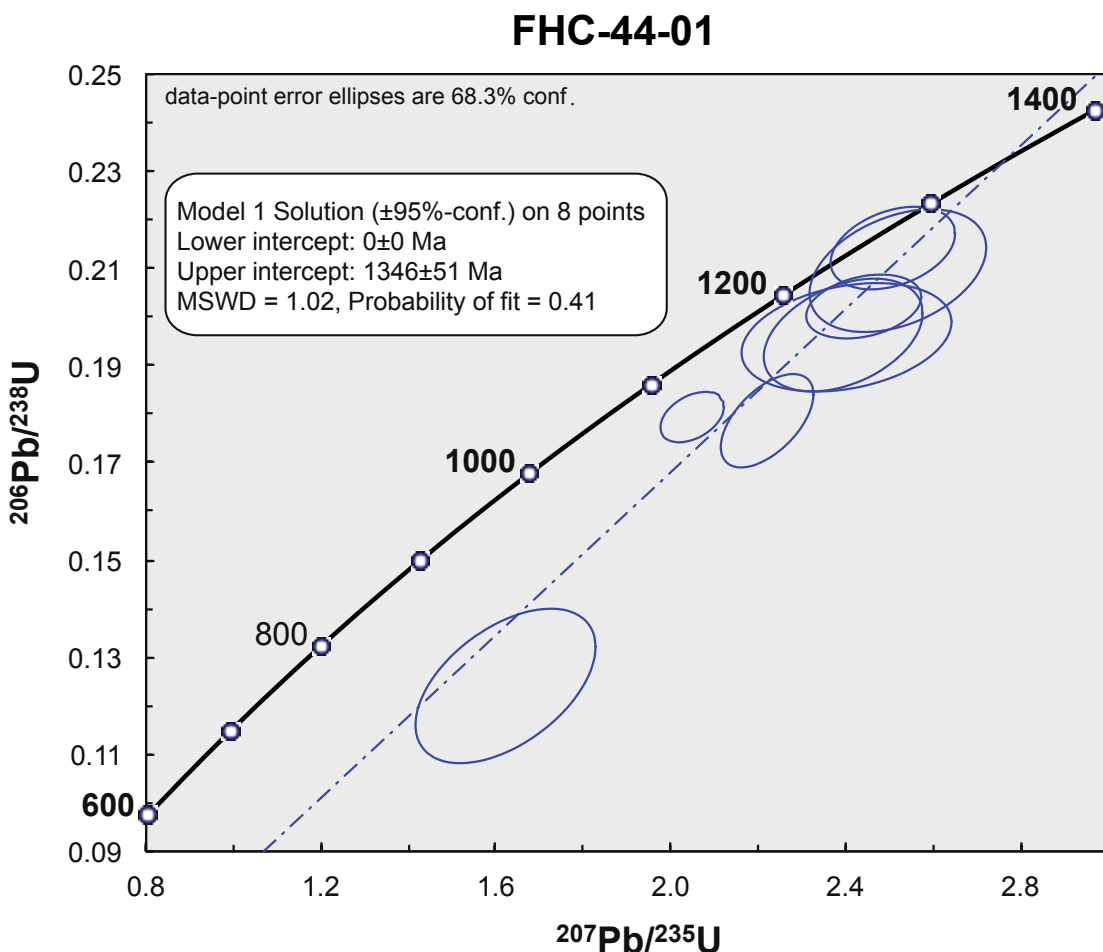


Figure 2-18: LA-ICPMS U-Pb zircon data for sample FHC-44-01 plotted on a Concordia diagram.

2-6-4 FHC-45-01 – RHYOLITE UNIT IN MT BELT

The morphologies of zircon grains from sample FHC-45-01 are all similar. They are generally are 100-200 um in size and luminesce brightly. In CL and BSE, some grains display well-preserved oscillatory zoning (e.g., grains 1297, 1537, 2699), whereas others show little or no zoning (e.g., grains 1020, 1091, 1613). Xenocrystic cores are visible in some grains (e.g., grains 65, 86, 367, 1537, 2717, 2853). Zircon grains contain a minimal

amount of cracks and inclusions, visible in BSE. Occasionally grains have a small resorption rim, which luminesces brightly (e.g., 1613).

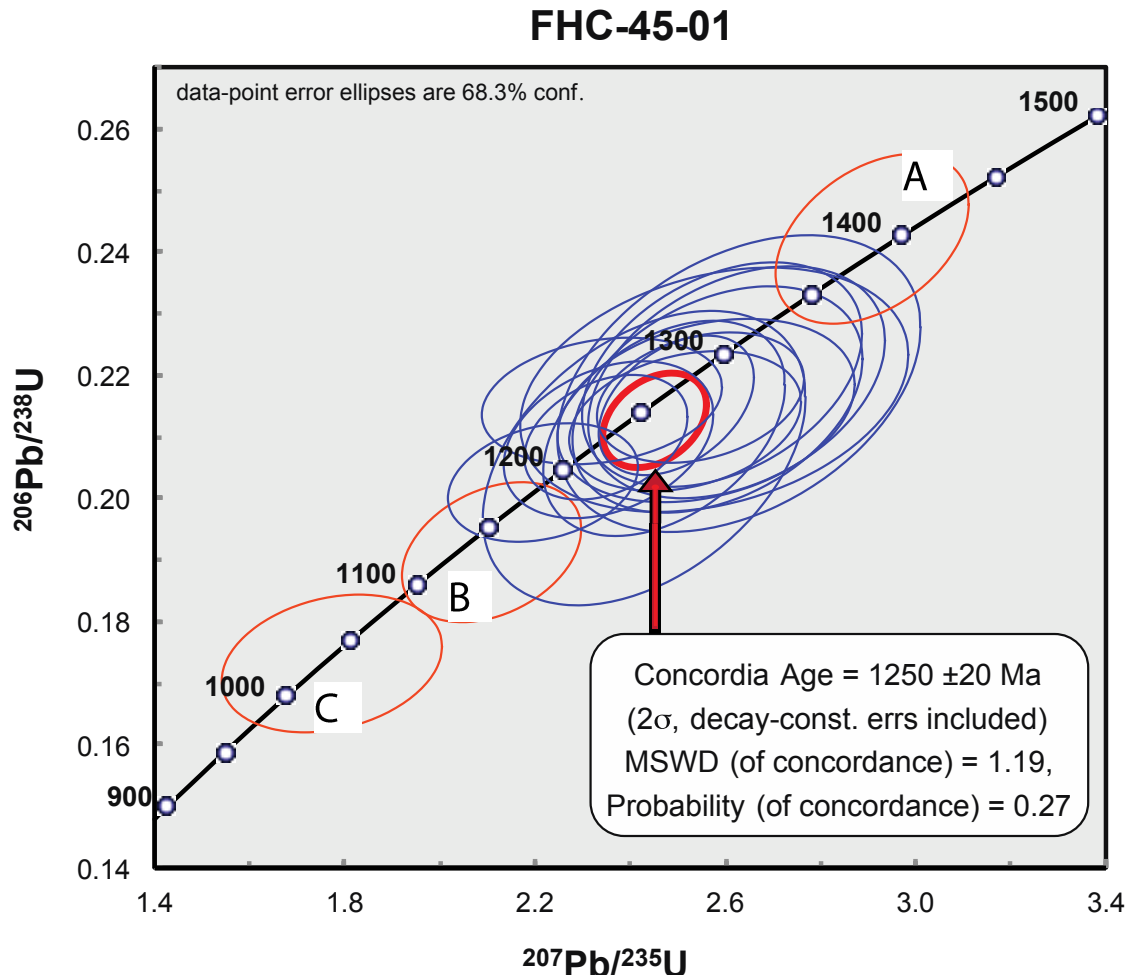


Figure 2-19: LA-ICPMS U-Pb zircon data for sample FHC-45-01 plotted on a Concordia diagram. Fifteen analyses shown in blue ellipses give a Concordia age of 1250 ± 20 Ma (2σ). Three analysis labeled “A”, “B” and “C”, shown as orange ellipses, are excluded from the age calculation.

Eighteen analyses of 17 zircon grains plot along the U-Pb concordia from ca. 1400 to 1000 Ma (Table 2-3). Fifteen analyses shown in blue ellipses give a Concordia age of 1250 ± 20 Ma (2σ) (Figure 2-19). Three analyses labeled “A”, “B” and “C” in Figure

2-19 are outliers. Analysis A, which includes an apparent xenocrystic core in grain 65 (Figures 2-13 to 2-15), has a Concordia age of 1388 ± 65 Ma (2σ). Analyses B and C are from grain 86 and have Concordia ages of 1140 ± 67 Ma and 1031 ± 73 Ma (2σ), respectively. Analysis C was positioned on the dark CL rim of the grain, whereas Analysis B overlapped in part with the brighter CL xenocrystic core of the grain. Thorium/U ratios for all grains range from 0.50 to 1.15, typical of magmatic values, except for grain 86, which has lower Th/U ratios of 0.12 (rim) and 0.24 (overlapping rim and core).

2-6-5 SAMPLE FHC-33-01A – ROAD BELT

The morphologies of the zircon grains from sample FHC-33-01A are complicated. Zircon grains range in size from 100-400 μm , display complex oscillatory zoning, sector zoning, and cauliflower (bimodal zoning) texture. Zircon grains exhibit variable amount of cracking, inclusions, and small voids, while CL is variable from almost non-existent to bright. Some grains (e.g., 85, 889, 1155, 2098) exhibit somewhat brighter CL cores than rims, which may represent xenocrystic domains.

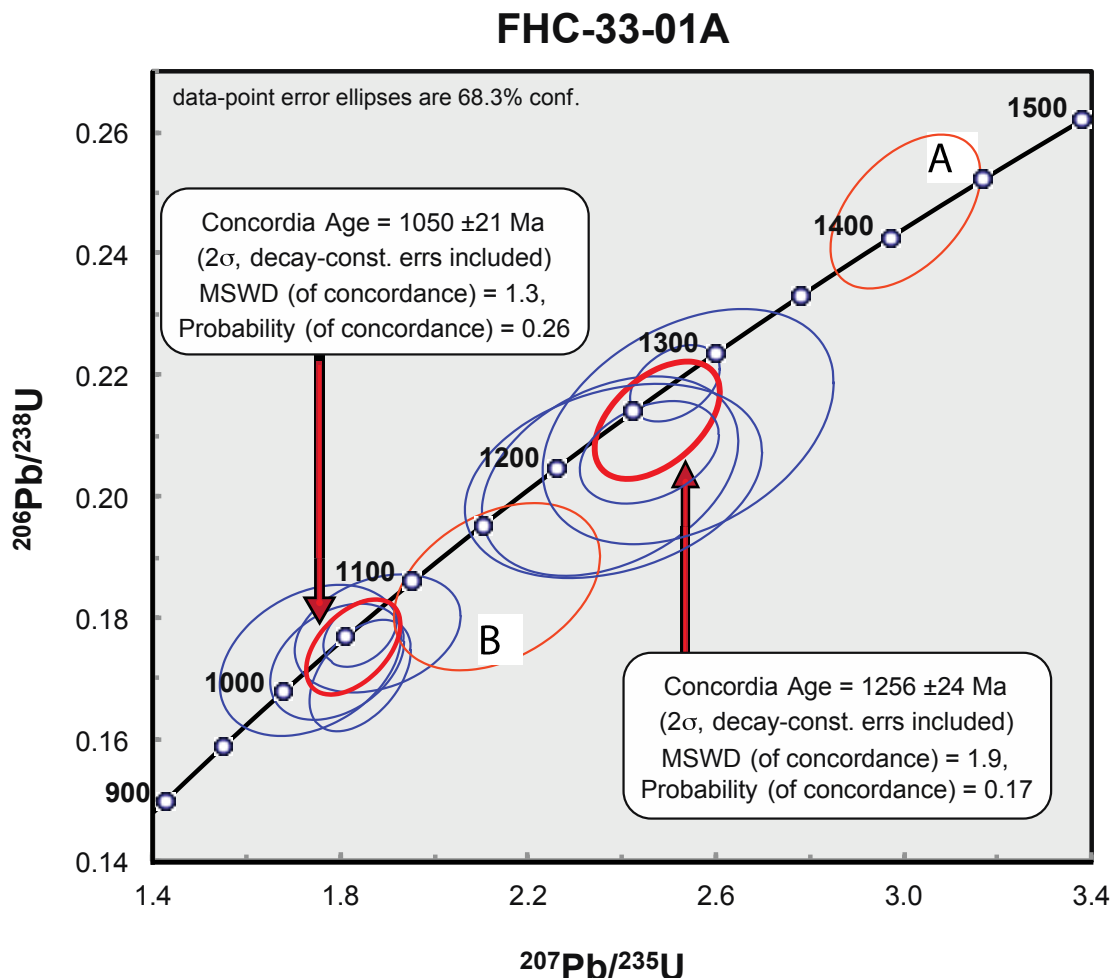


Figure 2-20: LA-ICPMS U-Pb zircon data for sample FHC-33-01A plotted on a Concordia diagram. There are two clusters of analyses shown as blue ellipses and two outliers (labeled “A” and “B”) shown as orange ellipses. See text for details.

Twelve U-Pb zircon analyses (Table 2-3) plot along the U-Pb Concordia, ranging from ca. 1400 to 1000 Ma, similar to sample FHC-45-01 (rhyolite from MT Belt). The oldest analysis (labeled “A” in Figure 2-20) has a Concordia age of 1410 ± 53 Ma (2σ); it represents a brighter CL core of grain 2098 that may be xenocrystic. All of the other analyses cluster in two populations, except for one grain (labeled “B” in Figure 2-20) that

plots in between the two clusters. The younger population (5 analyses; grains 198, 889, 1237, 1411, 1657) has a Concordia age of 1050 ± 21 Ma (2σ). The grains contain similar morphologies, where they luminesce poorly, have minimal oscillatory zoning, and occasionally display erratic internal textures. Thorium/U ratios of zircon grains analyzed in this younger population range from 0.07-0.53. The older population (5 analyses; grains 85, 388, 773, 986, 1155) has a Concordia age of 1256 ± 24 Ma (2σ). The older grains appear to preserve a complicated magmatic/restoration history, compared to the younger grains, which are smaller and less internally complicated. Thorium/U ratios from zircon grains in this older population range from 0.24-2.76.

2-6-6 SAMPLE FHC-34-03 – ROAD BELT

The morphologies of zircon grains from sample FHC-34-03 are fairly consistent. Zircon grains are 100-200 μm in size, long and slender, with bright luminescing oscillatory growth zoning. Grains exhibit small pits/voids largely in the center of the grains, perhaps representing xenocrystic cores inadvertently plucked out of the mount during polishing.

FHC-34-03

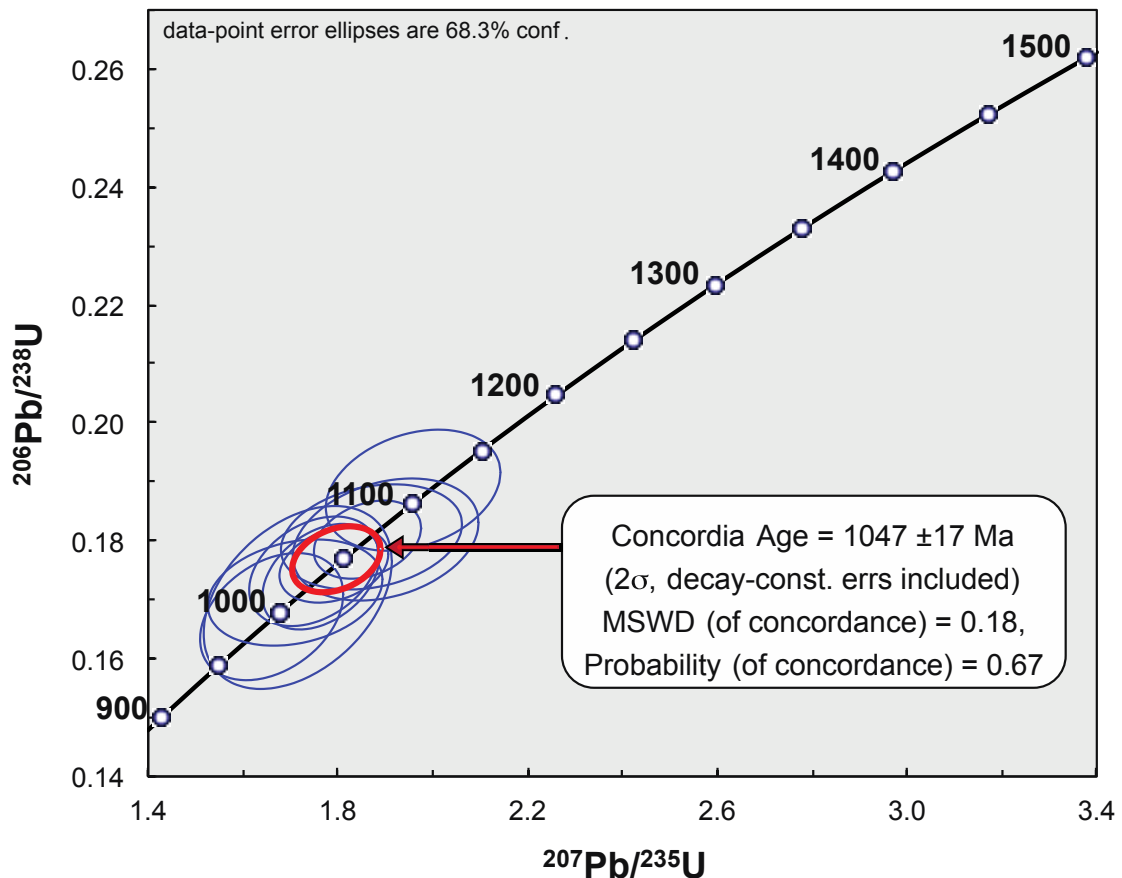


Figure 2-21: LA-ICPMS U-Pb zircon data for sample FHC-34-03 plotted on a Concordia diagram.

Ten zircon grains analyzed in this sample give a Concordia age of 1047 ± 17 Ma (2σ) as seen in Figure 2-21, Thorium/U ratios from zircon grains analyzed in this sample are very low, ranging from 0.04-0.10, which are typical of metamorphic ratios, except for one grain (2578), which has a Th/U of 0.21 (Table 2-3).

2-7 DISCUSSION

2-7-1 RECOGNITION OF NEW SUPRACRUSTAL PACKAGE

The recognition of the Fox Harbour bimodal volcanic package in southeastern Labrador has important economic, and scientific implications. This area of the Grenville Province is important in that it is thought to be the boundary between three lithotectonic terranes with differing Grenvillian metamorphic histories in the area. The detailed history of the area, as shown with this project is complex, with multiple phases of deformation, and metamorphism throughout.

Understanding the affect that metamorphism had on the rocks in the Fox Harbour area may aide in the identification of similar packages throughout the Grenville Province.

2-7-2 U-PB AGE OF VOLCANIC PACKAGE

In-situ U-Pb zircon age determinations were made on all three of the identified bimodal volcanic belts in the Fox Harbour project area, and identified two major age populations: one at ca. 1300 Ma, which is interpreted as the magmatic age of the rocks, and the other at ca. 1050 Ma, which is thought to present a high-grade metamorphic age. The magmatic zircon grains tend to have higher Th/U ratios (typically 0.5 – 1.1) compared to the metamorphic zircon grains (typically <0.20), as is commonly reported in high-grade metamorphic terranes elsewhere (Hoskin and Schaltegger, 2003). Chemical abrasion TIMS was conducted on one sample, from the South Belt (FHWT-6-02), and dated the magmatic age very precisely. All 3 belts exhibit zircons with the ca. 1300 Ma age, whereas the MT Belt and Road Belt also have zircons with the ca. 1050 Ma high-

grade metamorphic age. This is consistent with the idea that magmatic and tectonic events in the belts were related.

Xenocrystic cores in two zircon grains from the MT Belt (sample FHC-45-01) and Road Belt (sample FHC-33-01A) gave ages of ca. 1400 Ma, which may represent the age of the source rocks or country rocks of the felsic magmas of the Fox Harbour volcanic belts. If they were derived from the source rocks, they would be residual zircon that did not completely melt during the crustal melting event that produced the rhyolite magmas. If the xenocrystic zircon were derived from the country rocks, they would have formed as contaminants partially assimilated by the rhyolite magmas as they rose through the crust.

2-7-2-1 *1300 Ma age population*

The magmatic age population recorded in the Fox Harbour area is most precisely and accurately dated by the CA-TIMS U-Pb zircon age of 1300 ± 2.5 Ma (2σ) for rhyolite sample FHWT-6-02 from the South Belt. Less precise LA-ICPMS U-Pb zircon ages within error of this result are: 1297 ± 21 Ma (2σ), also from sample FHWT-6-02; and 1346 ± 51 Ma (2σ), derived from a discordant population of zircon grains from sample FHC-44-01 from the MT Belt. This zircon population is taken to be the age of formation for the rhyolitic units within the bimodal volcanic package. It is assumed that other supracrustal units (i.e.: basalt, quartzite, metasediments) in the area were also deposited around the same time as the rhyolite units.

LA-ICPMS U-Pb zircon ages of 1250 ± 20 Ma (2σ) from sample FHC-45-01 from the MT Belt and 1256 ± 24 Ma (2σ) from sample FHC-33-01A from the Road Belt also likely represent magmatic zircon crystallization at ca. 1300 Ma. The magmatic zircon grains in both samples are strongly overprinted by the ca. 1050 Ma metamorphic event and we suspect that the LA-ICPMS analysis intersected micron-scale metamorphic domains, resulting in integrated (mixed) ages that are somewhat younger than 1300 Ma.

The alternative interpretation is that magmatism in the MT Belt and Road Belt was some 50 Ma younger than in the South Belt. Current data are not sufficient to say whether one interpretation is right over the other. CA-TIMS U-Pb analyses of these samples would be needed to resolve this question unambiguously.

2-7-2-2 *1050 Ma age population*

The metamorphic age recorded in the Fox Harbour area is ~ 1050 Ma. This age presumably reflects new zircon growth, perhaps by dissolution reprecipitation (Geisler et al., 2007) during the Grenville deformation/metamorphism in this area of southeastern Labrador.

The metamorphic zircon population is most well-represented by the Concordia age of 1047 ± 17 Ma (2σ), based on 10 grains from sample FHC-34-03 from the Road Belt; and 1050 ± 21 Ma (2σ), based on 5 grains from sample FHC-33-01A, also from the Road Belt. Two zircon Concordia ages from the MT Belt, may represent the same ca. 1050 Ma event, or a slightly younger event: One grain from sample FHC-45-01 has an

age of 1031 ± 73 Ma (2σ), and three grains from sample FH-10-02 (8.4m) give an age of 1018 ± 30 Ma (2σ).

Kamo et al. (2011) dated an amazonite pegmatite on Battle Island, approximately 20 km from the main area of study in this project (Figure 2-22a). The amazonite pegmatite dated by Kamo et al. (2011) is texturally very similar, and is assumed to be the same as those found throughout the MT Belt, and Road Belt (specifically those found in the Foxtrot area of MT Belt, seen in Figure 2-22b). The time of emplacement for the amazonite pegmatite on Battle Harbour was taken to be 1024 ± 3 Ma (Kamo et al., 2011). This is based on three analyses, which define a co-linear line with the concordant analysis (Figure 2-22d) (Kamo et al., 2011). Based on findings by Kamo et al. (2011), and findings in this study, the large boudinaged pegmatites found mainly within the MT Belt, and also the Road Belt, are also interpreted to be Grenvillian in age (~1050 Ma). Cathodoluminescence images of the zircon grains show often well-defined oscillatory zoning, along with a much lower Th/U ratio, suggesting they are metamorphic in nature. These zircon grains (and amazonite pegmatites) are believed to have formed during a melting event that focused on the HFSE enriched rhyolitic units in the Fox Harbour area (i.e., mineralized units in the MT Belt, and Road Belt). This melting event explains the well developed oscillatory zoning observed in the zircon of this age, where a simple metamorphic event would not produce such zircon textures.

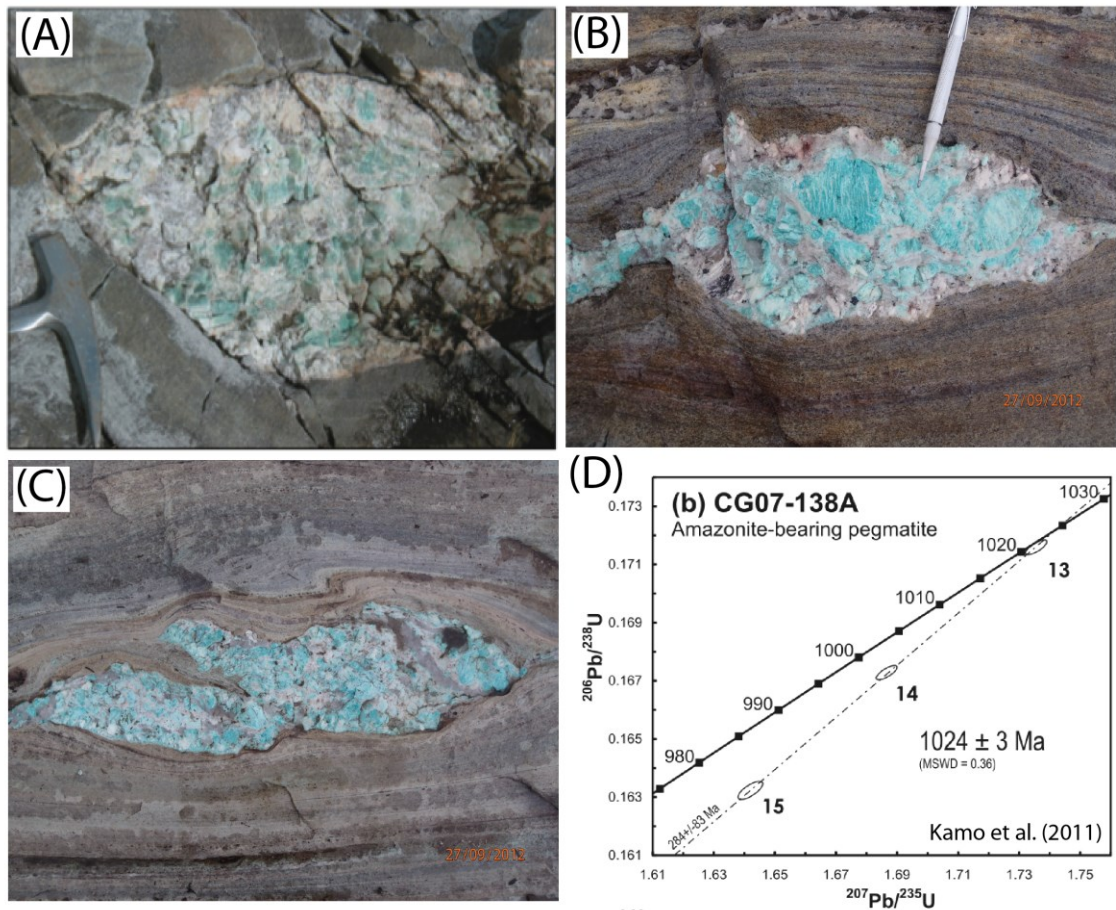


Figure 2-22: Photos of representative amazonite-bearing pegmatites from the Foxtrot Project within the MT Belt, and Battle Island, located 20 km to the southeast of the main project area. (A) Amazonite-bearing pegmatite located on Battle Island (Kamo et al., 2011). (B and C) Amazonite-bearing pegmatites located in the Foxtrot Project, within the MT Belt. (D) Concordia diagram for the amazonite-bearing pegmatite dated by Kamo et al. (2011).

It should be noted that the South Belt does not contain extensive pegmatites, like those found in the MT and Road Belts, and no Grenvillian age was recorded in the one sample dated in this belt. This suggests that melting (and zircon resetting/growth) did not occur as readily in the South Belt during Grenvillian Orogenesis.

2-7-3 TECTONIC IMPLICATIONS

The occurrence of a supracrustal package in this area of the Grenville Province is not completely unexpected, as supracrustal rocks have been identified in the northern Grenville Province (namely units in the Pinware terrane, the Wakeham Group, and Seal Lake). Nonetheless, there had been no previous evidence that a significant 1.3 Ga magmatic event occurred in this particular region. Supracrustal rocks in the Pinware terrane have been assumed to be much older (i.e.: 1600-1700 Ma) than the age of the Grenville metamorphism, but recent studies have revealed that this is not universally the case (Tucker and Gower, 1994; Wasteneys et al., 1997; Kamo et al., 2011).

It is believed that between ca. 1.5 to 1.3 Ga, there existed a continental-margin arc along the Laurentian margin (Tucker and Gower, 1994; Corrigan, 1995; Corrigan and Hanmer, 1995; McLelland et al., 1996; Rivers and Corrigan, 2000; Davidson, 2008; Hynes and Rivers, 2010, Kamo et al., 2011). Continental-margin arcs can have been shown to exhibit variable architecture, and can be either compressional or extensional (Uyeda and Kanamori 1979; Royden 1993; Waschbusch and Beaumont 1996; Pope and Willett 1998; Rivers and Corrigan, 2000). They have been shown to fluctuate between the extensional and compressional depending on the velocity of the tectonic plates involved (Uyeda and Kanamori 1979; Royden 1993; Waschbusch and Beaumont 1996; Pope and Willett 1998; Rivers and Corrigan, 2000). A compressional regime creates features such as an advancing subduction boundary, large imbricated thrustal stacks, with no back-arc magmatic activity (Uyeda and Kanamori 1979; Royden 1993; Waschbusch and Beaumont 1996; Pope and Willett 1998; Rivers and Corrigan, 2000). An extensional arc has a retreating subduction boundary, with normal faults dominating, leaving the basement

largely undeformed, and active linear back-arcs (Uyeda and Kanamori 1979; Royden 1993; Waschbusch and Beaumont 1996; Pope and Willett 1998; Rivers and Corrigan, 2000).

The occurrence of the Fox Harbour HFSE enriched rhyolitic units (assumed to peralkaline based on indicator minerals present), along with basaltic rocks can be attributed to being formed in an extensional rifting event, likely in a back-arc regime. This back-arc regime is believed to have existed by at least 1300 Ma. The Grenville Province during this time was moderately active. Geological activity during Geon 13 includes large AMCG suites such as the Nain Plutonic Suite (1320-1270 Ma), the Adirondack Highlands (1336-1301 Ma) (McLlland and Chiarenzelli, 1990; Ryan, 1991; Connelly 1993; Connelly and Ryan, 1999; Rivers and Corrigan, 2000). Also present are many granitic intrusions such as Arrowhead Lake (1307 Ma), the Red Wine Intrusive Suite (1337-1317 Ma), and the Dysart—Mt. Holly granitoids (1400-1301 Ma) (Hill and Miller, 1990; Lumbers et al., 1990; Rivers, 1997; and River and Corrigan, 2000). A lot of activity is recorded in the Grenville Province during Geon 12, including small intrusions, up to large supracrustal packages. Intrusions include the Upper North River syenite (1296 Ma), Flowers River granite (1271 Ma), Harp, Mealy, and Sudbury dykes (1250 Ma, 1273 Ma, and 1235 Ma, respectively), the Tshenuktish granite (1298 Ma), and the Strange Lake granite (1240 Ma) (Krogh et al., 1987; Hill and Miller, 1990; Cadman et al., 1993; Dudas et al., 1994; Romer et al., 1995; Emslie et al., 1997; Cox et al., 1998; Miller et al., 1997). Supracrustal packages during this time include the Bancroft-Cabonga-Elzevir-Mazinaw-Sharbot Lake terranes (1290-1230 Ma), the Frontenac-Mont Laurier-Morin terranes (1300-1230 Ma), and the Seal Lake Group (1273-1250 Ma) (Hill and Miller,

1990; Sager-Kinsman and Parrish, 1993; Friedman and Martignole, 1995; Romer et al., 1995). Much of this geological activity noted above is believed to have formed in an extensional setting, some of which is continental rifting, and some of which likely formed in a back-arc.

Grenvillian orogenesis is interpreted to have began at \sim 1100 Ma, lasting 100 Ma, resulting from the collision of Laurentia and another continent, likely Amazonia (McLlland et al., 1996; Carr et al., 2000; Hanmer et al., 2000; Tohver et al., 2004; Tohyer et al., 2006; Gower et al., 2008; Rivers, 2008; Rivers 2009; Hynes and Rivers, 2010). The \sim 1050 Ma event recorded in the Fox Harbour rocks represents the Grenvillian deformation. It is believed that most of the deformation observed in this area occurred at this time, confirmed by the deformation observed in the amazonite pegmatites, which have been dated at 1024 ± 3 Ma (Kamo et al., 2011). Grenvillian deformation in this area is thought to have caused selective migmatization, where units that melt readily (i.e.: volatile rich, hydrous) were the focus of melting. This relationship is observed in the Foxtrot project, where the mineralized units often contain amazonite pegmatites, and lesser-mineralized units do not contain pegmatites/migmatites. The Road Belt, and the MT Belt recorded this 1050 Ma age.

As mentioned previously, supracrustal units accurately dated in the Pinware terrane are consistently older (1710-1600 Ma) than the Grenville metamorphism. Accretion of the Pinware terrane accretion is believed to have ended by 1450 Ma, meaning the Fox Harbour volcanic package formed much later than this event. A regional aeromagnetic map of Labrador completed by the government suggests that the area around Cartwright, Port Hope Simpson, St. Lewis, Battle Island, Mary's Harbour, down

to Red Bay may include a belt of ~1300 Ma supracrustal rocks, which is currently poorly defined and understood (Figure 2-23). The area described appears as a magnetic low (in comparison to known Pinware terrane), and extends upwards of 250 Km. U-Pb dating in the area of this study reveals that Pinware age (1520-1460 Ma) units do occur proximal to the Fox Harbour units, such as the Cape Charles and Wolf Cove quartz monzonites, and a granite vein just south of the project area, dated at 1490 ± 5 Ma, 1472 ± 3 Ma, $1509 +11 - 12$, respectively (Scott et al., 1993; Tucker and Gower, 1994). It is likely that Grenvillian deformation caused this area to be extremely dismembered, juxtaposing 1.4-1.7 Ga Pinwarian rocks against younger 1.3 Ga supracrustal packages, such as the Fox Harbour, and Battle Harbour supracrustal units. Further work understanding the character, structure, magmatic and depositional age of these rocks is needed to define the geological history precisely.

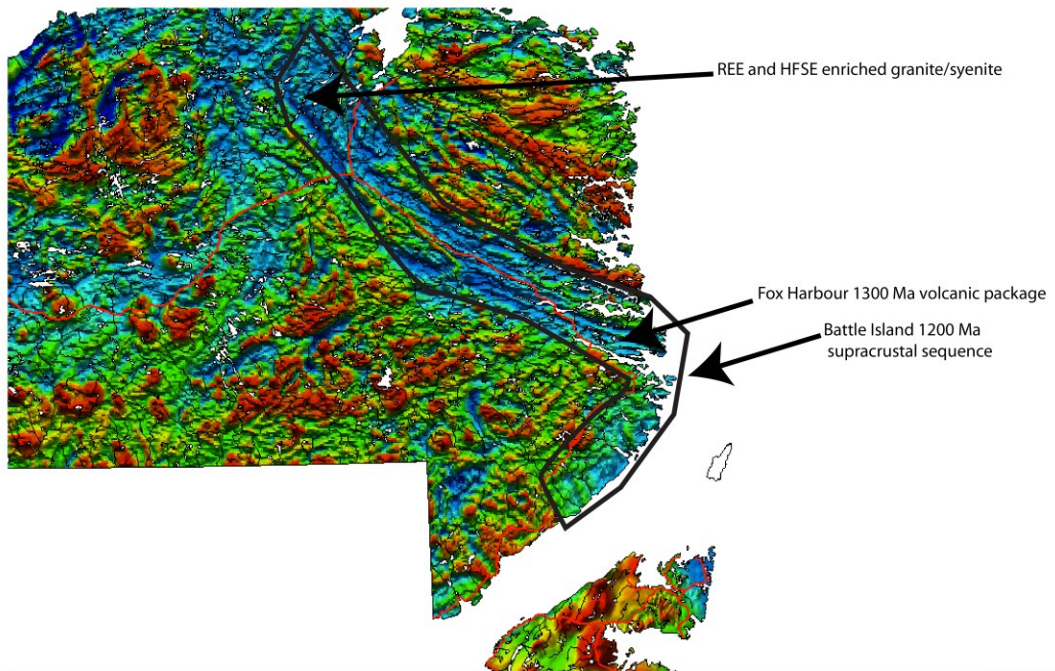


Figure 2-23: Airborne magnetometer survey for the southeastern coast of Labrador. The magnetic low, is thought to be a generalized outline of the Lake Melville terrane. It is possible that within this terrane, there is a 1300-1200 Ma belt of rocks. Arrows point to area of interest, such as the location of the Battle Island 1200 Ma supracrustal sequence, the 1300 Ma volcanic units, and samples collected by the Geological Survey of Newfoundland, enriched in HFSE.

2-8 CONCLUSIONS

The Fox Harbour area consists of a newly discovered structurally concordant supracrustal package within a amphibolite facies terrane. These units were formed at 1.3 Ga, in an extensional environment, coinciding with magmatism throughout much of the Grenville at this time. Many other units throughout the Grenville indicate the Laurentian margin was in an extensional setting during this time. These include large AMCG suites, small granitic to syenitic intrusions, mafic dyke swarms (Harp, Mealy, and Sudbury dykes), along with supracrustal packages (Bancroft-Cabonga-Elzevir-Mazinaw-Sharbot

Lake terrane, the Frontenac-Mont Laurier-Morin terrane, and the Seal Lake Group) (Krogh et al., 1987; Hill and Miller, 1990; Lumbers et al., 1990; McLelland and Chiarenzelli, 1990; Ryan, 1991; Cadman et al., 1993; Connelly 1993; Sager-Kinsman and Parrish, 1993; Dudas et al., 1994; Friedman and Martignole, 1995; Romer et al., 1995; Emslie et al., 1997; Miller et al., 1997; Rivers, 1997; Cox et al., 1998; Connelly and Ryan, 1999; and Rivers and Corrigan, 2000).

Lithological mapping completed in the project area revealed three extensive supracrustal belts, named the Road Belt, MT Belt and South Belt. *In-situ* U-Pb age determinations completed via LA-ICPMS, along with CA-TIMS U-Pb age determinations allowed for the recognition of two age populations. These rocks may have formed in an extensional back-arc environment around 1300 Ma within the continental margin arc, which is believed to have existed along the Laurentian margin between 1.5 and 1.3 Ga (Tucker and Gower, 1994; Corrigan, 1995; Corrigan and Hanmer, 1995; McLelland et al., 1996; Rivers and Corrigan, 2000; Hynes and Rivers, 2010). The second recorded age population is 1050 Ma, assumed to be the age of Grenvillian deformation and metamorphism for this area. This age, along with those recorded by Kamo et al. (2011) in an amazonite pegmatite reveal that much of the deformation that affects the Fox Harbour supracrustal package is Grenvillian in age. Grenvillian deformation in this area created large shear zones, regional to outcrop scale folds, and selective migmatization of certain units, and possibly causing the amazonite pegmatites observed throughout the project area.

A large magnetic low, seen in Figure 2-23 is thought to contain the generalized outline of the Lake Melville terrane. Within this terrane, there is a 1.2-1.3 Ga supracrustal

packages belt of rocks. This terrane, and possibly supracrustal packages are suggested to extend upwards of 250 km, and is possibly much longer than this. The occurrence of this belt of rocks, in the Lake Melville terrane, with an age recorded in it of 1.3 Ga, in the northern Grenville is extremely interesting. Many studies have been completed on similar supracrustal packages in the southern Grenville. The identification and interpretation of the Fox Harbour volcanic rocks will hopefully aid in the locating, and understanding the origin of similar rocks that may be unrecognized throughout the northern Grenville Province.

2-9 REFERENCES

- Arnaudov, V.; Pavlova, M.; Petrusenko, Sv. (1967): Lead content in certain amazonites. *Izvestiya na Geologicheskiy Institut, Bulgarska Akademiya na Naukite*, 16, 41-44 (in Bulgarian).
- Cadman, A. C., Heaman, L., Tarney, J., Wardle, R., & Krogh, T. E. (1993). U-Pb geochronology and geochemical variation within two Proterozoic mafic dyke swarms, Labrador. *Canadian Journal of Earth Sciences*, 30(7), 1490–1504.
- Carr, S., Easton, R., Jamieson, R., & Culshaw, N. (2000). Geologic transect across the Grenville orogen of Ontario and New York. *Canadian Journal of Earth Sciences*, 37(2-3), 193–216.
- Chiarenzelli, J. R., & McLlland, J. M. (1991). Age and regional relationships of granitoid rocks of the Adirondack Highlands. *The Journal of Geology*, 99(4), 571–590.

Connelly, J.N. 1993. U–Pb geochronological research agreement: final report for the Newfoundland Department of Mines and Energy, Labrador Mapping Section. Unpublished report on file with the Geological Survey Branch, Newfoundland Department of Mines and Energy.

Connelly, J., & Heaman, L. (1993). U-Pb geochronological constraints on the tectonic evolution of the Grenville Province, western Labrador. *Precambrian Research*, 63(1-2), 123–142.

Connelly, J. N., & Ryan, A. B. (1999). Age and tectonic implications of Paleoproterozoic granitoid intrusions within the Nain Province near Nain, Labrador. *Canadian Journal of Earth Sciences*, 36(5), 833–853.

Corfu, F., Hanchar, J., Hoskin, P., & Kinny, P. (2003). Atlas of zircon textures. *Reviews in Mineralogy and Geochemistry*, 53(1), 469.

Corriveau, L., & Bonnet, A.-L. (2005). Pinwarian (1.50 Ga) volcanism and hydrothermal activity at the eastern margin of the Wakeham Group, Grenville Province, Quebec. *Canadian Journal of Earth Sciences*, 42(10), 1749–1782.
doi:10.1139/e05-086.

Corrigan, D., 1995. Mesoproterozoic evolution of the south-central Grenville orogen: structural, metamorphic and geo-chronologic constraints from the Mauricie transect. Ph.D. Thesis, Carleton University, Ottawa.

Corrigan, D., Hanmer, S., 1995. Arc accretion, thickening, post- collisional extension and plutonism in the Grenville orogen; constraints from the Mauricie region, south-central Quebec. In: Precambrian '95, International Conference on Tectonics

and Metallogeny of Early/Mid Precambrian orogenic Belts, Program and Abstracts, Montreal, p. 106.

Corrigan, D., Rivers, T., & Dunning, G. (2000). U-Pb constraints for the plutonic and tectonometamorphic evolution of Lake Melville terrane, Labrador and implications for basement reworking in the northeastern Grenville Province* 1. *Precambrian Research*, 99(1-2), 65–90.

Cox, R. A., Dunning, G. R., & Indares, A. (1998). Petrology and U–Pb geochronology of mafic, high-pressure, metamorphic coronites from the Tshenukutish domain, eastern Grenville Province. *Precambrian Research*, 90(1), 59–83.

Davidson, A. (2008). Late Paleoproterozoic to mid-Neoproterozoic history of northern Laurentia: An overview of central Rodinia. *Precambrian Research*, 160(1-2), 5–22. doi:10.1016/j.precamres.2007.04.023.

Delaney, P. and Haley, J.T. (2011; *unpublished*). Report on mapping, prospecting, geochemical sampling, trenching, diamond drilling, and airborne radiometric/magnetometer survey on the Fox Harbour property, Port Hope Simpson, Labrador. 1st year assessment report, Alterra Resources Inc, pp. 429.

Dudàs, F.Ö, Davidson, A., and Bethune, K.M. 1994. Age of the Sudbury dykes and their metamorphism in the Grenville Province, Ontario. In Radiogenic age and isotope studies: Report 8. Geological Survey of Canada, Current research, 1994-F, 97–106.

Emslie, R.F. (1976). Mealy Mountains Complex, Grenville Province, southern Labrador.

In Report of activities, part A. Geological Survey of Canada, Paper 76-1A, 165–170.

Emslie, R.F., and Hunt, P.A. (1990). Ages and petrogenetic significance of igneous mangerite-charnockite suites associated with massif anorthosites, Grenville Province. *Journal of Geology*, 98, 213–231.

Emslie, R. F., Hamilton, M. A., & Gower, C. F. (1997). The Michael Gabbro and other Mesoproterozoic lithospheric probes in southern and central Labrador. *Canadian Journal of Earth Sciences*, 34, 1566–1580.

Friedman, R. M., & Martignole, J. (1995). Mesoproterozoic sedimentation, magmatism, and metamorphism in the southern part of the Grenville Province (western Quebec): U-Pb geochronological constraints. *Canadian Journal of Earth Sciences*, 32(12), 2103–2114.

Gerstenberger, H., & Haase, G. (1997). A highly effective emitter substance for mass spectrometric Pb isotope ratio determinations. *Chemical Geology*, 136(3), 309–312.

Giesler, T., Schaltegger, U., Tomaschek, F. (2007). Re-equilibration of zircon in aqueous fluids and melts, *Elements*, (4), 43–50, doi:10.2113/gselements.3.1.43.

Gower, C.F. (1985). Correlations between the Grenville Province and Sveconorwegian Orogenic Belt — Implications for Proterozoic Evolution of the Southern Margins

of the Canadian and Baltic Shields. *The Deep Proterozoic Crust in the North Atlantic Provinces*, 247–257. doi:10.1007/978-94-009-5450-2_15.

Gower, C.F. (1994). Distribution of pre-1400 Ma crust in the Grenville province: Implications for rifting in Laurentia-Baltica during geon 14. *Geology*, 22, 827-830.

Gower, C.F. (1996a). The evolution of the Grenville Province in eastern Labrador, Canada. *Geological Society London Special Publications*, 112(1), 197-218. doi: 10.1144/GSL.SP.1996.112.01.11

Gower, C.F. (1996b). Geology of the southeast Mealy Mountains Region, Grenville Province, Southeast Labrador. *Current Research, Newfoundland and Labrador Department of Natural Resources*. 96-1, 55-71.

Gower, C.F. (2003). Geological map of the Grenville Province in eastern Labrador. *Newfoundland and Labrador Department of Mines and Energy, Geological Survey, Map 2003-11*. Open file: LAB/1379.

Gower, C.F. (2005). Kinematic evidence for terrane displacements in the Grenville province. *Current Research, Newfoundland and Labrador Department of Natural Resources*. Report 05-01, pp. 73-92.

Gower, C. F. (2007). Protolith recognition of metamorphosed felsic volcanic/volcaniclastic rocks, with special reference to the Grenville Province in

- southeast Labrador. *Current Research. Newfoundland and Labrador Department of Natural Resources*. Report 07-01, pp. 11-23.
- Gower, C.F. (2009). Battle Island – A geological treasure in coastal eastern Labrador. Government of Newfoundland and Labrador, Department of Natural Resources, Geological Survey, Open File 003D/05/0031, 38 pages.
- Gower, C., & Owen, V. (1984). Pre-Grenvillian and Grenvillian lithotectonic regions in eastern Labrador-correlations with the Sveconorwegian Orogenic Belt in Sweden. *Canadian Journal of Earth Sciences*, 21(6), 678–693.
- Gower, C.F., Neuland, S., Newman, M., Smyth, J., 1987: Geology of the Port Hope Simpson map region, Grenville province, eastern Labrador, *Current Research (1987) Newfoundland Department of Mines and Energy, Mineral Development Division*, Report 87-1, 183-199.
- Gower, C. F., & Erdmer, P. (1988). Proterozoic metamorphism in the Grenville Province: a study in the Double Mer-Lake Melville area, eastern Labrador. *Canadian Journal of Earth Sciences*, 25(11), 1895–1905.
- Gower, C., Schärer, U., & Heaman, L. (1992). The Labradorian orogeny in the Grenville Province, eastern Labrador, Canada. *Canadian Journal of Earth Sciences*, 29(9), 1944–1957.
- Gower, C.F., van Nostrand, T. (1994). Geology of the Pinware River Region, southeast Labrador. *Current Research, Newfoundland and Labrador Department of Natural Resources*. 94-1, 347-369.

Gower, C., Hall, J., Kilfoil, G., Quinlan, G., & Wardle, R. (1997). Roots of the Labradorian orogen in the Grenville Province in southeast Labrador: Evidence from marine, deep-seismic reflection data. *Tectonics*, 16(5), 795–809.

Gower, C., & Krogh, T. (2002). A U–Pb geochronological review of the Proterozoic history of the eastern Grenville Province. *Canadian Journal of Earth Sciences*, 39(5), 795–829. doi: 10.1139/E01-090

Gower, C., Kamo, S., & Krogh, T. (2008a). Indenter tectonism in the eastern Grenville Province. *Precambrian Research*, 167(1-2), 201–212.

Gower, C., Kamo, S., Kwok, K., & Krogh, T. (2008b). Proterozoic southward accretion and Grenvillian orogenesis in the interior Grenville Province in eastern Labrador: Evidence from U-Pb geochronological investigations. *Precambrian Research*, 165(1-2), 61–95.

Hanmer, S., and Scott, D.J. (1990). Structural observations in the Gilbert River belt, Grenville Province, southeastern Labrador. *Current research, part C. Geological Survey of Canada*. Paper 90-1C, 1- 11.

Hanmer, S., Corrigan, D., Pehrsson, S., & Nadeau, L. (2000). SW Grenville Province, Canada: the case against post-1.4 Ga accretionary tectonics. *Tectonophysics*, 319(1), 33–51.

Heaman, L., Gower, C., & Perreault, S. (2004). The timing of Proterozoic magmatism in the Pinware terrane of southeast Labrador, easternmost Quebec and northwest Newfoundland. *Canadian Journal of Earth Sciences*, 41(2), 127–150.
doi:10.1139/e03-088.

- Hill, J.D., and Miller, R.R. 1990. A review of Middle Proterozoic epigenic felsic magmatism in Labrador. *In* Mid-Proterozoic Laurentia–Baltica. Edited by C.F. Gower, T. Rivers, and A.B. Ryan. Geological Association of Canada, Special Paper 38, pp. 417–431.
- Hoffman, P.F. (1989). Precambrian geology and tectonic history of North America. *In* The Geology of North America: an Overview. Geological Society of America, Boulder, Colo., The Geology of North America, Vol. A., pp. 447–512.
- Hoskin, P., & Schaltegger, U. (2003). The composition of zircon and igneous and metamorphic petrogenesis. *Reviews in Mineralogy and Geochemistry*, 53(1), 27.
- Hynes, A., & Rivers, T. (2010). Protracted continental collision-evidence from the Grenville Orogen. *Canadian Journal of Earth Sciences*, 47(5), 591–620.
- Kamo, S., Wasteneys, H., Gower, C., & Krogh, T. (1996). U-Pb geochronology of Labradorian and later events in the Grenville Province, eastern Labrador. *Precambrian Research*, 80(3-4), 239–260.
- Kamo, S. L., Heaman, L. M., & Gower, C. F. (2011). Evidence for post-1200 Ma — pre-Grenvillian supracrustal rocks in the Pinware terrane, eastern Grenville Province at Battle Harbour, Labrador. This article is one of a series of papers published in this Special Issue on the theme of Geochronology in honour of Tom Krogh. *Canadian Journal of Earth Sciences*, 48(2), 371–387. doi:10.1139/E10-052.
- Košler, J., & Sylvester, P. J. (2003). Present Trends and the Future of Zircon in Geochronology: Laser Ablation ICPMS. *Reviews in mineralogy and geochemistry*, 53(1), 243-275.

- Košler J., Forst L, Slama J. (2008). LAMDATE and LAMTOOL: Spreadsheet-based data reduction for laser ablation-ICPMS. In: Sylvester PJ (ed) Laser Ablation ICP-MS in the Earth Sciences: Current Practices and Outstanding Issues, Mineralogical Association of Canada p. 315-317.
- Krogh, T. E. (1973). A low-contamination method for hydrothermal decomposition of zircon and extraction of U and Pb for isotopic age determinations. *Geochimica et Cosmochimica Acta*, 37(3), 485–494.
- Krogh, T. E. (1982). Improved accuracy of U-Pb zircon ages by the creation of more concordant systems using an air abrasion technique. *Geochimica et Cosmochimica Acta*, 46, 637-649.
- Krogh, T.E., Corfu, F., Davis, D.W., Dunning, G.R., Heaman, L.M., Kamo, S.L., Machado, N, Greenough, J.D., and Nakamura, E. 1987. Precise U–Pb isotopic ages of diabase dykes and mafic to ultramafic rocks using trace amounts of baddeleyite and zircon. In Mafic dyke swarms. Edited by H.C. Halls and W.F. Fahrig. Geological Association of Canada, Special Paper 34, pp. 147–152.
- Ludwig K. R. (2008) Isoplot 3.6; A Geochronology Toolkit for Microsoft Excel. Berkeley Geochronology Center, pp. 77.
- Lumbers, S.B., Heaman, L.M., Vertolli, V.M., and Wu, T-W. 1990. Nature and timing of Middle Proterozoic magmatism in the Central Metasedimentary Belt, Grenville Province, Ontario. In Mid-Proterozoic Laurentia–Baltica. Edited by C.F. Gower, T. Rivers, and A.B. Ryan. Geological Association of Canada, Special Paper 38, pp. 243–276.

- Mattinson, J. M. (2005). Zircon U–Pb chemical abrasion (“CA-TIMS”) method: Combined annealing and multi-step partial dissolution analysis for improved precision and accuracy of zircon ages. *Chemical Geology*, 220(1-2), 47–66. doi:10.1016/j.chemgeo.2005.03.011.
- McLellan, J. M., & Chiarenzelli, J. (1990). Isotopic constraints on emplacement age of anorthositic rocks of the Marcy masiff, Adirondack Mts., New York. *The Journal of Geology*, 19–41.
- McLellan, J., & Daly, J.S., McLellan, J.M. (1996). The Grenville orogenic cycle (ca. 1350-1000 Ma): an Adirondack perspective. *Tectonophysics*, 265, 1-28.
- Miller, R. R., Heaman, L. M., & Birkett, T. C. (1997). U-Pb zircon age of the Strange Lake peralkaline complex: implications for Mesoproterozoic peralkaline magmatism in north-central Labrador. *Precambrian Research*, 81(1), 67–82.
- Plyusnin, G. S. (1969): Color of amazonites. *Zapiski Vsesoyuznogo Mineralogicheskogo Obshchestva*, 98, 3-17 (in Russian).
- Pope, D.C., and Willett, S.D. 1998. Thermal-mechanical model for crustal thickening in the central Andes driven by ablative subduction. *Geology*, 26: 511–514.
- Rivers, T. (1997). Lithotectonic elements of the Grenville Province: review and tectonic implications. *Precambrian Research*, 86(3-4), 117–154.
- Rivers, T., Ketchum, J., Indares, A., & Hynes, A. (2002). The High Pressure belt in the Grenville Province: architecture, timing, and exhumation. *Canadian Journal of Earth Sciences*, 39(5), 867–893. doi:10.1139/e02-025
- Rivers, T. (2008). Assembly and preservation of lower, mid, and upper orogenic crust in the Grenville Province--Implications for the evolution of large hot long-duration

- orogens. *Precambrian Research*, 167(3-4), 237–259.
doi:10.1016/j.precamres.2008.08.005.
- Rivers, T. (2009). The Grenville Province as a large hot long-duration collisional orogen - insights from the spatial and thermal evolution of its orogenic fronts. *Geological Society London Special Publications*, 327(1), 405–444. doi:10.1144/SP327.17.
- Rivers, T., & Corrigan, D. (2000). Convergent margin on southeastern Laurentia during the Mesoproterozoic: tectonic implications. *Canadian Journal of Earth Sciences*, 37(2-3), 359–383.
- Rivers, T., Ketchum, J., Indares, A., & Hynes, A. (2002). The High Pressure belt in the Grenville Province: architecture, timing, and exhumation. *Canadian Journal of Earth Sciences*, 39(5), 867–893. doi:10.1139/e02-025.
- Romer, R., Schärer, U., Wardle, R., & Wilton, D. (1995). U-Pb age of the Seal Lake Group, Labrador: relationship to Mesoproterozoic extension-related magmatism of Laurasia. *Canadian Journal of Earth Sciences*, 32(9), 1401–1410.
- Royden, L. H. (1993). Evolution of retreating subduction boundaries formed during continental collision. *Tectonics*, 12(3), 629. doi:10.1029/92TC02641.
- Ryan, B. (1991). Makhavinekh Lake pluton, Labrador, Canada: geological setting, subdivisions, mode of emplacement, and a comparison with Finnish rapakivi granites. *Precambrian Research*, 51(1-4), 193-225.
- Sager-Kinsman, E. A., & Parrish, R. R. (1993). Geochronology of detrital zircons from

- the Elzevir and Frontenac terranes, Central Metasedimentary Belt, Grenville Province, Ontario. *Canadian Journal of Earth Sciences*, 30(3), 465–473.
- Sánchez-García, T., Quesada, C., Bellido, F., & Dunning, G. R. (2008). Two-step magma flooding of the upper crust during rifting: The Early Paleozoic of the Ossa Morena Zone (SW Iberia). *Tectonophysics*, 461, 72-90.
doi:10.1016/j.tecto.2008.03.006.
- Schärer, U., & Krogh, T. (1986). Age and evolution of the Grenville Province in eastern Labrador from U-Pb systematics in accessory minerals. *Contributions to Mineralogy and Petrology*. (94), 438-451.
- Schärer, U., & Gower, C. (1988). Crustal evolution in eastern Labrador: Constraints from precise U-Pb ages. *Precambrian Research*, 38(4), 405–421.
- Scott, D., Machado, N., Hanmer, S., & Gariépy, C. (1993). Dating ductile deformation using U-Pb geochronology: examples from the Gilbert River Belt, Grenville Province, Labrador, Canada. *Canadian Journal of Earth Sciences*, 30(7), 1458–1469.
- Shand, S.J. (1927). On the relations between silica, alumina, and the bases in eruptive rocks, considered as a means of classification. *Geological Magazine*, (64), 446–446.
- Shand, S. J. (1951). *Eruptive Rocks*. New York: J. Wiley.
- Slama J., Košler J., Condon D.J., Crowley J.L., Gerdes A., Hanchar J.M., Horstwood

- M.S.A., Morris G.A., Nasdala L., Norberg N., Schaltegger U., Schoene B., Tubrett M.N., Whitehouse M.J. (2008). Plesovice zircon – a new natural reference material for U-Pb and Hf isotopic microanalysis. *Chemical Geology* (249), 1-35.
- Srivastava, R.M., Gauthier, J. (2012). Technical Report on the Foxtrot Deposit in Newfoundland and Labrador, Canada. NI-43-101 Report.
- Stacey, J.S., Kramers, J.D. (1975). Approximation of terrestrial lead isotope evolution by a two-stage model, *Earth and Planetary Science Letters*, (26), 207-221.
- Sylvester, P. J., & Ghaderi, M. (1997). ScienceDirect.com - Chemical Geology - Trace element analysis of scheelite by excimer laser ablation-inductively coupled plasma-mass spectrometry (ELA-ICP-MS) using a synthetic silicate glass standard. *Chemical Geology*, 141, 49-65.
- Szuzkiewicz, A. & Körber, T. (2010): "Amazonit" oder "Grüner Mikroklin" Zur Ursache der Grünfärbung von Kalifeldspäten aus dem Striegauer Granit. *Lapis* 35 (7-8), 75-77; 86. (in German).
- Tohver, E., Bettencourt, J. S., Tosdal, R., Mezger, K., Leite, W. B., & Payolla, B. L. (2004). Terrane transfer during the Grenville orogeny: tracing the Amazonian ancestry of southern Appalachian basement through Pb and Nd isotopes. *Earth and Planetary Science Letters*, 228(1), 161–176.

- Tohver, E., Teixeira, W., van der Pluijm, B., Geraldes, M. C., Bettencourt, J. S., & Rizzotto, G. (2006). Restored transect across the exhumed Grenville orogen of Laurentia and Amazonia, with implications for crustal architecture. *Geology*, 34(8), 669. doi:10.1130/G22534.1.
- Tucker, R., & Gower, C. (1994). A U-Pb geochronological framework for the Pinware terrane, Grenville Province, southeast Labrador. *The Journal of Geology*, 102(1), 67–78.
- Uyeda, S., & Kanamori, H. (1979). Back-arc opening and the mode of subduction. *J. geophys. Res.*, 84(3), 1049–1061.
- Van Breemen, O., and Corriveau, L. (2005). U-Pb age constraints on arenaceous and volcanic rocks of the Wakeham Group, eastern Grenville Province. *Canadian Journal of Earth Sciences*, 42(10), 1677–1697. doi:10.1139/e05-079.
- Van Nostrand, T., Dunphy, D., Eddy, D. (1992). Geology of the Alexis River map region, Grenville Province, southeastern Labrador. *Current Research, Newfoundland and Labrador Department of Mines and Energy, Geological Survey Branch*. 92-1, 399-412.
- Waschbusch, P., & Beaumont, C. (1996). Effect of a retreating subduction zone on deformation in simple regions of plate convergence. *J. geophys. Res.*, 101(B12), 28133. doi:10.1029/96JB02482.
- Wasteneys, H., Kamo, S., Moser, D., Krogh, T., Gower, C., & Owen, J. (1997). U-Pb geochronological constraints on the geological evolution of the Pinware terrane and adjacent areas, Grenville Province, southeast Labrador, Canada. *Precambrian Research*, 81(1-2), 101–128.

Wiedenback M., Alle P., Corfu F. (1995). Three natural zircon standards for U-Th-Pb,
Lu-Hf, trace element and REE analyses. Geostandards Newsletter 19: 1-23

CHAPTER 3 THE 1.3 Ga BIMODAL REE-ENRICHED FOX HARBOUR VOLCANIC BELTS: A STUDY OF THE LITHGEOCHEMICAL, MINERALOGICAL, AND ISOTOPIC CHARACTERISTICS

James T. Haley¹, Paul J. Sylvester¹, Randy R. Miller²

¹*Department of Earth Sciences, Memorial University, St. John's, NL, Canada,*

A1B 3X5

²*Search Minerals Inc., Toronto, ON, Canada, M5H 3B7*

E-mail: jhaley@mun.ca

ABSTRACT

The 1.3 Ga Fox Harbour volcanic packages contain a variety of supracrustal, and syn-supracrustal intrusive rocks. Geochemically, the rhyolites are peralkaline, and are further classified as pantellerites or comendites based on major element geochemistry. Rhyolitic major elements appear to have behaved largely immobile during metamorphism, generally decreasing with increasing SiO₂, with the exception of elements Na₂O, K₂O, and Al₂O₃, which display scatter throughout the Fox Harbour area, but could be due to primary hydrothermal activity after deposition, often seen in volcanic systems. Trace elements are also shown to be immobile, via utilizing a simple immobile vs immobile element plot. Electron probe microanalysis (EPMA) of the yttrium-niobate

mineral, initially analyzed using the SEM-MLA, is in fact fergusonite, and that REE are major elements in the structure, forming ~20-29 wt.% of the mineral. EPMA analysis of zircon reveals that the majority of the zircon grains show little compositional variation, except for a 1.05 Ga microporous zircon population that contains higher amounts of HFSE (U, Th, Nb, Ta, Y, Dy, Gd). *In-situ* Lu-Hf measurements reveal that the 1.3 Ga zircon grains have $\epsilon\text{Hf}(t)$ values between -0.65 to $+7.59$, and 1.05 Ga zircon have $\epsilon\text{Hf}(t)$ ranging between $+0.62$ to -4.21 . These findings suggest that the Fox Harbour volcanic packages were derived by partial melting of 1.9-1.5 Ga felsic crustal sources, and there was no flux of REE into or out of the packages during Grenvillian metamorphism.

3-1 INTRODUCTION

The *ca.* 1300 Ma Fox Harbour bimodal, basalt-rhyolite volcanic package, located in the northern Grenville Province of Labrador, Canada, was discovered during the 2010 mineral exploration season of Search Minerals Inc. (Delaney and Haley, 2013; *unpublished*). The volcanic units were initially studied and sampled by Search Minerals while looking for rare earth element (REE) mineralization. This package was intensely deformed, and metamorphosed during the Grenville Orogeny, a continental-scale collision, around 1050 Ma (Kamo et al., 2011; Haley et al., 2013).

A very large number (~10,000) of whole rock samples (hand, channel, and diamond drill hole samples) were collected throughout the Fox Harbour property by Search Minerals and analyzed for lithogeochemistry. In this paper, a small representative

subset of the lithogeochemistry of the ~10,000 samples is integrated with previous U-Pb zircon geochronology (Haley et al., 2013) of the rocks, and *in-situ* analyses of hafnium (Hf) isotopes of the zircon. The data are used to improve the understanding of the tectonic setting (Haley et al. 2013) and petrogenesis of the volcanism, and origin of the REE mineralization. Preliminary examination of the rocks using a scanning electron microscope (SEM) suggested that the main carrier of heavy REEs in the rocks is a yttrium-niobate mineral thought to be fergusonite (YNbO_4), and allanite. However, many minerals such as samarskite, euxenite, and pyrochlore, have compositions and physical properties similar to fergusonite, so electron microprobe analyses were used to investigate the REE mineralogy further.

3-2 GEOLOGICAL SETTING

The Grenville Province in Labrador generally consists of medium- to high- grade rocks (Gower, 1996; Rivers, 1997, 2002, 2008, and 2009). The Fox Harbour bimodal volcanic package is located adjacent to the towns of St. Lewis and Port Hope Simpson, Labrador. This area is known to contain three separate terranes (Lake Melville, Mealy Mountain, and Pinware terranes, as seen in Figure 3-1), which are distinguished by differing lithologies, structures, metamorphic facies, along with distinctive crystallization and metamorphic ages (Gower and Owen, 1984; Schärer and Krogh, 1986; Schärer and Gower, 1988; Gower et al., 1992; Scott et al., 1993; Tucker and Gower, 1994; Gower, 1994, 1996a, 1996b,, 2005, 2009; Gower et al., 1997; Kamo et al., 1996, 2011; Wasteneys et al. 1997; Rivers, 1997). The Fox Harbour volcanic package has not been

assigned to one of these terranes, as it lies in an area where the terranes are amalgamated (Figure 3-2) and highly deformed (Haley et al., 2013).

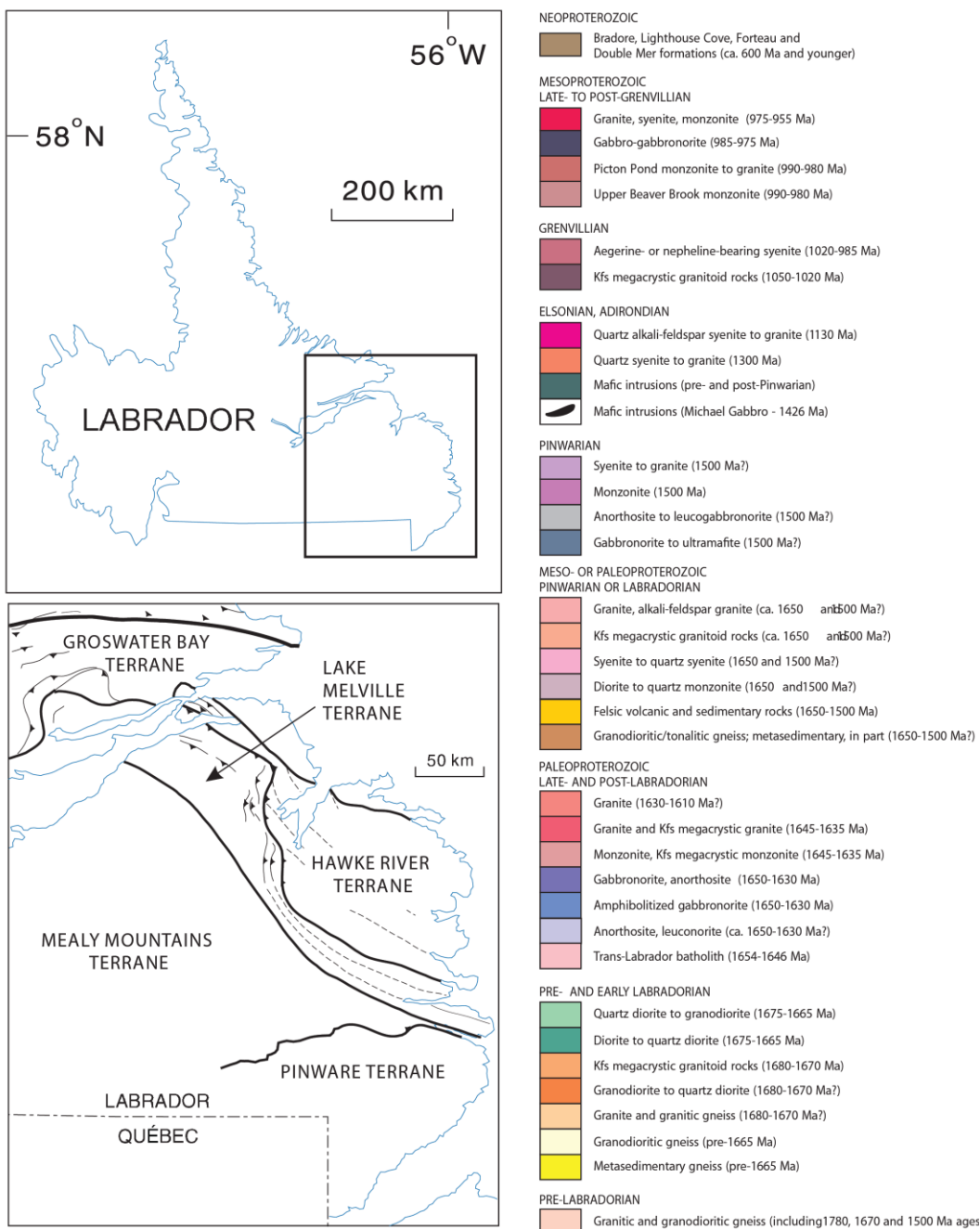


Figure 3-1: Generalized geological map of Labrador. Upper left inset depicts area drawn in the following figure, and lower left inset depicts lithotectonic terranes located in eastern Labrador (Gower, 2003).

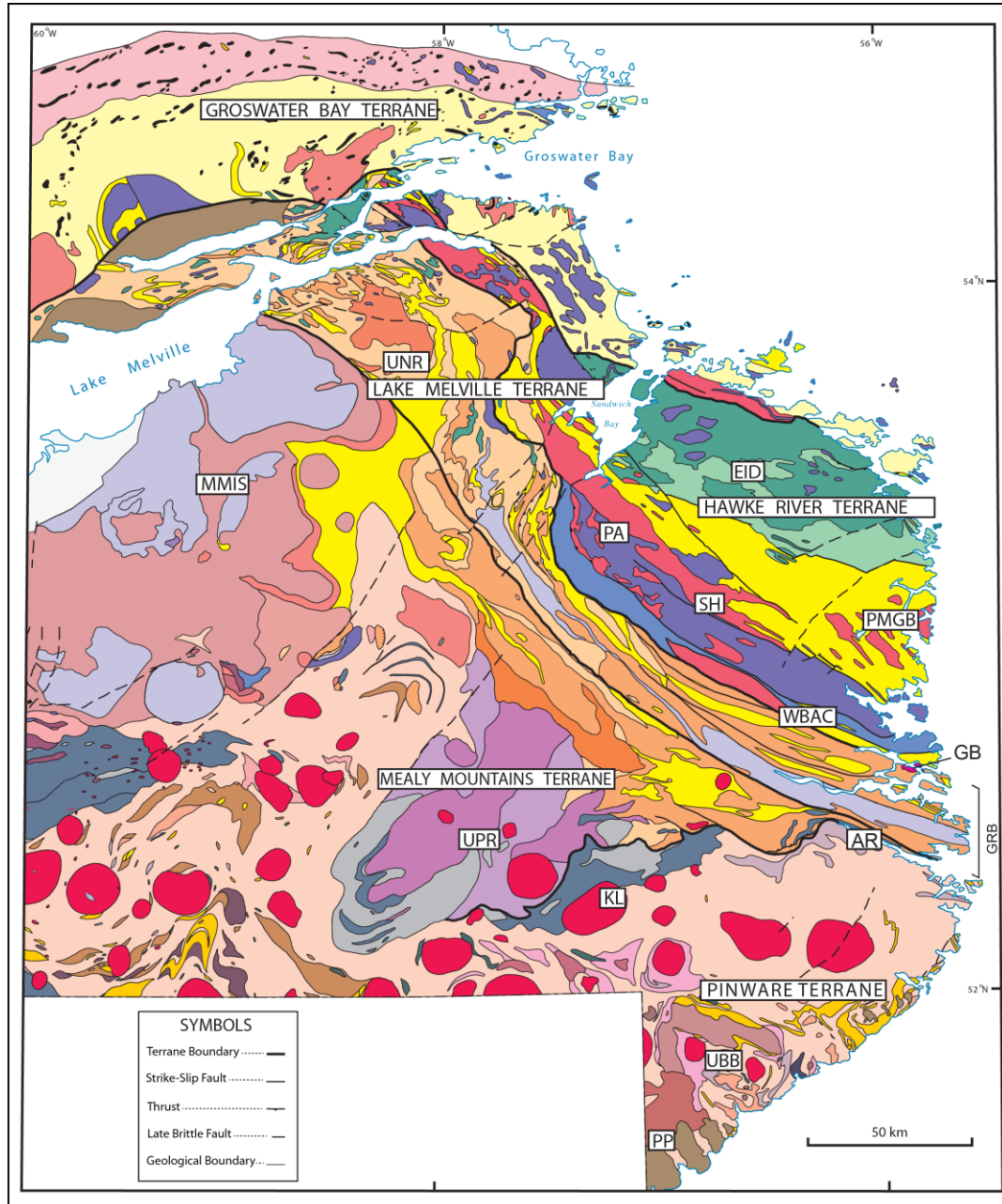


Figure 3-2: Geological map of the Grenville Province in eastern Labrador. Localities legend: AR - Alexis River anorthosite; EID - Earl Island domain; GB - Gilbert Bay pluton; GRB - Gilbert River belt; KL - Kyfanan Lake layered mafic intrusion; MMIS - Mealy Mountains Intrusive Suite; PA - Paradise Arm pluton; PMGB - Paradise metasedimentary gneiss belt; PP - Picton Pond pluton; SH - Sand Hill Big Pond gabbronorite; UBB - Upper Beaver Brook pluton; UNR - Upper North River pluton; UPR - Upper Paradise River pluton; WBAC - White Bear Arm complex (Gower, 2003).

The Fox Harbour area consists of three steeply dipping volcanic belts (Road, MT, and South Belt; seen in Figure 3-3). These volcanic belts are believed to have formed in an extensional crustal environment, at 1300 Ma, based on geological relationships and *in-situ* LA-ICPMS (laser ablation inductively coupled mass spectrometer), and CA-TIMS (chemical abrasion thermal ionization mass spectrometry) U-Pb dating of magmatic zircon (Haley et al., 2013). This package was then metamorphosed to amphibolite-facies during the Grenvillian Orogeny (1050 Ma), based on mineral assemblages and textures and U-Pb ages of hydrothermal-metamorphic zircon (Haley et al., 2013; Kamo et al., 2011).

It is believed that between 1.5 to 1.3 Ga, a continental-margin arc existed along the Laurentian margin (Tucker and Gower, 1994; Corrigan, 1995; Corrigan and Hanmer, 1995; McLelland et al., 1996; Rivers and Corrigan, 2000; Davidson, 2008; Hynes and Rivers, 2010, Kamo et al., 2011). The Grenville Province contains many occurrences of rift-related rocks, suggesting that the area was subjected to both compressional and extensional architecture.

Continental rifts often contain large amounts mafic rocks, along with less voluminous rhyolite packages, which are often peralkaline (White and McKenzie, 1989). Different models exist for their formation, such as (1) deep fractional crystallization of mantle magmas in intermediate crustal magmatic chambers (Kovalenko, 1977; Litvinovsky et al., 1996; Yarmolyuk et al., 2001; Vorontsov et al., 2004; Barberi et al., 1975; Civetta et al., 1998; Peccerillo et al., 2003); (2) anatetic melting of crustal rocks triggered by the heat of basic magmas (Davies and Macdonald, 1987); (3) partial melting

of basic rocks at the crustal base with the subsequent crystallization differentiation of obtained melts (Trua et al., 1999).

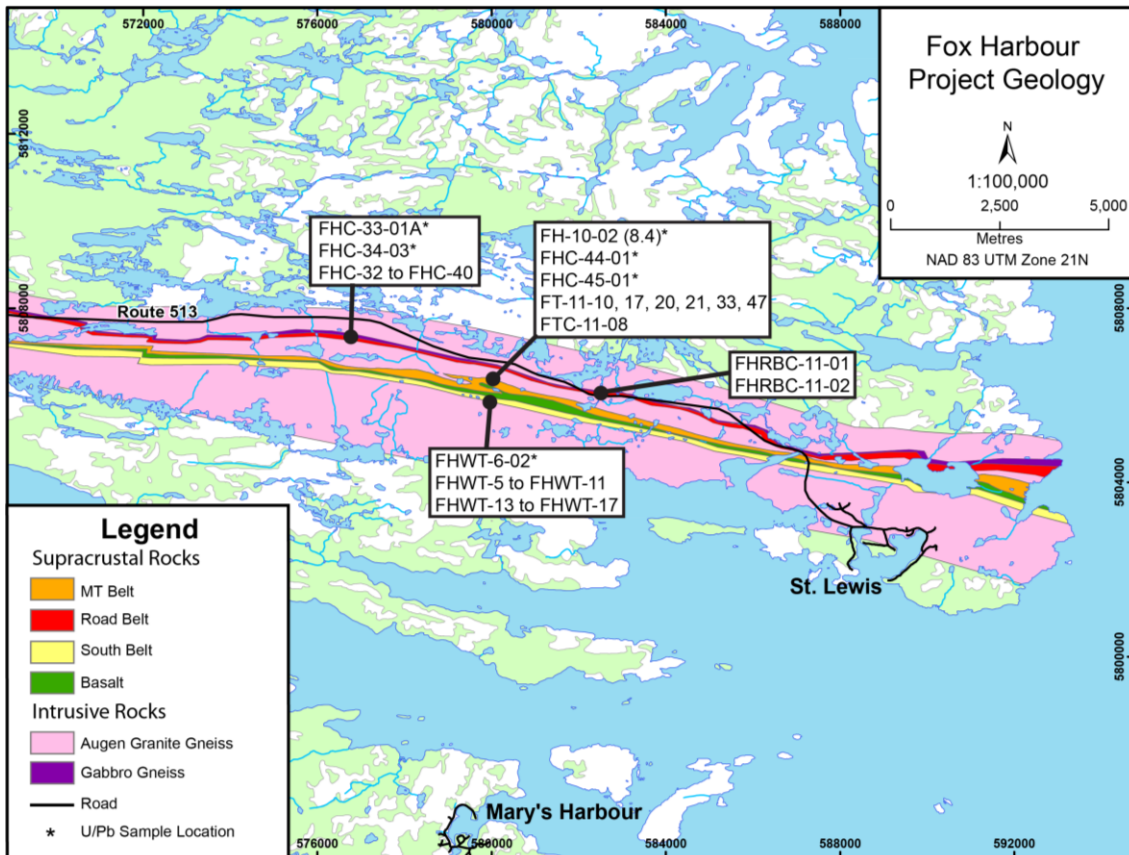


Figure 3-3: Fox Harbour geology, depicting three volcanic belts mapped and sampled. Sample locations are depicted. Due to the required scale of this map, the South Belt, and MT Belt appear to be touching, but that is not the case. Granitic augen gneiss separates these two belts along its entirety. Note: * depicts U-Pb and Hf sample location.

3-3 LOCAL GEOLOGY

3-3-1 SOUTH BELT

The South Belt is the most southern belt in the Fox Harbour area (Figure 3-3), and contains the thickest package of rhyolitic, and basaltic rocks (Haley et al., 2013). The rhyolite package is approximately 50-100 m in thickness, whereas the basaltic rocks are consistently 50-100 m for approximately 10 km (Haley et al., 2013). Rock types within the belt consist of highly deformed rhyolite (comendite, and pantellerite), basalt, quartzite, a discordant mafic sill, and an unmineralized rhyolite or aplite intrusion (Haley et al., 2013). The rhyolitic units have an extremely homogenous appearance on surface, weathering to a sandy material and are pink to grey in color (Haley et al., 2013). Mineralogy is dominated by orthoclase, albite, and quartz, with minor mineralogy consisting of biotite, magnetite, allanite, fluorite, chlorite and zircon (Haley et al., 2013).

3-3-2 MT BELT

The MT Belt is the central belt in the Fox Harbour area, and currently contains the most prospective occurrence of REE mineralization, termed the Foxtrot Deposit (Haley et al., 2013). Much like the South Belt, the lithological units within the belt range from rhyolite (comendite and pantellerite), basalt, quartzite, but also contains other units such as volcaniclastic/metasedimentary units, discordant mafic dyke/sills, and granitic dykes/sills. These units have been mapped to 1:10,000 at the surface (Figure 3-4), and have been traced to a depth of 500 m by diamond drill holes. As a result of the

exploration for REE, individual rhyolitic units have been identified via stratigraphic location, textures, and geochemistry.

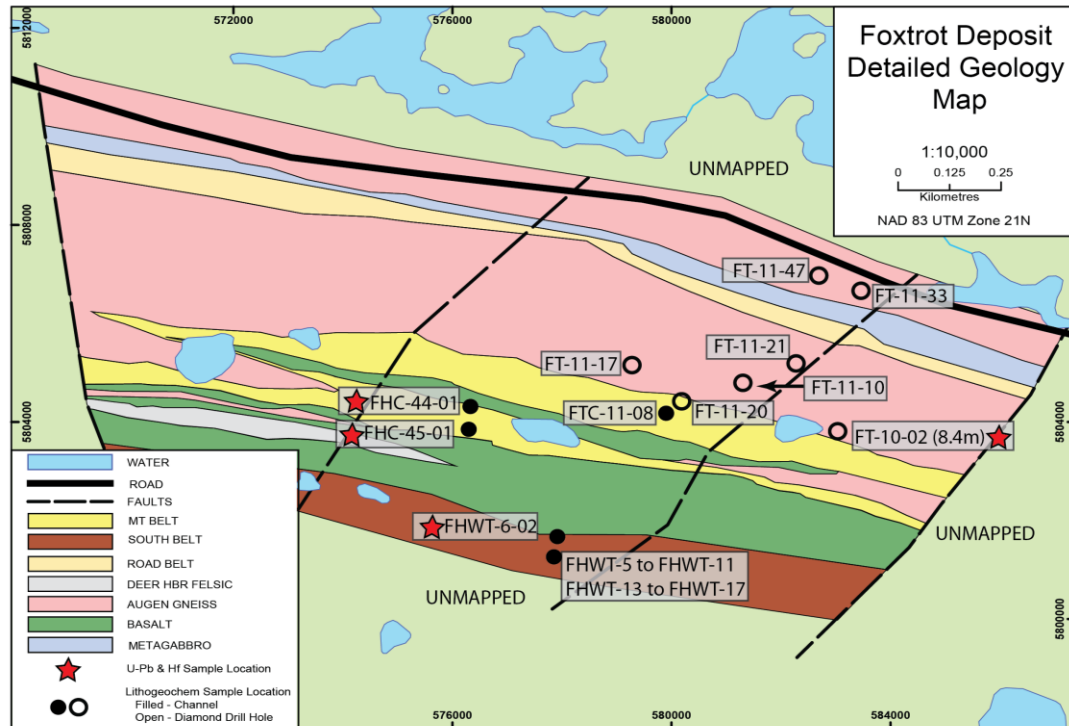


Figure 3-4: Geology map of the Foxtrot Deposit (MT Belt), along with the extent of the Road Belt and South Belt around the Foxtrot Deposit. U-Pb and Hf sample locations are indicated by red stars. Lithogeochemistry samples are indicated by either filled black circles (channel sample locations), or open black circles (diamond drill hole locations).

Rhyolitic unit names in the Foxtrot Deposit are as follows: FT2, FT2x, FT3, FT3b, FT4, FT5, and FTBuff (Figure 3-5). FT2 is the largest occurrence of rhyolite in the Foxtrot Deposit, and occurs as two 30-40 m sections separated by a 5-10 m thick unit of basalt. FT2 is characterized by its amphibole content, and slightly coarser grained nature. It is not considered prospective for REE mineralization, but is anomalous. FT2x occurs at

the bottom of FT2, and is characterized largely by its mineralogy and observed textures. FT2x contains “buck shot” equigranular magnetite grains (0.5-3 mm), along with Na-amphibole and Na-pyroxene which are extremely skeletal and observed reacting to magnetite and K-feldspar. FT3 is the most prospective rhyolite unit in the Foxtrot Deposit, and ranges in thickness from 4-27 m. FT3 is discerned from adjacent units largely by the occurrence of amazonite pods/blebs, which are thought to be migmatitic melts (Haley et al., 2013). FT3 is extremely fine-grained, and is green to grey in color. FT3b contains lesser amounts of amazonite, and less prospective for REE. FT4 contains amazonite, but is less prevalent in this unit. FT5 is a unit bound by basaltic unit approximately 10-15 m below the main rhyolite volcanic stratigraphy. FT5, unlike other rhyolite units in the area contains a lot of muscovite, which is not observed as readily in other units. FTBuff is a discordant microgranite/aplite intrusion, located largely in rhyolite units FT3b and FT4.

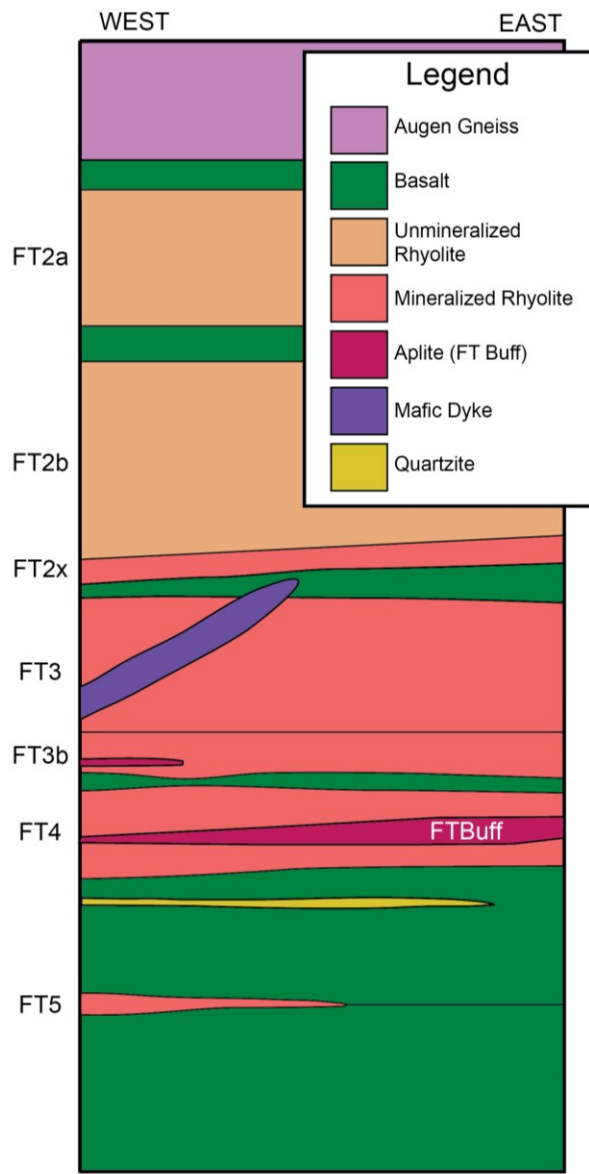


Figure 3-5: Stratigraphy observed in the Foxtrot Deposit.

3-3-3 ROAD BELT

The Road Belt is the most northern belt in the Fox Harbour area (Figure 3-3, and 3-4). The belt contains similar units to those found in the MT Belt, but appears to have undergone a greater amount of deformation (Haley et al., 2013).

The Road Belt is approximately 10-50 m across much of the strike, except for at the extreme east adjacent to the town of St. Lewis. In this area the belt is thickened, likely due to folding, and/or primary stratigraphic thickness. The Road Belt contains an amazonite-bearing unit, similar to that seen in the Foxtrot Deposit, suggesting a genetic link. Rock types consist of highly deformed rhyolite (comendite, pantellerite), basalt, and an aplitic/microgranite intrusion, much like the unit FTBuff, found in the Foxtrot Deposit, of the MT Belt.

3-4 ANALYTICAL TECHNIQUES

3-4-1 LITHOGEOCHEMICAL SAMPLING FROM CHANNEL SAMPLES AND DIAMOND DRILL CORE

All lithogeochemical samples discussed in this study have been taken from surficial exposures (i.e., channel sampled) and diamond drill core. Due to the steeply dipping ($60\text{--}75^\circ$) nature of the volcanic belts in the Fox Harbour area, channel sampling the surficial outcrop is effectively a horizontal diamond drill hole. This allows for the detailed stratigraphic interpretation and correlation of units at depth, discussed earlier in section 3.2.

Channel samples are 10 cm deep by 8 cm wide, and were cut using a gas-powered diamond saw from cleared outcrops. Each channel is cut into two vertical sections, similar to drill core, with a 6 cm thick section (weathering removed) being sent out for assay. A 2 cm thick section is stored in channel boxes for reference and to provide due diligence/verification samples. The channels are cut perpendicular to strike, pieced

together, logged, and photographed to produce geological and geochemical sections.

These channel samples, or horizontal drill holes, produce the same data as vertical diamond drill holes, except the data are from horizontal geological sections and the collected sample is 6 to 8 times bigger than NQ drill core.

Diamond drill holes (NQ drill core size, 47.6mm inside diameter) were designed to intersect mineralization across the strike of the Foxtrot Deposit, at depths of 50, 100, 150, 200, 250, 300, 350, 400, and 450 m. The diamond drill holes used in this study are FT-11-10, FT-11-17, FT-11-20, and FT-11-21 (Figure 3-4). Diamond drill hole FT-11-21 is the representative drill hole for the Foxtrot Deposit, with supplemental data from FT-11-17/20.

Diamond drill holes were logged according to company procedures, similar to channel sample logging. Drill core was then cut in half using a diamond bladed circular saw. Half of the core is kept for due-diligence purposes, and the other half is sent away for lithogeochemical analysis. Sample lengths tend to less than or equal to 1.0 m, while inducing as little lithological mixing as possible.

3-4-2 LITHOGEOCHEMICAL ANALYSIS

Lithogeochemical samples were crushed at Activation Laboratories Ltd., located in Goose Bay, Labrador. Samples were initially crushed 80%-mesh and riffled to produce a representative sample. This sample is then pulverized to 95%-200 mesh with the pulverizing mills being cleaned after every sample with cleaning sand. Samples were then transported to the Activation Laboratories (ActLabs) Ltd. analytical facility in Ancaster,

Ontario. A representative sample is treated by a lithium metaborate/tetraborate fusion and then analyzed by inductively coupled plasma/optical emission spectroscopy (ICP/OES) and mass spectrometry (ICP/MS). Mass balance is carried out as an additional quality control technique, and elemental totals of the oxides should be between 98.5% and 101%. For QA/QC purposes Search Minerals Inc. requires duplicates every 25 samples and two Search Minerals reproducibility standards every 50 samples. ActLabs analyses duplicates and splits approximately every 15 samples and also analyses 29 measured standards for QA/QC. ActLabs is an ISO/IEC 17025 accredited laboratory.

3-4-3 ELECTRON MICROPROBE ANALYSIS OF ZIRCON AND FERGUSONITE

Grains of zircon and the yttrium-niobate mineral thought to be fergusonite were located in polished thin sections using a FEI Quanta 650 field emission scanning electron microscope – mineral liberation analyzer (SEM-MLA) at Memorial University, St. John's, NL (Sylvester, 2012). The instrument is equipped with automated software for backscattered electron (BSE) imaging and energy dispersive X-ray (EDX) analysis. Rare earth element minerals in REE-enriched pegmatites, and A- to I-type granites/rhyolites commonly contain members of fergusonite, samarskite, euxenite, and pyrochlore groups (Ecrit, 2005). These minerals have the general chemical formula (Y, REE, U, Th)-(Nb, Ta, Ti) oxide.

A JXA JEOL-8900L electron probe micro-analyzer (EPMA) at McGill University, Montreal, Quebec, was utilized to determine the identity of the yttrium-niobate grains in polished sections of two samples. Zircon grains were also analyzed on

the EPMA to determine if magmatic and hydrothermal-metamorphic zircon had variable compositions associated with primary igneous crystallization and post-crystallization dissolution and re-precipitation. The analysed areas of the minerals were homogeneous in BSE images and free from inclusions, pore space and surface contamination. Operating conditions included a beam of 5 µm diameter, 20 kV accelerating voltage, and 20 nA beam current. Calibration standards and count times were: Ta ($K_2Ta_2O_6$, 100s); Na ($Na_2Nb_2O_6$, 20s); Ca (Diopside, 20s); Y (Y garnet, 20s); Fe (Fe_2O_3 , 20s); Eu (MAC_Eu, 100s); Si (Zircon, 20s); Ti (TiO_2 , 20s); Nb ($Na_2Nb_2O_6$, 20s); Mn (Spessartine, 20s); Er (MAC-Er, 50s); Pb (Vanadinite, 100s); Zr (Zircon, 20s); Ce (MAC-Ce, 50s); Th (ThO_2 , 100s); U (UO_2 , 100s); La (MAC-La, 50s); Nd (MAC-Nd, 100s); Pr (MAC-Pr, 100s); Dy (MAC-Dy, 50s); Sm (MAC-Sm, 50s); Gd (MAC-Gd, 50s); Yb (MAC-Yb, 50s); Hf (Zircon, 100s).

3-4-4 IN-SITU LUTETIUM-HAFNIUM ISOTOPE ANALYSIS OF ZIRCON

In-situ analysis of hafnium isotopes in zircon, coupled with U-Pb age provides further understanding of the primary, and metamorphic processes affecting this area. The six thin sections chosen by Haley et al. (2013) for *in-situ* U-Pb zircon dating were also analyzed for *in-situ* Hf isotopic analysis. *In-situ* Lu-Hf analyses were made on 40 or 49-um spots made directly over the *in-situ* U-Pb LA-ICPMS pits. Lu-Hf analyses were collected using a Finnigan NEPTUNE double focusing, high-resolution multi-collector inductively coupled mass spectrometer (MC-ICPMS) operated in static mode at Memorial University, St. Johns, NL. Ablation pits were made with Lambda Physik ComPex Pro 110

ArF excimer GeoLas laser ablation system operating at a wavelength of 193nm and a pulse width of 20 ns. Zircon grains were located in thin section via previously acquired BSE and cathodoluminescence images, collected by Haley et al. (2013).

Instrument operating conditions, data collection parameters and data reduction procedures are given in Souders et al. (2013). Reference zircons were measured along with the unknown zircons to monitor the accuracy of ^{176}Yb and ^{176}Lu interference and Lu and Hf isotope mass bias corrections. The reference zircon chosen for this study were Plešovice ($^{176}\text{Yb}/^{177}\text{Hf} = 0.003$ to 0.008) and FC-1 ($^{176}\text{Yb}/^{177}\text{Hf} = 0.02$ to 0.07), which were ablated at the beginning, middle, and end of the set of analyses for every thin section. The average value of $^{176}\text{Hf}/^{177}\text{Hf}$ for the Plešovice zircon was 0.282471 ± 0.000028 ($n=13$), compared to the accepted value of 0.282482 ± 0.000013 (Sláma et al., 2008). Analysis of the FC-1 zircon gave a value of 0.282180 ± 0.000073 ($n=15$), compared to the accepted value of 0.282182 ± 0.00014 (Vervoort, 2010).

Initial Hf-isotope ratios were calculated using ^{176}Lu decay constant of $1.867 \times 10^{-11}/\text{yr}$ (Söderlund et al., 2004). Epsilon Hf (t) values were calculated using the chondritic values of $^{176}\text{Lu}/^{177}\text{Hf} = 0.0336$ and $^{176}\text{Hf}/^{177}\text{Hf} = 0.282785$ (Bouvier et al., 2008). Depleted mantle model Hf ages are determined assuming $^{176}\text{Lu}/^{177}\text{Hf} = 0.010$ for felsic crustal sources (Pietranik et al., 2008) and a depleted mantle with a present day $^{176}\text{Hf}/^{177}\text{Hf}$ ratio of 0.28325 and $^{176}\text{Lu}/^{177}\text{Hf}$ ratio of 0.0388 (Griffin et al., 2000; updated by Andersen et al., 2009).

3-5 RESULTS

3-5-1 LITHOGEOCHEMISTRY

Major and trace element data for the lithogeochemical samples used in this study are tabulated in Appendix A. Sample locations are plotted on a map of the study area in the same Appendix.

The rhyolite units display diverse geochemical characteristics, which in many cases coincide with mineralogical and textural differences visible in hand specimen, and outcrop. Generally, the rhyolite units are peralkaline in nature (Figure 3-8c, and Figure 3-12c). Many of the units are characterized by sodic pyroxene (aegirine-augite) ± sodic amphibole (K-hastingsite, arfvedsonite, ferrorichterite), confirming that these units are peralkaline. Variably distressed aegirine-augite grains are depicted in Figure 3-6. The two most mineralized units are displayed in Figure 3-6 (FT2x, and FT3), as these units tend to have the most well preserved sodic minerals. Although not pictured with photomicrograph, small sodic amphibole grains have been recorded using the SEM-MLA. Aegirine-augite is much more abundant, although often skeletal, and reacting to magnetite and K-feldspar.

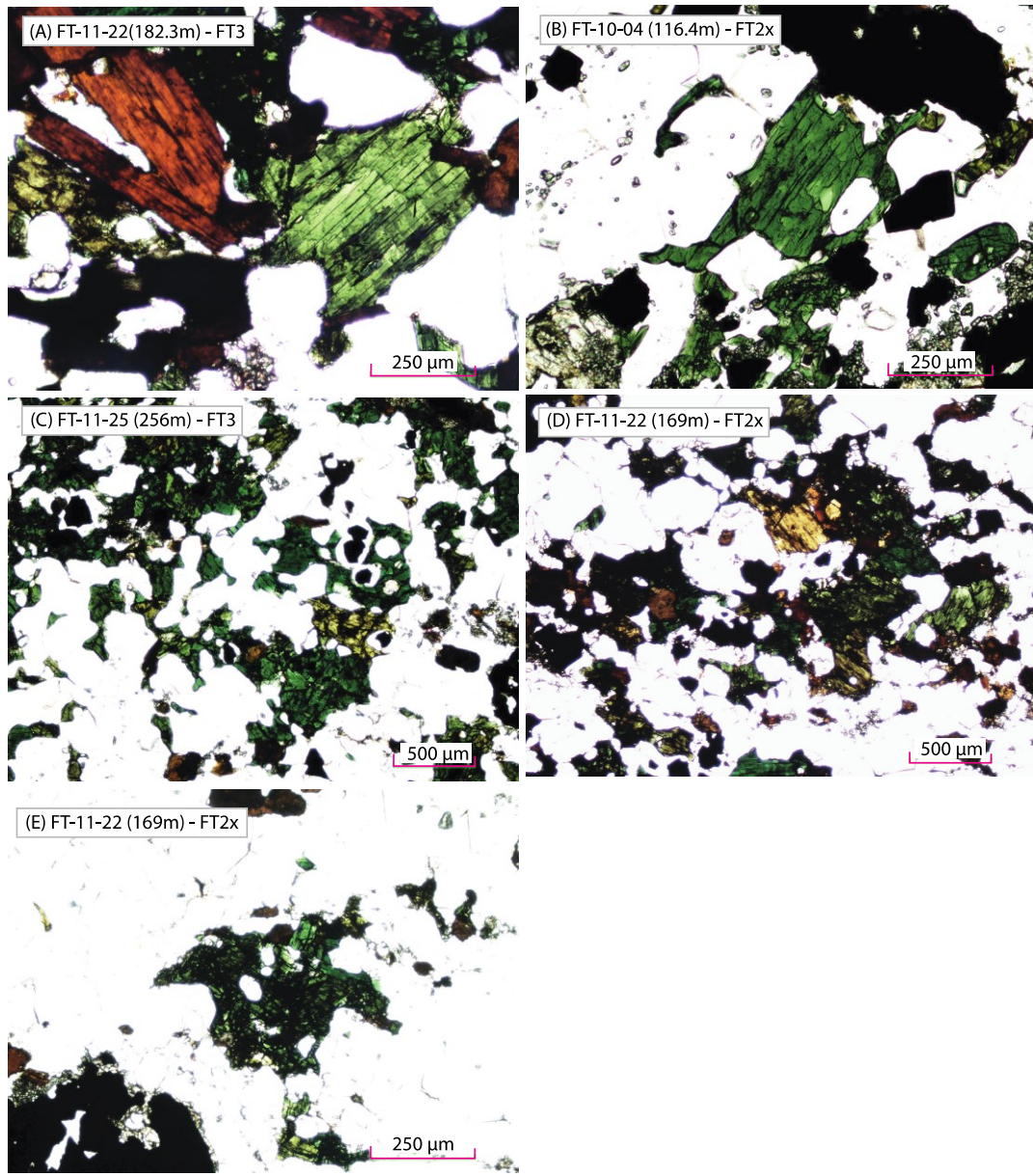


Figure 3-6: Photomicrographs from the most mineralized units in the Foxtrot Deposit, as these units have the most well preserved examples of aegirine-augite. (A) A large grain of aegirine-augite displaying 90° cleavage, from the interval FT-11-22 (182.3m), unit FT3. (B) Large grain of aegirine-augite from interval FT-10-04 (116.4m), unit FT2x. (C) Skeletal aegirine-augite displaying small “buck-shot” magnetite within the grains. A small rim of K-feldspar \pm qtz is present around each magnetite grain. From interval FT-11-25 (256m), unit FT3. (D) Mottled aegirine-augite grains in sample FT-11-22 (169m), from unit FT2x. (E) A heavily cleavaged grain of aegirine-augite, from sample FT-11-22 (169m), from unit FT2x.

A detailed description of the lithological units determined via surface and diamond drill hole, and channel logging is presented in Section 4.1. The focus of this lithogeochemical study will be the rhyolitic units, as sampling was focused on these units during exploration for REE. A small representative subset of the basaltic units present in each belt will be briefly described as well. As discussed earlier, a much more detailed interpretation has been created for the MT Belt, due to it being the focus of exploration within the project area (i.e., Foxtrot Deposit within the MT Belt).

Geochemical diagrams used will be those designed for use with altered, and metamorphosed volcanic rocks. These diagrams often use trace elements, as they are believed to be less mobile, and are more representative of the primary igneous geochemistry. Simple X-Y diagrams are utilized in testing the mobility of both major elements, and trace elements. Specific diagrams that will be discussed and used for interpretation are:

- (1) Winchester & Floyd's (1977) Nb/Y vs Zr/TiO₂, designed to distinguish rock type in altered volcanic rocks by utilizing immobile elements;
- (2) Shand's (1927) Index, as presented in Maniar and Piccoli (1989), which utilizes major element geochemistry to determine the degree of alumina saturation. Due to the metamorphosed nature (along with possible metasomatism) of the volcanic rocks in the Fox Harbour area, this index is likely not representative of the primary igneous geochemistry, and shouldn't be the sole determination of the alumina saturation.

- (3) Irvine and Baragar's (1971) AFM diagram, used to determine whether subalkaline basalts are tholeiitic or calc-alkaline (where A = $\text{Na}_2\text{O} + \text{K}_2\text{O}$, F = $\text{FeO} + (0.8998 \times \text{Fe}_2\text{O}_3)$, and M = MgO).
- (4) A diagram designed by Macdonald (1974) for mildly peralkaline volcanic rocks, using FeO vs Al_2O_3 ; (Rock types that apply plot in the com/pan field (comendite/pantellerite) on the Winchester and Floyd (1977) diagram. Macdonald's (1974) diagram subdivides the units to: comendite, comenditic trachyte, pantellerite, or pantelleritic trachyte.)
- (5) Harker diagrams, designed by Harker (1909), which are simple X-Y diagrams plotting SiO_2 on the x-axis, against other major oxides on the Y-axis; (Harker diagrams are readily affected by metamorphism and alteration, but are designed to show the evolution of magmas.)
- (6) Chondrite normalized REE diagrams, after Sun and McDonough (1989).
- (7) A La/Sm vs Gd/Lu diagram, which is utilized to quantify the variations observed on the chondrite normalized REE plots; (This diagram effectively plots the slope of the LREE, against the slope of the HREE. Geochemical assays that have similar LREE and HREE slopes plot as clusters.)
- (8) Various X-Y diagrams, plotting incompatible, immobile elements on the axes; (These diagrams vary between each unit, and are utilized in determining various geochemical patterns not readily visible in previously mentioned diagrams.)

All lithogeochemical sample locations (diamond drill holes, and channels) are shown in Figure 3-3, and 3-4

3-5-1-1 *South Belt Lithogeochemistry*

The entire South Belt (north to south) has been channel sampled to observe geochemical variations across the belt (Channel names: FHWT-5 – 11, and FHWT-13 – 17), as seen in Figure 3-7. These channels, cut perpendicular to the strike of the belt demonstrates that the rock type of the South Belt is extremely homogenous, and lithological distinctions are extremely difficult to discern in hand sample. This is partly due to the extremely fine-grained nature of the belt, making absolute mineral identification difficult in hand sample, as discussed in Section 3.1, and Haley et al. (2013). Variations consist of slight differences in phenocryst size, amount of quartz veins, and magnetite content. Although difficult to determine in hand sample, this approach has revealed several notable geochemical features of the belt that would have been otherwise overlooked. Samples that included more than one lithological unit (i.e., mixtures of two rock units) were excluded from interpretation.

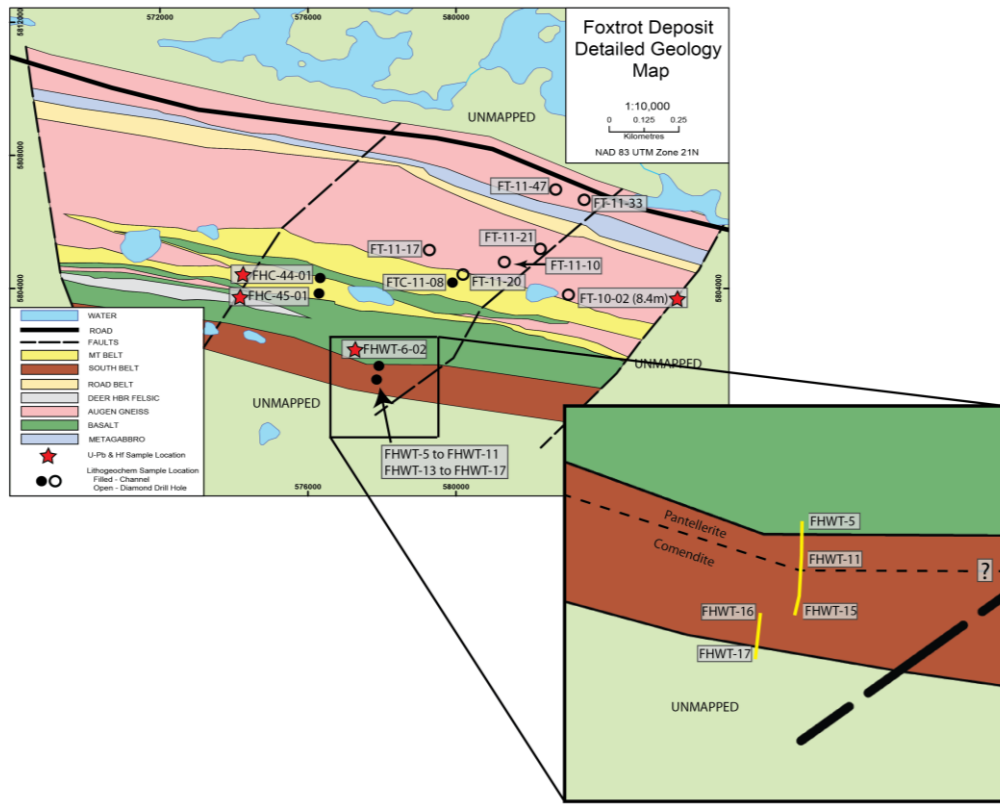


Figure 3-7: Geology map of the Foxtrot Deposit. Inset depicts close up of general location for lithogeochemical samples analyzed for the South Belt. U-Pb and Hf sample locations are indicated by red stars. Lithogeochemistry samples are indicated by either filled black circles (channel sample locations), or open black circles (diamond drill hole locations). Inset depicts close up of channel locations chosen in the South Belt (yellow lines). Also depicted is a proposed boundary between the pantelleritic and comenditic units within the South Belt.

Analyzed rhyolite samples plot in the comendite/pantellerite field (Figure 3-8a) on the Zr/TiO₂ vs Nb/Y diagram (Winchester and Floyd, 1977; Maniar and Picolli, 1989). Using the Al₂O₃ vs FeO plot (Figure 3-8c) designed by Macdonald (1974), to differentiate peralkaline rhyolites, the rhyolite units are further classified as comendite and pantellerite (Macdonald, 1974). Basaltic units in the South Belt are generally subalkaline basalts (Figure 3-8a), but a number of samples plot in the alkaline basalt field, and andesite field

(Winchester and Floyd, 1977). These slight geochemical variations are not discernable in hand sample, as all the rocks described as basalt look similar. Geochemically, the rhyolite units in the South Belt roughly display pantellerite lithogeochemistry in the north, and more of a comenditic lithogeochemistry in the south. This transition occurs roughly in the center of channel FHWT-11, as shown in the inset of Figure 3-7. A proposed lithogeochemical boundary has been created for the South Belt, as indicated by the dashed line in Figure 3-7. This boundary is used to indicate the location of pantellerite dominant (north) versus comendite dominant (south) throughout the South Belt, although both comendites and pantellerites are seen on either side of this boundary.

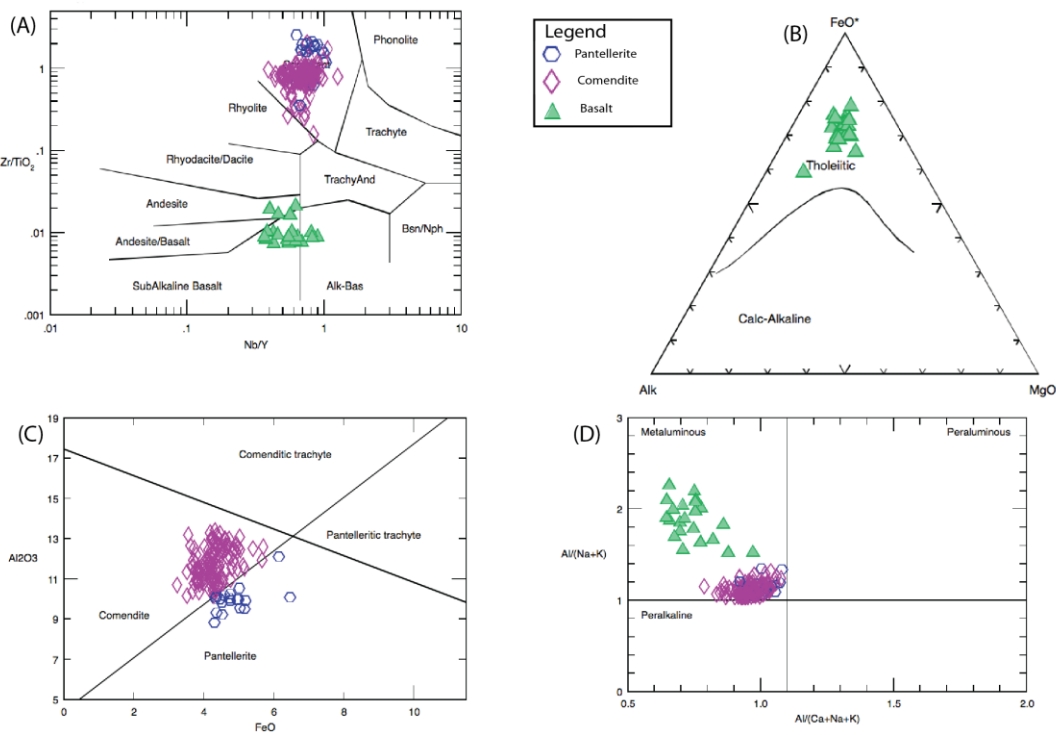


Figure 3-8: Geochemical diagrams for the South Belt. (A) Rhyolite and basaltic units plotted on Winchester and Floyd's (1977) diagram for determining rock type; (B) Basaltic units plotted on Irvine and Baragar's (1971) diagram, used to determine if the subalkaline basalts are calc-alkaline or tholeiitic; (C) Rhyolite units plotted on Macdonald's (1974) diagram, utilized in mildly peralkaline volcanic rocks; (D) Rhyolite and basaltic units plotted on Shand's (1927) Index, after Maniar and Piccoli (1989).

The contents of all major elements decrease with increasing SiO₂ (Figure 3-9), while a few elements such as Na₂O, K₂O, and CaO are slightly more clustered. (Harker, 1909).

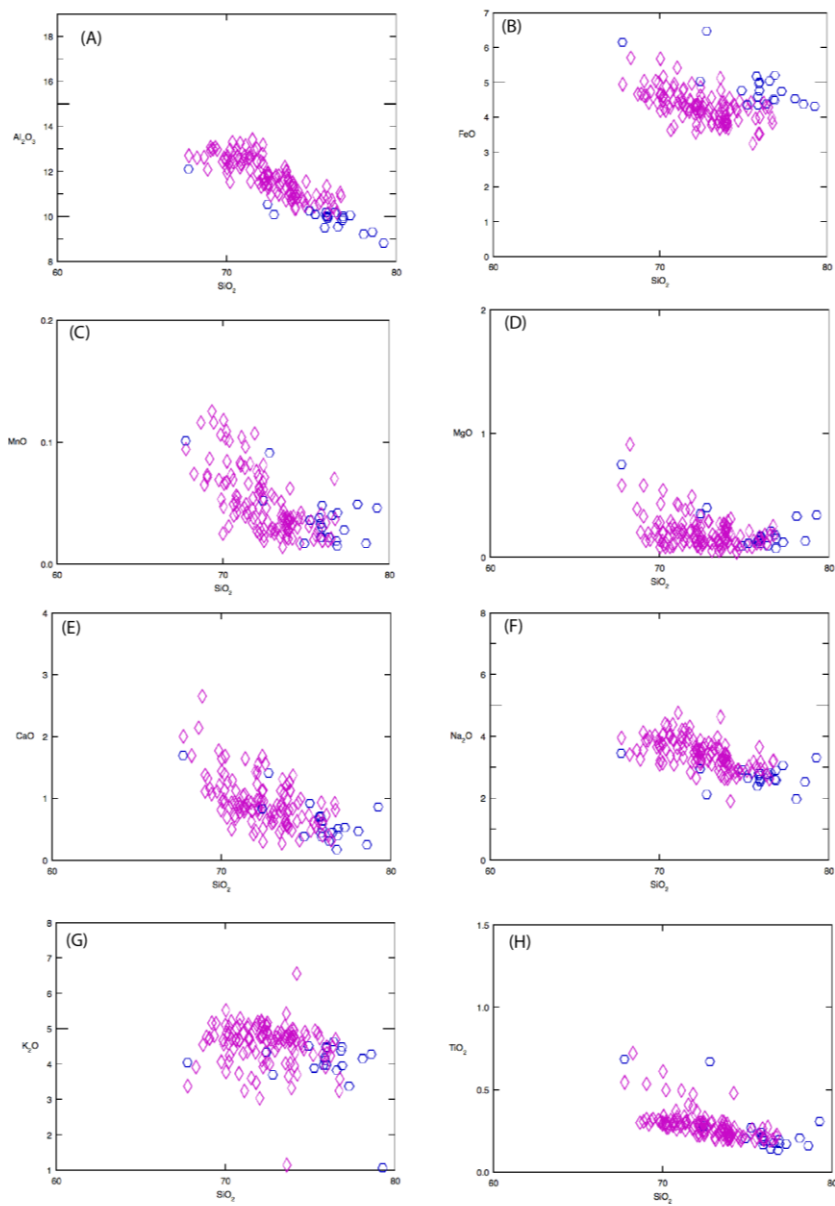


Figure 3-9: Harker Diagrams for the South Belt, displaying the rhyolitic (comendite – pink diamond, and pantellerite – blue square) units (Harker, 1909). (A) SiO_2 vs Al_2O_3 , (B) SiO_2 vs FeO , (C) SiO_2 vs MnO , (D) SiO_2 vs MgO , (E), SiO_2 vs CaO , (F) SiO_2 vs Na_2O , (G) SiO_2 , vs K_2O , and (I) SiO_2 vs TiO_2 .

Trace elements are shown to have quite a complicated relationship, in which the X-Y immobile vs immobile plot (i.e.: Zr vs Y) displays variable ratios depending on the amount of each element present. The ratio ranges from ~5 to ~13, with the majority of the samples ranging between 6-10 (Figure 3-10a). The Zr vs Y diagrams also displays that the pantellerite units have higher concentrations of these elements with respect to the comendites. Chondrite normalized spider diagrams display very similar REE patterns for all units, with small variations in the slope of the LREE and HREE (Figure 3-10b). The La/Sm vs Gd/Lu plot shows the small slope differences displayed on the Chondrite normalized plot, where the pantellerites generally plot on the left side of this diagram. The La vs Dy (i.e.: LREE vs HREE) plot displays the tendency of the pantellerite units to have more HREE with respect to LREE. This is displayed as a very slight distinction in slopes between the pantellerite (ratio of 2-4) and comendites (2.5-8).

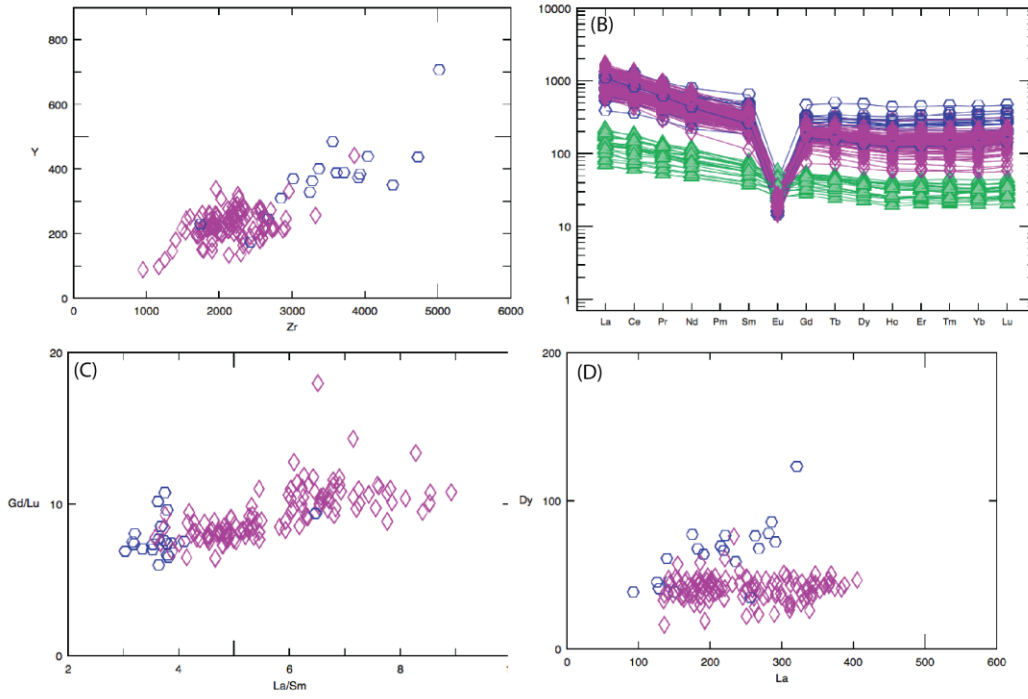


Figure 3-10: (A) Zr vs Y diagram for the rhyolite units of the South Belt, (B) Chondrite normalized spider diagrams for the rhyolite and basaltic units of the South Belt, (C) La/Sm vs Gd/Lu diagram for the rhyolite units in the South Belt, (D) La vs Dy diagram for the rhyolite units of the South Belt.

3-5-1-2 MT Belt Lithogeochemistry

For the purposes of this study, a single representative drill hole (FT-11-21) intersecting a representative section of the entire Foxtrot Deposit will be presented. Supplemental data from both channel samples (FTC-11-08), and diamond drill holes (FT-11-17, and FT-11-20) will be utilized to ensure every unit is adequately represented. All

diamond drill hole collar locations, along with channel sample locations are presented in Figure 3-11.

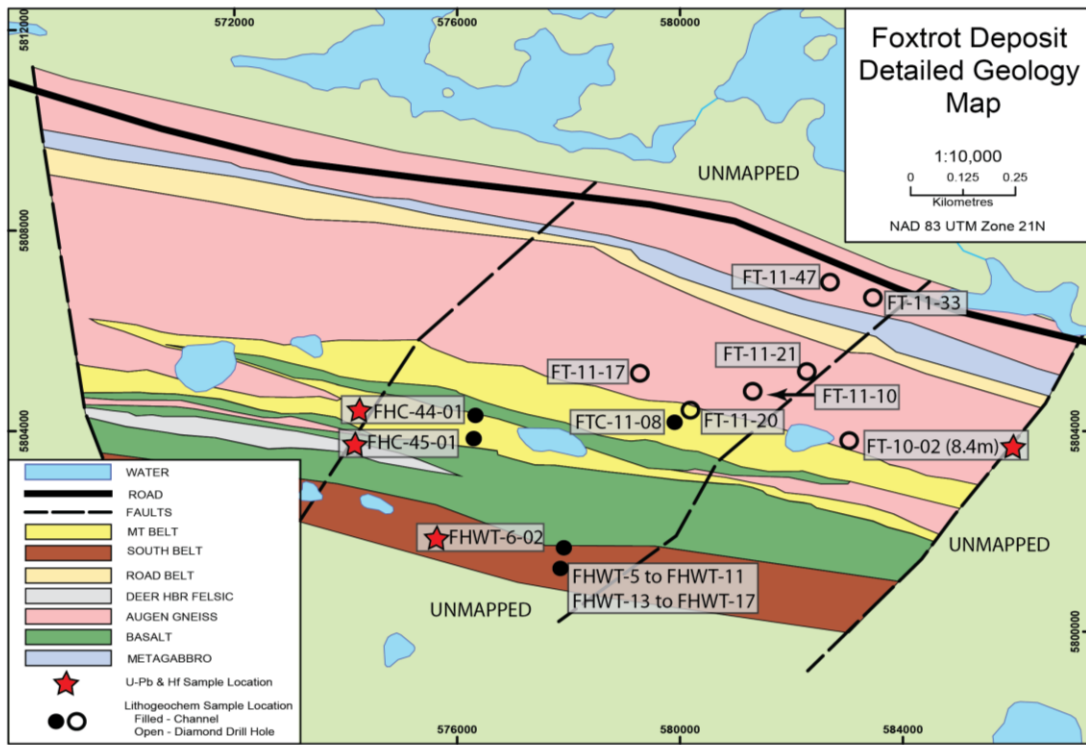


Figure 3-11: Geology map of the Foxtrot Deposit, within the MT Belt. U-Pb and Hf sample locations are indicated by red stars. Lithogeochemistry samples are indicated by either filled black circles (channel sample locations), or open black circles (diamond drill hole locations).

All rhyolitic units are peralkaline, largely determined via indicator minerals mentioned earlier, such as sodic amphiboles, and sodic pyroxenes. Units FT2, FT2x, FT3, FT3b, FT4, and FT5 plot in the comendite/pantellerite field on the Nb/Y vs Zr/TiO₂ diagram, while FTBuff plots in the rhyolite field (Winchester and Floyd, 1977). Basaltic units plot in the subalkaline basalt field, with some samples plotting in the andesite/basalt

field (Winchester and Floyd, 1977). Basaltic samples are further classified as tholeiitic on the AFM diagram (Irvine and Baragar, 1971). Using the Al_2O_3 vs FeO plot, units FT2, FT2x, FT3, FT3b, FT4, and FT5 are further classified as comendite and pantellerite (Macdonald, 1974). Lithological unit FT2 largely plots in the comendite field, with a small amount of scatter to the pantellerite field. Rock unit FT2x plots in the pantellerite field, as a sub-horizontal line. Units FT3, FT3b, and FT4 also plot in the pantellerite field, but occur as clusters, with unit FT3 and FT3b having lower Al_2O_3 (i.e.: plotting lower on the FeO vs Al_2O_3 plot). FT5 plots in both the comendite and pantellerite field.

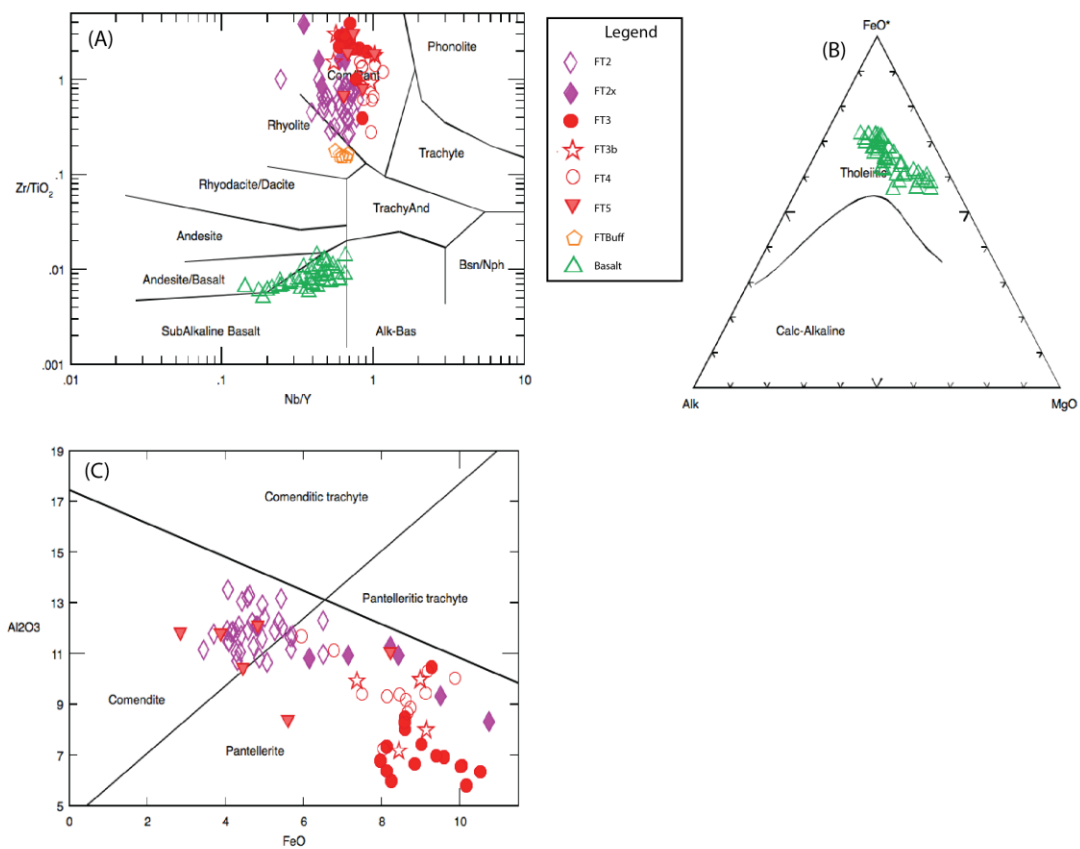


Figure 3-12: (A) Nb/Y vs Zr/TiO_2 diagram for the rhyolitic, basaltic, and aplite units of the MT Belt (Winchester and Floyd, 1977), (B) AFM diagram for the basaltic units of the MT Belt, (C) FeO vs Al_2O_3 diagram for the rhyolite, and aplite intrusions of the MT Belt (Macdonald, 1974).

Major elements in the MT Belt are slightly more scattered than in the South Belt. Major elements FeO , CaO , TiO_2 , and P_2O_5 decrease with increasing SiO_2 content. Major elements Al_2O_3 , Na_2O , and K_2O are generally clustered when plotted against SiO_2 .

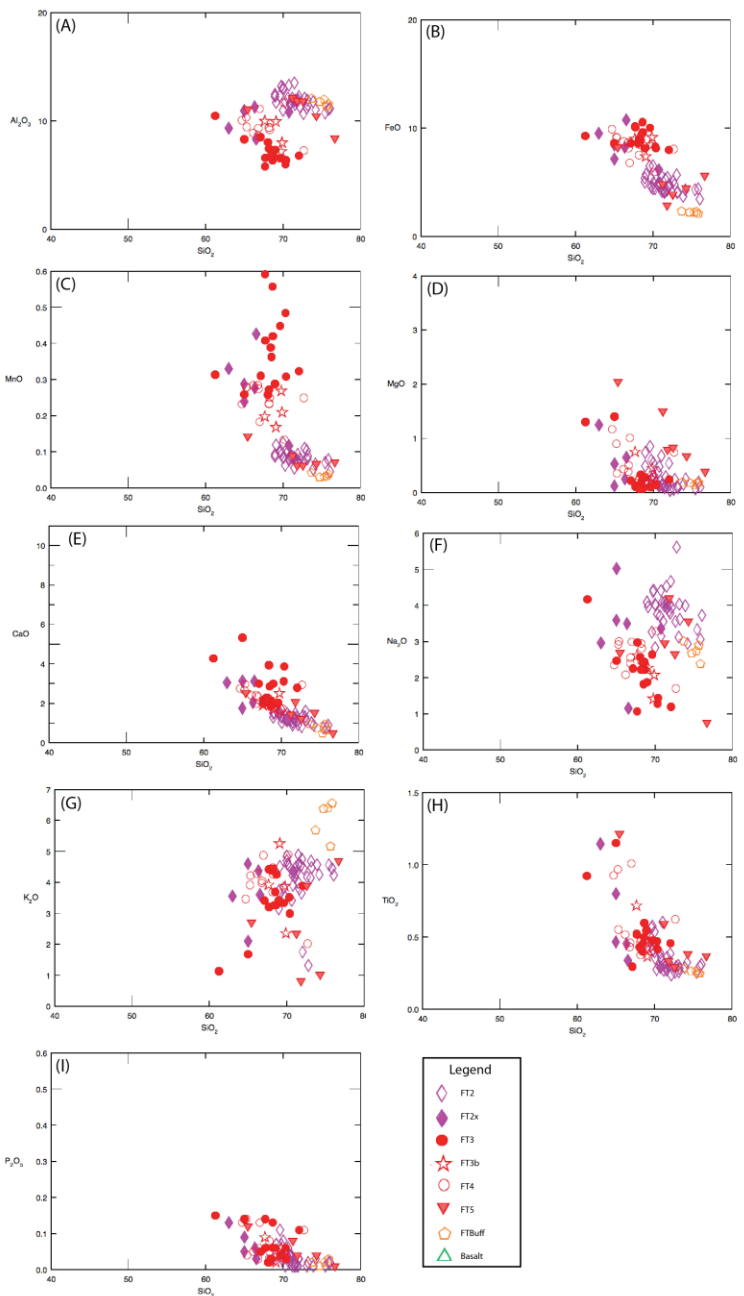


Figure 3-13: Harker Diagrams for MT Belt, displaying the rhyolitic (comendite and pantellerite) units FT2, FT2x, FT3, FT3b, FT4, and FT5, along with the microgranite intrusion FTBuff (Harker, 1909). (A) SiO_2 vs Al_2O_3 , (B) SiO_2 vs FeO , (C) SiO_2 vs MnO , (D) SiO_2 vs MgO , (E) SiO_2 vs CaO , (F) SiO_2 vs Na_2O , (G) SiO_2 vs K_2O , (H) SiO_2 vs MnO , (I) SiO_2 vs TiO_2 .

Using an immobile vs immobile element plot, such as Zr vs Y, or Zr vs Dy, we are able to determine if these elements acted as immobile elements during metamorphism. The Zr vs Y plot displays a consistent slope of approximately 10:1, while the Zr vs Dy plot displays a consist ratio of 5:1. This indicates that although elemental variation between different elements exist, (i.e.: Zr vs Dy, and Zr vs Y) and contain different slopes, they are consistent throughout the geochemical spectrum observed in the area, suggesting they acted as immobile elements during all post crystallization processes (volcanic, hydrothermal, other weathering processes, deformation, and metamorphism). As with the South Belt, chondrite normalized spider diagrams display very similar REE patterns, showing very little variation between each rhyolite unit. Unit FT5 has a shallow LREE slope, and a steeper HREE slope than the rest of the units; this is also seen in the La/Sm vs Gd/Lu plot.

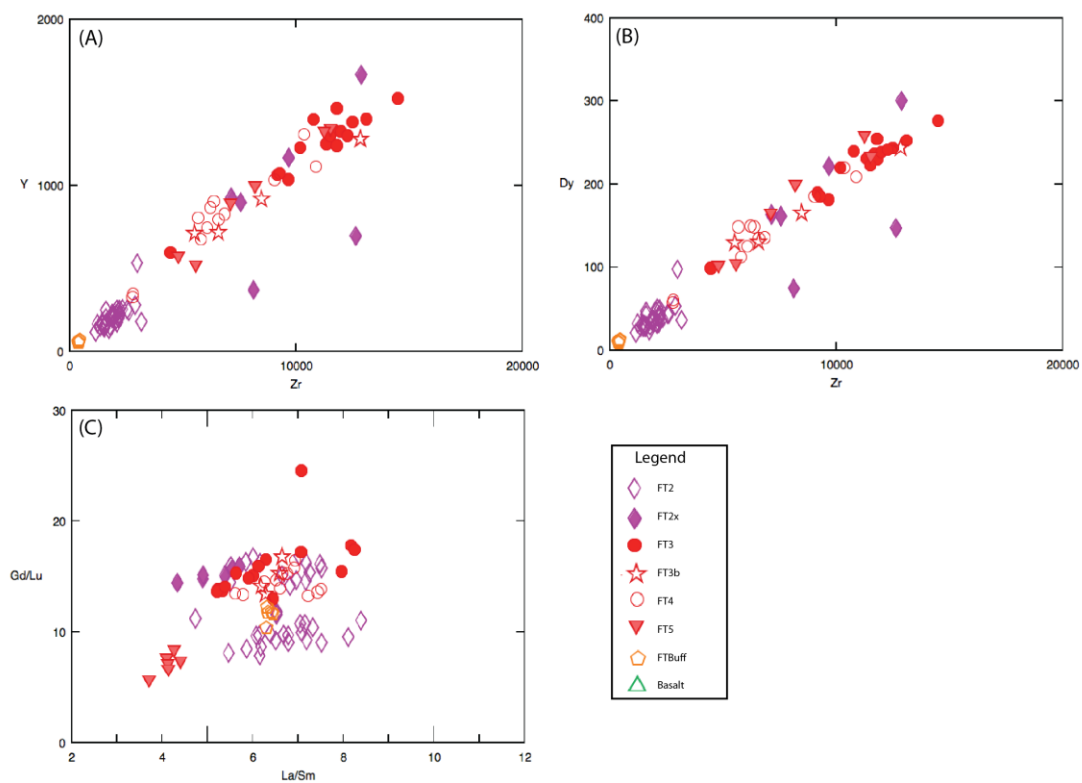


Figure 3-14: Geochemical diagrams for the MT Belt. (A) Y vs Zr diagram for the rhyolite and aplite units of the MT Belt, (B) Zr vs Dy diagram for the rhyolite and aplite units of the MT Belt, (C) La/Sm vs Gd/Lu diagram for the rhyolite and aplite units of the MT Belt.

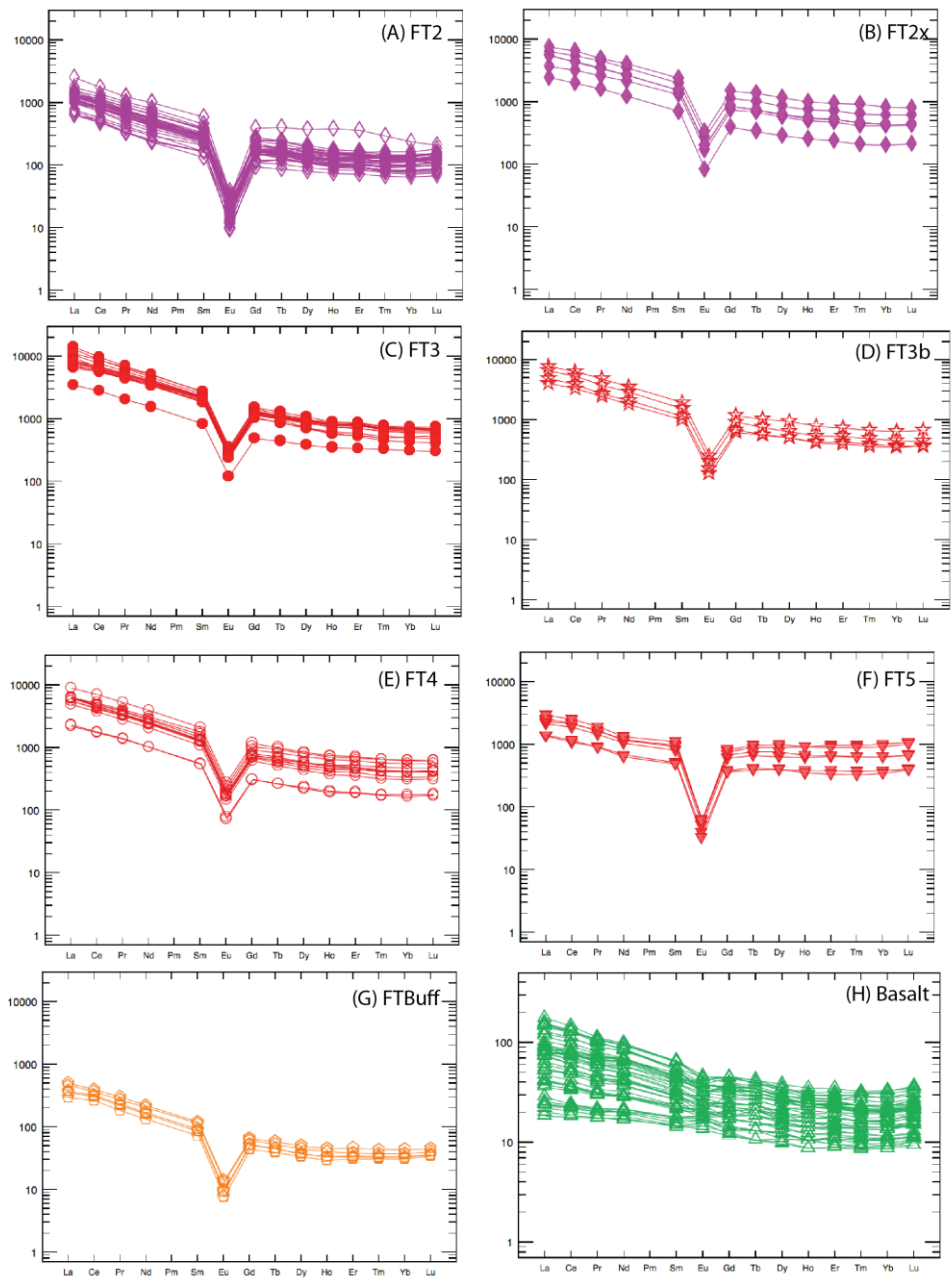


Figure 3-15: Spider diagrams for each unit in the MT Belt. (A) FT2, (B) FT2x, (C) FT3, (D) FT3b, (E) FT4, (F) FT5, (G) FTBuff, and (H) Basalt.

3-5-1-3 *Road Belt Lithogeochemistry*

The deepest diamond drill holes designed to intersect the Foxtrot Deposit also intersected the Road Belt. Two diamond drill hole intersections (FT-11-33, and FT-11-47), along with surficial data from channels (FHC-32—40, and FHRBC-11-01—FHRBC-11-02) will be presented in this study (see Figure 3-4). Naming of these units (i.e.: like the Foxtrot Deposit naming scheme) is difficult, and not possible yet. Therefore, all rock names are based on lithogeochemical signatures. Samples that included more than one lithological unit (i.e., mixtures), and the granitic augen gneiss were excluded.

Many of the rhyolite samples that were analyzed for lithogeochemistry from the Road Belt are peralkaline, as determined by the presence of sodic amphiboles, and sodic pyroxenes. Units that were deemed peralkaline plot in the comendite/pantellerite field (Figure 3-16a) while other lesser mineralized (non peralkaline) rhyolites plot in the rhyolite field, while the microgranite/aplite dyke plots in the rhyodacite/dacite field on the diagram designed by Winchester and Floyd (1977) (Figure 3-16a).

Geochemical units have been separated based on a few different criteria. Pantellerites in the Road Belt tend to contain a high amount of magnetite, sodic pyroxenes, titanite, and amazonite. Often times this mineralogy has been disturbed, and is difficult to determine prior to the acquisition of geochemical data. Comendite units in the Road Belt are extremely difficult to discern from adjacent highly mylonitized, and migmatized granitic augen gneiss prior to obtaining lithogeochemistry results. Magnetite content, and the presence of skeletal sodic pyroxenes (similar to those seen in Figure 3-6) are the only way to distinguish from the granitic augen gneiss in drill core. Filled and

hollow red circles are pantellerites. The pantellerites have been separated by their REE/Zr ratio (Figure 3-18a and b), where filled red circles have a higher REE/Zr, and vice-versa. This REE/Zr ratio assumes that all REE are acting the same, and the ratio remains generally the same throughout. The pantellerites are also the most mineralized samples with regards to REE and HFSE. Pink diamonds are comendites, and tend to be moderately mineralized with respect to REE and HFSE. Blue squares are metaluminous rhyolites, which have been separated from the pantellerites (red circles), and moderately mineralized comendites (pink diamonds) using the Winchester and Floyd (1977) plot.

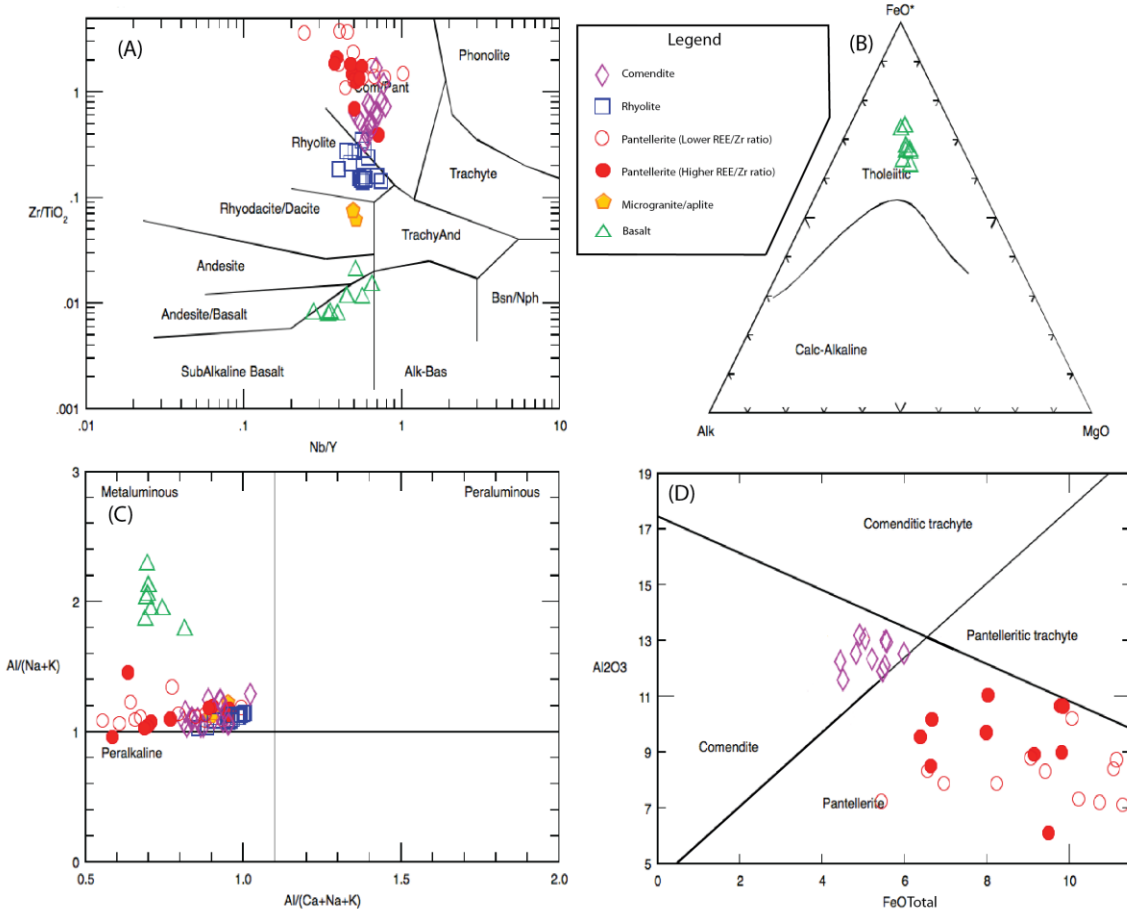


Figure 3-16: Geochemical diagrams for the Road Belt. (A) Nb/Y vs Zr/TiO_2 diagram for the rhyolitic, basaltic, and aplite units of the Road Belt (Winchester and Floyd, 1977), (B) AFM diagram for the basaltic units of the Road Belt, (C) Shand's (1927) Index, as presented by Maniar and Piccoli (1989) for the rhyolite, basaltic, and aplite units of the Road Belt, (D) FeO vs Al_2O_3 diagram for the rhyolite, and aplite intrusions of the Road Belt.

Major elements in the Road Belt are quite scattered, possibly due to the fact that they have been affected by metamorphism and/or there are primary lithogeochemical differences between the units. The more mineralized pantelleritic units (i.e.: those containing magnetite, amazonite, sodic pyroxene \pm sodic amphiboles) show much more variation than the lesser mineralized comendites. The pantelleritic units display erratic

Al_2O_3 , Na_2O , and K_2O , much lower than adjacent units (Figure 3-17a, e, f), possibly due to post deposition metasomatic alteration often observed in subaerial volcanics. FeO appears to have remained fairly immobile, with the pantellerites plotting above the comenditic units, but generally decreasing with increasing SiO_2 (Figure 3-17b). Generally the rhyolite units (non-peralkaline) appear as clusters, which have likely not undergone the same metasomatic alteration and/or metamorphism. CaO and TiO_2 appear to have remained immobile, and decrease with increasing SiO_2 (Figure 3-17e, and h).

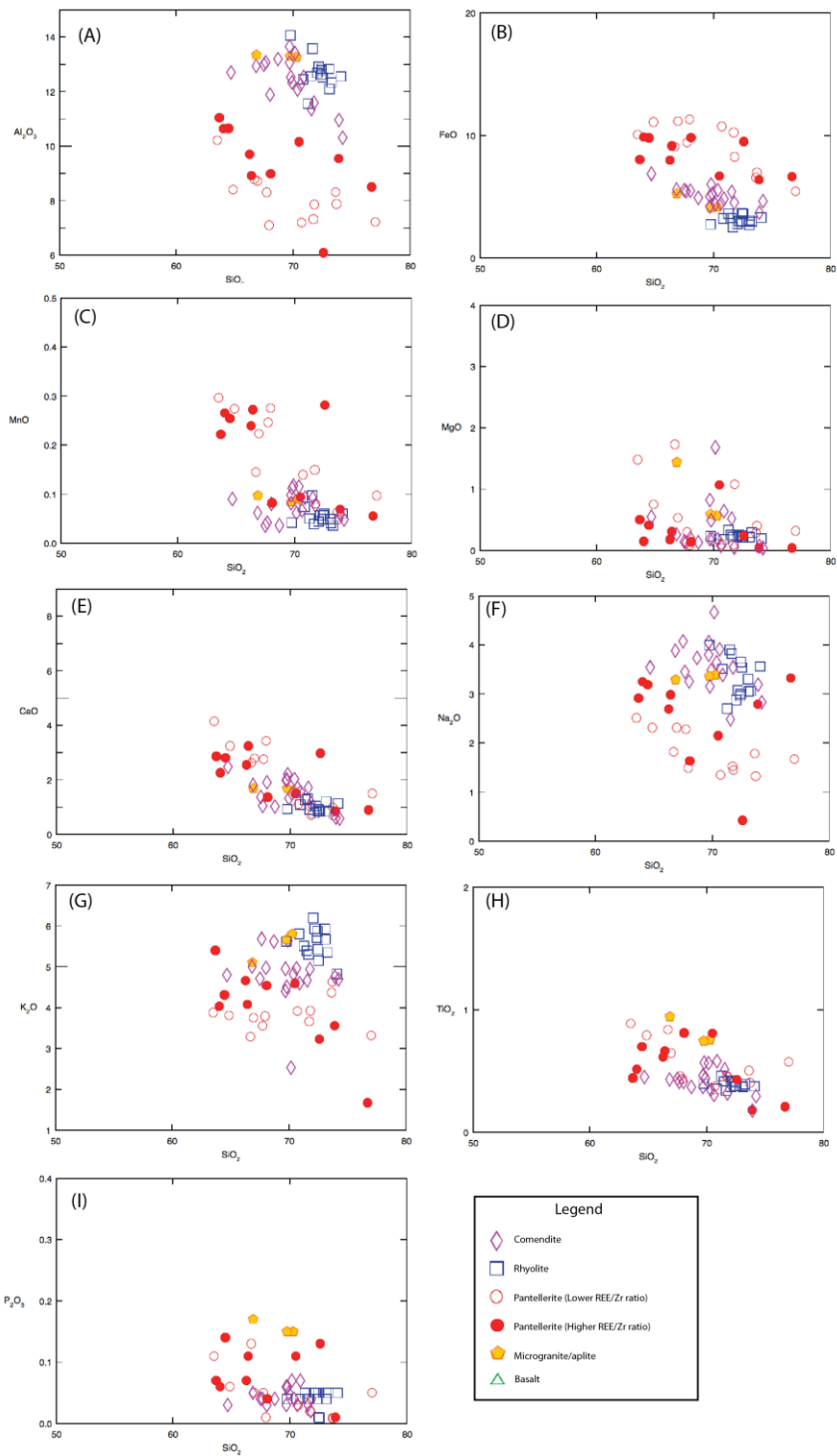


Figure 3-17: Harker Diagrams for the Road Belt, displaying the rhyolitic units (Harker, 1909). (A) SiO_2 vs Al_2O_3 , (B) SiO_2 vs FeO , (C) SiO_2 vs MnO , (D) SiO_2 vs MgO , (E), SiO_2 vs CaO , (F) SiO_2 vs Na_2O , (G) SiO_2 , vs K_2O , (H) SiO_2 vs MnO , (I) SiO_2 vs TiO_2 .

Much like the previously discussed belts, the trace elements appear to be relatively immobile, where individual rock types follow the same ratio through the entire geochemical spectrum. The first most prominent distinction is that of the pantelleritic units, which clearly display two trends on a simple XY immobile vs immobile plots (i.e.: Zr vs La, La vs Hf) (Figure 3-18a and b). These two trends have been termed higher REE/Zr pantellerite and lower REE/Zr pantellerite, where these units generally display a correlation between the Zr and REE content. The higher REE/Zr pantellerites have an approximate ratio of 10:1, whereas the lower REE/Zr pantellerites have a ratio of approximately 15:1. This suggests a slightly different unit (possibly a different volcanic package) is present in the Road Belt. The general patterns of the Chondrite-normalized REE spider plots are consistent within units, with more variability in the pantelleritic units (Figure 3-19a and b), which is expected with slightly different units present. Light REE slopes vs HREE slopes can be compared by using the plot La/Sm vs Gd/Lu (Figure 3-18c), and in the case of the Road Belt, it displays the variability described previously. The pantellerites are scattered, which is expected when observing the spider diagram for these units, as they tend to be slightly variable. Comenditic units are less scattered, agreeing with the consistency of the Chondrite-normalized spider diagrams for these units. The aplite/microgranite plots in a small cluster (Figure 3-18c).

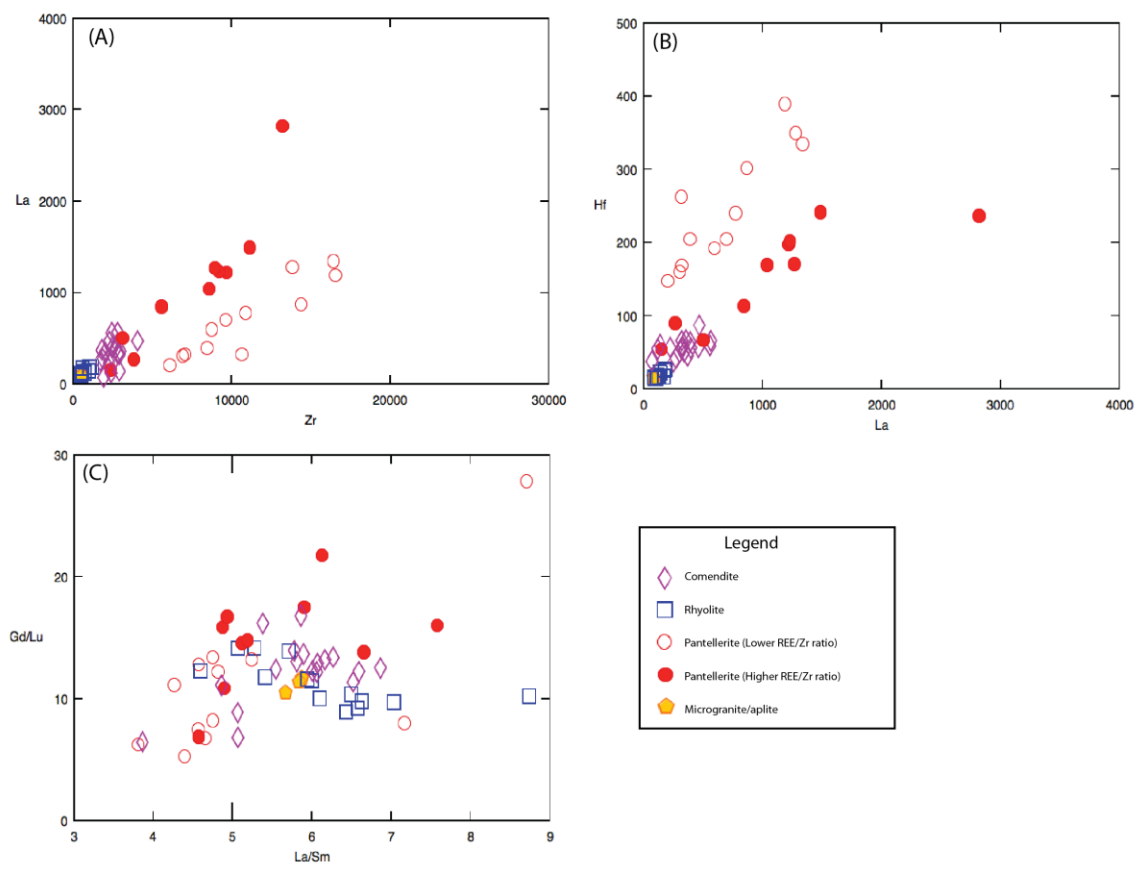


Figure 3-18: Geochemical diagrams for the rhyolitic units of the Road Belt (A) Zr vs La, (B) La vs Hf, and (C) La/Sm vs Gd/Lu.

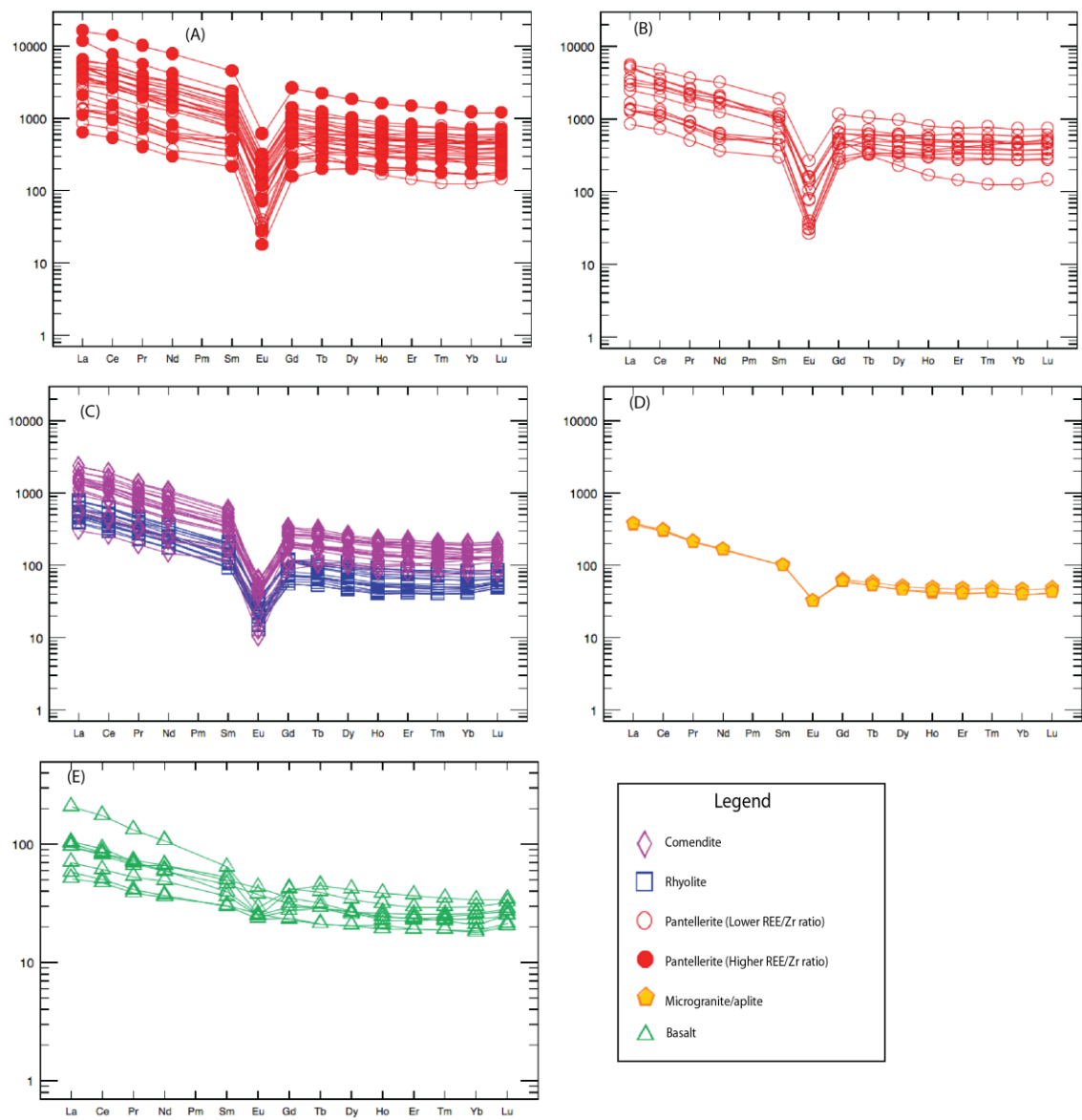


Figure 3-19: Spider diagrams for the rhyolitic, basaltic, and aplitic units of the Road Belt. (A) Pantellerite (higher REE/Zr ratio), (B) Pantellerite (lower REE/Zr ratio), (C) Comendite and rhyolite (D) microgranite/aplite, and (E) basalt.

3-5-2 ELECTRON MICROPROBE ANALYSIS

3-5-2-1 Electron Microprobe Analysis of Fergusonite

Two thin sections, one from the MT Belt, and one from the South Belt (FT-11-10 (187.5m) and FHWT-17-13) were chosen for the analysis (Figure 3-11). Sample FHWT-17-13 is from the comenditic southern section of the South Belt (Figure 3-7). The MT Belt sample, FT-11-10 (187.5m) is a pantellerite from the unit FT3, discussed in detail in section 3.2.

Ercit (2005) developed a method of differentiating the yttrium-niobate mineral groups of fergusonite, samarskite, euxenite, and pyrochlore. The method involved using statistical discrimination of certain elements that are commonly found in these mineral groups. These elements, and elements groups consist of Na, Ca, Pb, Fe*, Y, LREE, HREE, U*, Ti, Nb, and Ta* (Ecrit, 2005). The variables utilized in the following diagram are CV1 and CV2, otherwise known as canonical variables 1 and 2, and are further discussed in Ercit (2005). The mathematical formulas used to create these variables are:

$$\begin{aligned}\mathbf{CV1} = & 0.172 \mathbf{Na} - 0.027 \mathbf{Ca} + 0.058 \mathbf{Fe^*} \\ & + 0.069 \mathbf{Pb} - 0.306 \mathbf{Y} - 0.167 \mathbf{LREE} \\ & - 0.237 \mathbf{HREE} - 0.093 \mathbf{U^*} + 0.108 \mathbf{Ti} \\ & - 0.016 \mathbf{Nb} - 0.013 \mathbf{Ta^*} + 5.60 \text{ (oxide wt.\%)}\end{aligned}$$

$$\begin{aligned}\mathbf{CV2} = & 0.275 \mathbf{Na} + 0.089 \mathbf{Ca} - 0.152 \mathbf{Fe^*} \\ & + 0.414 \mathbf{Pb} + 0.148 \mathbf{Y} + 0.249 \mathbf{LREE} \\ & + 0.118 \mathbf{HREE} + 0.067 \mathbf{U^*} + 0.305 \mathbf{Ti} + 0.066 \mathbf{Nb} \\ & + 0.083 \mathbf{Ta^*} - 10.01 \text{ (oxide wt.\%)}\end{aligned}$$

Using this statistical method of differentiating these (Y, REE, U, Th) – (Nb, Ta, Ti) oxide minerals, it was confirmed that the REE-bearing mineral in the Fox Harbour area is in fact fergusonite, as seen in Figure 3-20.

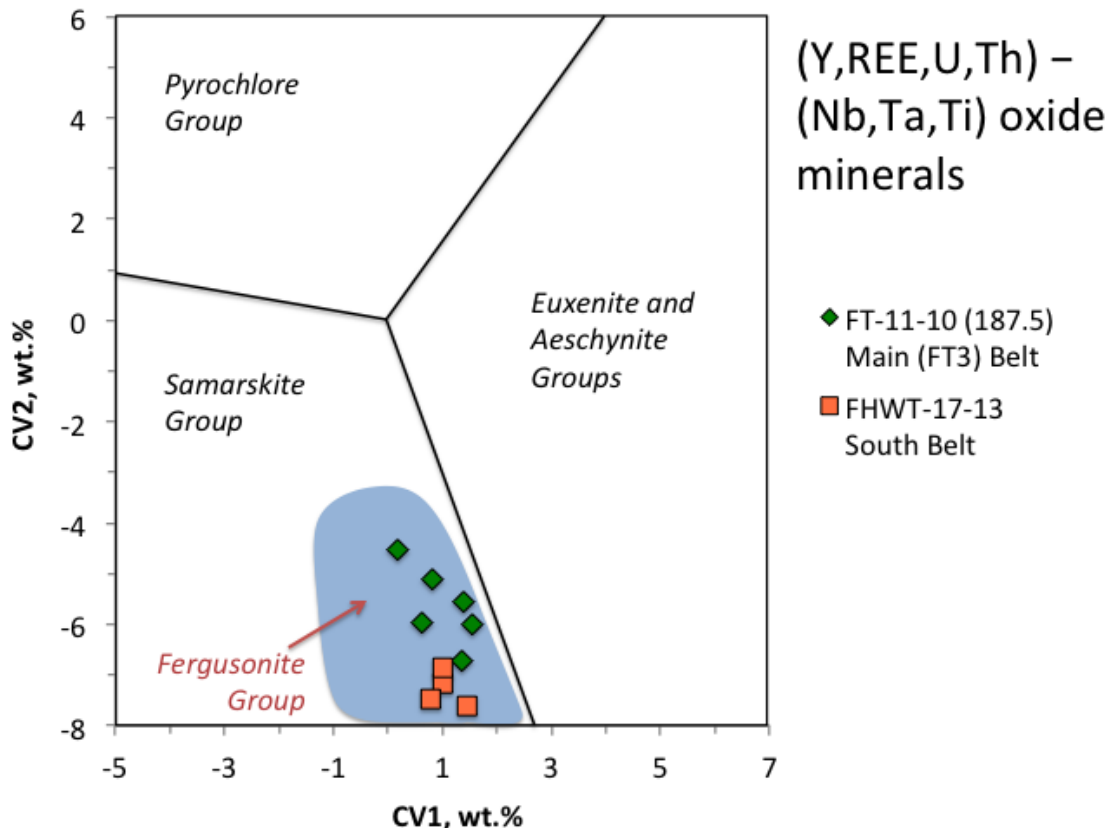


Figure 3-20: Plot designed by Ercit (2005) utilized in distinguishing yttrium-niobate mineral groups. Both samples from Fox Harbour (FT-11-10 (187.5m), and FHWT-17-13) plot in the fergusonite group field, as indicated by a filled blue field.

REE are major elements in the analyzed fergusonite, forming a total of ~20 – 29 wt.% of the mineral (Table 1). Chondrite-normalized REE patterns are fairly consistent from grain to grain, with HREE enriched relative to LREE and large negative Eu

anomalies. The LREE pattern has a positive slope increasing from La to Sm, whereas the HREE pattern is much more flat, ranging from slightly positive to slightly negative (Figure 3-21, and 3-22).

There are some differences in the fergusonite between the two analyzed samples. South Belt comendite sample FHWT-17-13 displays more strongly LREE depleted patterns with concentrations of La at \sim 100 – 1000 \times chondrites and Sm at \sim 10,000 to 50,000 \times chondrites. Negative Eu anomalies are very large, with Eu/Eu* (chondrite-normalized Eu/mean of chondrite-normalized Sm and Gd) of \sim 0.001 – 0.002. HREE are enriched at \sim 100,000 \times chondrites.

For fergusonite grains in MT Belt pantellerite sample FT-11-10 (187.5 m), LREE tend to be more enriched than in sample FHWT-17-13: concentrations of La range from \sim 5,000 – 10,000 \times chondrites whereas Sm are at \sim 50,000 to 100,000 \times chondrites. Negative Eu anomalies are variable, with Eu/Eu* of \sim 0.001 – 0.09. HREE are enriched at \sim 100,000 \times chondrites, as in sample FHWT-17-13.

Table 3-1: Electron microprobe analyses (wt.%) for fergusonite

FT-11-10 (187.5) Main (FT3) Belt						FHWT-17-13 South Belt				
	YNb-1	YNb-2	YNb-3	YNb-4	YNb-5	YNb-6	YNb-1	YNb-2	YNb-3	YNb-4
SiO ₂	2.09	2.62	1.80	3.56	3.56	0.51	0.18	0.02	0.35	0.25
TiO ₂	0.60	0.85	0.38	0.58	0.65	0.29	0.82	0.13	0.87	0.73
FeO*	0.36	0.53	0.54	0.96	0.39	1.17	0.77	1.47	0.09	0.17
MnO	0.19	0.25	0.31	0.49	0.43	0.12	<0.01	0.04	<0.01	<0.01
CaO	1.80	2.23	1.53	3.91	3.26	0.67	0.09	0.35	0.04	0.11
Na ₂ O	<0.01	<0.01	<0.01	0.02	<0.01	<0.01	<0.01	0.01	<0.01	<0.01
Nb ₂ O ₅	44.89	43.61	45.70	44.58	44.37	45.96	47.21	48.18	48.29	46.43
Ta ₂ O ₅	0.53	0.50	1.62	1.58	1.06	1.22	0.65	0.74	0.26	0.42
UO ₂	0.60	0.53	0.59	0.66	0.21	0.63	0.28	0.89	0.23	0.35
ThO ₂	0.67	2.23	0.94	1.36	1.82	0.59	1.32	0.08	0.47	0.25
PbO	0.03	0.07	0.08	0.13	0.09	<0.01	0.06	0.14	0.02	0.06
ZrO ₂	0.09	0.12	0.07	0.09	0.13	0.04	0.06	0.11	0.05	0.08
HfO ₂	0.07	0.05	0.05	0.11	<0.01	<0.01	<0.01	<0.01	0.04	0.06
Y ₂ O ₃	19.84	18.61	24.42	19.34	19.81	22.85	27.79	28.95	29.15	28.26
La ₂ O ₃	0.091	0.166	0.137	0.278	0.541	0.116	0.001	0.013	0.041	0.005
Ce ₂ O ₃	1.12	1.32	0.77	1.80	2.69	0.97	0.04	0.07	0.05	0.09
Pr ₂ O ₃	0.75	0.71	0.22	0.47	0.53	0.54	0.03	0.02	0.02	0.03
Nd ₂ O ₃	6.07	6.14	1.78	2.67	3.16	4.55	0.61	0.17	0.55	0.63
Sm ₂ O ₃	2.20	2.24	0.73	0.90	1.01	1.73	0.53	0.25	0.56	0.59
Eu ₂ O ₃	0.043	0.104	0.001	0.052	<0.001	0.098	<0.001	<0.001	<0.001	<0.001
Gd ₂ O ₃	6.05	5.73	4.63	3.95	4.17	5.54	5.12	2.97	5.43	5.19
Tb ₂ O ₃	0.99	0.93	0.83	0.72	0.75	0.92	0.94	0.62	0.99	0.93
Dy ₂ O ₃	5.90	5.54	5.50	4.83	5.03	5.65	6.50	4.80	6.78	6.22
Ho ₂ O ₃	1.08	0.99	1.05	0.87	0.98	1.02	1.17	1.09	1.26	1.16
Er ₂ O ₃	2.45	2.21	2.57	1.95	2.48	2.27	2.60	3.23	2.95	2.73
Tm ₂ O ₃	0.34	0.32	0.37	0.32	0.36	0.34	0.42	0.63	0.44	0.45
Yb ₂ O ₃	2.04	1.94	2.23	2.21	2.31	2.22	2.88	5.05	2.81	3.20
Lu ₂ O ₃	0.27	0.26	0.30	0.35	0.33	0.32	0.45	0.88	0.40	0.51
TOTAL	101.13	100.79	99.14	98.72	100.14	100.33	100.48	100.90	102.14	98.88
Structural formulae calculated on the basis of 2 (A + B) cations and 4 (O)										
Ti	0.020	0.028	0.013	0.018	0.021	0.010	0.027	0.004	0.028	0.025
Si	0.091	0.113	0.079	0.148	0.149	0.023	0.008	0.001	0.015	0.011
Fe(3+)	0.000	0.000	0.000	0.000	0.000	0.024	0.009	0.031	0.001	0.006
Nb	0.881	0.851	0.901	0.840	0.840	0.927	0.947	0.952	0.951	0.946
Ta	0.006	0.006	0.019	0.018	0.012	0.015	0.008	0.009	0.003	0.005
Zr	0.002	0.002	0.002	0.002	0.003	0.001	0.001	0.002	0.001	0.002
Hf	0.001	0.001	0.001	0.002	0.000	0.000	0.000	0.000	0.001	0.001
B cations	1.000	1.001	1.014	1.028	1.024	1.000	1.000	1.000	1.000	0.995
Ca	0.084	0.103	0.072	0.175	0.146	0.032	0.004	0.016	0.002	0.005
Na	0.000	0.000	0.000	0.002	0.000	0.000	0.000	0.001	0.000	0.000
Fe(2+)	0.013	0.019	0.020	0.033	0.014	0.019	0.019	0.023	0.002	0.000
Mn	0.007	0.009	0.011	0.017	0.015	0.005	0.000	0.001	0.000	0.000
Y	0.458	0.428	0.567	0.429	0.441	0.543	0.656	0.674	0.676	0.677
La	0.001	0.003	0.002	0.004	0.008	0.002	0.000	0.000	0.001	0.000
Ce	0.018	0.021	0.012	0.027	0.041	0.016	0.001	0.001	0.001	0.001
Pr	0.012	0.011	0.004	0.007	0.008	0.009	0.000	0.000	0.000	0.001
Nd	0.094	0.095	0.028	0.040	0.047	0.073	0.010	0.003	0.009	0.010
Sm	0.033	0.033	0.011	0.013	0.015	0.027	0.008	0.004	0.008	0.009
Eu	0.001	0.002	0.000	0.001	0.000	0.001	0.000	0.000	0.000	0.000
Gd	0.087	0.082	0.067	0.055	0.058	0.082	0.075	0.043	0.078	0.077
Tb	0.014	0.013	0.012	0.010	0.010	0.013	0.014	0.009	0.014	0.014
Dy	0.083	0.077	0.077	0.065	0.068	0.081	0.093	0.068	0.095	0.090
Ho	0.015	0.014	0.015	0.012	0.013	0.014	0.016	0.015	0.017	0.017
Er	0.033	0.030	0.035	0.025	0.032	0.032	0.036	0.044	0.040	0.038
Tm	0.005	0.004	0.005	0.004	0.005	0.005	0.006	0.009	0.006	0.006
Yb	0.027	0.025	0.030	0.028	0.029	0.030	0.039	0.067	0.037	0.044
Lu	0.004	0.003	0.004	0.004	0.004	0.004	0.006	0.012	0.005	0.007
Pb	0.000	0.001	0.001	0.001	0.001	0.000	0.001	0.002	0.000	0.001
U	0.006	0.005	0.006	0.006	0.002	0.006	0.003	0.009	0.002	0.004
Th	0.007	0.022	0.009	0.013	0.017	0.006	0.013	0.001	0.005	0.003
A cations	1.000	0.999	0.986	0.972	0.976	1.000	1.000	1.000	1.000	1.005
CV1	1.55	1.38	0.64	0.17	0.83	1.35	1.01	0.78	1.46	1.01
CV2	-5.99	-5.55	-5.96	-4.54	-5.10	-6.71	-7.15	-7.46	-7.63	-6.87

Note: Tb₂O₃, Ho₂O₃, Tm₂O₃, Lu₂O₃ are calculated values determined by interpolation from chondrite-normalized REE pattern. Fe(3+) calculated from total FeO* to make total number of B cations equal 1 (or approach 1 were the total Fe is insufficient). CV1 and CV2 are discrimination variables for the chemical classification of (Y,REE,U,Th)-(Nb,Ta,Ti) oxide minerals from the three-group model of Ercit (2005).

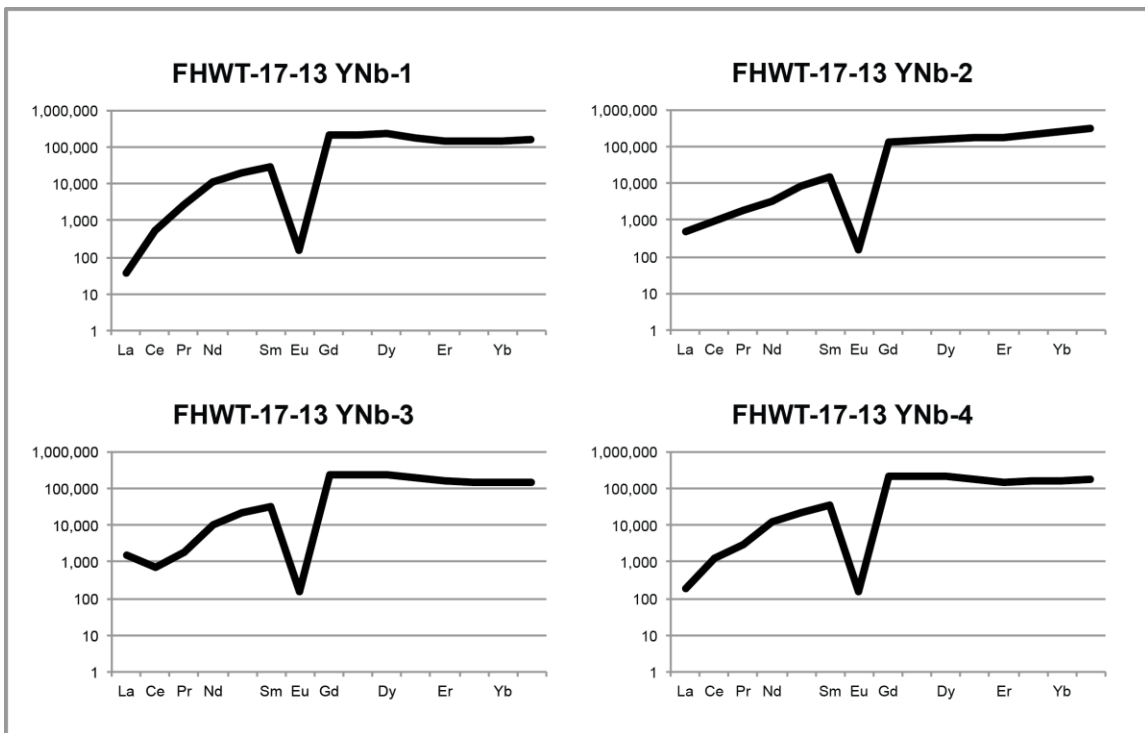


Figure 3-21: Chondrite-normalized REE patterns for fergusonite grains from sample FHWT-17-13.

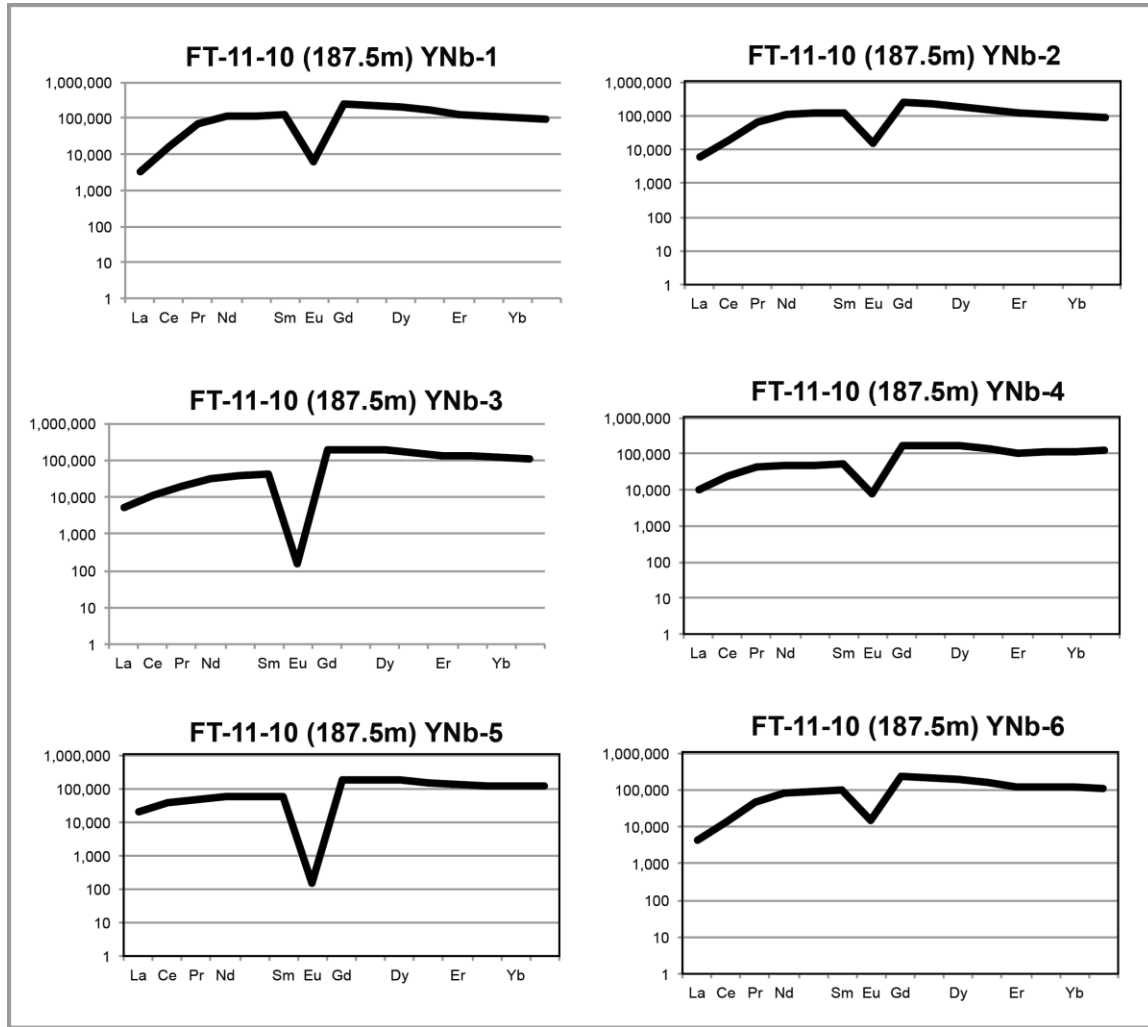


Figure 3-22: Chondrite-normalized REE patterns for fergusonite grains from sample FT-11-10 (187.5m).

3-5-2-2 *Electron Microprobe Analysis of Zircon*

Zircon from the Fox Harbour area often exhibits very interesting morphologies, and textures. Some of the textures observed consist of well- to poorly- defined oscillatory zoning, bimodal (cauliflower zoning), sector zoning, local recrystallization, along with variable amounts of cracking, and microporous voids/pits (Haley et al., 2013). Features

within the zircon correlate with the analyzed *in-situ* U-Pb age (Haley et al., 2013).

Attempting to understand the geochemical signature of the different age populations allows for further understanding of the processes that affected these rocks.

A total of four thin sections were chosen for EPMA analysis on zircon. All three belts are represented by thin sections, along with a sample of the granitic augen gneiss. Thin sections include FHWT-17-13 – South Belt, FT-11-10 (187.5m) – MT Belt (unit FT3), FHC-32-01 – Road Belt, and FT-10-05 (13.8 m) – granitic augen gneiss. Most of the interesting zircon morphologies observed in the Fox Harbour area are represented in this dataset.

Sample FHWT-17-13, from the South Belt included a large cluster of zircon grains, with approximately 9 analyses from in and around this cluster. All grains are almost featureless in BSE, with only small cracks present throughout the grains. Sample FT-11-10 (187.5m) from unit FT3 within the MT Belt contains eight analyses throughout the entire thin section. Grain morphology in this sample is consistent, ranging in size from 50-100 μm , often displaying small pits/voids in the center of the grain. Sample FHC-32-01, from the Road Belt contains the most variable zircon morphology from those analyzed in this study. As discussed in Haley et al. (2013), there are many different zircon textures present in the Fox Harbour area. The majority of the grains in sample FHC-32-01 are fairly simple, displaying simple growth zoning, minimal cracking with the occasional pit/void. Occasionally, there are large zircon grains (100-500 μm), displaying voids/pits throughout the entire grain. A number of these grains are present in sample FHC-32-01, and will be discussed in the following.

The diagram utilized when attempting to interpret EPMA zircon data is a simple X vs Y diagram, utilizing the atoms per formula unit (APFU). In this study, the X-axis will always be Zr (APFU), as the mineral of interest is zircon. The Y-axes chosen consist of U+Th (APFU), Nb+Ta (APFU) and Y+Gd+Dy+Yb (APFU), utilized to show the variability of the HFSE and REE elements in zircon. As can be seen in Figure 3-23, there is a small amount of variability within zircon grains within samples analyzed for the Fox Harbour area.

Sample FHWT-17-13 (South Belt) is fairly consistent on all plots, with the majority of them plotting around 0.99 Zr (APFU). Generally the Y-axes are consistent as well, with average values of 0.0001 (U+Th), 0.0001 (Nb+Ta), and 0.005 (Y+Gd+Dy+Yb). One grain plots with a slightly lower Zr value at 0.965, and higher Y-axes values of 0.0009 (U+Th), 0.000 (Nb+Ta), and 0.0273 (Y+Gd+Dy+Yb). Morphologically, this grain does not look different than the other zircon grains analyzed.

Sample FT-11-10 (187.5m), which is from the MT Belt (FT3), is very similar to the South Belt sample. The grains analyzed plot around 0.95-0.99 Zr (APFU). Uranium-Th in the zircon grains range from 0.000-0.0014, Nb-Ta ranges from 0.0000-0.0018, while Y+Gd+Dy+Yb ranges from 0.0002-0.0081. A single zircon grains appears to be an outlier with a lower Zr value (0.95), and higher U+Th (0.0014), Nb+Ta (0.0018), and average Y+Gd+Dy+Yb (0.0046). Morphologically, the grain does not look different than other zircon grains analyzed.

Sample FHC-32-01, from the Road Belt is the most interesting sample analyzed for this study. As mentioned previously, it contains variable zircon morphologies, which have correlated well with interesting patterns observed in the zircon chemistry. There are

two general populations of zircon in this sample. The first geochemical population is similar to the previous samples, with Zr values ranging from 0.97-1.0, U+Th values of 0.0002-0.0016, Nb+Ta values of 0.0000-0.0006, and Y+Gd+Dy+Yb values of 0.0023-0.0214. Morphologically, these zircon grains are very similar to those seen in previous samples, and are the dominant grain type in the Fox Harbour area. The second population of zircon in this sample is the previously mentioned large microporous grains. As seen in Figure 3-23, this population has much lower Zr values, generally ranging from 0.926-0.943 APFU, which is lower than the general population of grains analyzed. Y-axes values range from 0.0025-0.0048 (U+Th), 0.0012-0.0082 (Nb+Ta), and 0.0130-0.0802 (Y+Gd+Dy+Yb). Similar grains were analyzed for U/Pb and Hf in Haley et al. (2013) with variable success. Many of the disturbed zircon grains (i.e.: those with pits/voids, erratic zoning, and those with embayments) were the younger population (~1050 Ma).

The final sample analyzed by the EPMA was sample FT-10-05 (13.8m), which is a sample of granitic augen gneiss. This sample contains a simple population of zircon, morphologically, and chemically speaking. Zircon grains are small, featureless in BSE, and contain erratic zoning when viewed in CL. Zirconium values range from 0.986-0.997 APFU. The Y-axes values are also quite low in comparison to other samples analyzed in the Fox Harbour area. Y-axes value range from 0.0000-0.0003 (U+Th), 0.0000-0.0000 (Nb+Ta), and 0.0000-0.0005 (Y+Gd+Dy+Yb). Zircon in this sample contains much less variability than the rhyolite units throughout the Fox Harbour area, which is expected.

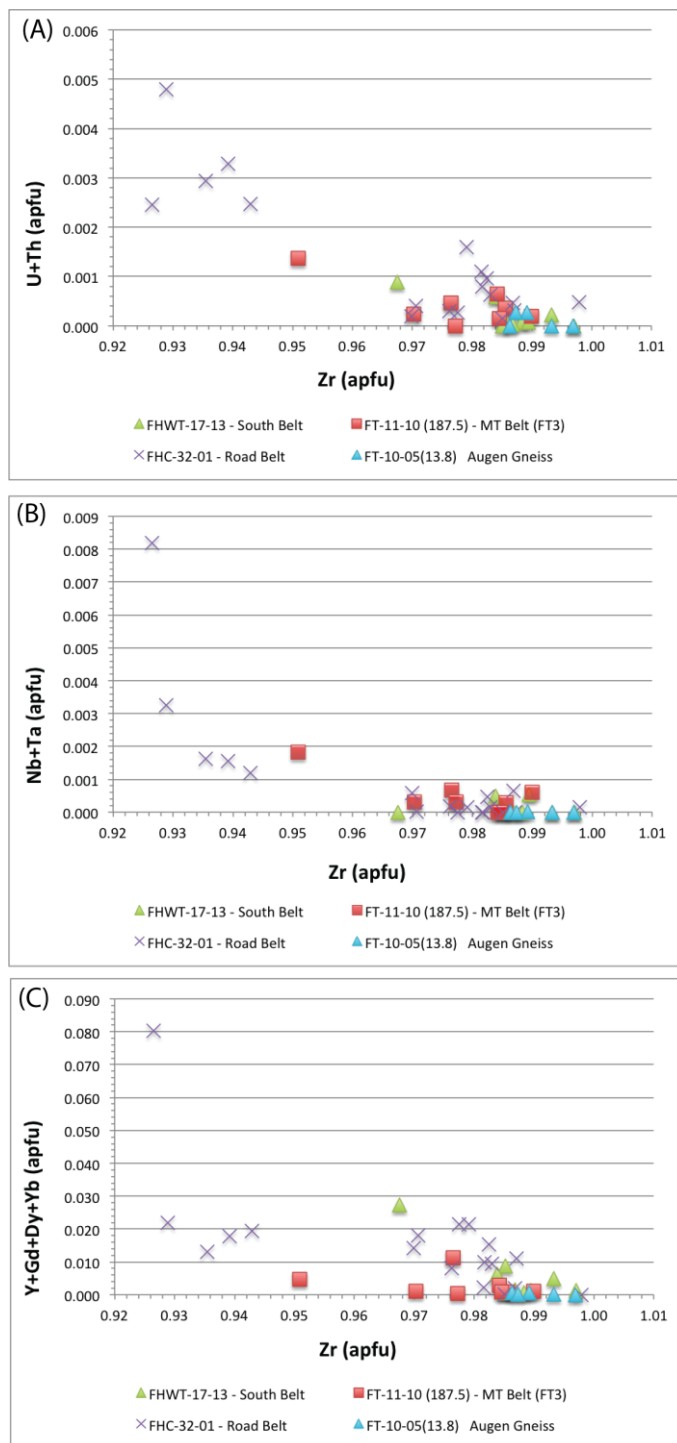


Figure 3-23: EPMA data for zircon in the Fox Harbour area displayed as simple X vs Y A.P.F.U (atoms per formula unit) plots. (A) Zr vs $\text{U}+\text{Th}$, (B) Zr vs $\text{Nb}+\text{Ta}$, (C) Zr vs $\text{Y}+\text{Gd}+\text{Dy}+\text{Yb}$.

Table 3-2: Electron microprobe analyses (wt.%) for zircon

	FT-11-10 (187.5) Main (FT3) Belt							
	zircon-1 area 7	zircon-2 area 7	zircon-3 area 7	zircon-4 area 9	zircon-5 area 9	zircon-6 area 10	zircon-7 area 10	zircon-8 area 11
SiO ₂	32.46	32.28	32.11	32.17	33.76	32.91	32.06	32.46
TiO ₂	0.012	0.000	0.028	0.017	0.032	0.005	0.000	0.001
FeO*	0.099	0.143	0.285	0.259	0.049	0.077	0.081	0.238
MnO	0.004	0.000	0.019	0.017	0.027	0.011	0.000	0.014
CaO	0.004	0.000	0.066	0.005	0.061	0.072	0.036	0.038
Na ₂ O	0.012	0.000	0.000	0.000	0.014	0.000	0.000	0.000
Nb ₂ O ₅	0.021	0.044	0.048	0.000	0.106	0.022	0.000	0.023
Ta ₂ O ₅	0.000	0.000	0.000	0.000	0.045	0.000	0.000	0.000
UO ₂	0.037	0.027	0.048	0.076	0.168	0.013	0.022	0.000
ThO ₂	0.015	0.002	0.019	0.017	0.034	0.021	0.000	0.000
PbO	0.008	0.023	0.017	0.018	0.000	0.043	0.020	0.000
ZrO ₂	65.94	66.08	64.93	65.41	64.35	64.81	64.89	64.76
HfO ₂	1.490	1.424	1.496	1.386	1.415	1.396	1.457	1.272
Y ₂ O ₃	0.027	0.047	0.618	0.152	0.225	0.041	0.049	0.014
Gd ₂ O ₃	0.008	0.000	0.038	0.007	0.000	0.000	0.000	0.024
Dy ₂ O ₃	0.027	0.015	0.000	0.027	0.070	0.047	0.000	0.000
Yb ₂ O ₃	0.000	0.006	0.078	0.017	0.033	0.000	0.000	0.000
TOTAL	100.16	100.09	99.80	99.58	100.39	99.46	98.61	98.85
Structural formulae calculated on the basis of 4 oxygens								
Si	0.995	0.992	0.990	0.993	1.023	1.010	0.997	1.005
Nb	0.000	0.001	0.001	0.000	0.001	0.000	0.000	0.000
Ta	0.000	0.000	0.000	0.000	0.000	0.000	0.000	0.000
Zr	0.986	0.990	0.977	0.984	0.951	0.970	0.985	0.977
Hf	0.015	0.015	0.015	0.014	0.014	0.014	0.015	0.013
U	0.000	0.000	0.000	0.001	0.001	0.000	0.000	0.000
Th	0.000	0.000	0.000	0.000	0.000	0.000	0.000	0.000
Ti	0.000	0.000	0.001	0.000	0.001	0.000	0.000	0.000
Y	0.000	0.001	0.010	0.002	0.004	0.001	0.001	0.000
Gd	0.000	0.000	0.000	0.000	0.000	0.000	0.000	0.000
Dy	0.000	0.000	0.000	0.000	0.001	0.000	0.000	0.000
Yb	0.000	0.000	0.001	0.000	0.000	0.000	0.000	0.000
Ca	0.000	0.000	0.002	0.000	0.002	0.002	0.001	0.001
Na	0.001	0.000	0.000	0.000	0.001	0.000	0.000	0.000
Fe(2+)	0.003	0.004	0.007	0.007	0.001	0.002	0.002	0.006
Mn	0.000	0.000	0.000	0.000	0.001	0.000	0.000	0.000
Pb	0.000	0.000	0.000	0.000	0.000	0.000	0.000	0.000
SUM	2.001	2.002	2.005	2.003	2.002	2.002	2.001	2.003
Nb+Ta	0.0003	0.0006	0.0007	0.0000	0.0018	0.0003	0.0000	0.0003
U+Th	0.0004	0.0002	0.0005	0.0006	0.0014	0.0002	0.0002	0.0000
Y+Gd+Dy+Yb	0.0008	0.0010	0.0113	0.0030	0.0046	0.0011	0.0008	0.0005

Table 3-2 (continued): Electron microprobe analyses (wt.%) for zircon

FHWT-17-13 South Belt									
	zircon-1	zircon-2	zircon-3	zircon-4 light domain	zircon-5 dark domain	zircon-6	zircon-7 light domain (core)	zircon-8 dark domain (rim)	zircon-9
SiO ₂	32.65	32.53	32.78	32.34	32.81	32.50	32.56	32.43	32.25
TiO ₂	0.006	0.000	0.000	0.000	0.018	0.028	0.020	0.000	0.000
FeO*	0.226	0.032	0.033	0.082	0.488	0.096	0.042	0.015	0.016
MnO	0.000	0.000	0.000	0.000	0.000	0.002	0.000	0.004	0.009
CaO	0.004	0.003	0.000	0.010	0.005	0.000	0.013	0.000	0.009
Na ₂ O	0.000	0.000	0.000	0.000	0.000	0.000	0.000	0.000	0.000
Nb ₂ O ₅	0.000	0.005	0.000	0.000	0.000	0.035	0.036	0.000	0.000
Ta ₂ O ₅	0.000	0.000	0.000	0.000	0.000	0.006	0.000	0.000	0.000
UO ₂	0.002	0.008	0.000	0.039	0.000	0.000	0.051	0.000	0.020
ThO ₂	0.009	0.024	0.004	0.088	0.000	0.010	0.035	0.000	0.013
PbO	0.071	0.040	0.026	0.018	0.027	0.012	0.000	0.007	0.049
ZrO ₂	66.39	66.05	66.38	64.40	66.44	66.12	66.12	66.90	66.32
HfO ₂	1.048	1.040	1.155	1.060	0.880	0.931	1.330	0.965	1.035
Y ₂ O ₃	0.000	0.465	0.071	1.356	0.034	0.025	0.312	0.026	0.213
Gd ₂ O ₃	0.006	0.043	0.000	0.130	0.018	0.000	0.035	0.048	0.007
Dy ₂ O ₃	0.047	0.060	0.029	0.123	0.000	0.080	0.094	0.042	0.075
Yb ₂ O ₃	0.000	0.019	0.005	0.263	0.000	0.000	0.000	0.000	0.078
TOTAL	100.46	100.32	100.48	99.91	100.72	99.84	100.65	100.44	100.09
Structural formulae calculated on the basis of 4 oxygens									
Si	0.997	0.995	0.999	0.996	0.997	0.997	0.994	0.991	0.991
Nb	0.000	0.000	0.000	0.000	0.000	0.000	0.000	0.000	0.000
Ta	0.000	0.000	0.000	0.000	0.000	0.000	0.000	0.000	0.000
Zr	0.988	0.985	0.987	0.968	0.985	0.989	0.984	0.997	0.993
Hf	0.011	0.011	0.012	0.011	0.009	0.010	0.014	0.010	0.011
U	0.000	0.000	0.000	0.000	0.000	0.000	0.000	0.000	0.000
Th	0.000	0.000	0.000	0.001	0.000	0.000	0.000	0.000	0.000
Ti	0.000	0.000	0.000	0.000	0.000	0.001	0.000	0.000	0.000
Y	0.000	0.008	0.001	0.022	0.001	0.000	0.005	0.000	0.003
Gd	0.000	0.000	0.000	0.001	0.000	0.000	0.000	0.000	0.000
Dy	0.000	0.001	0.000	0.001	0.000	0.001	0.001	0.000	0.001
Yb	0.000	0.000	0.000	0.002	0.000	0.000	0.000	0.000	0.001
Ca	0.000	0.000	0.000	0.000	0.000	0.000	0.000	0.000	0.000
Na	0.000	0.000	0.000	0.000	0.000	0.000	0.000	0.000	0.000
Fe(2+)	0.006	0.001	0.001	0.002	0.012	0.002	0.001	0.000	0.000
Mn	0.000	0.000	0.000	0.000	0.000	0.000	0.000	0.000	0.000
Pb	0.001	0.000	0.000	0.000	0.000	0.000	0.000	0.000	0.000
SUM	2.003	2.001	2.000	2.006	2.005	2.001	2.000	2.000	2.001
Nb+Ta	0.0000	0.0001	0.0000	0.0000	0.0000	0.0005	0.0005	0.0000	0.0000
U+Th	0.0001	0.0002	0.0000	0.0009	0.0000	0.0001	0.0006	0.0000	0.0002
Y+Gd+Dy+Yb	0.0005	0.0088	0.0015	0.0273	0.0007	0.0012	0.0063	0.0013	0.0050

Table 3-2 (continued): Electron microprobe analyses (wt.%) for zircon

	FHC-32-01 Road Belt- Part 1								
	zircon-1 micro porous grain 216	zircon-2 light domain grain 216	zircon-3 light domain grain 223	zircon-4 dark domain grain 223	zircon-5 grey domain grain 245	zircon-6 grey domain grain 372	zircon-7 grey domain grain 477	zircon-8 light domain grain 490	zircon-9 light core grain 566
SiO ₂	30.57	32.04	31.89	31.87	31.79	32.32	32.00	32.18	32.25
TiO ₂	0.039	0.014	0.024	0.034	0.008	0.000	0.000	0.000	0.012
FeO*	0.810	0.182	0.014	0.014	0.066	0.616	0.064	0.041	0.102
MnO	0.181	0.028	0.000	0.009	0.009	0.000	0.000	0.000	0.006
CaO	0.080	0.042	0.000	0.012	0.004	0.032	0.010	0.009	0.008
Na ₂ O	0.063	0.004	0.000	0.000	0.000	0.003	0.000	0.000	0.000
Nb ₂ O ₅	0.573	0.000	0.021	0.011	0.000	0.000	0.011	0.002	0.000
Ta ₂ O ₅	0.000	0.000	0.022	0.000	0.000	0.000	0.000	0.000	0.000
UO ₂	0.165	0.117	0.018	0.064	0.022	0.022	0.102	0.048	0.072
ThO ₂	0.180	0.041	0.119	0.005	0.017	0.000	0.127	0.011	0.044
PbO	0.045	0.000	0.029	0.000	0.037	0.022	0.032	0.007	0.009
ZrO ₂	56.13	64.76	64.87	65.89	64.22	65.77	64.94	63.87	65.22
HfO ₂	1.309	1.492	1.014	0.991	1.020	1.229	0.921	1.070	1.075
Y ₂ O ₃	3.812	0.109	0.779	0.000	1.086	0.010	1.065	0.858	0.455
Gd ₂ O ₃	0.546	0.000	0.088	0.002	0.093	0.000	0.119	0.043	0.063
Dy ₂ O ₃	0.720	0.026	0.089	0.003	0.107	0.009	0.166	0.173	0.062
Yb ₂ O ₃	0.316	0.022	0.069	0.000	0.141	0.000	0.123	0.183	0.131
TOTAL	95.54	98.88	99.04	98.91	98.62	100.03	99.68	98.49	99.51
Structural formulae calculated on the basis of 4 oxygens									
Si	0.966	0.996	0.990	0.990	0.992	0.993	0.989	1.003	0.995
Nb	0.008	0.000	0.000	0.000	0.000	0.000	0.000	0.000	0.000
Ta	0.000	0.000	0.000	0.000	0.000	0.000	0.000	0.000	0.000
Zr	0.926	0.982	0.982	0.998	0.978	0.985	0.979	0.971	0.982
Hf	0.014	0.015	0.010	0.010	0.011	0.013	0.009	0.011	0.011
U	0.001	0.001	0.000	0.000	0.000	0.000	0.001	0.000	0.000
Th	0.001	0.000	0.001	0.000	0.000	0.000	0.001	0.000	0.000
Ti	0.001	0.000	0.001	0.001	0.000	0.000	0.000	0.000	0.000
Y	0.064	0.002	0.013	0.000	0.018	0.000	0.018	0.014	0.007
Gd	0.006	0.000	0.001	0.000	0.001	0.000	0.001	0.000	0.001
Dy	0.007	0.000	0.001	0.000	0.001	0.000	0.002	0.002	0.001
Yb	0.003	0.000	0.001	0.000	0.001	0.000	0.001	0.002	0.001
Ca	0.003	0.001	0.000	0.000	0.000	0.001	0.000	0.000	0.000
Na	0.004	0.000	0.000	0.000	0.000	0.000	0.000	0.000	0.000
Fe(2+)	0.021	0.005	0.000	0.000	0.002	0.016	0.002	0.001	0.003
Mn	0.005	0.001	0.000	0.000	0.000	0.000	0.000	0.000	0.000
Pb	0.000	0.000	0.000	0.000	0.000	0.000	0.000	0.000	0.000
SUM	2.031	2.004	2.001	2.000	2.005	2.008	2.003	2.004	2.002
Nb+Ta	0.0082	0.0000	0.0005	0.0002	0.0000	0.0000	0.0002	0.0000	0.0000
U+Th	0.0025	0.0011	0.0010	0.0005	0.0003	0.0002	0.0016	0.0004	0.0008
Y+Gd+Dy+Yb	0.0802	0.0023	0.0153	0.0001	0.0214	0.0003	0.0216	0.0182	0.0100

Table 3-2 (continued): Electron microprobe analyses (wt.%) for zircon

	FHC-32-01 Road Belt- Part 2								
	zircon-10 micro porous grain 566	zircon-11 light domain grain 1300	zircon-12 micro porous grain 1300	zircon-13 light domain grain 1465	zircon-14 grey domain grain 1689	zircon-15 micro porous grain 1684	zircon-16 micro porous grain 1684	zircon-17 grey domain grain 1892	zircon-18 grey domain grain 1892
SiO ₂	32.90	32.24	32.13	32.02	32.33	32.10	32.77	32.50	32.36
TiO ₂	0.051	0.000	0.000	0.000	0.018	0.004	0.000	0.000	0.000
FeO*	0.100	0.027	0.135	0.037	0.026	0.447	0.276	0.026	0.069
MnO	0.000	0.000	0.047	0.004	0.000	0.126	0.011	0.000	0.010
CaO	0.049	0.023	0.036	0.007	0.000	0.202	0.024	0.012	0.014
Na ₂ O	0.087	0.003	0.071	0.000	0.000	0.077	0.119	0.000	0.000
Nb ₂ O ₅	0.115	0.046	0.083	0.000	0.000	0.072	0.231	0.000	0.000
Ta ₂ O ₅	0.000	0.000	0.000	0.019	0.068	0.062	0.000	0.021	0.000
UO ₂	0.172	0.067	0.172	0.052	0.003	0.191	0.127	0.043	0.022
ThO ₂	0.245	0.000	0.173	0.038	0.024	0.271	0.553	0.000	0.023
PbO	0.070	0.016	0.030	0.035	0.028	0.028	0.114	0.010	0.026
ZrO ₂	61.46	65.42	60.90	64.77	64.02	60.98	61.15	64.72	66.07
HfO ₂	1.659	1.123	1.236	1.094	1.016	1.431	1.678	1.105	1.074
Y ₂ O ₃	0.683	0.092	0.937	0.454	0.707	0.925	1.044	0.411	0.565
Gd ₂ O ₃	0.065	0.007	0.091	0.064	0.081	0.068	0.129	0.066	0.008
Dy ₂ O ₃	0.049	0.000	0.108	0.085	0.099	0.060	0.139	0.062	0.065
Yb ₂ O ₃	0.055	0.044	0.164	0.035	0.075	0.109	0.190	0.000	0.106
TOTAL	97.76	99.10	96.31	98.72	98.50	97.15	98.56	98.97	100.41
Structural formulae calculated on the basis of 4 oxygens									
Si	1.027	0.997	1.020	0.997	1.004	1.014	1.021	1.005	0.991
Nb	0.002	0.001	0.001	0.000	0.000	0.001	0.003	0.000	0.000
Ta	0.000	0.000	0.000	0.000	0.001	0.001	0.000	0.000	0.000
Zr	0.935	0.987	0.943	0.983	0.970	0.939	0.929	0.976	0.987
Hf	0.017	0.012	0.013	0.011	0.011	0.015	0.017	0.011	0.011
U	0.001	0.000	0.001	0.000	0.000	0.001	0.001	0.000	0.000
Th	0.002	0.000	0.001	0.000	0.000	0.002	0.004	0.000	0.000
Ti	0.001	0.000	0.000	0.000	0.000	0.000	0.000	0.000	0.000
Y	0.011	0.002	0.016	0.008	0.012	0.016	0.017	0.007	0.009
Gd	0.001	0.000	0.001	0.001	0.001	0.001	0.001	0.001	0.000
Dy	0.000	0.000	0.001	0.001	0.001	0.001	0.001	0.001	0.001
Yb	0.001	0.000	0.002	0.000	0.001	0.001	0.002	0.000	0.001
Ca	0.002	0.001	0.001	0.000	0.000	0.007	0.001	0.000	0.000
Na	0.005	0.000	0.004	0.000	0.000	0.005	0.007	0.000	0.000
Fe(2+)	0.003	0.001	0.004	0.001	0.001	0.012	0.007	0.001	0.002
Mn	0.000	0.000	0.001	0.000	0.000	0.003	0.000	0.000	0.000
Pb	0.001	0.000	0.000	0.000	0.000	0.000	0.001	0.000	0.000
SUM	2.008	2.000	2.010	2.003	2.001	2.018	2.013	2.003	2.003
Nb+Ta	0.0016	0.0006	0.0012	0.0002	0.0006	0.0016	0.0033	0.0002	0.0000
U+Th	0.0029	0.0005	0.0025	0.0006	0.0002	0.0033	0.0048	0.0003	0.0003
Y+Gd+Dy+Yb	0.0130	0.0020	0.0195	0.0094	0.0142	0.0179	0.0218	0.0081	0.0109

Table 3-2 (continued): Electron microprobe analyses (wt.%) for zircon

FT-10-05(13.8) Augen Gneiss					
	zircon-1 grain 97-1	zircon-2 grain 97-2	zircon-3 gran 260	zircon-4 grain 245	zircon-5 grain 485
SiO ₂	32.24	32.19	32.19	32.14	32.09
TiO ₂	0.042	0.162	0.003	0.024	0.005
FeO*	0.541	0.102	0.139	0.208	0.228
MnO	0.006	0.000	0.006	0.011	0.017
CaO	0.004	0.090	0.057	0.055	0.051
Na ₂ O	0.000	0.000	0.000	0.000	0.000
Nb ₂ O ₅	0.001	0.000	0.000	0.000	0.000
Ta ₂ O ₅	0.000	0.000	0.000	0.000	0.000
UO ₂	0.033	0.000	0.000	0.000	0.039
ThO ₂	0.007	0.000	0.000	0.000	0.000
PbO	0.020	0.000	0.022	0.000	0.026
ZrO ₂	66.28	65.76	66.40	66.86	65.58
HfO ₂	1.462	1.596	1.536	1.529	1.624
Y ₂ O ₃	0.000	0.000	0.000	0.000	0.000
Gd ₂ O ₃	0.000	0.055	0.009	0.000	0.016
Dy ₂ O ₃	0.053	0.000	0.000	0.002	0.000
Yb ₂ O ₃	0.000	0.000	0.000	0.000	0.000
TOTAL	100.68	99.96	100.36	100.83	99.67
Structural formulae calculated on the basis of 4 oxygens					
Si	0.987	0.990	0.987	0.983	0.991
Nb	0.000	0.000	0.000	0.000	0.000
Ta	0.000	0.000	0.000	0.000	0.000
Zr	0.989	0.986	0.993	0.997	0.987
Hf	0.015	0.016	0.016	0.016	0.017
U	0.000	0.000	0.000	0.000	0.000
Th	0.000	0.000	0.000	0.000	0.000
Ti	0.001	0.004	0.000	0.001	0.000
Y	0.000	0.000	0.000	0.000	0.000
Gd	0.000	0.001	0.000	0.000	0.000
Dy	0.001	0.000	0.000	0.000	0.000
Yb	0.000	0.000	0.000	0.000	0.000
Ca	0.000	0.003	0.002	0.002	0.002
Na	0.000	0.000	0.000	0.000	0.000
Fe(2+)	0.014	0.003	0.004	0.005	0.006
Mn	0.000	0.000	0.000	0.000	0.000
Pb	0.000	0.000	0.000	0.000	0.000
SUM	2.007	2.003	2.002	2.003	2.004
Nb+Ta	0.0000	0.0000	0.0000	0.0000	0.0000
U+Th	0.0003	0.0000	0.0000	0.0000	0.0003
Y+Gd+Dy+Yb	0.0005	0.0006	0.0001	0.0000	0.0002

3-5-3 IN-SITU LUTETIUM-HAFNIUM ANALYSIS OF ZIRCON

Lutetium and Hf isotopes were analyzed on the two main age populations of zircon identified in the study by Haley et al. (2013). These two age populations are the primary age of formation of the rhyolite units, at \sim 1300 Ma, and the age of high-grade Grenvillian deformation \sim 1050 Ma (Haley et al., 2013). There is a third, less present age population, consisting of inherited zircon grains. A total of two zircon grains are considered inherited, dated at 1388 ± 65 Ma, and 1410 ± 53 Ma (Haley et al., 2013). The Lu-Hf isotope results are presented in Figure 3-24, and 3-25, while all Lu-Hf isotope measurements are presented in Table 3-3.

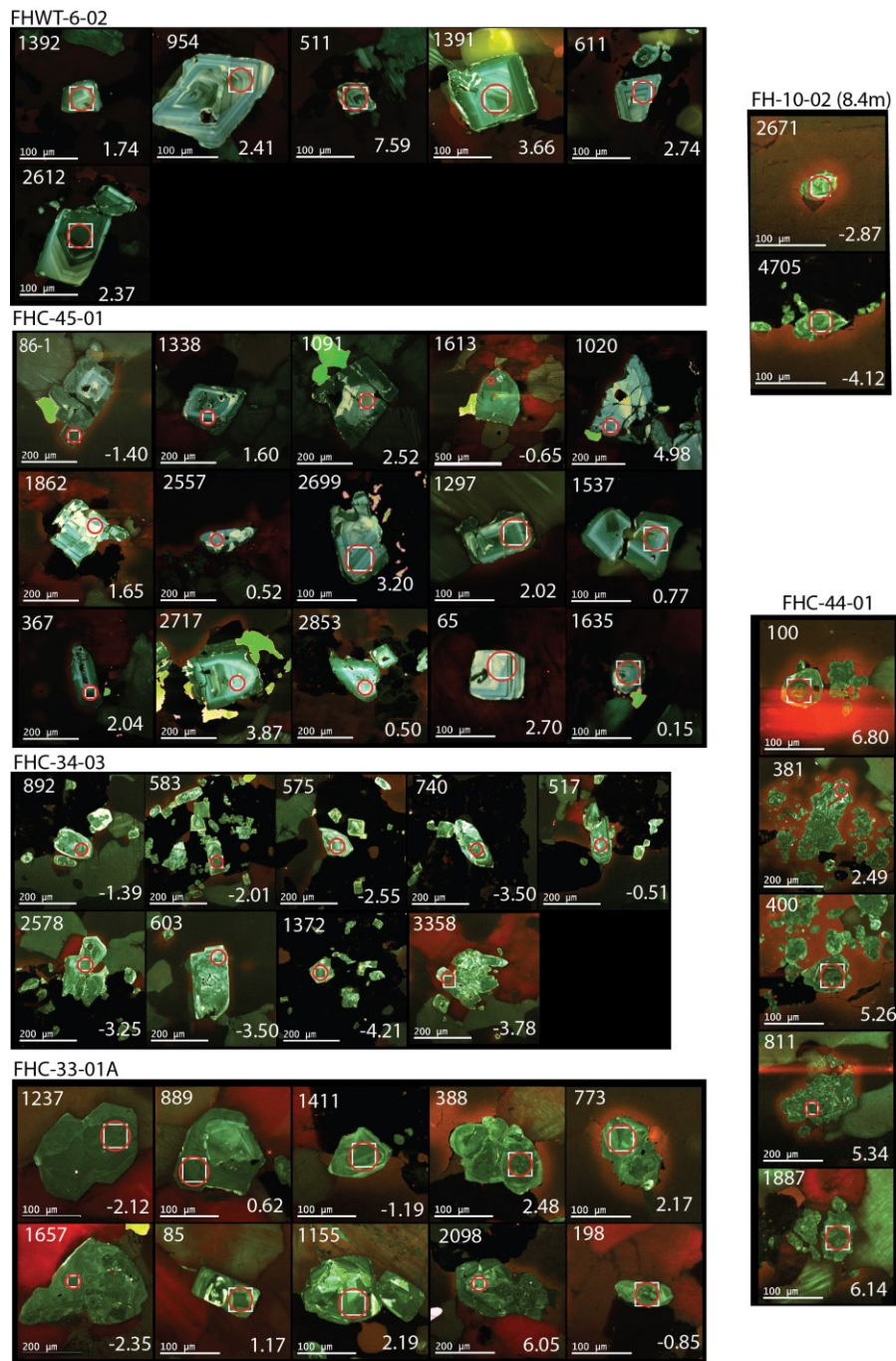


Figure 3-24: Cathodoluminescence images of zircon from the Fox Harbour area. *In-situ* U-Pb 40x40 µm spots depicted by white box. *In-situ* Hf analysis (40µm, or 49µm circles) depicted by red circle, directly overtop U-Pb spot.

A total of six zircon grains were analyzed for sample FHWT-6-02, located in the South Belt. These analyses have $\epsilon\text{Hf}(t)$ values ranging from +1.74 to +7.59. All grains analyzed in this sample contain the magmatic age of 1300 ± 2.5 Ma (Haley et al., 2013).

A total of two grains were analyzed for sample FH-10-02 (8.4 m), located in the MT Belt. Analyzed grains have $\epsilon\text{Hf}(t)$ values ranging from -2.97 to -4.12, and have a U-Pb age of 1018 Ma (Haley et al., 2013).

A total of six zircon grains were analyzed for sample FHC-44-01, located in the MT Belt. All grains analyzed have $\epsilon\text{Hf}(t)$ values ranging from +1.46 to +6.80, and a U-Pb magmatic age of 1346 ± 51 Ma (Haley et al., 2013).

A total of 13 zircon grains were analyzed for sample FHC-45-01, located in the MT Belt. All grains analyzed have $\epsilon\text{Hf}(t)$ values ranging from -4.12 to +4.98. Sample FHC-45-01 has three *in-situ* U-Pb ages, 1031 ± 73 Ma, 1250 ± 20 Ma, and 1388 ± 65 Ma, of which the majority of the zircon grains analyzed are 1250 ± 20 Ma (Haley et al., 2013).

A total of 12 zircon grains were analyzed for sample FHC-33-01A, located in the Road Belt. All grains analyzed have $\epsilon\text{Hf}(t)$ values ranging from -2.35 to +6.05. Sample FHC-33-01A has three *in-situ* U-Pb ages, 1050 ± 21 Ma, 1256 ± 24 Ma, and 1410 ± 53 Ma (Haley et al., 2013).

A total of nine zircon grains were analyzed for sample FHC-34-03, from the Road Belt. All grains analyzed have $\epsilon\text{Hf}(t)$ values ranging from -4.21 to -0.51, and a metamorphic age of 1047 ± 17 Ma (Haley et al., 2013).

All of the analyzed zircon analyses plot below the Hf isotope evolution curves for depleted and arc mantle (Figure 3-25). Most of the *ca.* 1300 Ma grains have $\epsilon\text{Hf}(t)$

values of ~ 0 to $+5$, whereas most of the *ca.* 1050 Ma grains have $\epsilon\text{Hf}(t)$ values of ~ 0 to -5 .

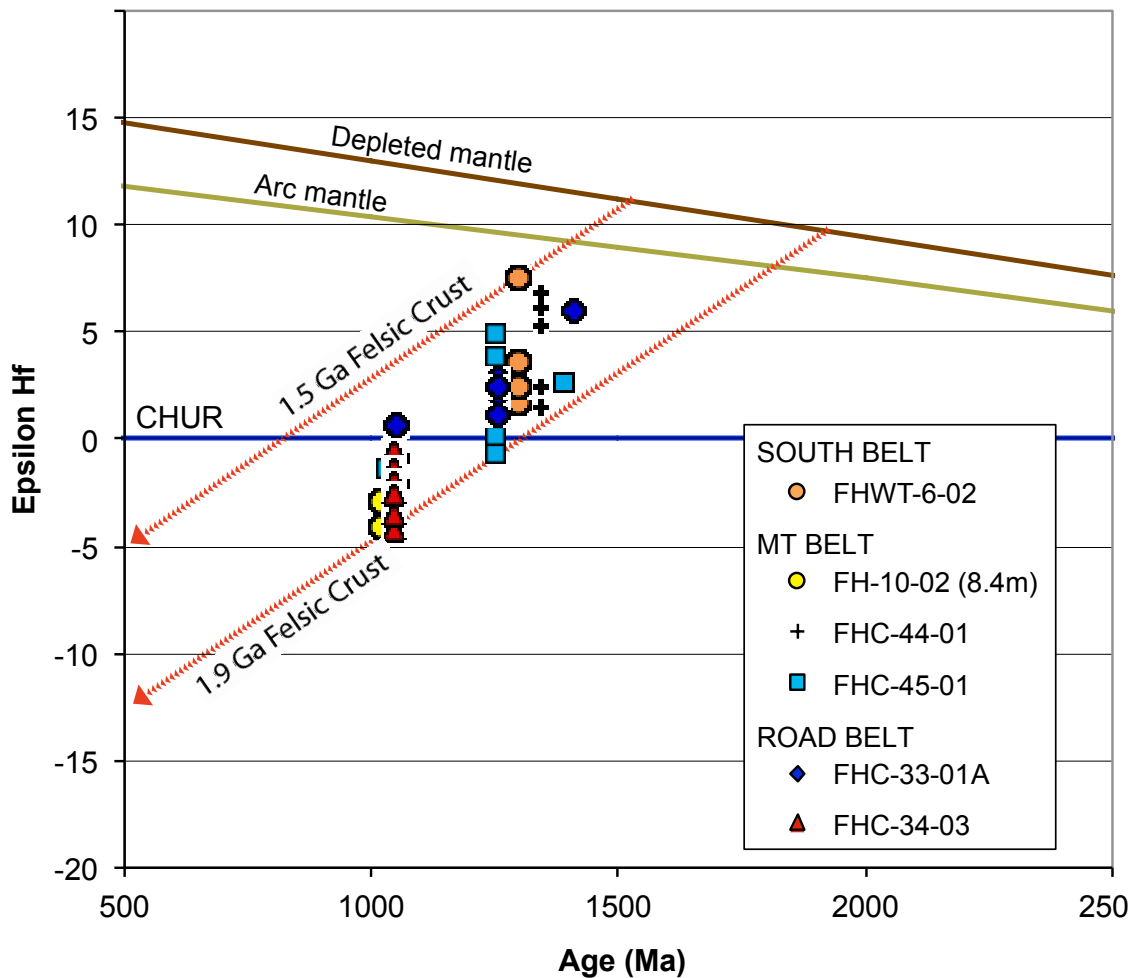


Figure 3-25: $\epsilon\text{Hf}(t)$ results for zircon from the Fox Harbour area. U-Pb zircon ages obtained via *in-situ* LA-ICPMS analysis (Haley et al., 2013). Lutetium decay constant from Söderlund et al. (2004). CHUR values from Bouvier et al. (2008). Model depleted mantle from Griffin et al. (2000); updated by Andersen et al. (2009). Model arc mantle from Dhuime et al. (2011). Model Hf evolution lines for felsic crustal sources assuming $^{176}\text{Lu}/^{177}\text{Hf} = 0.010$ (Pietranik et al., 2008).

Table 3-3: Lu-Hf isotope measurements of zircon from Fox Harbour volcanic rocks by LA-MC-ICPMS

Grain ¹	Age ² (Ma)	$\pm 2s$	Hf ³ (ppm)	$^{176}\text{Hf}/^{177}\text{Hf}$	$\pm 2\text{SE}$	$^{176}\text{Lu}/^{177}\text{Hf}$	$\pm 2\text{SE}$	$^{176}\text{Hf}/^{177}\text{Hf}_{(\text{t})}^{\text{4}}$	$\varepsilon\text{Hf}_{(\text{T})}^{\text{5}}$	$\pm 2\text{SE}$	T_{DM}^{6} (Ga)
SAMPLE FHC-33-01A (Road Belt)											
Metamorphic grains											
889	1050	21	8722	0.282153	3.8E-05	0.000778	2.7E-06	0.282137	0.62	1.35	1.69
1657	1050	21	6806	0.282065	3.3E-05	0.000569	2.4E-06	0.282053	-2.35	1.16	1.84
1141	1050	21	8226	0.282099	3.5E-05	0.000646	7.0E-06	0.282086	-1.19	1.24	1.78
198	1050	21	3804	0.282118	6.5E-05	0.001090	3.2E-05	0.282096	-0.85	2.30	1.76
1237	1050	21	7553	0.282082	3.4E-05	0.001117	2.5E-05	0.282060	-2.12	1.19	1.83
Magmatic grains											
986	1256	24	8928	0.282082	2.5E-05	0.000679	4.3E-06	0.282066	2.77	0.89	1.74
1155	1256	24	7653	0.282097	3.2E-05	0.002008	1.2E-04	0.282050	2.19	1.13	1.77
1008	1256	24	8979	0.282064	3.5E-05	0.000959	1.6E-05	0.282041	1.89	1.24	1.79
85	1256	24	4722	0.282032	4.6E-05	0.000488	2.1E-05	0.282021	1.17	1.64	1.83
773	1256	24	7757	0.282063	3.9E-05	0.000583	1.9E-05	0.282049	2.17	1.39	1.77
388	1256	24	4524	0.282092	6.9E-05	0.001454	1.6E-05	0.282058	2.48	2.45	1.76
Inherited grain											
2098	1410	53	4746	0.282078	5.7E-05	0.000691	1.1E-05	0.282059	6.05	2.01	1.70
SAMPLE FHC-34-03 (Road Belt)											
Metamorphic grains											
603	1047	17	7196	0.282039	5.8E-05	0.000795	8.6E-06	0.282023	-3.50	2.05	1.90
2978	1047	17	7922	0.282047	2.8E-05	0.000871	8.6E-06	0.282030	-3.25	1.00	1.88
3358	1047	17	3426	0.282034	7.9E-05	0.000943	2.9E-05	0.282015	-3.78	2.79	1.91
517	1047	17	4351	0.282117	5.3E-05	0.000478	4.3E-06	0.282107	-0.51	1.87	1.74
892	1047	17	8042	0.282091	3.5E-05	0.000414	9.3E-06	0.282082	-1.39	1.23	1.79
1372	1047	17	8029	0.282014	3.9E-05	0.000546	2.0E-06	0.282003	-4.21	1.39	1.93
583	1047	17	4246	0.282085	3.9E-05	0.000995	5.6E-06	0.282065	-2.01	1.40	1.82
740	1047	17	4554	0.282034	4.6E-05	0.000543	4.7E-06	0.282023	-3.50	1.63	1.90
575	1047	17	6337	0.282059	4.0E-05	0.000458	9.3E-06	0.282050	-2.55	1.41	1.85
SAMPLE FHC-44-01 (MT Belt)											
Magmatic grains											
400	1346	51	2820	0.282132	6.1E-05	0.002131	1.3E-05	0.282078	5.26	2.16	1.69
811	1346	51	6501	0.282099	3.7E-05	0.000734	2.0E-05	0.282080	5.34	1.32	1.68
1887	1346	51	3311	0.282131	7.4E-05	0.001087	3.3E-05	0.282103	6.14	2.61	1.64
100	1346	51	3676	0.282153	6.2E-05	0.001229	4.2E-05	0.282122	6.80	2.20	1.61
381	1346	51	3815	0.282021	5.6E-05	0.000813	3.6E-05	0.282000	2.49	1.98	1.83
636	1346	51	3990	0.281983	4.8E-05	0.000457	1.3E-05	0.281971	1.46	1.71	1.89

Table 3-3 (Continued)

Grain ¹	Age ² (Ma)	$\pm 2s$	Hf ³ (ppm)	$^{176}\text{Hf}/^{177}\text{Hf}$	$\pm 2\text{SE}$	$^{176}\text{Lu}/^{177}\text{Hf}$	$\pm 2\text{SE}$	$^{176}\text{Hf}/^{177}\text{Hf}_{(t)}$ ⁴	$\varepsilon\text{Hf}_{(T)}$ ⁵	$\pm 2\text{SE}$	T_{DM} ⁶ (Ga)
SAMPLE FH-10-02 (8.4m) (MT Belt)											
Metamorphic grains											
2671	1018	30	4765	0.282078	3.9E-05	0.001005	1.6E-05	0.282059	-2.87	1.37	1.84
4705	1018	30	4084	0.282041	5.1E-05	0.000882	5.6E-06	0.282024	-4.12	1.80	1.91
SAMPLE FHC-45-01 (MT Belt)											
Metamorphic grain											
86-1	1031	73	4262	0.282154	5.8E-05	0.003161	5.1E-05	0.282092	-1.40	2.05	1.78
Magmatic grains											
1297	1250	20	4844	0.282122	4.1E-05	0.003127	2.9E-05	0.282049	2.02	1.47	1.78
1862	1250	20	4467	0.282077	5.0E-05	0.001641	1.4E-05	0.282038	1.65	1.78	1.80
1613	1250	20	4266	0.282040	6.2E-05	0.002809	1.8E-05	0.281973	-0.65	2.21	1.92
1091	1250	20	4057	0.282085	5.9E-05	0.000954	2.3E-06	0.282063	2.52	2.09	1.75
1635	1250	20	2463	0.282040	7.5E-05	0.001855	2.1E-05	0.281996	0.15	2.65	1.88
1338	1250	20	3630	0.282100	6.9E-05	0.002666	5.4E-05	0.282037	1.60	2.44	1.80
2699	1250	20	3725	0.282123	6.0E-05	0.001734	2.0E-05	0.282082	3.20	2.14	1.72
367	1250	20	3404	0.282114	6.7E-05	0.002765	6.0E-06	0.282049	2.04	2.38	1.78
2717	1250	20	3322	0.282124	5.9E-05	0.000984	4.5E-06	0.282101	3.87	2.08	1.68
1020	1250	20	3360	0.282165	6.2E-05	0.001404	6.4E-06	0.282132	4.98	2.21	1.62
1657	1250	20	4762	0.282095	3.7E-05	0.001892	8.5E-05	0.282050	2.07	1.30	1.78
Inherited grain											
65	1388	65	3179	0.282006	5.3E-05	0.001041	6.6E-06	0.281979	2.70	1.87	1.86
SAMPLE FHWT-6-02 (South Belt)											
Magmatic grains											
611	1297	21	2454	0.282080	6.7E-05	0.001703	4.1E-05	0.282039	2.74	2.37	1.78
2612-1	1297	21	3035	0.282048	5.1E-05	0.000822	7.7E-06	0.282028	2.37	1.80	1.80
511	1297	21	2399	0.282216	7.2E-05	0.001630	2.0E-05	0.282176	7.59	2.54	1.53
1392	1297	21	4018	0.282033	4.3E-05	0.000912	7.6E-06	0.282011	1.74	1.54	1.83
1391	1297	21	3634	0.282119	8.5E-05	0.002214	2.5E-05	0.282065	3.66	3.02	1.73
954	1297	21	4098	0.282052	3.7E-05	0.000912	9.6E-06	0.282029	2.41	1.32	1.80

¹ Grain numbers are the same as those analyzed for U-Pb geochronology by LA-ICPMS

² Ages determined by U-Pb geochronology by LA-ICPMS

³ Hf concentrations determined from sensitivity of 178Hf (V) in Plešovice zircon using Hf=11167 ppm (Sláma et al., 2008).

⁴ Initial Hf-isotope ratio calculated using ^{176}Lu decay constant ($1.867 \times 10^{-11}/\text{yr}$) of Söderlund et al. (2004)

⁵ Epsilon values calculated using chondritic values of $^{176}\text{Lu}/^{177}\text{Hf}=0.0336$ and $^{176}\text{Hf}/^{177}\text{Hf}=0.282785$ (Bouvier et al., 2008)

⁶ T_{DM} (Ga) are the model Hf ages for felsic crustal sources assuming $^{176}\text{Lu}/^{177}\text{Hf} = 0.010$ (Pietranik et al., 2008) and model depleted mantle with present day $^{176}\text{Hf}/^{177}\text{Hf}$ ratio of 0.28325 and $^{176}\text{Lu}/^{177}\text{Hf}$ ratio of 0.0388 (Griffin et al., 2000; updated by Andersen et al., 2009)

3-6 DISCUSSION

Geochemically, the rhyolitic units from the Fox Harbour display a very interesting story. Generally, the rhyolite units are comendites and pantellerites; rock types denoted to units that are peralkaline. Many of the REE mineralized samples contain sodic- pyroxenes

\pm sodic- amphiboles, minerals often found in peralkaline rocks. The more mineralized samples also plot in the peralkaline field on Shand's Index, utilized for determining the alumina saturation for rocks (Maniar and Piccoli, 1989), although it should be noted that Shand's Index is often inconsistent with altered volcanic rocks, as is the case in this project area. Therefore, the peralkaline nature of these rocks is determined by the presence of sodic amphibole, and sodic pyroxene, which are commonly found in peralkaline rocks. It appears as though the units in the Fox Harbour area have been subjected to variable amounts of post-depositional metasomatism, which often affects subaerial volcanic rocks of this nature. The observed Na, Al, and K mobility is possibly due to alteration of the volcanic piles after deposition, and that the removal of these elements is not due to metamorphism. This metasomatism appears to have had variable geochemical affect on the rhyolitic units, concentrating on the highly mineralized units. The chondrite-normalized REE diagrams for all three belts are very similar, with only small variations discernable between them.

Electron microprobe analysis confirmed the occurrence of fergusonite as a major REE carrier mineral in the rocks. The two samples analyzed, one from the South Belt, and one from the MT Belt have slightly different REE patterns. Fergusonite grains from the MT Belt (FT-11-10 (187.5 m)) display variable geochemistry, such as variable negative Eu anomalies, and somewhat variable LREE slopes between grains. Fergusonite grains from the South Belt (FHWT-17-13) show more consistent REE patterns, each with more strongly depleted LREE slopes, along with large negative Eu anomalies. The variation of fergusonite chemistry is likely primary, although remobilization during Grenvillian

deformation cannot be ruled out. Although not analyzed, allanite is also a major REE-mineral present in the Fox Harbour area.

Electron microprobe analysis of zircon records differences in zircon grains throughout the Fox Harbour area. The majority of the grains plot similarly, with small amounts of U, Th, Nb, Ta, Y, Gd, Dy, or Yb. A small population of zircon grains, mostly found in sample FHC-32-01, although morphologically similar grains are present in other non-analyzed samples, displays a much different chemistry. These grains have much lower Zr (APFU) values, likely due to the fact that the U, Th, Nb, Ta, Y, Gd, Dy, and Yb have replaced Zr in the crystal structure. These grains look drastically different in backscatter and CL imaging, appearing as large microporous grains with voids/pits throughout. EPMA confirmed that these pits are not inclusions of minerals. U-Pb dating of these particular grains concluded that they were of the ~1050 Ma age population found in the Fox Harbour package of rocks (Haley et al., 2013). Based on the data presented in this study, an interesting conclusion can be displayed. The author suggests that there was a zircon dissolution and reprecipitation event during 1050 Ma Grenvillian high-grade metamorphism. Zircon features in the Fox Harbour are very similar to those found in Giesler et al. (2007), and Schwartz et al. (2010); studies conducted on the re-equilibration of zircon in aqueous fluids and melts.

In-situ Lu-Hf measurements integrated with *in-situ* U-Pb age determinations allow for the interpretation of the magma source. Zircon grains with an age of ~1.3 Ga have slightly variable $\epsilon\text{Hf}(t)$ values, ranging between -0.65 to +7.59, as seen in Figure 3-25. This suggests that the magmas that formed the ~1.3 Ga Fox Harbour units were derived

by partial melting 1.5 to 1.9 Ga felsic crustal sources. This finding suggests that any of the terranes in southeastern Labrador could have been the source for the magmas that created the Fox Harbour volcanics. Labradorian rocks, ranging in age from approximately 1.6-1.7 Ga characterize both the Lake Melville, and Mealy Mountain terranes. The Pinware terrane contains a broad range of magmatic ages, ranging from ~1650 Ma to ~950 Ma. The older ~1.6 Ga rocks are highly deformed supracrustal packages, found locally throughout the Pinware terrane. Much of the Pinware terrane has been dated at approximately ~1.45 Ga, meaning that it is possibly too young to be the source for the Fox Harbour magmas.

The metamorphic 1.05 Ga zircon grains have $\epsilon_{\text{Hf}}(t)$ values, ranging between +0.62 to -4.21, as seen in Figure 3-25. The Lu/Hf ratios for the 1.3 Ga primary magmatic and 1.05 Ga metamorphic grains are very similar such that the younger grains fall along the same Hf-isotope crustal evolution array for 1.5 to 1.9 Ga sources as the older grains. This suggests that the 1.05 Ga amphibolite grade Grenvillian metamorphism was a closed system for Lu-Hf isotopes, with no flux of REE into or out of the rocks, which would have affected the analyzed Lu/Hf ratios. This is a very interesting finding, as it suggests that the HFSE and REE were simply remobilized within the volcanic packages, and not removed or added during the Grenville metamorphism.

Based on the findings in this discussion, along with those presented by Haley et al. (2013), this package of volcanic to sub-volcanic rocks tells a very interesting story. Rhyolite units that have been dated confirmed a date of formation at 1.3 Ga (Haley et al., 2013). Although not quantified, it is believed that the subalkaline basalts, quartzite, and

aplitic intrusions are of similar age. The rhyolite units were derived from partial melts of 1.5 to 1.9 Ga felsic crustal sources. All lithotectonic terranes in this area of the Grenville Province contain 1.5 to 1.9 Ga felsic crust, therefore a definitive source cannot be confidently identified. As shown by the *in-situ* Hf isotopic analysis of zircon, there was no flux of REE in or out of the volcanic packages. Therefore, all HFSE and REE present in the rhyolitic units are primary, with the possibility of some secondary mobilization within the rhyolite units, presumably during deformation. Lithogeochemistry suggests that REE mobility between units was minimal to nil, as shown by the XY incompatible vs incompatible, which plot at a consistent ratio across the full geochemical spectrum with respect to each element taken into consideration (i.e.: Zr vs Y, or La vs Dy, etc).

The 1.3 Ga rhyolites in the Fox Harbour area formed during an extensional phase, often found in the Grenville Province, as suggested by Haley et al. (2013). This means that the rhyolites (and adjacent supracrustal units) are likely anorogenic in origin. A-type granites, can form by a number of processes, such as (i) differentiation from an OIB (oceanic island basalts)-like basaltic magma, (ii) differentiation from a continental tholeiite basaltic magma, or (iii) melting of lower continental crust. Based on the findings of this study, it is believed that the Fox Harbour rhyolite package was formed by the partial melting of lower continental (felsic) crust. REE enrichment likely occurred at this time via extreme fractional crystallization of the magma. It has been shown that there was no infiltration of REE during the 1.05 Ga metamorphic event, but there must be redistribution and concentration of certain elements during this time. This is present in the Fox Harbour area in the form of 1.05 Ga zircon grains that are very large, and microporous, often associated with zircon that has been reprecipitated.

3-7 CONCLUSIONS

The 1.3 Ga Fox Harbour REE enriched peralkaline volcanic units were derived from partial melts of 1.5-1.9 Ga felsic crustal sources. The 1.5-1.9 Ga crustal source is still poorly defined, but could be any of the terranes present in the area, such as the Lake Melville (1.7-1.2 Ga), Mealy Mountains (1.7-0.9 Ga), or Pinware terrane (1.65-0.9 Ga). The 1.05 Ga amphibolite facies Grenvillian metamorphism induced no flux of HFSE into or out of the volcanic units, and these elements were simply remobilized within. The main REE-bearing mineral in the Fox Harbour area is fergusonite, and contains slightly variable geochemistry based on which volcanic belt it is present in. Although not analyzed, allanite is probably an important mineral in the Fox Harbour area, and is observed in all mineralized units throughout the area. Microporous zircon in the Fox Harbour area dated at 1.05 Ga Ma record slight differences in chemistry, likely associated with the dissolution and reprecipitation of hydrothermal zircon during Grenville deformation.

3-8 REFERENCES

Andersen, T., Simonsen, S.L. & Haug, L.E. (2009). LAM-ICPMS Lu-Hf isotope data on magmatic zircons from felsic and intermediate intrusions in the Oslo Rift: Constraints on the mantle source. Abstracts, NGF Winter Conference, Bergen, Jan. 2009. *Norsk Geologisk Forening Abstracts and Proceedings*, (1), 3-4.

Barberi F., Ferrara G., & Santacrose R. (1975). Transitional Basalt-Pantellerite Sequence of Fractional Crystallization, the Boina Centre (Afar Rift, Ethiopia). *Journal of Petrology*. (16), 22–56.

Bouvier, A., Vervoort, J. D., & Patchett, P. J. (2008). The Lu–Hf and Sm–Nd isotopic composition of CHUR: Constraints from unequilibrated chondrites and implications for the bulk composition of terrestrial planets. *Earth and Planetary Science Letters*.

Civetta, L., D'Antonio, M., Orsi, G., and Tilton, G. R. (1998). The Geochemistry of Volcanic Rocks from Pantelleria Island, Sicily Channel: Petrogenesis and Characteristics of the Mantle Source Region. *Journal of Petrology*, (39), 1453– 1491.

Corrigan, D., 1995. Mesoproterozoic evolution of the south- central Grenville orogen: structural, metamorphic and geo- chronologic constraints from the Mauricie transect. Ph.D. Thesis, Carleton University, Ottawa.

Corrigan, D., Hanmer, S., 1995. Arc accretion, thickening, post- collisional extension and plutonism in the Grenville orogen; constraints from the Mauricie region, south-central Quebec. In: Precambrian '95, International Conference on Tectonics and Metallogeny of Early/Mid Precambrian orogenic Belts, Program and Abstracts, Montreal, p. 106.

Davidson, A. (2008). Late Paleoproterozoic to mid-Neoproterozoic history of northern Laurentia: An overview of central Rodinia. *Precambrian Research*, 160(1-2), 5–22.
doi:10.1016/j.precamres.2007.04.023

Davies, G. R. and Macdonald, R. (1987) Crustal Influences in the Petrogenesis of the

Naivasha Basalt–Comendite Complex: Combined Trace Element and Sr–Nd–Pb

Isotope Constraints. *Journal of Petrology*, (28-6), 1009–1031.

Delaney, P., Haley, J.T. (2011; *unpublished*). Report on mapping, prospecting, geochemical sampling, trenching, diamond drilling, and airborne radiometric/magnetometer survey on the Fox Harbour property, Port Hope Simpson, Labrador. 1st year assessment report for Alterra Resources Inc, pp. 429.

Dhuime, B., Hawkesworth, C., & Cawood, P. (2011). When continents formed. *Science*, (331), 154-155.

Ercit, T.S. (2005). Identification and alteration trends of granitic-pegmatite-hosted (Y, REE, U, Th)-(Nb, Ta, Ti) oxide minerals: a statistical approach, *The Canadian Mineralogist*, (43), 1291-1303.

Giesler, T., Schaltegger, U., Tomaschek, F. (2007). Re-equilibration of zircon in aqueous fluids and melts, *Elements*, (3), 43-50.

Gower, C.F. (1985). Correlations between the Grenville Province and Sveconorwegian Orogenic Belt — Implications for Proterozoic Evolution of the Southern Margins of the Canadian and Baltic Shields. *The Deep Proterozoic Crust in the North Atlantic Provinces*, 247–257. doi:10.1007/978-94-009-5450-2_15.

Gower, C.F. (1994). Distribution of pre-1400 Ma crust in the Grenville province: Implications for rifting in Laurentia-Baltica during geon 14. *Geology*, 22, 827-830.

Gower, C.F. (1996a). The evolution of the Grenville Province in eastern Labrador, Canada.

Geological Society London Special Publications, 112(1), 197-218. doi:

10.1144/GSL.SP.1996.112.01.11

Gower, C.F. (1996b). Geology of the southeast Mealy Mountains Region, Grenville Province, Southeast Labrador. *Current Research, Newfoundland and Labrador Department of Natural Resources*. 96-1, 55-71.

Gower, C.F. (2003). Geological map of the Grenville Province in eastern Labrador. *Newfoundland and Labrador Department of Mines and Energy, Geological Survey, Map 2003-11*. Open file: LAB/1379.

Gower, C.F. (2005). Kinematic evidence for terrane displacements in the Grenville province. *Current Research, Newfoundland and Labrador Department of Natural Resources*. Report 05-01, pp. 73-92.

Gower, C. F. (2007). Protolith recognition of metamorphosed felsic volcanic/volcaniclastic rocks, with special reference to the Grenville Province in southeast Labrador. *Current Research, Newfoundland and Labrador Department of Natural Resources*. Report 07-01, pp. 11-23.

Gower, C.F. (2009). Battle Island – A geological treasure in coastal eastern Labrador. Government of Newfoundland and Labrador, Department of Natural Resources, Geological Survey, Open File 003D/05/0031, 38 pages.

Gower, C., & Owen, V. (1984). Pre-Grenvillian and Grenvillian lithotectonic regions in

- eastern Labrador-correlations with the Sveconorwegian Orogenic Belt in Sweden.
Canadian Journal of Earth Sciences, 21(6), 678–693.
- Gower, C.F., Neuland, S., Newman, M., Smyth, J., (1987). Geology of the Port Hope Simpson map region, Grenville province, eastern Labrador, *Current Research (1987 Newfoundland Department of Mines and Energy, Mineral Development Division, Report 87-1*, 183-199.
- Gower, C. F., & Erdmer, P. (1988). Proterozoic metamorphism in the Grenville Province: a study in the Double Mer-Lake Melville area, eastern Labrador. *Canadian Journal of Earth Sciences*, 25(11), 1895–1905.
- Gower, C., Schärer, U., & Heaman, L. (1992). The Labradorian orogeny in the Grenville Province, eastern Labrador, Canada. *Canadian Journal of Earth Sciences*, 29(9), 1944–1957.
- Gower, C.F., van Nostrand, T. (1994). Geology of the Pinware River Region, southeast Labrador. *Current Research, Newfoundland and Labrador Department of Natural Resources*. 94-1, 347-369.
- Gower, C., Hall, J., Kilfoil, G., Quinlan, G., & Wardle, R. (1997). Roots of the Labradorian orogen in the Grenville Province in southeast Labrador: Evidence from marine, deep-seismic reflection data. *Tectonics*, 16(5), 795–809.
- Gower, C., & Krogh, T. (2002). A U–Pb geochronological review of the Proterozoic history of the eastern Grenville Province. *Canadian Journal of Earth Sciences*, 39(5), 795–

829. doi: 10.1139/E01-090

Gower, C., Kamo, S., & Krogh, T. (2008). Indentor tectonism in the eastern Grenville Province. *Precambrian Research*, 167(1-2), 201–212.

Gower, C., Kamo, S., Kwok, K., & Krogh, T. (2008). Proterozoic southward accretion and Grenvillian orogenesis in the interior Grenville Province in eastern Labrador: Evidence from U-Pb geochronological investigations. *Precambrian Research*, 165(1-2), 61–95.

Griffin, W.L., Pearson, N.J., Belousova, E., Jackson, S.E., van Achter-bergh, E., O'Reilly, S.Y. & Shee, S.R. (2000). The Hf isotope composition of cratonic mantle: LAM-MC-ICPMS analysis of zircon megacrysts in kimberlites. *Geochimica et Cosmochimica Acta* (64), 133-147.

Haley, J.T., Sylvester, P.J., Miller, R.R. (2013). Discovery of 1.3 Ga REE-enriched bimodal volcanism in the Grenville Province of southeastern Labrador, Canada.

Harker, A., (1909). The Natural History of Igneous Rocks. London, Methuen, 384 pp.

Hynes, A., & Rivers, T. (2010). Protracted continental collision-evidence from the Grenville Orogen. *Canadian Journal of Earth Sciences*, 47(5), 591–620.

Irvine, T. N., & Baragar, W. (1971). A Guide to the Chemical Classification of the Common Volcanic Rocks. *Canadian Journal of Earth Sciences*, (8) 523-548.

Kamo, S., Wasteneys, H., Gower, C., & Krogh, T. (1996). U-Pb geochronology of

Labradorian and later events in the Grenville Province, eastern Labrador.

Precambrian Research, 80(3-4), 239–260.

Kamo, S. L., Heaman, L. M., & Gower, C. F. (2011). Evidence for post-1200 Ma — pre-Grenvillian supracrustal rocks in the Pinware terrane, eastern Grenville Province at Battle Harbour, Labrador. This article is one of a series of papers published in this Special Issue on the theme of Geochronology in honour of Tom Krogh. *Canadian Journal of Earth Sciences*, 48(2), 371–387. doi:10.1139/E10-052

Kovalenko V. I., *Petrology and Geochemistry of Rare-Metal Granites* (Nauka, Novosibirsk, 1977) (in Russian).

Litvinovsky B. A., Zanvilevich A. N., Shadaev M. G., and Lyapunov S. M. (1996). The Role of Fractional Crystallization in the Formation of a Bimodal Trachybasalt-Trachyte Series: Malo-Khamardabanskaya Volcano-Tectonic Structure, Transbaikalia, *Petrologiya*, (4), 26–45 (in Russian).

Macdonald, R. (1974). Nomenclature and petrochemistry of the peralkaline oversaturated extrusive rocks. *Bulletin volcanologique*, 38(2), 498–516.

Maniar, P.D., Piccoli, P.M. (1989). Tectonic discrimination of granitoids, *Geological Society of America Bulletin*, 101(5), 635–643.

doi:10.1130/00167606(1989)101<0635:TDOG>2.3.CO;2

McLlland, J., Daly, J.S., & McLlland, J.M. (1996). The Grenville orogenic cycle (ca. 1350–1000 Ma): an Adirondack perspective. *Tectonophysics*, 265, 1-28.

- Peccerillo A., Barberio M. R., and Yirgu G. (2003). Relationships between Mafic and Peralkaline Silicic Magmatism in Continental Rift Settings: A Petrological, Geochemical and Isotopic Study of the Gedemsa Volcano, Central Ethiopian Rift. *Journal of Petrology*, (44), 2003–2032.
- Pietranik, A.B., Hawkesworth, C.J., Storey, C.D., Kemp, A.I.S., Sircombe, M.J., Whitehouse, M.J., Bleeker, W. (2008). Episodic, mafic crust formation from 4.5 to 2.8 Ga: New evidence from detrital zircons, Slave craton, Canada, *Geology*, 36(11), 875-878, doi:10.1130/G24861A.1
- Rivers, T. (1997). Lithotectonic elements of the Grenville Province: review and tectonic implications. *Precambrian Research*, 86(3-4), 117–154.
- Rivers, T. (2008). Assembly and preservation of lower, mid, and upper orogenic crust in the Grenville Province--Implications for the evolution of large hot long-duration orogens. *Precambrian Research*, 167(3-4), 237–259. doi:10.1016/j.precamres.2008.08.005.
- Rivers, T. (2009). The Grenville Province as a large hot long-duration collisional orogen - insights from the spatial and thermal evolution of its orogenic fronts. *Geological Society London Special Publications*, 327(1), 405–444. doi:10.1144/SP327.17.
- Rivers, T., & Corrigan, D. (2000). Convergent margin on southeastern Laurentia during the Mesoproterozoic: tectonic implications. *Canadian Journal of Earth Sciences*, 37(2-3), 359–383.
- Rivers, T., Ketchum, J., Indares, A., & Hynes, A. (2002). The High Pressure belt in the

- Grenville Province: architecture, timing, and exhumation. *Canadian Journal of Earth Sciences*, 39(5), 867–893. doi:10.1139/e02-025.
- Schärer, U., & Krogh, T. (1986). Age and evolution of the Grenville Province in eastern Labrador from U-Pb systematics in accessory minerals. *Contributions to Mineralogy and Petrology*. (94), 438-451.
- Schärer, U., & Gower, C. (1988). Crustal evolution in eastern Labrador: Constraints from precise U-Pb ages. *Precambrian Research*, 38(4), 405–421.
- Schwartz, J.J., John, B.E., Cheadle, M.J., Wooden, J.L., Mazdab, F., Swapp, S., Grimes, C.B. (2010). Dissolution-reprecipitation of igneous zircon in mid-ocean ridge gabbro, Atlantis Bank, southwest Indian Ridge, *Chemical Geology*, (274), 68-81.
- Scott, D., Machado, N., Hanmer, S., & Gariépy, C. (1993). Dating ductile deformation using U-Pb geochronology: examples from the Gilbert River Belt, Grenville Province, Labrador, Canada. *Canadian Journal of Earth Sciences*, 30(7), 1458–1469.
- Shand, S.J. (1927). On the relations between silica, alumina, and the bases in eruptive rocks, considered as a means of classification. *Geological Magazine*, (64), 446-446.
- Shand, S. J. (1951). *Eruptive Rocks*. New York: J. Wiley.
- Slama J., Košler J., Condon D.J., Crowley J.L., Gerdes A., Hanchar J.M., Horstwood M.S.A., Morris G.A., Nasdala L., Norberg N., Schaltegger U., Schoene B., Tubrett M.N., Whitehouse M.J. (2008). Plesovice zircon – a new natural reference material for U-Pb

- and Hf isotopic microanalysis. *Chem Geol* 249: 1-35
- Souders, A., Sylvester, P., Myers, J., 2012. Mantle and crustal sources of Archean anorthosite: a combined in situ isotopic study of Pb–Pb in plagioclase and Lu–Hf in zircon. *Contributions to Mineralogy and Petrology* 1–24.
- Sun, S. S., & McDonough, W. F. (1989). Chemical and isotopic systematics of oceanic basalts: implications for mantle composition and processes. *Geological Society*, (42), 313-345.
- Sylvester P.J. (2012). Use of the Mineral Liberation Analyzer (MLA) for mineralogical studies of sediments and sedimentary rocks. In Quantitative Mineralogy and Micro-Analysis of Sediments and Sedimentary Rocks (P. Sylvester, ed.). *Mineral Association of Canada Short Course Series* (42), p. 1-16.
- Trua T., Daniel C., and Mazzuoli R. (1999). Crustal Control in the Genesis of Plio-Quaternary Bimodal Magmatism of the Main Ethiopian Rift (MER): Geochemical and Isotopic (Sr, Nd, Pb) Evidence. *Chemical Geology*, (155), 201–231.
- Tucker, R., & Gower, C. (1994). A U-Pb geochronological framework for the Pinware terrane, Grenville Province, southeast Labrador. *The Journal of Geology*, 102(1), 67–78.
- Vorontsov A. A., Yarmolyuk V. V., and Baikin D. N. (2004). Structure and Composition of the Early Mesozoic Volcanic Series of the Tsagan–Khurtei Graben, Western

Transbaikalia: Geological, Geochemical, and Isotopic Data. *Geokhimiya*, (11), 1186–1202 (in Russian).

Yarmolyuk V. V., Litvinovsky B. A., Kovalenko V. I. (2001). Formation Stages and Sources of the Peralkaline Granitoid Magmatism of the Northern Mongolia–Trans- baikalia Rift Belt during the Permian and Triassic. *Petrologiya* (9), 351–389 (in Russian).

Wasteneys, H., Kamo, S., Moser, D., Krogh, T., Gower, C., & Owen, J. (1997). U-Pb geochronological constraints on the geological evolution of the Pinware terrane and adjacent areas, Grenville Province, southeast Labrador, Canada. *Precambrian Research*, 81(1-2), 101–128.

White, R., & McKenzie, D. (1989). Magmatism at rift zones: The generation of volcanic continental margins and flood basalts. *J. Geophys. Res.*, 94(B6), 7685.
doi:10.1029/JB094iB06p07685

Winchester, J. A., & Floyd, P. A. (1977). Geochemical discrimination of different magma series and their differentiation products using immobile elements. *Chemical Geology*, (20), 325–343. doi:10.1016/0009-2541(77)90057-2

SUMMARY

The data presented in this thesis provide the first description of the Fox Harbour volcanic packages available in literature. Three individual volcanic belts have been discovered (South Belt, MT Belt, and Road Belt), each with slightly different lithological units. Rock types consist of peralkaline rhyolitic units (comendite and pantellerite, determined geochemically), subalkaline tholeiitic basalt, discordant mafic and granitic dykes/sills, and quartzite.

U-Pb zircon geochronology conducted on representative samples from each volcanic belt identified two main age populations. The first is 1.3 Ga, taken to be the age of formation for the rhyolite units, and inferred age of formation for adjacent supracrustal units. The second is 1.05 Ga, taken to be the age that Grenvillian metamorphism affected this area of southeastern Labrador, subjecting the area to amphibolite facies metamorphism.

Zircon analyzed for U-Pb was also analyzed for Lu-Hf, to determine if findings were consistent. Hafnium isotopes in ca. 1.3 Ga zircon suggest that partial melting of 1.5-1.9 Ga felsic crustal sources derived Fox Harbour supracrustal packages. Although an interesting finding, a definitive source cannot be identified as the majority of southeastern Labrador ranges in age from 1.5-1.9 Ga. Hafnium isotopes in zircon containing an age of 1.05 Ga follow the same Hf-isotope crustal evolution array for 1.5 to 1.9 Ga sources. This suggests that the 1.05 Ga high-grade Grenvillian metamorphism was a closed system for

Lu-Hf isotopes, and there was no flux of REE into or out of the rocks. This means that the REE present in the packages currently were present when deposited.

APPENDIX A

LITHOGEOCHEMICAL DATA

Lithogeochemical data tables for each belt. Note that data are broken into a number of sections in order to allow the data to display properly.

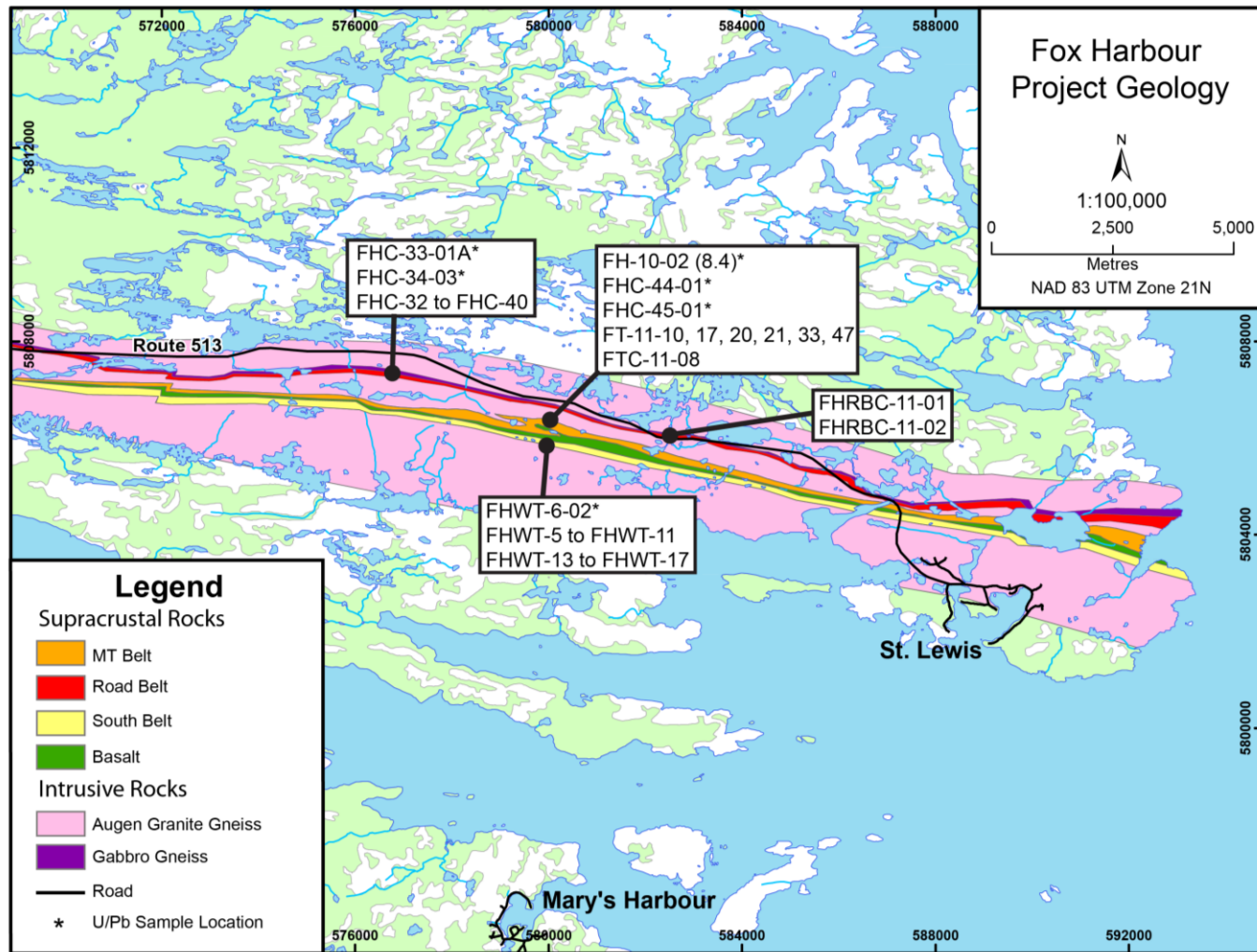


Figure A-1: Geology map of the Fox Harbour project area, displaying all samples locations.

Table A1-1: Lithogeochemical data for the South Belt

Sample	Channel* Number	SiO ₂	Al ₂ O ₃	Fe ₂ O ₃	FeO	MnO	MgO	CaO	Na ₂ O	K ₂ O	TiO ₂	P ₂ O ₅	LOI	Total
A103237	FHWT50D1	75.92	9.97	5.52	4.96	0.022	0.11	0.38	2.6	4.48	0.167	<0.01	0.26	99.43
A103238	FHWT50D2	75.96	9.92	5.29	4.76	0.03	0.17	0.63	2.54	4.45	0.204	<0.01	0.36	99.56
A103239	FHWT50D3	76.57	9.54	5.61	5.04	0.04	0.21	0.45	2.82	3.82	0.177	<0.01	0.16	99.39
A103240	FHWT50D4	45.23	13.99	16.73	15.04	0.408	5.61	5.96	1.78	4.56	3.678	0.45	1.22	99.62
A103241	FHWT50D5	76.89	9.92	5.78	5.2	0.042	0.15	0.51	2.58	3.95	0.173	<0.01	0.15	100.1
A103242	FHWT50D6	75.96	9.98	5.56	5	0.048	0.16	0.51	2.79	3.97	0.188	<0.01	0.3	99.46
A103243	FHWT50D7	77.3	10.04	5.27	4.74	0.028	0.12	0.53	3.06	3.37	0.171	<0.01	0.28	100.2
		0												
103244	FHWT60D1	71.13	13.14	4.86	4.37	0.104	0.42	0.78	4.76	3.24	0.495	0.03	0.64	99.6
103245	FHWT60D2	67.44	14.64	6.66	5.99	0.066	0.17	1.26	5.94	2.25	0.459	0.04	0.6	99.52
103246	FHWT60D3	65.21	15.17	7.28	6.54	0.083	0.21	1.65	5.74	2.59	0.49	0.04	0.99	99.45
103247	FHWT60D4	71.52	13.41	4.8	4.32	0.066	0.38	0.89	4.22	3.6	0.407	0.02	0.68	99.99
103248	FHWT60D5	54.32	14.25	13.4	12.05	0.229	3.54	4.82	2.78	2.98	1.891	0.34	2.06	100.6
103249	FHWT60D6	46.92	14.52	16.08	14.46	0.31	4.89	6.98	2.34	2.57	2.941	0.51	2.59	100.6
		0												
103250	FHWT70D1	79.28	8.81	4.79	4.31	0.046	0.34	0.86	3.31	1.06	0.307	0.03	0.75	99.59
103251	FHWT70D2	72.79	10.08	7.2	6.47	0.091	0.4	1.41	2.12	3.69	0.669	0.08	0.78	99.33
103252	FHWT70D3	43.21	14.21	16.79	15.09	0.351	5.55	6.16	2.02	3.47	3.868	0.5	3.6	99.74
103253	FHWT70D4	78.1	9.21	5.04	4.53	0.049	0.33	0.47	1.97	4.15	0.206	0.01	0.63	100.2
103254	FHWT70D5	75.88	10.01	4.83	4.34	0.022	0.14	0.44	2.74	4.1	0.206	0.02	0.46	98.85
103255	FHWT70D6	75.87	10.17	5.11	4.59	0.033	0.13	0.71	2.8	4.17	0.213	0.01	0.77	99.99
103256	FHWT70D7	76.88	10	4.97	4.47	0.015	0.07	0.4	2.9	4.48	0.195	<0.01	0.38	100.3
103257	FHWT70D8	75.45	10.59	4.92	4.42	0.00	0.08	0.6	2.84	4.87	0.19	0.02	0.83	100.4
103258	FHWT70D9	74.9	10.25	5.3	4.76	0.017	0.09	0.38	2.92	4.51	0.204	0.01	0.36	98.94
103259	FHWT71D0	76.39	10.16	4.87	4.38	0.022	0.09	0.31	2.78	4.63	0.141	0.01	0.5	99.92
103260	FHWT71D1	76.82	9.83	5.03	4.52	0.019	0.18	0.17	2.6	4.37	0.132	<0.01	0.3	99.46
103261	FHWT71D2	76.34	10.43	4.75	4.27	0.019	0.11	0.4	2.75	4.48	0.191	0.02	0.49	99.99
103262	FHWT71D3	54.34	13.1	11.85	10.65	0.366	3.33	10.37	0.77	1.73	1.374	0.17	3.28	100.7
103263	FHWT71D4	74.63	10.46	4.64	4.17	0.017	0.1	0.32	2.91	4.42	0.194	0.02	0.59	98.3
103264	FHWT71D5	75.99	10.82	4.45	4	0.019	0.14	0.4	2.94	4.49	0.21	0.02	0.61	100.1
103265	FHWT71D6	76.51	10.17	4.76	4.28	0.021	0.17	0.32	2.62	4.69	0.195	<0.01	0.33	99.8
103266	FHWT71D7	78.6	9.31	4.86	4.37	0.017	0.13	0.32	2.53	4.27	0.16	<0.01	0.32	100.5
103267	FHWT71D8	56.27	13.11	12.74	11.45	0.235	3.43	5.23	2.93	2.53	2.38	0.28	1.47	100.6
103268	FHWT71D9	74.47	10.77	4.82	4.33	0.03	0.11	0.63	2.86	4.6	0.211	0.01	0.32	98.85
103269	FHWT71D9	74.78	10.83	4.85	4.46	0.038	0.17	0.7	2.8	4.78	0.215	0.03	0.45	99.74
103270	FHWT72D1	75.17	10.45	4.81	4.32	0.031	0.09	0.73	2.89	4.26	0.236	0.01	0.53	99.22
103271	FHWT72D2	75.79	9.5	5.75	5.17	0.038	0.13	0.7	2.39	3.97	0.242	0.02	0.23	98.75
103272	FHWT72D3	75.73	10.85	4.39	3.95	0.028	0.11	0.63	3.03	4.27	0.227	<0.01	0.42	99.68
103273	FHWT72D4	76.21	10.71	4.9	4.41	0.034	0.18	0.73	2.95	4.23	0.273	0.01	0.26	100.5
103274	FHWT72D5	51.31	13.95	13.08	11.76	0.277	4.92	3.67	3.05	3.86	2.008	0.36	2.57	99.06
103275	FHWT72D6	71.04	12.5	5.01	5.41	0.083	0.43	0.91	3.37	4.29	0.301	0.02	0.57	99.54
103276	FHWT72D7	76.75	10.9	4.26	3.83	0.037	0.18	0.81	3.21	3.58	0.226	0.01	0.36	100.3
103277	FHWT72D8	76.7	11.04	4.42	3.97	0.07	0.25	0.92	3.19	3.24	0.212	<0.01	0.36	100.4
103278	FHWT72D9	62.38	14.69	7.23	6.5	0.151	2.15	3.01	3.99	2.85	1.24	0.55	1.86	100.1
103279	FHWT72D6	47.54	14.57	15.29	13.75	0.301	5.31	6.55	2.38	3.21	2.516	0.39	1.21	99.28
103280	FHWT72D7	66.62	16.3	3.34	3	0.1	0.49	1.66	3.52	7.23	0.571	0.12	0.52	100.5
103280	FHWT72D8	74.22	11.14	4.67	4.2	0.033	0.31	0.83	1.9	6.55	0.478	0.06	0.47	100.7
		0												
103278	FHWT80D1	75.24	10.09	4.84	4.35	0.036	0.11	0.92	2.65	3.88	0.269	0.01	0.14	98.19
103279	FHWT80D2	44.91	15.25	13.47	12.11	0.352	7.52	7.07	2.4	3.07	1.69	0.19	2.52	98.44
103280	FHWT80D3	74.07	10.9	4.21	3.78	0.038	0.13	1.13	3.02	3.94	0.23	0.02	0.43	98.11
103281	FHWT80D4	43.9	15.09	14.93	13.42	0.29	5.78	8.95	1.87	3.34	1.88	0.19	2.23	98.45
103282	FHWT80D5	73.91	11.5	4.74	4.26	0.038	0.14	0.98	3.71	3.32	0.241	0.01	0.25	98.84
103283	FHWT80D6	73.87	10.87	4.29	3.86	0.033	0.15	1.21	2.63	4.92	0.247	0.01	0.85	99.08
103284	FHWT80D7	74.03	10.89	4.28	3.85	0.036	0.12	1.26	2.74	4.76	0.216	0.01	0.56	98.91
103285	FHWT80D8	73.1	10.98	5.07	4.56	0.054	0.11	0.79	3.09	4.52	0.262	<0.01	0.43	98.42
103286	FHWT80D9	72.27	11.46	4.83	4.34	0.059	0.09	0.75	3.28	4.89	0.255	0.01	0.34	98.24
103287	FHWT80D0	73.51	10.72	4.32	3.88	0.051	0.1	0.87	3.08	4.62	0.248	<0.01	0.45	97.97
103288	FHWT80D1	70.02	12.15	4.65	4.18	0.047	0.08	1.44	3.1	5.52	0.29	0.01	0.53	97.86
103289	FHWT80D2	72.52	11.78	4.71	4.23	0.071	0.1	0.95	3.22	4.86	0.33	0.01	0.48	99.03
103290	FHWT80D3	72.42	11.79	4.64	4.17	0.067	0.07	0.86	3.31	5.06	0.25	<0.01	0.31	98.79
103291	FHWT80D4	73.52	11.3	4.29	3.86	0.04	0.05	1.12	2.88	4.75	0.308	0.01	0.18	98.47
103292	FHWT80D5	74.56	10.68	4.69	4.22	0.037	0.04	0.93	2.67	4.51	0.227	0.02	0.15	98.5
103293	FHWT80D6	73.65	10.95	5.31	4.77	0.039	0.06	0.83	2.74	4.77	0.254	0.02	0.06	98.68
103294	FHWT80D7	55.73	18.3	9.65	8.68	0.1	0.13	3.52	7.33	1.01	0.658	0.01	0.58	97.01
103295	FHWT80D8	74.69	11.55	4.35	3.91	0.042	0.07	0.99	2.92	4.9	0.208	0.02	0.17	99.91
		0												
103296	FHWT90D1	43.39	14.23	16.68	15	0.263	5.36	7.7	2.93	2.58	3.821	0.49	1.78	99.24
103297	FHWT90D2	73.63	11.67	5.7	5.12	0.044	0.21	1.31	4.63	1.14	0.305	0.01	0.3	98.94
103298	FHWT90D3	72.23	11.79	4.6	4.14	0.029	0.09	0.97	3.51	3.92	0.301	0.02	0.58	98.03

Table A1-2: Lithogeochemical data for the South Belt

Sample	Channel* Number	SiO ₂	Al ₂ O ₃	Fe ₂ O ₃	FeO	MnO	MgO	CaO	Na ₂ O	K ₂ O	TiO ₂	P ₂ O ₅	LOI	Total
103299	FHW ^T 90D4	74.17	10.79	5.05	4.54	0.021	0.08	0.48	3.14	4.67	0.245	0.01	0.32	98.98
103300	FHW ^T 90D5	73.83	10.69	4.8	4.32	0.022	0.11	0.57	3.34	4.01	0.199	<0.01	0.43	98
103301	FHW ^T 90D6	45.85	14.49	15.41	13.85	0.306	5.2	5.4	2.66	4.18	3.271	0.42	2.13	99.31
103302	FHW ^T 90D7	44.08	14.67	16.6	14.92	0.288	5.32	7.19	2.83	3.04	3.767	0.53	0.99	99.29
103303	FHW ^T 90B	73.54	12	4.54	4.08	0.037	0.09	0.9	3.57	4.01	0.281	0.02	0.48	99.46
		0												
103304	FHW ^T 10D1	42.91	14.27	16.6	14.92	0.299	5.42	8.01	2.89	2.55	3.625	0.5	1.7	98.79
103305	FHW ^T 10D2	72.87	11.72	4.51	4.05	0.027	0.29	0.8	3.21	4.63	0.295	0.02	0.62	98.97
103306	FHW ^T 10D3	70	12.49	5.16	4.64	0.025	0.14	0.81	3.71	5.1	0.289	0.02	0.57	98.32
103307	FHW ^T 10D4	73	11.1	4.73	4.25	0.029	0.12	0.6	3.38	4.75	0.251	0.01	0.44	98.42
103308	FHW ^T 10D5	72.47	11.27	4.66	4.19	0.029	0.15	1.13	3.57	4.64	0.257	0.01	0.96	99.14
103309	FHW ^T 10D6	72.48	11.92	4.13	3.71	0.019	0.19	0.3	3.44	5.17	0.239	0.01	0.52	98.43
103310	FHW ^T 10D7	75.58	10.69	3.6	3.24	0.024	0.13	0.54	3.16	4.73	0.209	0.01	0.43	99.1
103311	FHW ^T 10D8	73.6	11.6	4.08	3.67	0.014	0.11	0.27	3.21	5.42	0.196	<0.01	0.57	99.07
103312	FHW ^T 10D9	72.46	11.43	4.54	4.08	0.023	0.12	0.51	3.49	4.91	0.227	<0.01	0.43	98.15
103313	FHW ^T 10D10	73.09	11.8	4.19	3.77	0.025	0.05	0.62	3.7	4.89	0.21	0.01	0.4	98.99
103314	FHW ^T 10D11	73.29	11.55	4.49	4.04	0.029	0.16	0.89	3.58	4.89	0.235	0.01	0.6	99.73
103315	FHW ^T 10D12	75.99	10.15	3.92	3.52	0.019	0.11	0.59	3.16	4.3	0.195	<0.01	0.43	98.88
103316	FHW ^T 10D13	72.18	11.44	4.19	3.77	0.025	0.21	0.82	3.54	4.78	0.221	0.01	0.55	97.97
103317	FHW ^T 10D14	73.79	10.98	4.22	3.79	0.029	0.27	0.61	3.24	4.68	0.225	0.01	0.53	98.58
103318	FHW ^T 10D15	73.56	11.81	4.46	4.01	0.026	0.27	0.51	3.55	4.77	0.23	<0.01	0.59	99.78
103319	FHW ^T 10D16	74.01	11.26	4.34	3.9	0.035	0.24	0.81	3.38	4.78	0.207	<0.01	0.66	99.73
103320	FHW ^T 10D7	73.13	11.39	4.26	3.83	0.028	0.18	0.71	3.47	4.73	0.196	<0.01	0.46	98.57
103321	FHW ^T 10D8	73.9	11.28	4.47	4.02	0.036	0.2	0.78	3.39	4.72	0.221	0.01	0.44	99.44
103322	FHW ^T 10D9	72.04	11.32	4.58	4.12	0.027	0.17	0.47	3.47	4.76	0.222	0.01	0.43	97.75
103323	FHW ^T 10D20	73.96	11.41	4.19	3.77	0.028	0.25	0.53	3.19	4.99	0.223	<0.01	0.46	99.25
103324	FHW ^T 10D21	74.03	10.35	4.31	3.87	0.062	0.29	1.26	2.63	4.95	0.211	<0.01	0.09	99.1
103325	FHW ^T 10D22	74.09	10.37	4.09	3.68	0.031	0.19	1.12	3.12	4.32	0.193	<0.01	0.9	98.43
103376	FHW ^T 10D23	73.89	11.48	4.31	3.87	0.028	0.22	0.57	3.44	4.75	0.201	0.01	0.57	99.46
103377	FHW ^T 10D24	73.94	10.78	4.14	3.72	0.021	0.21	0.57	3.2	4.44	0.208	<0.01	0.61	98.12
103378	FHW ^T 10D25	75.3	10.94	4.68	4.21	0.035	0.21	0.48	3.03	4.94	0.258	0.02	0.49	100.4
422276	FHW ^T 10D26	73.81	10.74	4.93	4.43	0.033	0.26	0.65	3.24	4.66	0.294	0.01	0.46	99.09
		0												
422277	FHW ^T Q1	44.31	14.9	16.08	14.46	0.291	5.72	6.91	2.95	2.15	3.517	0.44	1.65	88.93
422278	FHW ^T Q1	66.89	14.97	4.92	4.42	0.083	0.47	1.94	4.96	2.28	0.316	0.02	1.1	97.94
422279	FHW ^T Q1	72.14	13.18	3.96	3.56	0.046	0.13	1.42	3.37	5.16	0.236	<0.01	1.12	100.8
422280	FHW ^T Q1	70.67	12.65	4.03	3.62	0.04	0.29	1.29	3.35	5	0.307	0.03	0.87	98.52
422281	FHW ^T Q1	69.06	13.08	5.59	5.03	0.073	0.58	1.38	3.55	4.73	0.534	0.06	0.96	99.61
422282	FHW ^T Q1	70.85	12.53	4.15	3.73	0.042	0.19	0.9	3.88	5.1	0.258	0.01	0.43	98.34
422283	FHW ^T Q1	75.92	11.34	3.92	3.52	0.041	0.16	0.93	3.65	3.91	0.264	0.01	0.32	100.5
422284	FHW ^T Q1	44.25	14.79	15.56	13.99	0.351	5.38	6.24	3.12	4.06	3.497	0.53	1.42	99.19
422285	FHW ^T Q1	71.3	12.55	5.06	4.55	0.046	0.22	1.04	3.99	4.35	0.338	0.03	0.38	99.32
422286	FHW ^T Q1	71.76	12.46	4.62	4.15	0.034	0.2	0.93	3.9	5.01	0.264	0.01	0.58	99.76
422287	FHW ^T Q1	71.35	12.61	4.47	4.02	0.039	0.27	0.83	3.97	5.11	0.254	0.02	0.67	99.6
422288	FHW ^T Q1	72.68	11.56	4.89	4.4	0.035	0.12	0.64	3.72	4.69	0.274	<0.01	0.33	98.95
422289	FHW ^T Q1	73.44	12.19	4.22	3.79	0.022	0.13	0.45	3.97	4.69	0.251	0.01	0.31	99.68
422290	FHW ^T Q1	70.34	13.29	4.66	4.19	0.031	0.08	0.69	4.4	5.2	0.272	0.02	0.37	99.34
422291	FHW ^T Q1	51.32	14.5	12.68	11.4	0.222	5.28	6.3	2.97	2.43	1.725	0.22	1.57	99.22
422292	FHW ^T Q1	46.16	14.83	14.67	13.19	0.274	6.22	7.52	2.99	2.19	2.276	0.31	1.59	99.04
422293	FHW ^T Q1	71.38	12.06	5.29	4.76	0.049	0.21	1.06	3.58	4.75	0.305	0.02	0.54	99.23
422294	FHW ^T Q1	72.42	10.54	5.58	5.02	0.052	0.35	0.83	2.95	4.33	0.279	0.02	0.48	97.83
422295	FHW ^T Q1	72.44	11.45	5.14	4.62	0.054	0.25	1.68	3.11	4.66	0.281	0.02	0.7	99.79
422296	FHW ^T Q1	71.43	11.54	5.35	4.81	0.042	0.13	1.64	3.31	4.69	0.306	0.01	0.64	99.07
422297	FHW ^T Q1	68.88	12.08	5.2	4.67	0.065	0.2	2.65	3.25	4.76	0.307	0.02	1.21	98.64
422298	FHW ^T Q1	72.45	11.89	5.41	4.86	0.061	0.33	1.12	3.2	5.09	0.305	0.02	0.65	100.5
422299	FHW ^T Q1	70.86	12.32	5.5	4.94	0.055	0.23	1.12	3.09	5.28	0.332	0.02	0.75	99.56
422300	FHW ^T Q1	72.19	11.7	4.82	4.33	0.063	0.27	0.85	2.65	5.05	0.287	0.01	0.82	98.71
422251	FHW ^T Q1	72.61	10.94	4.77	4.29	0.046	0.11	1.56	3.61	4	0.263	0.02	0.64	98.57
422252	FHW ^T Q1	73.5	12	4.7	4.23	0.051	0.13	0.79	3.67	5.07	0.267	0.02	0.41	100.6
422253	FHW ^T Q1	72.12	12.78	4.83	4.34	0.057	0.13	0.97	3.64	5.21	0.298	0.01	0.52	100.6
422254	FHW ^T Q1	72.13	11.68	4.71	4.23	0.072	0.25	1.23	3.19	4.78	0.279	0.02	0.55	98.89
		0												
422255	FHW ^T Q3	70.62	12.67	5.23	4.7	0.049	0.23	0.5	3.99	4.7	0.293	0.02	0.5	98.8
422256	FHW ^T Q3	72.91	11.81	4.66	4.19	0.057	0.29	0.69	3.78	4.38	0.303	0.02	0.67	99.56
422257	FHW ^T Q3	70.85	12.32	5.38	4.84	0.048	0.11	0.67	3.89	4.66	0.316	0.03	0.5	98.78
422258	FHW ^T Q3	70.79	12.18	4.97	4.47	0.056	0.09	0.94	3.91	4.67	0.291	0.02	0.58	98.51
422259	FHW ^T Q3	70.2	12.42	5.09	4.58	0.067	0.19	0.93	3.74	4.83	0.288	0.01	0.73	98.5
422260	FHW ^T Q3	72.42	11.94	4.59	4.13	0.081	0.15	1.11	3.87	4.04	0.293	0.03	0.52	99.04
422261	FHW ^T Q3	70.24	12.16	4.73	4.25	0.084	0.1	1.68	4.06	4.24	0.272	0.02	0.9	98.51
422262	FHW ^T Q3	70.5	12.83	4.79	4.31	0.073	0.16	0.85	4.35	4.43	0.316	0.03	0.43	98.75
422263	FHW ^T Q3	71.36	12.81	4.86	4.37	0.096	0.1	0.79	4.2	4.71	0.296	0.03	0.7	99.96

Table A1-3: Lithogeochemical data for the South Belt

Sample	Channel* Number	SiO ₂	Al ₂ O ₃	Fe ₂ O ₃	FeO	MnO	MgO	CaO	Na ₂ O	K ₂ O	TiO ₂	P ₂ O ₅	LOI	Tc
422264	FHWTD3	71.62	12.96	4.71	4.23	0.082	0.15	0.96	3.85	4.52	0.317	0.02	0.85	
422265	FHWTD3	67.77	12.7	5.5	4.94	0.094	0.58	2	3.95	3.37	0.544	0.06	1.24	
422266	FHWTD3	70.61	12.99	4.75	4.27	0.069	0.08	0.93	4.04	4.67	0.28	0.02	0.78	
422267	FHWTD3	71.79	13.02	4.69	4.22	0.045	0.12	0.63	4.09	4.33	0.395	0.02	0.69	
422268	FHWTD3	70.03	11.93	6.31	5.67	0.118	0.28	1.64	3.65	3.77	0.61	0.07	0.65	
		0		0										
422269	FHWTD4	65.28	15.91	5.19	4.67	0.095	0.45	1.89	4.91	3.69	0.627	0.11	0.86	
422270	FHWTD4	58.24	16.18	8.7	7.82	0.175	0.86	3.16	4.25	4.13	0.994	0.19	1.01	
422271	FHWTD4	52.49	13.09	15.25	13.71	0.223	3.31	6.21	2.88	2.53	2.311	0.3	0.95	
422272	FHWTD4	63.71	15.06	8.04	7.23	0.147	0.59	2.61	4.67	2.56	0.88	0.17	0.66	
422273	FHWTD4	50.72	12.95	15.74	14.15	0.228	3.78	6.31	2.73	2.93	2.395	0.31	1.53	
422274	FHWTD4	69.69	12.5	6.71	6.03	0.094	0.86	2.24	3.7	3.07	0.761	0.1	0.69	
422275	FHWTD4	60.57	15.95	8.3	7.46	0.147	1.48	3.25	5.42	2.12	1.774	0.12	1.07	
422301	FHWTD4	62.5	14.33	8.52	7.66	0.149	0.9	2.22	4.26	3.67	1.016	0.15	1.09	
422302	FHWTD4	70.79	13.26	4.97	4.47	0.051	0.26	0.72	4.38	3.73	0.37	0.02	0.47	
422303	FHWTD4	71.8	12.43	4.99	4.49	0.054	0.39	0.8	4.31	3.47	0.472	0.04	0.58	
422304	FHWTD4	61.66	14.26	7.51	6.75	0.114	0.42	2.99	4.28	4.45	0.768	0.12	1.65	
422305	FHWTD4	69.88	14.06	4.6	4.14	0.036	0.05	0.9	5.15	3.77	0.653	0.01	0.32	
422306	FHWTD4	68.16	14.63	5.07	5.56	0.044	0.05	1.08	5.11	3.99	0.578	<0.01	0.5	
422307	FHWTD4	66.93	14.11	5.42	4.87	0.068	0.08	1.78	4.88	4.06	0.854	<0.01	0.84	
422308	FHWTD4	66.21	13.4	6.79	6.1	0.073	0.1	2.41	4.76	3.43	1.164	0.01	0.76	
422309	FHWTD4	63.91	14.04	6.78	6.1	0.135	0.21	3.24	4.25	4.35	0.902	0.1	1.77	
422310	FHWTD4	67.7	13.67	6.74	6.06	0.082	0.14	1.74	4.73	3.97	0.859	0.06	0.63	
422311	FHWTD4	60.88	15.25	7.88	7.08	0.158	0.3	2.46	4.38	4.99	0.858	0.15	1.17	
422312	FHWTD4	62.54	14.89	8.03	7.22	0.141	0.88	2.91	4.28	3.31	1.065	0.16	0.75	
422313	FHWTD4	51.29	12.63	16.3	14.65	0.232	4.01	7.4	2.85	1.25	2.571	0.33	0.53	
422314	FHWTD4	57.04	14.9	9.62	8.65	0.136	3.62	4.06	3.97	2.66	1.407	0.34	1.37	
422315	FHWTD4	70.06	12.94	6.51	5.85	0.076	0.08	1.12	4.71	3.28	0.598	<0.01	0.44	
422316	FHWTD4	64.88	14.67	7.23	6.5	0.119	0.21	1.64	4.57	4.43	0.775	0.09	0.83	
422317	FHWTD4	69.35	14.06	5.87	5.28	0.085	0.08	0.84	4.79	4.34	0.521	0.05	0.41	
422318	FHWTD4	70.84	13.77	5.78	5.2	0.071	0.17	0.97	5.31	2.78	0.501	0.02	0.4	
		0		0										
322456	FHWTD6 ^a	71.92	11.5	5.52	4.96	0.107	0.49	0.42	3.18	5.18	0.28	0.02	0.33	
322457	FHWTD6 ^a	72.17	12.35	4.72	4.24	0.061	0.18	1.54	3.56	4.11	0.281	<0.01	0.5	
322458	FHWTD6 ^a	72.03	12.44	4.81	4.32	0.076	0.29	1.43	3.86	3.03	0.369	0.02	0.36	
322459	FHWTD6 ^a	44.29	14.86	15.62	14.04	0.256	6.44	8.06	2.73	2.75	2.629	0.3	1.3	
322460	FHWTD6 ^a	70.07	12.65	5.17	4.65	0.066	0.43	0.95	3.22	4.88	0.339	0.02	0.63	
322461	FHWTD6 ^a	68.27	12.6	6.34	5.7	0.074	0.91	1.69	3.41	3.91	0.721	0.09	0.53	
322463	FHWTD6 ^a	73.72	11.47	4.92	4.42	0.037	0.17	1.08	3.25	3.65	0.276	0.04	0.46	
322464	FHWTD6 ^a	71.84	11.89	4.94	4.44	0.038	0.21	0.8	2.84	5.12	0.267	0.02	0.26	
322465	FHWTD6 ^a	74.23	10.89	4.7	4.23	0.039	0.18	1.37	2.88	3.7	0.271	0.02	0.38	
322466	FHWTD6 ^a	52.99	13.44	13.86	12.46	0.273	5.06	4.55	2.35	3.91	1.99	0.27	1.33	
322467	FHWTD6 ^a	70.2	11.53	5.74	5.16	0.067	0.54	1.39	3.14	4.06	0.497	0.05	0.69	
322468	FHWTD6 ^a	72.37	11.6	4.95	4.45	0.038	0.13	0.96	3.56	4.33	0.298	0.02	0.5	
322469	FHWTD6 ^a	69.91	12.55	5.55	4.99	0.053	0.16	1.21	3.83	4.55	0.309	0.02	0.76	
322470	FHWTD6 ^a	69.19	12.99	5.13	4.61	0.086	0.13	1.32	3.87	5.16	0.29	0.03	0.71	
		0		0										
322471	FHWTD7 ^a	70.38	12.42	5.43	4.88	0.101	0.11	1.26	3.59	4.7	0.292	0.02	0.66	
322472	FHWTD7 ^a	69.76	12.43	5.61	5.04	0.069	0.22	1.11	4.03	4.06	0.316	0.02	0.79	
322473	FHWTD7 ^a	67.76	12.1	6.84	6.15	0.101	0.75	1.69	3.45	4.04	0.684	0.08	0.83	
322474	FHWTD7 ^a	41.76	13.63	19.31	17.36	0.301	6.46	6.52	2.28	3.19	3.041	0.37	2.72	
322475	FHWTD7 ^a	69.06	12.93	5.13	4.61	0.071	0.33	1.11	4.12	4.71	0.322	0.03	0.64	
321918	FHWTD7 ^a	71.08	12.69	4.92	4.42	0.081	0.2	0.86	3.62	4.87	0.278	0.05	0.58	
321919	FHWTD7 ^a	69.87	12.6	4.91	4.41	0.106	0.28	1.77	3.65	4.67	0.303	0.06	0.82	
321920	FHWTD7 ^a	68.67	12.62	5.18	4.66	0.116	0.39	2.14	3.55	4.54	0.3	0.03	1.14	
321921	FHWTD7 ^a	69.34	13.08	4.91	4.41	0.125	0.19	1.16	3.87	4.8	0.311	0.04	0.58	
321922	FHWTD7 ^a	70.16	12.35	4.97	4.47	0.103	0.13	0.98	3.77	4.58	0.292	0.03	0.58	

Table A1-4: Lithogeochemical data for the South Belt

Sample	Channel* Number	Sc	Be	V	Cr	Co	Ni	Cu	Zn	Ga	Ge	As	Rb	Sr	Y	Zr	Nb	Mo	Ag	In	Sn	Sb	Cs
A103237	FHW75#1	<1	11	7	<20	<1	<20	<10	100	51	3	<5	454	20	328	3249	293	<2	<0.2	51	<0.5	<0.5	
A103238	FHW75#2	<1	16	<5	<20	<1	<20	<10	170	51	2	<5	439	20	401	3367	276	<2	<0.2	49	<0.5	<0.5	
A103239	FHW75#3	<1	22	<5	<20	<1	<20	20	390	56	3	<5	410	24	389	3715	318	3	<0.2	55	<0.5	<0.5	
A103240	FHW75#4	31	6	284	80	47	50	50	980	29	3	<5	615	123	58	282	40	4	1.2	<0.2	6	<0.5	5.9
A103241	FHW75#5	<1	15	<5	<20	<1	<20	10	360	57	3	<5	359	25	350	4381	221	<2	<0.2	51	<0.5	<0.5	
A103242	FHW75#6	<1	11	<5	<20	4	<20	<10	280	60	3	<5	397	22	369	3016	277	<2	<0.2	50	<0.5	<0.5	
A103243	FHW75#7	<1	15	<5	<20	<1	<20	10	240	55	2	<5	296	30	309	2850	210	<2	<0.2	39	<0.5	<0.5	
103244	FHW76#1	2	17	17	<20	2	<20	50	120	52	2	<5	154	65	227	1808	166	<2	<0.2	16	<0.5	<0.5	
103245	FHW76#2	<1	17	11	<20	2	<20	<10	190	57	3	<5	108	71	363	2564	228	3	<0.2	21	<0.5	<0.5	
103246	FHW76#3	1	19	15	<20	1	<20	30	260	63	3	<5	130	80	377	2598	200	3	<0.2	21	<0.5	<0.5	
103247	FHW76#4	<1	17	17	<20	3	<20	110	180	52	2	<5	180	53	227	1883	178	<2	<0.2	21	<0.5	<0.5	
103248	FHW76#5	31	4	185	40	33	<20	50	270	25	2	<5	230	184	50	363	20	<2	1.1	<0.2	3	<0.5	1.3
103249	FHW76#6	33	9	292	50	43	30	60	440	31	2	<5	271	116	65	215	28	<2	0.6	<0.2	9	<0.5	1.3
103250	FHW77#1	1	17	23	<20	3	<20	50	300	44	2	<5	127	58	388	3614	399	<2	<0.2	51	<0.5	<0.5	
103251	FHW77#2	4	25	37	<20	5	<20	10	930	59	3	<5	454	49	707	5016	516	2	<0.2	85	<0.5	<0.5	
103252	FHW77#3	32	7	298	60	46	40	50	880	26	2	<5	387	149	59	335	34	9	1.2	<0.2	5	<0.5	1.6
103253	FHW77#4	1	30	5	<20	2	<20	10	240	48	2	<5	400	23	363	3279	267	<2	<0.2	54	<0.5	<0.5	
103254	FHW77#5	<1	29	6	<20	1	<20	<10	90	56	2	<5	366	20	373	3910	319	<2	<0.2	60	<0.5	<0.5	
103255	FHW77#6	<1	30	<5	<20	<1	<20	<10	110	57	2	<5	394	24	439	4041	323	<2	<0.2	64	<0.5	<0.5	
103256	FHW77#7	<1	24	<5	<20	<1	<20	<10	80	55	2	<5	403	15	384	3931	292	<2	<0.2	55	<0.5	<0.5	
103257	FHW77#8	<1	41	<5	<20	<1	<20	<10	<50	59	3	<5	560	18	441	3857	331	<2	<0.2	63	<0.5	<0.5	
103258	FHW77#9	<1	34	<5	<20	<1	<20	<10	40	58	3	<5	484	18	485	3560	383	<2	<0.2	64	<0.5	<0.5	
103259	FHW77#10	<1	30	<5	<20	<1	<20	<10	<50	55	2	<5	538	10	253	2612	214	<2	<0.2	42	<0.5	<0.5	
103260	FHW77#11	<1	19	<5	<20	<1	<20	<10	<50	52	2	<5	441	9	222	2018	221	<2	<0.2	39	<0.5	<0.5	
103261	FHW77#12	<1	20	<5	<20	<1	<20	<10	<50	51	2	<5	405	15	265	2273	237	<2	<0.2	41	<0.5	<0.5	
103262	FHW77#13	25	7	179	110	30	80	30	760	29	3	<5	250	132	39	113	21	<2	<0.5	<0.2	7	<0.5	1.7
103263	FHW77#14	<1	16	<5	<20	<1	<20	<10	<50	51	2	<5	415	14	205	2023	157	<2	<0.2	32	<0.5	<0.5	
103264	FHW77#15	<1	16	<5	<20	1	<20	<10	<50	52	2	<5	425	15	209	2123	168	<2	<0.2	33	<0.5	<0.5	
103265	FHW77#16	<1	17	6	<20	<1	<20	<10	<50	56	2	<5	478	14	257	3321	272	<2	<0.2	53	<0.5	<0.5	
103266	FHW77#17	<1	10	10	<20	<1	<20	<10	<50	51	2	<5	411	13	245	2671	235	<2	<0.2	43	<0.5	<0.5	
103267	FHW77#18	22	12	190	40	32	30	100	460	35	2	<5	313	135	111	924	63	2	<0.2	14	<0.5	2.5	
103268	FHW77#19	<1	17	<5	<20	<1	<20	<10	40	54	2	<5	377	18	272	2348	168	<2	<0.2	35	<0.5	<0.5	
103269	FHW77#20	<1	21	<5	<20	<1	<20	<10	110	55	3	<5	379	20	310	2267	198	<2	<0.2	38	<0.5	<0.5	
103270	FHW77#21	<1	18	<5	<20	<1	<20	<10	40	57	3	<5	323	20	332	2960	219	2	<0.2	41	<0.5	<0.5	
103271	FHW77#22	<1	20	<5	<20	<1	<20	<10	50	54	3	<5	304	21	437	4725	304	3	<0.2	47	<0.5	<0.5	
103272	FHW77#23	<1	19	<5	<20	<1	<20	<10	30	55	2	<5	299	22	264	2317	181	<2	<0.2	34	<0.5	<0.5	
103273	FHW77#24	<1	24	<5	<20	<1	<20	<10	130	55	2	<5	309	24	286	2330	205	<2	<0.2	40	<0.5	<0.5	
103274	FHW77#25	22	21	181	70	41	80	60	520	35	2	<5	607	64	66	420	41	1.4	<0.2	12	<0.5	5	
103275	FHW77#26	2	32	16	<20	2	<20	<10	130	69	2	<5	348	39	271	2189	185	3	<0.2	58	<0.5	<0.5	
103276	FHW77#27	1	26	7	<20	<1	<20	<10	40	51	2	<5	235	31	270	2304	185	<2	<0.2	36	<0.5	<0.5	
103277	FHW77#28	1	28	9	<20	1	<20	<10	90	57	2	<5	246	36	248	2188	184	<2	<0.2	38	<0.5	<0.5	
103278	FHW77#29	23	3	56	<20	9	<20	<10	30	22	2	<5	67	296	41	207	19	<2	0.7	<0.2	4	<0.5	1.3
103279	FHW77#30	30	4	221	160	52	130	110	600	23	2	<5	332	151	32	141	12	<2	0.7	<0.2	3	1	1.9
103280	FHW78#1	1	13	<5	<20	<1	<20	<10	30	100	45	2	<5	261	27	180	1403	106	<2	<0.2	20	0.8	<0.5
103281	FHW78#2	30	8	216	140	49	110	30	530	30	2	<5	335	147	47	139	26	<2	0.7	<0.2	6	1.2	1.5
103282	FHW78#3	<1	16	7	<20	1	<20	30	150	53	2	<5	211	28	199	1681	133	<2	<0.2	24	1	<0.5	
103283	FHW78#4	1	17	10	20	<1	<20	10	90	49	2	<5	355	20	215	1774	139	<2	<0.2	27	1.1	<0.5	
103284	FHW78#5	<1	16	9	<20	<1	<20	<10	110	50	2	<5	345	18	220	1894	140	<2	<0.2	26	0.8	<0.5	
103285	FHW78#6	<1	14	6	<20	<1	<20	<10	120	54	2	<5	375	16	237	1918	154	<2	<0.2	31	1.1	<0.5	
103286	FHW78#7	<1	15	<5	<20	<1	<20	<10	140	55	2	<5	415	15	217	1841	131	<2	<0.2	30	0.9	<0.5	
103287	FHW78#8	<1	18	<5	<20	<1	<20	<10	150	52	2	<5	390	13	273	2283	186	<2	<0.2	33	1	<0.5	
103288	FHW78#9	1	19	<5	<20	<1	<20	<10	110	57	3	<5	433	20	307	2033	160	<2	<0.2	36	1.1	0.6	
103289	FHW78#10	1	18	<5	<20	<1	<20	<10	110	57	2	<5	426	15	242	2093	174	<2	<0.2	35	1.1	<0.5	
103290	FHW78#11	<1	15	<5	<20	<1	<20	<10	100	56	2	<5	410	14	193	1692	130	<2	<0.2	26	1.1	<0.5	
103291	FHW78#12	<1	10	8	<20	<1	<20	<10	110	50	2	<5	286	28	251	1599	131	<2	<0.2	35	1	0.5	
103292	FHW78#13	<1	12	11	<20	<1	<20	<10	130	49	2	<5	260	34	285	2182	112	<2	<0.2	32</td			

Table A1-5: Lithogeochemical data for the South Belt

Sample	Channel* Number	Sc	Be	V	Cr	Co	Ni	Cu	Zn	Ga	Ge	As	Rb	Sr	Y	Zr	Nb	Mo	Ag	In	Sn	Sb	Cs
103299	FHW-T90D4	<1	17	<5	<20	<1	<20	<10	210	55	2	<5	414	17	272	2712	247	<2	<0.2	47	0.7	<0.5	
103300	FHW-T90D5	<1	22	<5	<20	<1	<20	<10	200	52	2	<5	391	20	278	2569	218	<2	<0.2	42	0.7	<0.5	
103301	FHW-T90D6	32	14	247	50	43	40	120	970	33	2	<5	494	139	76	290	68	3	1	<0.2	14	0.8	3.3
103302	FHW-T90D7	32	5	295	50	46	40	80	400	27	2	<5	320	195	50	296	31	2	1.1	<0.2	5	0.8	2.2
103303	FHW-T90D8	<1	15	<5	<20	<1	<20	<10	90	57	2	<5	305	25	279	2549	210	<2	<0.2	37	0.8	<0.5	
103304	FHW-T10D1	31	5	294	60	51	60	110	560	27	2	<5	269	149	53	323	34	5	1.3	<0.2	5	0.9	2.2
103305	FHW-T10D2	1	14	5	<20	<1	<20	<10	310	54	2	<5	336	34	193	1721	150	<2	<0.2	27	0.6	<0.5	
103306	FHW-T10D3	<1	13	<5	<20	<1	<20	<10	360	60	2	<5	420	29	246	2353	194	<2	<0.2	34	0.8	<0.5	
103307	FHW-T10D4	<1	14	<5	<20	<1	<20	<10	460	56	2	<5	437	19	262	2193	203	<2	<0.2	37	0.8	<0.5	
103308	FHW-T10D5	<1	18	<5	<20	<1	<20	<10	340	54	2	<5	398	19	252	2188	190	<2	<0.2	34	0.8	<0.5	
103309	FHW-T10D6	<1	13	<5	<20	<1	<20	<10	180	54	2	<5	431	19	217	1938	203	<2	<0.2	38	0.8	0.7	
103310	FHW-T10D7	<1	12	<5	<20	<1	<20	<10	200	49	2	<5	390	16	204	1754	168	<2	<0.2	31	0.9	0.6	
103311	FHW-T10D8	<1	10	<5	<20	<1	<20	<10	190	53	2	<5	428	15	261	2408	258	<2	<0.2	30	0.7	1.4	
103312	FHW-T10D9	<1	16	<5	<20	<1	<20	<10	300	55	3	<5	424	17	258	1970	182	<2	<0.2	31	0.7	<0.5	
103313	FHW-T10D10	<1	15	<5	<20	<1	<20	<10	130	55	2	<5	401	24	244	1554	180	<2	<0.2	35	1	<0.5	
103314	FHW-T10D11	<1	19	<5	<20	<1	<20	<10	170	56	3	<5	437	19	279	2338	226	<2	<0.2	41	0.7	<0.5	
103315	FHW-T10D12	<1	15	<5	<20	<1	<20	<10	140	48	3	<5	385	16	221	1976	186	<2	<0.2	33	0.8	<0.5	
103316	FHW-T10D13	<1	17	<5	<20	<1	<20	<10	140	55	3	<5	433	18	260	1948	190	<2	<0.2	37	0.8	<0.5	
103317	FHW-T10D14	<1	18	<5	<20	<1	<20	<10	120	52	2	<5	390	21	243	1883	162	<2	<0.2	36	0.7	<0.5	
103318	FHW-T10D15	<1	15	<5	<20	<1	<20	<10	100	56	2	<5	401	20	220	1921	197	<2	<0.2	39	0.8	<0.5	
103319	FHW-T10D16	<1	16	<5	<20	<1	<20	<10	150	53	2	<5	409	17	252	2123	187	<2	<0.2	35	0.8	<0.5	
103320	FHW-T10D17	<1	17	<5	<20	<1	<20	<10	90	52	2	<5	400	18	258	1876	167	<2	<0.2	35	1.1	<0.5	
103321	FHW-T10D18	<1	18	<5	<20	<1	<20	<10	100	54	2	<5	414	14	246	1726	157	<2	<0.2	36	0.7	<0.5	
103322	FHW-T10D19	<1	15	<5	<20	<1	<20	<10	90	56	2	<5	429	14	241	2253	207	<2	<0.2	40	0.7	<0.5	
103323	FHW-T10D20	<1	17	<5	<20	<1	<20	<10	100	53	2	<5	417	18	277	2121	201	<2	<0.2	38	0.8	<0.5	
103324	FHW-T10D21	<1	19	<5	<20	<1	<20	<10	170	48	2	<5	431	18	262	1865	182	<2	<0.2	35	1	<0.5	
103325	FHW-T10D22	<1	17	<5	<20	<1	<20	<10	70	50	2	<5	367	15	215	1491	141	<2	<0.2	30	0.8	<0.5	
103326	FHW-T10D23	<1	19	<5	<20	<1	<20	<10	70	54	2	<5	398	15	212	1710	165	<2	<0.2	32	0.6	<0.5	
103327	FHW-T10D24	<1	17	<5	<20	<1	<20	<10	70	50	2	<5	365	15	204	1543	120	<2	<0.2	28	0.7	<0.5	
103328	FHW-T10D25	<1	20	<5	<20	<1	<20	<10	100	51	2	<5	422	19	338	1956	222	<2	<0.2	51	0.6	0.9	
422276	FHW-T0D26	<1	22	<5	<20	<1	<20	<10	110	54	2	<5	388	18	320	2260	190	<2	<0.2	51	1	0.6	
422277	FHW-T0D1	31	3	281	100	51	50	90	210	27	2	<5	142	208	55	358	32	2	1	<0.2	4	<0.5	1.6
422278	FHW-T0D1	2	22	15	<20	<1	<20	<10	540	62	2	<5	127	73	241	1576	138	4	<0.2	34	<0.5	0.5	
422279	FHW-T0D1	2	19	8	<20	<1	<20	<10	340	62	2	<5	345	23	231	1930	154	6	<0.2	42	<0.5	<0.5	
422280	FHW-T0D1	2	21	12	<20	2	<20	<10	390	60	2	<5	360	22	243	1949	142	6	<0.2	44	<0.5	<0.5	
422281	FHW-T0D1	4	19	34	<20	5	<20	10	370	58	3	<5	309	32	220	1883	134	7	<0.2	44	<0.5	0.8	
422282	FHW-T0D1	2	17	10	<20	1	<20	<10	200	58	3	<5	304	26	223	1938	136	4	<0.2	38	<0.5	<0.5	
422283	FHW-T0D1	2	14	10	<20	2	<20	30	250	51	3	<5	191	46	250	1980	110	2	<0.2	28	<0.5	<0.5	
422284	FHW-T0D1	30	9	283	80	47	30	60	750	33	2	<5	399	143	61	351	49	4	1	<0.2	12	<0.5	8.6
422285	FHW-T0D1	<1	19	7	<20	2	<20	10	370	62	3	<5	292	48	241	2130	195	3	<0.2	33	<0.5	<0.5	
422286	FHW-T0D1	<1	23	<5	<20	<1	<20	<10	300	62	3	<5	334	22	230	2156	215	<2	<0.2	33	<0.5	<0.5	
422287	FHW-T0D1	<1	20	<5	<20	<1	<20	<10	290	62	3	<5	334	19	204	1782	172	<2	<0.2	28	<0.5	0.5	
422288	FHW-T0D1	<1	15	<5	<20	<1	<20	<10	210	62	3	<5	346	15	213	1776	182	<2	<0.2	35	<0.5	<0.5	
422289	FHW-T0D1	<1	13	11	<20	<1	<20	<10	120	58	3	<5	268	21	165	1906	161	4	<0.2	28	<0.5	<0.5	
422290	FHW-T0D1	<1	15	<5	<20	<1	<20	<10	180	64	3	<5	284	26	223	1957	184	3	<0.2	28	<0.5	<0.5	
422291	FHW-T0D1	24	6	188	120	47	47	90	390	33	2	<5	198	173	96	703	63	16	3.1	<0.2	10	<0.5	2.3
422292	FHW-T0D1	30	3	242	150	58	120	110	210	25	2	<5	174	194	37	212	17	4	1	<0.2	2	<0.5	1.6
422293	FHW-T0D1	<2	22	<5	<20	<1	<20	<10	300	62	3	<5	246	32	269	2563	208	4	<0.2	36	<0.5	<0.5	
422294	FHW-T0D1	1	18	8	<20	2	<20	10	360	60	3	<5	377	17	230	1743	192	6	<0.2	40	<0.5	<0.5	
422295	FHW-T0D1	<1	21	<5	<20	<1	<20	<10	420	60	3	<5	369	27	219	1925	169	3	<0.2	38	<0.5	<0.5	
422296	FHW-T0D1	<1	20	<5	<20	<1	<20	<10	340	61	3	<5	295	29	226	2096	146	2	<0.2	31	<0.5	<0.5	
422297	FHW-T0D1	<1	27	<5	<20	<1	<20	<10	260	64	3	<5	313	36	265	2179	178	<2	<0.2	31	<0.5	0.6	
422298	FHW-T0D1	<1	20	5	<20	<1	<20	<10	240	63	3	<5	367	25	230	2256	190	<2	<0.2	31	<0.5	0.9	
422299	FHW-T0D1	1	17	<5	<20	<1	<20	<10	160	65	3	<5	344	31	246	2615	199	<2	<0.2	28	<0.5	0.8	
422300	FHW-T0D1	<1	20	<5	<20	<1	<20	<10	280	62	3	<5	387	28	233	2309	178	4	<0.2	33	<0.5	0.9	
422301	FHW-T0D1	<1	19	<5	<20	<1	<20	<10	250	57	3	<5	232	25	229	2951	163	<2	<0.2</				

Table A1-6: Lithogeochemical data for the South Belt

Sample	Channel* Number	Sc	Be	V	Cr	Co	Ni	Cu	Zn	Ga	Ge	As	Rb	Sr	Y	Zr	Nb	Mo	Ag	In	Sn	Sb	Cs	
422264	FHWTD3	1	11	5	<20	<1	<20	10	230	64	2	<5	182	37	267	2510	336	7	<0.2	13	<0.5	0.6		
422265	FHWTD3	3	10	30	<20	5	<20	30	250	58	2	<5	131	76	150	1771	101	6	<0.2	12	<0.5	0.8		
422266	FHWTD3	<1	9	<5	<20	1	<20	10	190	64	3	<5	198	40	147	1901	119	6	<0.2	12	<0.5	<0.5		
422267	FHWTD3	<1	6	6	<20	<1	<20	20	140	62	2	<5	114	32	119	1257	74	7	<0.2	9	<0.5	<0.5		
422268	FHWTD3	7	5	18	<20	2	<20	<10	120	36	2	<5	77	124	88	959	74	6	<0.2	7	<0.5	<0.5		
422269	FHWTD4	9	6	17	<20	3	<20	30	140	38	2	<5	82	185	101	1356	74	3	<0.2	8	<0.5	0.5		
422270	FHWTD4	17	6	35	<20	7	<20	60	260	39	2	<5	109	229	115	2141	86	2	<0.2	10	<0.5	0.8		
422271	FHWTD4	37	3	317	30	44	30	50	210	29	2	<5	107	178	51	376	29	<2	1.8	<0.2	4	<0.5	1.2	
422272	FHWTD4	16	7	27	<20	5	<20	20	200	37	2	<5	72	194	79	1044	65	3	<0.2	8	<0.5	0.7		
422273	FHWTD4	38	2	353	30	48	40	70	210	26	2	<5	126	177	39	247	15	<2	1.2	<0.2	3	<0.5	6	
422274	FHWTD4	10	5	68	<20	9	<20	40	120	43	2	<5	80	131	55	632	42	<2	3.2	<0.2	6	<0.5	1.4	
422275	FHWTD4	13	8	95	<20	16	20	20	250	51	2	<5	111	156	128	800	103	3	3.9	<0.2	14	<0.5	2.9	
422301	FHWTD4	12	8	28	<20	5	<20	20	200	36	2	<5	124	139	104	1247	79	2	<0.2	10	<0.5	2.5		
422302	FHWTD4	<1	10	8	<20	<1	<20	20	130	50	2	<5	119	37	149	1793	86	<2	<0.2	9	<0.5	<0.5		
422303	FHWTD4	3	6	15	<20	1	<20	20	90	41	2	<5	89	48	98	1177	70	<2	<0.2	8	<0.5	1		
422304	FHWTD4	12	6	18	<20	<1	<20	<10	120	37	2	<5	114	93	93	107	1453	88	<2	<0.2	8	<0.5	0.5	
422305	FHWTD4	1	4	<5	<20	<1	<20	<10	70	47	1	<5	75	67	127	1500	110	12	<0.2	12	<0.5	<0.5		
422306	FHWTD4	1	6	9	<20	<1	<20	<10	90	50	1	<5	83	77	156	173	117	5	<0.2	13	<0.5	<0.5		
422307	FHWTD4	1	8	8	<20	<1	<20	<10	130	50	2	<5	101	48	163	1127	125	21	<0.2	14	<0.5	<0.5		
422308	FHWTD4	2	5	17	<20	<1	<20	<10	140	47	2	<5	74	63	184	1795	144	13	<0.2	15	<0.5	<0.5		
422309	FHWTD4	7	7	7	<20	<1	<20	<10	250	38	2	<5	145	99	128	1518	105	6	<0.2	12	<0.5	0.6		
422310	FHWTD4	3	7	7	<20	<1	<20	<10	170	48	2	<5	105	76	131	1081	119	11	<0.2	14	<0.5	<0.5		
422311	FHWTD4	12	9	7	<20	<1	<20	<10	230	37	2	<5	164	161	93	1071	80	6	<0.2	9	<0.5	0.9		
422312	FHWTD4	13	7	27	<20	5	<20	50	180	31	2	<5	132	218	118	2103	96	5	<0.2	10	<0.5	1		
422313	FHWTD4	39	1	361	<20	36	20	60	130	20	2	<5	39	224	41	229	15	<2	0.9	<0.2	3	<0.5	0.7	
422314	FHWTD4	14	5	91	30	24	50	20	150	25	1	<5	139	265	63	656	38	<2	2.8	<0.2	5	<0.5	3	
422315	FHWTD4	2	10	<5	<20	<1	<20	<10	60	160	57	2	<5	89	63	77	365	37	7	1.6	<0.2	5	<0.5	0.6
422316	FHWTD4	8	6	<5	<20	<1	<20	<10	30	160	43	2	<5	143	126	78	631	49	5	2.8	<0.2	6	<0.5	0.9
422317	FHWTD4	3	6	<5	<20	<1	<20	<10	140	58	2	<5	157	57	62	485	34	11	2.1	<0.2	4	<0.5	<0.5	
422318	FHWTD4	2	7	8	<20	<1	<20	<10	140	63	2	<5	81	52	68	504	38	10	2.3	<0.2	5	<0.5	0.8	
322456	FHWTD161	<1	26	5	<20	<1	<20	20	250	52	3	<5	332	29	197	2031	102	<2	<0.2	29	0.9	0.9		
322457	FHWTD162	<1	20	<5	30	<1	<20	10	530	58	3	<5	197	38	241	2220	118	<2	<0.2	22	0.9	<0.5		
322458	FHWTD163	2	14	15	<20	2	<20	40	220	54	3	<5	112	107	211	2236	114	7	<0.2	25	0.9	0.5		
322459	FHWTD164	30	3	271	90	57	100	50	180	24	2	<5	198	199	38	233	21	3	1.2	<0.2	4	0.9	2.8	
322460	FHWTD165	1	14	15	<20	3	<20	80	210	56	3	<5	297	30	200	2208	113	4	<0.2	27	0.9	1		
322461	FHWTD166	4	13	42	30	7	<20	30	170	51	3	<5	226	78	182	1905	99	2	<0.2	23	0.9	1.4		
322463	FHWTD168	<1	19	13	<20	<1	<20	<10	160	50	3	<5	166	54	54	236	2113	121	<2	<0.2	29	0.9	<0.5	
322464	FHWTD169	<1	14	14	<20	1	<20	<10	140	51	2	<5	254	49	232	2130	116	2	<0.2	26	0.9	<0.5		
322465	FHWTD1610	<1	15	11	20	1	<20	30	170	49	3	<5	189	52	52	225	2242	107	<2	<0.2	26	0.9	<0.5	
322466	FHWTD1611	29	5	222	180	43	100	50	400	33	2	<5	277	110	53	326	30	<2	1.8	<0.2	8	0.9	2.7	
322467	FHWTD1612	3	15	23	30	4	<20	20	290	55	3	<5	254	32	199	273	115	6	<0.2	29	0.9	1		
322468	FHWTD1613	<1	15	8	<20	<1	<20	<10	170	56	2	<5	235	26	213	2468	116	7	<0.2	27	0.9	<0.5		
322469	FHWTD1614	<1	19	<5	20	<1	<20	30	290	62	3	<5	276	24	246	2917	127	4	<0.2	35	0.8	<0.5		
322470	FHWTD1615	<1	19	<5	<20	<1	<20	<10	230	64	3	<5	300	27	249	2645	140	11	<0.2	26	1	0.6		
322471	FHWTD171	<1	20	<5	<20	<1	<20	<10	240	64	3	<5	293	24	215	2623	135	9	<0.2	28	1.1	<0.5		
322472	FHWTD172	<1	38	<5	<20	<1	<20	<10	270	64	3	<5	258	21	216	2909	120	4	<0.2	33	1	0.5		
322473	FHWTD173	5	16	49	<20	7	<20	30	280	56	3	<5	207	59	174	2435	116	9	<0.2	25	1.1	0.6		
322474	FHWTD174	29	8	262	80	64	140	20	440	38	2	<5	259	113	50	263	41	<2	1.4	<0.2	10	1.1	3.7	
322475	FHWTD175	1	15	<5	<20	<1	<20	<10	350	63	3	<5	230	40	219	2733	107	8	<0.2	20	0.9	0.7		
321918	FHWTD176	<1	13	<5	<20	<1	<20	<10	60	360	58	3	<5	295	27	201	2499	115	6	<0.2	21	1.1	1.2	
321919	FHWTD177	<1	14	<5	<20	<1	<20	<10	300	59	3	<5	259	33	216	2760	130	8	<0.2	19	1.1	1		
321920	FHWTD178	<1	20	<5	<20	<1	<20	<10	10	530	59	3	<5	308	27	235	2587	129	6	<0.2	23	1.2	1.9	
321921	FHWTD179	1	16	<5	<20	<1	<20	<10	320	60	3	<5	300	27	216	2604	121	9	<0.2	21	1.2	1		
321922	FHWTD1710	1	15	<5	<20	<1	<20	<10	290	57	3	<5	300	23	220	2622	116	7	<0.2	20	1.2	0.9		
321923	FHWTD1711	1	13	<5	<20	<1	<20	<10	30	330	58	3	<5	302	33	203	2567	113	11	<0.2	19	1	0.5	
321924	FHWTD1712	<1	13	<5	<20	<1	<20	<10	370	59	3	<5	311	23	211	2732	105	7	<0.2	21	0.9	0.6		
321925	FHWTD1713	<1	17	<5	<20	<1	<20	<10	360	63	2	<5	323	18	212	2874	186	7	<0.2	28	0.6	<0.5		

Table A1-7: Lithogeochemical data for the South Belt

Sample	Channel Number	Ba	Bi	La	Ce	Pr	Nd	Sm	Eu	Gd	Tb	Dy	Ho	Er	Tm	Yb	Lu	Hf	Ta	W	Tl	Pb	Th	U	
A103237	FHW75-01	32	< 0.4	191	432	53.1	208	54	1.23	49.7	8.7	63.8	13.6	41.8	6.57	44.8	6.77	92.8	18.6	2	1.6	35	52	12	
A103238	FHW75-02	39	< 0.4	215	470	58.1	328	57.4	1.31	55.3	10.6	69.3	14.7	45.1	7.06	46.8	7.3	85.9	18.3	1	1.4	41	51	10.7	
A103239	FHW75-03	45	0.5	265	579	72.2	280	71.3	1.63	66.3	12.1	76.2	15.8	48.6	7.6	49.8	7.3	96.6	20.3	2	1.2	161	57.7	12.9	
A103240	FHW75-04	296	< 0.4	31.4	72.6	9.7	44.4	10.9	2.68	11	1.8	11.1	2.3	6.8	1	6.5	0.99	7.2	1.9	< 1	2.6	134	3.1	1.1	
A103241	FHW75-05	58	< 0.4	268	586	72.4	282	70.7	1.51	63.7	10.9	67.6	13.9	41.1	6.33	42.5	6.64	123	16.6	2	1.2	134	43.2	12.4	
A103242	FHW75-06	51	0.6	291	620	79.9	313	77.5	1.65	70.4	11.9	72.2	14.7	42.8	6.4	42.5	6.55	84	16.2	2	1.7	133	46.5	10.9	
A103243	FHW75-07	92	< 0.4	236	524	65.6	260	65.1	1.38	57.3	9.7	58.8	12	36	5.42	36.3	5.64	78	14.1	1	1.1	131	36.7	9.5	
103244	FHW76-01	172	< 0.4	359	786	82.8	320	55.8	2.51	43.2	6.9	42.1	8.6	25.8	3.83	24.5	3.67	43.9	7.8	< 1	0.5	43	26.7	4.6	
103245	FHW76-02	159	< 0.4	541	1220	134	526	97.2	3.84	75.5	12.3	73.5	14.4	41.3	5.93	37.8	5.63	59.8	10.9	1	1.3	58	40.2	6.3	
103246	FHW76-03	165	< 0.4	589	1330	144	559	101	3.71	77.9	12.6	75.1	14.6	41.9	5.87	37.4	5.65	59.2	10.2	< 1	0.4	107	36.7	5.9	
103247	FHW76-04	342	0.6	366	824	87	332	60.2	2.44	45.8	7.2	42.9	8.5	25	3.71	24.5	3.59	46.9	8.7	< 1	0.5	255	29.1	4.9	
103248	FHW76-05	627	< 0.4	48.2	113	13.1	56.6	11.4	2.51	10	1.7	9.6	1.9	5.4	0.81	5.3	0.84	8.9	0.9	< 1	1.1	47	5.9	1.1	
103249	FHW76-06	334	< 0.4	40	96.9	11.9	52.2	12.2	2.32	10.9	1.9	11.3	2.1	6.1	0.9	5.7	0.89	5.5	1	< 1	1.1	47	3.2	1.1	
103250	FHW77-01	131	< 0.4	175	456	50.2	201	52.3	1.54	53.3	11.2	77.2	15.9	47.5	7.42	50.1	7.56	107	22.4	< 1	0.4	86	71.6	13.9	
103251	FHW77-02	81	0.6	321	795	91.5	374	100	2.75	97.4	18.9	123	25.1	74.7	11.8	78	12.1	147	28.4	1	1.5	89	79.2	17.1	
103252	FHW77-03	316	< 0.4	33.6	82.6	10.1	46.8	11	2.86	10.7	1.8	10.8	2.1	6.3	0.92	5.8	0.91	8.1	1.8	< 1	1.4	94	3.4	1	
103253	FHW77-04	76	< 0.4	140	363	42.1	170	46.1	1.29	46.9	9.3	60.9	12.8	39.8	6.31	43	6.81	103	17.1	< 1	0.9	67	48.1	12.1	
103254	FHW77-05	46	< 0.4	219	545	61.5	246	60.2	1.56	55.8	10.5	66.4	13.8	42.4	6.88	47.1	7.29	121	19.7	< 1	0.9	36	55.5	12.9	
103255	FHW77-06	46	< 0.4	282	674	75.8	296	68.7	1.73	62.3	11.6	78	16.6	49.8	7.83	53.4	8.27	121	21.2	< 1	1	44	53.6	12.8	
103256	FHW77-07	34	< 0.4	183	453	53.2	217	57.2	1.47	54.7	10.5	67.4	14	42.5	6.79	47.3	7.44	116	18.9	< 1	1	29	54.3	12	
103257	FHW77-08	45	< 0.4	233	517	65.7	247	65.1	1.63	63.1	11.5	75.9	16.4	49.2	7.63	52.5	8.13	110	21.6	< 1	1.5	32	62.1	13.5	
103258	FHW77-09	36	< 0.4	286	633	79.9	299	74.1	1.79	68.5	13.2	85.6	18.6	56.7	8.7	59.4	9.25	101	24.2	1	1.4	39	74.1	14.5	
103259	FHW77-10	29	< 0.4	143	328	40.2	148	37.6	0.94	35.7	6.8	45.2	10	30.7	4.89	34.3	5.38	74.3	13.5	< 1	1.7	35	39.7	9.2	
103260	FHW77-11	32	< 0.4	129	299	36.4	133	33.8	0.84	30.8	6	40.6	8.9	27.4	4.37	30.1	4.74	57.3	13.6	< 1	1.5	32	39.4	8	
103261	FHW77-12	67	< 0.4	155	344	42	154	37.4	1.02	35.1	6.9	46.7	10.4	31.8	5.02	34.4	5.42	63.5	14.9	< 1	1.3	55	44.3	8.6	
103262	FHW77-13	97	2.3	16.9	37	5.03	22.2	5.7	1.48	6.1	1	5.9	1.2	3.7	0.52	3.4	0.52	2.8	0.5	< 1	1	124	1.4	0.5	
103263	FHW77-14	48	< 0.4	149	328	38.4	139	32.9	0.93	30.2	5.6	36.6	7.8	23.2	3.56	24.3	3.84	53.3	10.8	< 1	1.3	25	30.8	6.6	
103264	FHW77-15	49	< 0.4	141	315	36.9	134	32.6	0.95	31.1	5.8	37.9	8.2	24.3	3.69	24.9	4.02	57.4	11.4	< 1	1.3	26	31	6.8	
103265	FHW77-16	45	< 0.4	152	360	42.8	156	41.3	1.12	39.1	7.3	47.9	10.3	31.1	4.84	33.2	5.28	90.4	17.2	< 1	1.4	38	47.3	10.5	
103266	FHW77-17	38	< 0.4	126	297	35.7	133	35.7	0.95	35.3	6.7	45	9.8	30.2	4.74	32.1	5.04	74.6	15	1	1.3	34	44	9.1	
103267	FHW77-18	156	< 0.4	78.7	178	21.3	81.6	18.8	2.14	17.5	3	18.6	3.8	11.5	1.76	12.1	1.92	23.9	4.2	1	1.2	56	13.1	2.8	
103268	FHW77-19	41	< 0.4	202	432	51.9	192	44.4	1.18	40.2	7.1	45.2	9.6	29.6	3.18	30.5	5.09	59.5	12.2	6	1.2	36	34.6	7.6	
103269	FHW77-20	52	< 0.4	241	502	61.4	221	51.9	1.35	52.6	10.9	32.8	5.02	33.8	5.29	58.1	13	1	1.1	40	49.4	7.9			
103270	FHW77-21	45	< 0.4	221	501	62.4	237	58.7	1.53	54.6	9.8	60.7	12.4	37.4	5.72	37.8	5.89	81.4	14.5	2	0.9	42	48.1	9.2	
103271	FHW77-22	51	< 0.4	186	403	46.5	181	43.5	1.19	40.4	7.2	45.9	9.8	30.4	4.62	31.3	4.94	62	11.9	< 1	0.9	39	32.9	7.2	
103272	FHW77-23	59	< 0.4	186	403	46.5	181	43.5	1.19	40.4	7.2	45.9	9.8	30.4	4.62	31.3	4.94	62	11.9	< 1	0.9	39	32.9	7.2	
103273	FHW77-24	74	< 0.4	197	433	53.1	199	47.3	1.27	49.2	9.7	48.6	10.2	30.6	4.75	32	4.94	66	13	< 1	0.8	32	35.5	7.4	
103274	FHW77-25	209	< 0.4	43.3	94.1	11.5	45.6	10.6	1.6	10.1	1.7	10.6	2.2	40.3	7.5	47	9.9	40.3	6.1	1.6	1.04	11.2	2.1	1.3	
103275	FHW77-26	95	< 0.4	204	202	43.5	52.8	193	44.8	1.31	40.3	7.5	47	9.9	30.4	4.69	46.9	3.21	61.4	11	< 1	0.9	43	38.9	5.9
103276	FHW77-27	108	< 0.4	251	527	63.4	231	50.7	1.45	44.4	7.7	48.5	10.1	30.1	4.6	31.1	4.89	63.3	11.7	2	0.7	44	47.5	7.2	
103277	FHW77-28	84	< 0.4	241	500	59.9	213	45.9	1.32	30.5	7.1	44.4	9.2	37.9	4.26	29.5	4.65	60.3	11.1	< 1	0.7	48	41.3	7	
103278	FHW77-29	1933	< 0.4	51.7	108	13.3	52.0	10.2	3.38	8.6	1.3	7.4	1.4	4.2	0.64	4.3	0.68	4.8	1.1	< 1	0.3	14	8.8	2.4	
103279	FHW77-26	969	< 0.4	32.2	72.4	9.33	28.7	8.7	2.27	8.4	1.3	7.6	1.5	4.3	0.66	4.4	0.7	6	1	< 1	0.4	26	4.1	0.9	
103280	FHW77-27	1839	< 0.4	120	225	25.4	90.1	13.8	2.62	9.4	1.3	7.2	1.4	4.2	0.66	4.6	0.76	10.6	0.9	< 1	0.6	27	18.1	2.9	
103300	FHW77-28	599	< 0.4	262	541	64.5	234	41.8	2.66	30.5	4.9	28.5	5.7	23.2	2.57	33.3	7.1	1.1	0.8	33	38.3	6.2			
103278	FHW78-01	69	< 0.4	150	332	41.1	165	39.5	1.08	35.4	6.3	38.4	8.2	25.5	4.11	28.2	4.79	42.7	13.3	< 1	0.7	45	37.1	6.2	
103279	FHW78-02	211	< 0.4	16.6	37.1	4.96	22.6	5.7	1.51	5.7	0.9	5.7	1.1	3.4	0.55	3.9	0.67	2.9	0.7	< 1	1.3	67	2.2	0.6	
103280	FHW78-03	64	< 0.4	186	378	44.5	168	34.7	1.01	29.9	5	29.7	6	18.1	2.95	22.4	3.82	31.3	10.7	< 1	0.8	54	30.3	4.7	
103281	FHW78-04	326	0.8	26	47.5	6.81	29.8	7.2	1.67	7.4	1.2	7.1	1.4	4.4	0.7	5.3	0.93	3	1.3	< 1	1.3	78	2.2	0.6	

Table A1-8: Lithogeochemical data for the South Belt

Sample	Channel Number	Ba	Bi	La	Ce	Pr	Nd	Sm	Eu	Gd	Tb	Dy	Ho	Er	Tm	Yb	Lu	Hf	Ta	W	Tl	Pb	Th	U	
103299	FHW79-04	53	< 0.4	142	326	38.5	141	36.6	1.04	36.6	7.2	47.2	10	30.9	4.94	33.5	5.32	80.8	15.7	< 1	1.5	62	35.9	9.7	
103300	FHW79-05	57	< 0.4	167	366	44	160	39.5	1.11	37.8	7.4	46.8	9.6	29.3	4.55	30.5	4.75	76.7	14.5	< 1	1.4	52	41.6	9.3	
103301	FHW79-06	427	0.6	32.6	74.1	9.37	39.1	9.7	2.35	10.5	1.9	11.7	2.4	7.4	1.16	7.5	1.16	7.4	2.3	< 1	2.4	70	3.5	1.4	
103302	FHW79-07	356	< 0.4	30.6	71	8.83	37.4	8.9	2.54	9.3	1.6	9.2	1.8	5.2	0.78	5.1	0.78	7.3	1.6	< 1	1.5	70	3.3	1	
103303	FHW79-08	47	< 0.4	182	399	47.5	173	42.5	1.18	40.7	7.6	47.5	9.7	28.9	4.44	29.7	4.63	74.8	13.4	< 1	0.9	39	36.1	8.1	
103304	FHW710-01	305	< 0.4	31.7	74.3	9.37	39.2	9.5	2.61	9.7	1.6	9.6	1.8	5.3	0.81	5.2	0.81	7.7	1.6	< 1	1	63	4.1	1.5	
103305	FHW710-02	50	< 0.4	135	289	32.9	117	27.5	0.87	26.7	5.2	32.6	6.6	19.7	3.12	21.7	3.42	49.8	9.5	< 1	1	60	26.5	5.8	
103306	FHW710-03	55	< 0.4	198	402	47.5	168	38.2	1.15	36.5	6.8	42.8	9	25.9	4.18	27.9	4.44	68.4	12.3	< 1	1.2	110	37.5	7.4	
103307	FHW710-04	43	0.5	165	358	42.1	156	38.3	1.12	37.6	7.1	45.2	9	27.6	4.44	29.6	4.6	67.9	13.5	< 1	1.3	132	37.9	7.2	
103308	FHW710-05	44	< 0.4	231	473	55.6	198	43.5	1.22	39	7	43.3	8.6	25.6	4.05	27.3	4.31	64.8	12.1	< 1	1.3	99	36.6	6.7	
103309	FHW710-06	63	0.7	136	296	33.6	119	28.3	0.9	28.1	5.5	36.5	7.6	22.5	3.55	24.7	3.87	58.4	12.7	< 1	1.3	59	29.6	6.7	
103310	FHW710-07	49	0.5	160	343	37.8	133	30.3	0.92	29.1	5.6	34.9	7	20.4	3.26	22.6	3.53	53.2	11.3	< 1	1.2	56	26.4	6.1	
103311	FHW710-08	51	1	145	313	35.3	127	31.1	1.01	32	6.7	44.6	9.1	28.2	4.61	31.1	4.99	73.6	15	< 1	1.3	53	45	9.9	
103312	FHW710-09	38	0.7	202	414	48.4	169	38.3	1.18	35.7	6.9	44.5	8.3	24	3.75	24.2	3.89	60.4	11.5	< 1	1.2	46	57.3	7.5	
103313	FHW710-10	34	< 0.4	157	328	38.3	135	32.2	0.98	31.6	6.2	40.9	8.1	23.7	3.8	24.6	3.84	45.9	10.5	< 1	1.1	51	30.5	6.1	
103314	FHW710-11	34	< 0.4	207	431	51.3	182	41.4	1.23	38.9	7.5	48.7	10	29.9	4.72	32.4	5.09	71.1	14.5	< 1	1.1	35	42.4	8	
103315	FHW710-12	30	< 0.4	187	386	46	161	36.5	1.05	33.4	6.3	38.8	7.9	23.7	3.69	26	4.07	59.9	11.9	< 1	1	35	36.3	7.1	
103316	FHW710-13	36	< 0.4	181	380	45.4	162	38.3	1.17	37.3	7.1	45.3	9.2	27.1	4.16	28.7	4.52	60.2	12.8	< 1	1.1	27	39.5	7.5	
103317	FHW710-14	38	0.4	189	396	47.3	169	38.2	1.15	35.8	6.8	42.6	8.8	25.7	4.02	28.4	4.42	56	11.7	< 1	1	27	33.1	6.6	
103318	FHW710-15	36	0.8	152	337	39.1	139	33.5	1.01	31.5	6.1	39	8	23.7	3.7	25.9	4.1	59.2	12.4	< 1	1	23	32.1	7.2	
103319	FHW710-16	37	0.5	170	362	42.8	155	36.2	1.07	35	6.7	42.4	8.7	25.6	3.85	27.2	4.36	64.8	12.1	< 1	1	26	32.5	6.8	
103320	FHW710-17	36	< 0.4	185	389	46.2	166	38.1	1.12	36.8	6.9	43.5	8.9	26.6	4.1	28.7	4.48	56.9	12	< 1	1	24	39.2	7.4	
103321	FHW710-18	37	< 0.4	178	377	44.8	161	37.7	1.14	36.1	6.6	40.6	8.4	24.8	3.94	28	4.47	53.8	10.7	< 1	1	22	18.8	5.6	
103322	FHW710-19	36	0.4	164	355	41.1	147	34.2	1.01	32.1	6.2	40	8.2	24.8	3.88	27.6	4.4	66.9	13.1	< 1	1	22	45.4	8.2	
103323	FHW710-20	48	0.5	196	416	49.1	175	40.9	1.17	38.4	7.4	46	9.5	28.9	4.5	29.6	4.63	65.6	13.5	< 1	1.1	24	39.2	7.4	
103324	FHW710-21	90	< 0.4	174	367	43	155	35.8	1.05	33.9	6.5	41.4	8.5	26	4.19	28.4	4.4	55.4	11.5	< 1	1.1	28	34.4	6.2	
103325	FHW710-22	39	< 0.4	176	361	42.8	152	34.1	1.01	31.9	5.6	36	7.2	21.7	3.44	23.8	3.83	45.9	9.4	< 1	1	21	28.8	5.3	
103376	FHW710-23	44	< 0.4	187	392	45	161	35	1.02	31.8	5.7	35.3	7.1	21.2	3.39	23.9	3.77	51.7	10.4	< 1	1.1	19	33.1	5.8	
103377	FHW710-24	40	< 0.4	163	346	40.6	147	33.8	0.98	31.4	5.4	33.7	6.9	20.7	3.33	23	3.69	45.7	9.7	< 1	1	22	21.2	5.5	
103378	FHW710-25	46	0.4	186	409	47.6	172	44.4	1.29	45.5	9	57.9	11.4	32.9	4.83	31	4.81	62.4	13.4	< 1	1.2	34	23.7	7.8	
422276	FHW710-26	44	< 0.4	155	355	41.9	157	41.4	1.2	46.9	8.8	56.9	11.7	34.5	5.28	35	5.54	72	16.3	2	1	28	30.1	8.1	
422277	FHW711	346	< 0.4	42	94.2	12.3	53.1	11.4	2.74	11.1	1.8	10.7	2.1	6.2	0.89	5.8	0.92	7.7	2.4	1	0.7	25	5.9	1.1	
422278	FHW711	159	< 0.4	254	543	61.7	229	44.4	1.43	38.7	6.6	39.3	7.7	23.4	3.54	24.3	3.99	41.2	10.6	< 1	0.5	152	31	5.7	
422279	FHW711	49	0.8	203	438	49.2	183	37.2	1.28	34.2	6.4	40.4	8.4	25.6	3.92	26.2	4.19	55.9	13.4	2	1.1	79	32.9	6.6	
422280	FHW711	53	< 0.4	211	454	51.3	191	38.9	1.4	35.8	6.6	41.5	8.5	25.5	3.82	25.5	4.03	54.7	13.3	< 1	1.1	105	35.1	6.6	
422281	FHW711	93	< 0.4	208	448	50.7	188	37.8	1.46	34	6.2	38	7.8	23.5	3.53	23.8	3.82	52.9	12.2	< 1	1	91	29.5	5.6	
422282	FHW711	78	< 0.4	221	475	54.2	203	41.4	1.35	37.1	6.6	40.9	8.2	24.7	3.71	25.3	4	55.1	12.6	< 1	0.9	91	31.9	6.6	
422283	FHW711	113	< 0.4	266	572	64.9	244	48.8	1.6	43.8	7.6	46.7	9.2	26.7	3.88	25.3	3.98	54.2	11.4	< 1	0.5	96	39.9	5.9	
422284	FHW711	249	< 0.4	34.3	75.1	75.1	10.1	44.6	10.2	2.68	10.6	1.7	10.9	2.2	6.7	0.99	6.4	1.05	7.8	2.7	< 1	1.6	82	4	1.1
422285	FHW711	67	< 0.4	286	555	68	232	47.1	1.47	39.9	7.4	43.6	8.8	25.6	3.78	25.5	4.11	55.7	11.7	< 1	0.7	113	31.9	6.9	
422286	FHW711	44	< 0.4	262	508	61.8	211	44.2	1.38	38.1	7.1	43.3	8.7	25.8	3.9	26.6	4.3	59.8	13.7	< 1	0.9	102	31.9	6.6	
422287	FHW711	51	0.4	246	475	57.7	193	39	1.24	32.4	5.8	35.2	7	20.8	3.13	21.4	3.54	47	10.3	< 1	0.9	84	25.6	4.9	
422288	FHW711	41	< 0.4	177	387	44.7	155	35.3	1.09	32.1	6	37.3	7.4	22	3.33	22.8	3.71	51.7	12.4	< 1	0.9	50	30.4	5.9	
422289	FHW711	78	< 0.4	178	379	42.9	145	30	0.98	25.9	4.9	30	6	18	2.72	18.6	3.13	55.3	11.3	< 1	0.8	57	28.4	5	
422290	FHW711	75	< 0.4	252	499	59.4	200	40.8	1.33	34.4	6.5	40	8.1	24.2	3.68	25.2	4.03	52.4	12.2	< 1	0.8	72	32	6	
422291	FHW711	372	< 0.4	99.8	207	23.9	83.9	17.7	1.87	15.9	2.8	16.9	3.4	9.8	1.42	9.7	1.58	17.9	3.6	< 1	0.8	71	10.2	2.2	
422292	FHW711	392	< 0.4	20.6	47.5	6.06	25.5	6.3	1.91	6.5	1.1	6.6	1.4	3.9	0.57	3.8	0.61	5.1	1	< 1	0.7	37	2	0.6	
422293	FHW711	91	< 0.4	307	606	74.3	257	52.7	1.59	43.7	7.9	48.8	9.9	29.8	4.62	31.4	5.15	67.7	13.2	< 1	0.9	35	39.8	7.6	
422294	FHW711	47	0.8	221	276	103	29.2	0.92	30.7	6	38.4	7.8	23	3.56	24.7	4.1	53	13.3	< 1	1	43	28.1	7.4		
422295	FHW711	80	< 0.4	299	577	69.																			

Table A1-9: Lithogeochemical data for the South Belt

Sample	Channel Number	Ba	Bi	La	Ce	Pr	Nd	Sm	Eu	Gd	Tb	Dy	Ho	Er	Tm	Yb	Lu	Hf	Ta	W	Tl	Pb	Th	U
422264	FHWT-13	82	< 0.4	303	565	65.1	220	44.6	2	41.3	7.7	50.7	10.9	31.4	4.34	25.2	3.57	53.9	10.4	< 1	0.6	64	32.9	18.4
422265	FHWT-13	155	< 0.4	311	565	64.4	210	36.4	1.27	27.6	4.4	26.1	5.2	15.5	2.32	15.4	2.57	35.7	6.3	< 1	0.5	40	18.5	3.5
422266	FHWT-13	94	< 0.4	339	615	70	227	38	1.23	27.9	4.4	25.9	5.2	15.5	2.37	15.6	2.59	38.7	6.4	2	0.6	41	19.6	4.2
422267	FHWT-13	99	< 0.4	251	446	52.2	169	30.3	1.17	23.5	3.8	22.1	4.2	12.1	1.76	11.2	2.52	4.3	< 1	0.3	27	11.5	2.3	
422268	FHWT-13	957	< 0.4	136	265	27.9	92.3	17.5	1.58	15.3	2.7	16.2	3.3	9.7	1.51	10.4	1.73	22.3	4.8	< 1	0.4	34	12.4	2.2
422269	FHWT-14	1335	< 0.4	145	293	32.3	108	20.9	2.81	16.9	2.9	18.1	3.7	10.9	1.6	10.4	1.67	28.6	4.7	< 1	0.3	66	13.7	2.7
422270	FHWT-14	1333	< 0.4	174	365	41.5	143	27.3	4.22	21.7	3.6	21.2	4.3	12.5	1.82	12.1	1.98	40.3	4.4	< 1	0.5	45	13.8	3.3
422271	FHWT-14	495	< 0.4	35	77.6	9.4	36.3	8.5	2.06	8.4	1.5	9	1.9	5.4	0.79	5.1	0.82	8.8	1.6	< 1	0.5	16	6.6	1.3
422272	FHWT-14	1084	< 0.4	142	290	31.8	107	19.8	3.3	15.7	2.6	15	2.9	8.6	1.26	8.3	1.36	21.4	3.5	< 1	0.3	34	11.5	2
422273	FHWT-14	425	< 0.4	31.5	69.7	8.55	33.5	7.6	2	7.3	1.3	7.4	1.5	4.1	0.6	4.1	0.66	5.9	0.9	< 1	0.6	15	5.6	1
422274	FHWT-14	380	< 0.4	127	257	27.8	93.2	16.2	1.41	12.2	2	11.3	2.1	6.2	0.9	5.9	0.95	14.4	2.3	< 1	0.3	27	8.1	1.7
422275	FHWT-14	373	< 0.4	60.5	134	15.4	56	15	1.77	16.4	3.2	20.3	4.1	11.7	1.67	10.5	1.57	22.8	6.6	< 1	0.5	19	15.7	2.3
422301	FHWT-14	992	< 0.4	121	257	29.4	105	21.4	3	18.2	3	18.1	3.6	10.4	1.51	9.9	1.51	26.2	4.1	< 1	0.5	30	15	2.3
422302	FHWT-14	110	< 0.4	312	620	72.7	251	47.9	2.09	37.7	5.8	31.3	5.7	15.4	2.13	13.4	2.1	33	4.2	< 1	0.4	34	13.5	2.5
422303	FHWT-14	195	< 0.4	193	394	43.3	148	27	1.44	21.3	3.3	18.9	3.6	10.3	1.49	9.5	1.49	22.8	3.6	< 1	0.3	21	10.6	2
422304	FHWT-14	772	< 0.4	275	495	54.5	179	28.7	3.04	21.3	3.2	18.3	3.5	10.2	1.47	9.6	1.58	25.9	3.9	< 1	0.5	25	11.6	2.2
422305	FHWT-14	414	< 0.4	97.7	204	21.3	71.5	15.9	0.57	15.5	2.9	19	4	12	1.77	11.6	1.77	30.4	6.1	< 1	0.3	25	13.7	3
422306	FHWT-14	520	< 0.4	126	262	28.6	97.3	22.4	0.78	21.8	3.9	24.2	4.8	13.9	1.98	12.3	1.83	29.6	6.9	< 1	0.3	31	18.4	3
422307	FHWT-14	368	< 0.4	115	244	27.2	94.2	22	0.72	21.5	3.8	23.7	4.8	13.6	1.95	12.7	1.89	26.5	6.6	< 1	0.5	28	15.7	2.9
422308	FHWT-14	369	< 0.4	104	224	25.4	90.1	21.9	0.82	22.1	3.9	24.6	5.2	15.5	2.26	14.8	2.22	36.1	7.1	< 1	0.3	25	15.6	3.4
422309	FHWT-14	800	< 0.4	105	222	25.6	92.7	20.8	2.58	19.7	3.3	20.3	4	11.7	1.71	11.2	1.73	25.2	5.5	< 1	0.6	34	13.8	2.8
422310	FHWT-14	578	< 0.4	55.9	129	15.7	59.8	17.2	1.42	18	3.4	21.4	4.3	12.6	1.88	11.8	1.68	29.3	7.4	< 1	0.5	28	18.3	3.1
422311	FHWT-14	1314	< 0.4	121	248	28.2	101	20.1	3.59	17.4	2.9	16.7	3.3	9.6	1.42	9.3	1.46	23.4	4.5	< 1	0.8	43	12.5	2.2
422312	FHWT-14	1032	< 0.4	225	434	49.4	169	30.2	3.75	23.6	3.8	21.9	4.3	13	1.91	12.7	2	40.1	5.1	< 1	0.7	36	19.2	3.8
422313	FHWT-14	322	< 0.4	19.2	44.3	5.81	24.4	6.2	1.84	6.7	1.2	7.3	1.5	4.4	0.65	4.2	0.65	5.4	0.9	< 1	0.2	12	4.9	0.8
422314	FHWT-14	671	< 0.4	87	180	20.2	72.3	14.2	2.08	12	1.9	10.8	2.1	6	0.87	5.7	0.9	15	2	< 1	0.6	21	10.7	2.3
422315	FHWT-14	199	< 0.4	74.1	132	14.3	50	10.4	0.52	10.3	1.6	9.7	1.9	5.5	0.83	5.8	1	7.8	1.6	< 1	0.4	23	3.4	0.7
422316	FHWT-14	938	< 0.4	82.7	164	18.7	67.9	13.7	2.43	12.3	2	11.8	2.3	6.7	0.99	6.7	1.13	13.3	2.5	< 1	0.6	27	6.4	1.3
422317	FHWT-14	317	< 0.4	61.9	118	13.2	47.7	9.8	0.94	9.4	1.5	8.6	1.7	5	0.74	5.4	0.95	10.6	1.8	< 1	0.6	15	4.2	0.8
422318	FHWT-14	161	< 0.4	42.5	81.2	8.99	32.7	7.7	0.32	8.2	1.5	8.9	1.8	5.3	0.8	5.7	1	11.1	2	< 1	0.3	16	3.9	1
322456	FHWT-16-1	127	< 0.4	249	502	58.6	204	41.2	1.33	37.5	6.5	38	7.6	22.2	3.46	23.8	3.93	52	9	2	0.9	65	28.8	5.2
322457	FHWT-16-2	71	< 0.4	342	667	77.5	268	52	1.59	45.2	7.6	45.4	9.2	26.5	4.02	27.3	4.43	58.5	9.3	3	0.5	159	32	5.5
322458	FHWT-16-3	150	< 0.4	259	515	59.8	206	40.9	1.38	36.7	6.5	40.1	8.2	24.3	3.71	24.8	4.02	58.3	9.4	< 1	0.3	66	30.7	5.8
322459	FHWT-16-4	232	< 0.4	24	49.3	7.05	29.9	7.5	2.05	8.3	1.3	7.7	1.5	4.2	0.62	4	0.64	5.7	1.3	1	0.8	21	2.2	0.5
322460	FHWT-16-5	77	< 0.4	281	555	63.4	218	41.3	1.32	35.9	6.1	37	7.7	22.3	3.52	23.6	3.88	54.6	8.5	2	0.6	26	27.5	5.4
322461	FHWT-16-6	141	< 0.4	261	512	59.5	205	39.9	1.55	34.5	5.7	34.4	6.9	20.5	3.2	21.3	3.52	47.9	7.6	2	0.6	27	24.5	4.7
322463	FHWT-16-8	93	< 0.4	290	575	67.3	235	48.1	1.48	44.5	7.7	45.9	9.3	26.6	4.07	26.9	4.31	58	9.9	3	0.4	47	33.3	5.4
322464	FHWT-16-9	114	< 0.4	294	581	67.8	235	47	1.43	43	7.5	43.9	8.9	25.4	3.83	25.5	4.12	55.2	9.3	2	0.6	46	30.8	5.8
322465	FHWT-16-10	86	< 0.4	312	608	71.1	245	48.3	1.47	43.6	7.3	43.3	8.7	24.8	3.77	25	4.04	59.3	8.7	1	0.4	48	29.7	5.8
322466	FHWT-16-11	360	< 0.4	45.4	91.1	11.8	45.1	10.2	1.79	10.5	1.7	10	2	6	0.9	5.8	0.93	8.5	1.5	1	0.9	36	5.1	0.9
322467	FHWT-16-12	98	< 0.4	269	525	61.9	216	43.2	1.35	38.5	6.5	38.6	7.8	23.2	3.53	23.4	3.86	59.9	8.6	2	0.7	70	26.7	5
322468	FHWT-16-13	74	< 0.4	262	521	61.2	214	43.8	1.29	40.6	6.7	41.4	8.3	24.4	3.66	24.2	3.84	65.8	9.7	1	0.6	68	30	5.2
322469	FHWT-16-14	60	< 0.4	317	628	74.2	260	52.6	1.56	48.5	8.2	48.1	9.5	27.9	4.14	27.3	4.41	76.5	10.7	2	0.6	50	33.3	6
322470	FHWT-16-15	84	< 0.4	347	684	79.8	277	55.7	1.6	50.4	8.5	50.2	9.9	29.1	4.38	28.8	4.57	70.6	10.5	2	0.8	84	35.1	6
322471	FHWT-17-1	80	< 0.4	328	658	76	263	53.4	1.5	46.8	7.8	45.1	8.7	25.8	3.84	25.3	4.11	68.8	10.1	2	0.9	72	34	5.3
322472	FHWT-17-2	66	< 0.4	347	688	80.4	277	54.7	1.55	47.2	7.7	43.7	8.5	24.8	3.73	25.2	4.19	68.5	8.4	1	0.7	103	30.9	4.9
322473	FHWT-17-3	129	< 0.4	257	507	58.2	202	39.7	1.44	34.3	5.8	34.7	7.1	21.3	3.34	22.2	3.66	61.7	8.8	2	0.6	114	28.4	4.7
322474	FHWT-17-4	303	< 0.4	27.2	58.3	8.34	35	8.8	2.07	9.8	1.6	9.4	1.9	5.6	0.85	5.5	0.89	6.5	1.6	2	1	18	2.7	0.7
322475	FHWT-17-5	73	< 0.4	335	647	74.8	259	49.9	1.42	43.9	7.2	41.6	8.3	25	3.77	25.5	4.25	63.4	8.3	2	0.7	48	28.9	5.4
321918	FHWT-17-6	54	< 0.4	328	616	67.5	23																	

Table A2-1: Lithogeochemical data for the MT Belt

Sample	Felsic Belt Unit	SiO ₂	Al ₂ O ₃	Fe ₂ O ₃	FeO	MnO	MgO	CaO	Na ₂ O	K ₂ O	TiO ₂	P ₂ O ₅	LOI	Total
510539	FT2	69.62	12.3	7.22	6.5	0.099	0.85	1.53	3.26	3.82	0.566	0.11	0.63	100
510540	FT2	51.44	14.61	11.8	10.62	0.197	5.08	6.41	3.71	1.89	2.18	0.33	1.18	98.83
510541	FT2	44.75	15.56	14.96	13.46	0.204	5.89	7.78	3.49	1.52	2.958	0.54	0.88	98.54
510542	FT2	45.13	16.44	14.93	13.43	0.2	5.93	6.98	3.86	1.77	2.8	0.52	0.95	99.52
510543	FT2	44	16.07	14.66	13.19	0.205	5.98	8.1	3.56	1.34	2.833	0.51	0.88	98.12
510544	FT2	45.92	15.31	14.66	13.19	0.214	5.73	6.37	3.26	2.63	2.836	0.55	1.2	98.68
510545	FT2	43.58	15.71	15.21	13.69	0.218	5.24	8.68	2.72	2.85	2.786	0.58	1.83	99.4
510546	FT2	50.35	14.4	13.37	12.03	0.196	5.36	6.34	3.02	2.98	2.329	0.39	1.87	100.6
510547	FT2	44.84	15.7	14.9	13.41	0.272	6.2	6.82	3.62	2.19	2.966	0.53	1.27	99.3
510548	FT2	48.82	14.58	13.59	12.23	0.296	5.31	5.9	3.59	2.56	2.635	0.41	1.03	98.72
510549	FT2	72.06	12.23	5.21	4.69	0.071	0.54	1.3	4.66	1.75	0.385	0.03	0.52	98.75
510550	FT2	68.99	12.42	5.56	5	0.087	0.74	1.5	4.09	3.14	0.464	0.04	0.79	97.84
510551	FT2	45.53	15.3	12.94	11.64	0.319	7.91	5.4	3.4	3.08	1.581	0.18	5.04	100.7
510552	FT2	68.97	12.24	5.97	5.37	0.093	0.49	1.29	4.09	3.72	0.427	0.03	0.54	97.86
510553	FT2	71.63	11.89	5.86	5.27	0.078	0.29	1.26	4.07	3.79	0.361	0.02	0.49	99.73
510554	FT2	71.92	12.01	6.07	5.46	0.093	0.2	1.22	4.04	3.65	0.321	0.01	0.42	99.97
510555	FT2	50.28	15.03	13.31	11.98	0.266	5.71	4.17	4.06	2.93	2.014	0.42	2.18	100.4
510556	FT2	70.27	11.71	4.89	4.4	0.062	0.19	1.26	3.76	4.54	0.274	0.01	0.66	97.61
510557	FT2	73.89	11.77	4.11	3.7	0.052	0.15	1.01	3.99	4.57	0.29	0.01	0.41	100.2
510558	FT2	76.09	11.15	3.82	3.44	0.045	0.1	0.9	3.72	4.23	0.311	0.02	0.42	100.8
510559	FT2	69.09	11.68	6.36	5.72	0.119	0.24	1.53	3.96	4.51	0.529	0.07	0.35	98.45
510560	FT2	70.01	13.04	4.91	4.42	0.084	0.31	1.31	4.03	4.84	0.398	0.08	0.57	99.58
510561	FT2	70.48	13.25	3.7	3.33	0.064	0.59	1.46	4.06	4.9	0.53	0.13	0.83	100
510562	FT2	70.1	12.92	5.5	4.95	0.084	0.26	1.02	4	4.58	0.354	0.03	0.66	99.5
510563	FT2	70.63	12.09	5.37	4.83	0.101	0.37	1.17	3.71	3.41	0.298	0.06	0.54	97.77
510564	FT2	47.31	16.09	13.97	12.57	0.245	6.27	7.21	3.01	3.24	1.931	0.27	1.26	100.8
510565	FT2	69.81	13.21	5.08	4.57	0.079	0.25	1.54	4.42	3.52	0.407	0.03	0.41	98.79
510566	FT2	70.75	13.29	5.14	4.62	0.082	0.11	1.12	4.41	4.23	0.388	0.02	0.39	99.92
510567	FT2	71.49	13.51	4.52	4.07	0.055	0.09	4.53	4.09	4.38	0.07	0.35	99.74	
510568	FT2	69.77	13.16	6.03	5.43	0.101	0.5	1.44	4.38	3.54	0.574	0.07	0.54	100.2
510569	FT2	68.42	14.27	6.07	5.47	0.139	0.17	1.57	4.3	4.71	0.427	0.04	0.3	100.4
510570	FT2	55.31	15.2	11.14	10.02	0.222	3.2	4.21	4.64	3.64	1.962	0.37	0.83	100.7
510571	FT2	46.67	15.05	15.16	13.64	0.281	4.73	6.54	3.85	3.31	2.867	0.59	1.01	100.1
510572	FT2	53.35	14.76	11.57	10.41	0.202	3.72	3.42	4.36	3.72	1.881	0.35	1.38	98.7
510573	FT2	45.97	14.36	16.74	15.06	0.26	5.33	3.48	3.13	5.32	2.58	0.52	1.8	99.49
510574	FT2	62.62	14.5	7.26	6.53	0.131	1.95	2.06	5.54	2.25	0.838	0.12	0.75	98.02
510575	FT2	46.02	16.5	12.74	11.46	0.271	7.37	5.94	3.21	3.21	1.758	0.26	1.59	98.97
510576	FT2	46.96	17.15	12.81	11.53	0.265	7.16	6.89	3.73	2.17	1.53	0.24	1.56	100.5
510577	FT2	44.33	18.21	11.96	10.76	0.24	6.71	8.62	3.16	1.84	1.416	0.32	1.81	98.63
510578	FT2	45.47	17.84	13.11	11.8	0.302	7.05	6.89	3.62	1.98	1.811	0.25	1.46	99.79
510579	FT2	45.24	17.11	13.54	12.18	0.216	7.13	7.77	3.46	2.07	1.736	0.28	1.24	99.79
510580	FT2	45.46	17.19	13.98	12.58	0.301	6.1	7.72	3.22	2.83	2.204	0.34	1.28	100.6
510581	FT2	51.1	15.26	12.2	10.98	0.235	2.94	6.09	3.95	2.91	2.298	0.46	1.46	98.9
510582	FT2	56.42	13.99	11.74	10.56	0.238	2.21	5.4	3.96	2.64	2.135	0.46	1.06	100.2
510583	FT2	52.39	14.4	12.71	11.44	0.22	4.1	6.51	3.85	2.2	2.336	0.4	1.01	100.1
510584	FT2	74.22	11.02	4.77	4.29	0.066	0.25	0.9	2.94	4.25	0.323	0.03	0.42	99.17
510585	FT2	64.68	11.68	8.74	7.86	0.148	1.68	2.77	3.39	3.82	1.133	0.18	0.6	98.82
510586	FT2	75.86	11.06	4.87	4.38	0.078	0.19	0.74	3.06	4.45	0.297	0.02	0.37	101
510587	FT2	71.06	11.65	6.29	5.66	0.089	0.68	1.35	3.55	4.15	0.602	0.04	0.59	100
510588	FT2	75.47	10.71	4.78	4.3	0.07	0.07	0.75	3.33	4.56	0.254	0.01	0.35	100.4
510589	FT2	72.63	10.65	5.64	5.07	0.072	0.06	0.82	3.55	4.17	0.254	<0.01	0.31	98.15
510590	FT2	70.01	10.97	7.24	6.51	0.125	0.55	1.69	2.83	4.7	0.536	0.04	0.66	99.35
510591	FT2	73.24	11.44	4.55	4.09	0.088	0.09	1.13	3.61	4.47	0.282	0.02	0.39	99.31
510592	FT2	71.98	11.91	5.09	4.58	0.073	0.13	1.1	3.78	4.75	0.301	0.03	0.59	99.74
510593	FT2	70.81	10.82	5.41	4.87	0.076	0.48	1.48	3.15	3.91	0.361	0.04	1.05	97.6
510594	FT2	50.94	12.87	13.25	11.92	0.218	4.03	6.29	3.62	2.12	2.504	0.41	1.49	97.75
510595	FT2	49.25	13.05	14.32	12.89	0.251	4.27	7.1	3.49	2.38	2.548	0.48	1.11	98.24
510596	FT2	71.21	12.09	4.83	4.35	0.087	0.16	1.14	3.99	4.31	0.306	0.01	0.61	98.75
510597	FT2	71.51	11.86	4.66	4.19	0.084	0.12	1.04	4.04	4.88	0.274	0.01	0.62	99.09
510598	FT2	71.22	11.83	4.6	4.14	0.085	0.12	1.29	4.08	4.5	0.27	0.02	0.46	98.46
510599	FT2	43.92	14.61	15.64	14.07	0.273	6.09	7.63	3.33	2.62	2.676	0.31	1.55	98.64
510600	FT2	71.82	11.82	4.73	4.26	0.075	0.15	1.48	3.84	4.54	0.297	0.01	0.72	99.48
510601	FT2	71.58	11.49	4.55	4.09	0.077	0.12	1.21	3.92	4.6	0.271	0.01	0.69	98.52
510602	FT2	73.13	11.91	4.49	4.04	0.08	0.1	1.6	4.03	4.68	0.258	<0.01	0.67	100.9
510603	FT2	70.9	11.58	5.49	4.94	0.086	0.21	1.32	4.08	4.33	0.344	0.04	0.51	98.88
510604	FT2	72.15	11.49	5.25	4.72	0.089	0.04	0.02	3.94	4.45	0.237	<0.01	0.33	98.97
510605	FT2	73.06	11.17	6.31	5.68	0.103	0.11	1.32	3.12	4.14	0.305	0.01	1.05	100.3
510606	FT2	51.25	13.56	13.74	12.41	0.243	4.22	5.25	4.19	3.08	2.218	0.26	1.53	99.58
510607	FT2	72.8	12.08	5.31	4.78	0.11	0.24	1.36	5.61	1.32	0.296	<0.01	0.44	99.61
510608	FT2x	70.78	10.91	6.84	6.15	0.117	0.11	1.16	3.36	4.35	0.288	0.03	0.4	98.24
510609	FT2x	48.61	12.39	14.39	12.95	0.402	3.85	5.58	4.32	3.94	2.676	0.51	1.7	98.37
510610	FT2x	65.01	10.93	7.93	7.14	0.239	0.53	3.13	5.02	2.1	0.799	0.09	0.44	96.21
510611	FT2x	63	9.32	10.57	9.51	0.33	1.25	3.05	2.96	3.55	1.144	0.13	0.75	96.05

Table A2-2: Lithogeochemical data for the MT Belt

Sample	Felsic Belt unit	SiO ₂	Al ₂ O ₃	Fe ₂ O ₃	FeO	MnO	MgO	CaO	Na ₂ O	K ₂ O	TiO ₂	P2O ₅
510612	FT2x	64.98	10.92	9.37	8.43	0.287	0.12	1.75	3.59	4.6	0.466	0.05
510613	FT2x	66.36	11.28	9.13	8.22	0.276	0.25	2.05	3.5	4.37	0.453	0.06
510614		48.9	13.19	15.62	14.05	0.237	3.7	6.7	4.52	2.67	2.83	0.47
510615	FT2x	66.55	8.31	11.95	10.75	0.426	0.65	3.12	1.15	3.6	0.338	0.03
510616	FT2-Like unit?	62.35	11.64	10.37	9.33	0.276	1.37	3.51	3.26	4	0.905	0.12
510617	FT2-Like unit?	61.87	11.17	10.65	9.4	0.285	1.31	3.62	2.93	3.77	0.864	0.11
510618	Pegmatite	71.2	12.28	8.49	3.2	0.1	0.29	1.64	3.56	5.85	0.357	0.03
510619	Pegmatite	72.35	13.03	8.48	3.13	0.073	0.33	1.21	3.22	5.47	0.477	0.05
510620		46.46	13.7	16.38	14.74	0.233	4.85	7.32	3.8	2.96	3.379	0.49
510621		42.98	12.95	15.76	14.18	0.254	4.53	6.9	4.47	2.79	3.117	0.52
510622	FT3	72.07	6.77	8.86	7.97	0.323	0.24	2.79	1.19	3.89	0.456	0.11
510623	FT3	70.32	5.98	9.17	8.25	0.484	0.15	3.12	1.28	3.51	0.472	0.06
510624	FT3	67.69	5.8	11.3	10.17	0.591	0.11	2.16	1.07	4.42	0.523	0.14
510625	FT3	68.66	6.33	11.7	10.53	0.557	0.07	1.81	2.43	3.27	0.498	0.13
510626	FT3	68.69	6.91	10.67	9.6	0.42	0.08	2.15	2.22	4.25	0.59	0.06
510627	FT3	67.73	6.58	11.18	10.06	0.408	0.13	1.99	2.97	3.2	0.516	0.06
510628	FT3	69.65	6.54	11.14	10.02	0.448	0.1	2.02	2.64	3.33	0.476	0.04
510629	FT3	68.43	6.66	9.84	8.83	0.388	0.33	3.93	2.43	3.26	0.403	0.03
510630	FT3	68.08	8.01	9.56	8.6	0.258	0.09	2.29	2.57	4.37	0.431	0.02
510631	FT3	68.2	7.42	10.03	9.02	0.272	0.07	2.18	2.22	4.44	0.419	0.02
510632	FT3	68.51	6.97	9.45	9.4	0.362	0.21	2.86	1.82	3.69	0.456	0.03
510633	FT3	68.96	7.33	9.04	8.13	0.288	0.28	3	1.87	3.41	0.544	0.06
510634	FT3	70.42	6.37	9.03	8.13	0.308	0.14	3.87	1.44	2.99	0.416	0.03
510635	FT3	67.15	8.49	9.55	9.5	0.31	0.22	3	2.25	3.41	0.405	0.05
510636	FT3	61.23	10.46	10.31	9.28	0.243	1.3	4.28	4.17	1.16	3.922	0.15
510638		46.01	14.3	15.41	13.87	0.252	5.4	6.8	3.01	3.56	3.349	0.51
510639		66	8.39	9.55	8.59	0.359	1.4	5.33	3.47	1.68	1.149	0.14
510640		43.88	14.69	16.27	14.64	0.24	5.91	8.06	3.06	2.64	3.02	0.37
510641		46.35	14.33	15.68	14.11	0.349	5.42	7.09	3.51	2.71	2.752	0.36
510642	FT4	72.71	7.25	8.95	8.05	0.249	0.74	2.93	1.7	2.02	0.622	0.11
510643	FT4	66.82	9.31	9.05	8.14	0.274	0.5	2.4	2.56	4.04	0.46	0.06
510644	FT4	65.34	9.44	10.15	9.13	0.279	0.35	2.96	3	4.22	0.551	0.04
510645	FT4	68.27	9.18	9.58	8.62	0.25	0.29	2.27	2.81	4.26	0.482	0.05
510646	FT4	68.22	9.38	9.4	8.46	0.232	0.24	2.05	2.46	4.47	0.46	0.08
510647	FT4	68.21	9.4	8.33	7.5	0.234	0.24	2.28	2.94	3.68	0.374	0.03
510648	FT4	66.79	8.65	9.62	8.66	0.284	0.38	1.98	2.39	3.97	0.433	0.03
510649	FT4	66.19	8.86	9.71	8.74	0.283	0.43	2.39	2.08	4.28	0.516	0.05
510650	FT4											
510651	FT Buff	73.72	12.05	2.59	2.33	0.042	0.19	0.94	3.01	5.68	0.28	< 0.02
510652	FT Buff	75.65	11.36	2.25	0.033	0.18	0.03	2.89	5.16	0.249	< 0.01	
510653	FT Buff	68.62	11.86	6.55	5.71	0.04	1.74	2.6	5.06	0.861	0.09	
510654	FT4	74	11.38	2.37	2.13	0.024	0.06	0.68	2.54	6.29	0.261	0.02
510655	FT4	66.98	11.12	7.54	6.78	0.183	1.01	2.32	2.99	4.87	0.007	0.13
510656	FT Buff	72.02	11.31	4.19	3.77	0.09	0.68	1.84	2.31	6.01	0.237	0.05
510657	FT4	70.16	11.68	6.61	5.95	0.133	0.29	1.72	3.29	4.89	0.455	0.05
510658	FT4	65.25	10.31	10.2	9.18	0.279	0.9	2.66	2.91	3.91	0.966	0.14
510659	FT4	64.68	10.03	10.98	9.88	0.232	1.17	2.75	2.35	3.46	0.926	0.13
510660	46.34	15.59	13.84	12.45	2.21	7.11	8.79	3.21	1.44	2.376	0.37	
510661	45.19	15.54	13.4	12.06	0.195	7.72	9.19	2.98	1.39	2.146	0.33	
510662	45.48	16.17	11.95	10.75	0.196	9.71	8.92	2.87	1.41	1.43	0.17	
510663	46.74	17.05	10.79	9.71	0.172	8.96	8.71	3.19	1.72	1.09	0.1	
510664	51.86	14.02	11.66	10.49	0.186	6.85	7.24	2.72	1.9	1.736	0.23	
510665	45.76	16.66	12.13	10.91	0.184	8.46	9.68	2.82	1.17	1.586	0.18	
510666	46.3	16.82	11.71	10.54	0.183	8.44	9.59	2.83	1.23	1.506	0.15	
510667	47.35	15.94	11.36	10.22	0.18	9.29	7.66	2.81	1.54	1.415	0.17	
510668	43.95	14.59	12.51	11.26	0.186	13.78	9	1.68	0.75	1.06	0.14	
510669	45.2	15.89	11.68	10.51	0.23	10.65	9.27	2.45	0.41	1.198	0.12	
510670	45.21	15.37	11.62	10.63	0.175	11.86	10.21	1.94	0.26	1.089	0.12	
510671	46.82	15.6	11.95	10.48	0.245	1.3	9.85	2.74	0.37	1.147	0.14	
510672	44.59	15.88	11.38	10.24	0.206	11.43	9.21	2.2	0.55	0.953	0.1	
510673	45.21	15.53	11.03	9.93	0.216	10.93	8.56	2.43	0.49	0.929	0.09	
510674	44.28	15.1	12.46	11.21	0.188	13.1	8.53	1.97	0.8	1.275	0.2	
510675	43.74	13.87	12.39	11.15	0.188	14.39	7.86	1.49	1.32	0.93	0.1	
510676	47.89	16.16	10.35	9.31	0.176	8.66	6.34	3.19	2.59	1.168	0.16	
510677	48.22	14.84	11.96	10.76	0.214	8.94	6.5	2.97	2.24	1.442	0.17	
510678	44.53	15.14	11.87	10.68	0.176	12.17	7.73	2.16	2	1.166	0.13	
510679	47.91	15.06	13.43	12.08	0.206	6.76	7.87	3.06	1.54	2.07	0.28	
507545	FT Buff	74.75	11.76	2.48	2.23	0.029	0.18	0.71	2.67	6.37	0.262	0.01
507546	FT Buff	75.33	11.95	2.46	2.21	0.03	0.14	0.49	2.74	6.4	0.264	0.02
507548	FT Buff	75.87	11.54	2.32	2.09	0.038	0.18	0.64	2.38	6.55	0.246	0.03

Table A2-3: Lithogeochemical data for the MT Belt

Sample	Felsic Belt unit	SiO ₂	Al ₂ O ₃	Fe ₂ O ₃	FeO	MnO	MgO	CaO	Na ₂ O	K ₂ O	TiO ₂	P ₂ O ₅	LOI	Total
511012	FT3b	69.9	7.98	10.16	9.14	0.209	0.45	1.57	2.07	2.35	0.474	0.04	0.35	95.54
511046	FT5	71.24	12.11	5.37	4.83	0.089	1.5	1.43	2.95	2.34	0.592	0.08	1.09	98.8
511049	FT5	74.3	10.44	4.95	4.45	0.066	0.67	1.52	3.56	1.02	0.382	0.04	0.64	97.59
511050	FT5	71.85	11.84	3.17	2.85	0.062	0.79	2.07	4.2	0.81	0.334	0.04	0.77	95.94
510312	FT3b	69.09	9.92	8.19	7.37	0.168	0.18	1.72	2.27	5.25	0.364	0.02	0.77	97.94
510313	FT3b	69.78	7.17	9.38	8.44	0.268	0.26	2.51	1.41	3.87	0.428	0.06	1.34	96.48
510340	FT5	65.46	11.07	9.14	8.22	0.143	2.04	2.54	2.69	2.7	1.213	0.12	0.71	97.82
510341	FT5	76.7	8.39	6.22	5.6	0.071	0.38	0.48	0.75	4.69	0.369	0.01	0.4	98.46
510342	FT5	72.56	11.8	4.31	3.88	0.062	0.83	1.22	2.65	3.88	0.292	<0.01	0.58	98.18

Table A2-4: Lithogeochemical data for the MT Belt

Sample	Felsic-Belt-unit	Sc	Be	V	Cr	Co	Ni	Cu	Zn	Ga	Ge	As	Rb	Sr	Y	Zr	Nb	Mo	Ag	In	Sn	Sb	Cs
S10539	FT2	6	12	24	<20	5	<20	20	410	43	3	<6	161	149	247	1626	129	2	<0.2	22	<0.5	0.5	
S10540	FT2	24	3	190	50	40	70	50	210	21	3	<6	97	194	38	273	18	<2	0.5	<0.2	4	<0.5	1.6
S10541	FT2	26	1	228	50	50	100	90	110	21	2	<6	61	312	35	217	10	<2	<0.5	<0.2	2	<0.5	2
S10542	FT2	27	1	212	50	51	90	50	110	20	2	<6	76	307	33	185	8	<2	<0.5	<0.2	2	<0.5	3.2
S10543	FT2	25	1	213	50	51	100	50	100	20	2	<6	60	336	32	199	9	<2	<0.5	<0.2	2	<0.5	2.3
S10544	FT2	25	2	209	50	49	100	70	170	20	2	<6	154	245	33	212	8	<2	<0.5	<0.2	2	<0.5	7.8
S10545	FT2	25	4	167	40	48	80	40	220	27	3	<6	197	260	36	209	17	<2	0.5	<0.2	13	<0.5	12.3
S10546	FT2	23	4	199	60	43	90	50	220	23	2	<6	214	200	37	254	20	2	0.5	<0.2	4	<0.5	9.6
S10547	FT2	26	1	227	50	51	100	80	170	21	2	<6	139	279	34	214	11	<2	0.6	<0.2	3	<0.5	9.9
S10548	FT2	27	5	215	60	42	90	80	270	24	3	<6	175	206	52	312	26	<2	0.6	<0.2	6	<0.5	6
S10549	FT2	2	13	17	<20	3	<20	20	250	55	4	<6	84	86	222	2056	105	6	<0.2	18	<0.5	0.7	
S10550	FT2	2	15	23	<20	4	<20	20	270	56	4	<6	162	73	251	2095	99	16	<0.2	20	<0.5	<0.5	
S10551	FT2	27	7	194	120	47	140	10	350	31	3	<6	334	127	40	120	24	3	<0.5	<0.2	6	<0.5	2.8
S10552	FT2	2	18	14	<20	3	<20	20	360	60	4	<6	215	60	276	2896	128	12	<0.2	27	<0.5	<0.5	
S10553	FT2	<4	18	7	<20	1	<20	20	350	62	4	<6	209	46	252	2225	120	8	<0.2	24	<0.5	<0.5	
S10554	FT2	<4	15	5	<20	<4	<20	<40	290	63	4	<6	142	50	178	3182	79	15	<0.2	17	<0.5	<0.5	
S10555	FT2	25	11	182	70	38	80	20	430	34	3	<6	342	136	83	885	48	5	1.7	<0.2	13	<0.5	5.6
S10556	FT2	<4	10	25	<20	<4	<20	10	190	58	3	<6	197	47	151	1807	75	8	<0.2	14	<0.5	<0.5	
S10557	FT2	<4	12	10	<20	<4	<20	10	270	55	3	<6	211	40	149	1357	70	8	<0.2	14	<0.5	<0.5	
S10558	FT2	<4	10	6	<20	<4	<20	40	230	52	2	<6	209	36	116	1165	80	5	<0.2	13	<0.5	<0.5	
S10559	FT2	6	12	<6	<20	<4	<20	<40	260	46	3	<6	215	59	130	1758	79	4	<0.2	15	<0.5	0.8	
S10560	FT2	5	14	12	<20	2	<20	<40	270	46	4	<6	260	80	166	1247	92	2	<0.2	18	<0.5	0.8	
S10561	FT2	8	10	29	<20	4	<20	10	140	25	2	<6	250	103	115	930	68	6	2.1	<0.2	11	<0.5	1.1
S10562	FT2	<4	12	9	<20	2	<20	30	330	61	4	<6	225	37	173	2099	102	10	<0.2	16	<0.5	1.1	
S10563	FT2	<4	28	6	<20	2	<20	10	400	67	5	<6	195	51	531	2993	130	11	<0.2	24	<0.5	0.9	
S10564	FT2	30	4	227	130	50	110	110	230	29	3	<6	327	202	38	267	25	4	0.7	<0.2	4	<0.5	2.4
S10565	FT2	1	11	9	<20	2	<20	10	240	63	4	<6	120	59	202	1602	158	5	<0.2	33	<0.5	<0.5	
S10566	FT2	<4	9	6	<20	<4	<20	10	240	64	4	<6	137	44	145	1502	99	6	<0.2	16	<0.5	<0.5	
S10567	FT2	<4	7	8	<20	<4	<20	20	180	61	3	<6	121	65	150	1554	80	4	<0.2	13	<0.5	<0.5	
S10568	FT2	3	9	22	<20	5	<20	20	320	60	3	<6	154	71	141	1537	99	8	<0.2	15	<0.5	1	
S10569	FT2	1	13	<6	<20	<4	<20	<40	280	53	5	<6	147	70	185	2266	108	7	<0.2	15	<0.5	<0.5	
S10570	FT2	21	9	143	40	27	50	60	460	34	3	<6	274	131	100	826	58	6	1.8	<0.2	8	<0.5	4.8
S10571	FT2	31	4	236	60	46	80	50	350	23	3	<6	299	188	39	266	18	4	0.8	<0.2	4	<0.5	4.1
S10572	FT2	16	12	141	40	32	60	10	430	39	4	<6	371	131	94	1004	63	2	<0.2	11	<0.5	6.3	
S10573	FT2	19	9	202	40	44	80	<40	510	44	3	<6	531	123	74	358	57	<2	0.9	<0.2	12	<0.5	7.4
S10574	FT2	8	9	62	20	14	40	20	280	46	3	<6	163	111	116	1340	73	5	<0.2	9	<0.5	2.1	
S10575	FT2	22	2	191	70	55	130	20	210	23	2	<6	224	206	21	129	11	<2	<0.5	<0.2	2	<0.5	2.7
S10576	FT2	19	6	169	60	55	130	50	280	26	2	<6	135	206	26	136	17	<2	<0.5	<0.2	4	<0.5	1.4
S10577	FT2	17	4	152	40	56	130	20	200	26	2	<6	116	241	18	100	7	3	<0.5	<0.2	2	<0.5	1.1
S10578	FT2	21	2	213	50	57	120	70	190	21	2	<6	115	207	21	138	8	<2	<0.5	<0.2	2	<0.5	1.9
S10579	FT2	20	2	186	60	59	130	60	140	21	2	<6	117	198	26	148	12	<2	0.6	<0.2	2	<0.5	1.5
S10580	FT2	23	3	223	70	55	110	40	320	24	2	<6	148	256	30	192	15	<2	<0.5	<0.2	3	<0.5	1.3
S10581	FT2	24	4	164	<20	31	30	70	270	34	3	<6	139	255	92	744	53	3	1.9	<0.2	11	<0.5	0.7
S10582	FT2	22	7	116	<20	24	20	40	290	33	3	<6	105	196	103	814	62	4	1.7	<0.2	14	<0.5	0.5
S10583	FT2	23	5	192	50	37	70	40	200	29	2	<6	92	194	62	479	38	2	1.1	<0.2	8	<0.5	0.6
S10584	FT2	1	10	10	<20	2	<20	20	370	51	3	<6	214	44	162	1484	110	8	<0.2	19	<0.5	0.6	
S10585	FT2	10	9	84	20	18	30	30	410	47	4	<6	414	79	141	1372	115	10	<0.2	18	<0.5	2.4	
S10586	FT2	<4	10	5	<20	1	<20	<40	340	58	3	<6	306	23	170	1617	115	7	<0.2	20	<0.5	1.2	
S10587	FT2	4	10	39	<20	6	<20	10	360	54	4	<6	296	49	159	1574	108	4	<0.2	20	<0.5	1.2	
S10588	FT2	<4	11	<6	<20	<4	<20	<40	350	59	3	<6	253	26	195	1910	142	5	<0.2	24	<0.5	0.7	
S10589	FT2	<4	11	<6	<20	<4	<20	<40	450	61	4	<6	203	32	217	2161	129	5	<0.2	26	<0.5	<0.5	
S10590	FT2	3	9	26	<20	5	<20	<40	510	51	4	<6	235	56	218	2208	142	4	<0.2	26	<0.5	1.2	
S10591	FT2	<4	11	<6	<20	<4	<20	<40	310	51	4	<6	214	45	172	1449	104	5	<0.2	22	<0.5	0.5	
S10592	FT2	<4	12	<6	<20	<4	<20	<40	370	60	5	<6	315	29	240	2612	159	6	<0.2	27	<0.5	<0.5	
S10593	FT2	2	18	14	<20	4	<20	<40	940	54	4	<6	248	31	240	2189	191	10	<0.2	35	<0.5	0.8	
S10594	FT2	30	5	292	40	38	40	70	670	26	3	<6	147	193	65	495	38	2	1.5	<0.2	6	<0.5	1.5
S10595	FT2	34	4	331	30	40	40	40	270	24	3	<6	203	247	47	361	20	<2	0.8	<0.2	5	<0.5	1.6
S10596	FT2	1	18	7	<20	2	<20	20	390	55	4	<6	233	44	252	2568	190	8	<0.2	29	<0.5	0.5	
S10597	FT2	<4																					

Table A2-6: Lithogeochemical data for the MT Belt

Sample	Felsic Belt Unit	Sc	Be	V	Cr	Co	Ni	Cu	Zn	Ga	Ge	As	Rb	Sr	Y	Zr	Nb	Mo	Ag	In	Sn	Sb	Cs
511012	FT3b	<4	93	11	<20	2	<20	20	1510	67	7	9	363	94	915	8485	938	<2	<0.2	139	<0.5	0.5	
511046	FT5	7	19	47	20	10	30	50	390	54	4	<6	295	123	573	4801	492	<2	<0.2	108	<0.5	1.9	
511049	FT5	2	22	22	<20	4	<20	20	520	57	4	<6	149	103	892	7122	912	<2	<0.2	114	<0.5	0.9	
511050	FT5	4	28	27	<20	4	<20	<10	350	54	5	<6	112	162	1342	11540		<2	<0.2	84	<0.5	0.8	
510312	FT3b	1	75	<6	<20	<4	<20	<10	670	55	4	7	500	65	710	5530	391	<2	<0.2	63	<0.5	<0.5	
510313	FT3b	<4	115	<6	<20	<4	<20	<10	1050	68	6	12	625	106	1276	12850	725	<2	<0.2	142	<0.5	0.6	
510340	FT5	9	31	94	30	17	30	70	930	50	4	<6	452	142	997	8207	639	<2	<0.2	96	<0.5	2.4	
510341	FT5	<4	5	10	<20	<4	<20	10	1170	64	4	<6	482	60	1324	11250	983	<2	0.2	171	<0.5	1.4	
510342	FT5	1	19	15	<20	4	<20	20	550	50	3	<6	416	85	522	5569	354	<2	<0.2	60	<0.5	1.6	

Table A2-9: Lithogeochemical data for the MT Belt

Sample	Felsic belt unit	Ba	Bi	La	Ce	Pr	Nd	Sm	Eu	Gd	Tb	Dy	Ho	Er	Tm	Yb	Lu	Hf	Ta	W	Tl	Pb	Th	U
S11012	FT3b	85	0.9	1590	3320	358	1360	239	12	191	28.4	165	30.7	89.5	12.7	77	11.4	165	31.1	4	1.7	186	224	19
S11046	FT5	392	0.5	326	667	88.8	322	79.4	2.33	80.3	16	102	22.3	65	9.65	65.4	10.5	123	26	4	1.2	171	73.2	20.8
S11049	FT5	124	0.5	516	1170	140	501	125	2.99	125	25.6	165	35.8	108	16.4	110	17.6	195	46.5	3	0.5	126	124	36.7
S11050	FT5	131	0.9	558	1320	159	567	150	3.77	159	33.6	233	52.9	163	25	174	28	304	67.8	5	0.5	159	146	56.4
S10312	FT3b	162	<0.4	962	2020	234	848	153	7.5	128	20.9	129	23.6	65.4	9.29	59.9	9.56	105	20.8	3	2.5	99	81.4	19.7
S10313	FT3b	84	0.6	1850	3940	460	1660	299	14.7	244	38.9	243	44.9	123	17.3	110	17.3	241	37.7	5	2.7	205	120	39.8
S10340	FT5	213	1.2	614	1340	159	552	144	3.49	145	29.3	199	38.8	111	16.5	110	17.3	190	40.5	5	2.1	196	118	27.7
S10341	FT5	164	<0.4	712	1560	184	629	172	3.56	174	36.7	258	52.4	151	23.1	158	26.2	258	60.3	7	1.9	228	158	32.4
S10342	FT5	214	<0.4	335	728	85.9	303	75.9	1.93	75.2	15.1	104	20.1	56.6	8.51	59.4	10.2	126	20.7	4	1.8	226	61.4	18.5

